THE
PHYSICAL REVIEW

A journal of experimental and theoretical physics established by E. L. Nichols in 1893

SECOND SERIES, VOL. 73, NO. 1 JANUARY 1, 1948

A Phase-Shift Analysis of the Scattering of Protons by Deuterons

CHARLES L. CRITCHFIELD*
Los Alamos Scientific Laboratory, Los Alamos, New Mexico
(Received September 22, 1947)

Numerical values for the *S*-wave and *P*-wave phase shifts are deduced from the observed angular distribution of protons scattered by deuterons. The experimental results used are those obtained at Los Alamos in the energy range, 1.5 to 3.5 Mev. In reducing the results to phase shifts the theoretical work on neutron-deuteron scattering, as presented by Buckingham and Massey, was used as a guide. It is found that the *p-d* phase shifts are qualitatively similar to the calculated *n-d* phase shifts, for the case of exchange forces between nucleons, except that the doublet *P*-wave is much more strongly refracted in the *p-d* results. The discrepancy may be evidence for a difference between the actual nuclear forces and the type of central, exchange forces assumed in the calculations. The results are definitely not similar to those for ordinary forces, however, and such forces would appear to be ruled out. Phase shifts in *S*- and *P*-waves alone are not sufficient to represent the *p-d* results in the range of energies used, but it is necessary to include interference with *D*-waves.

I. INTRODUCTION

THE angular distribution of protons, as scattered by deuterium gas, has been determined at the Los Alamos Laboratory.[1] Very complete and accurate results were obtained for five energies of incident protons, ranging from 1.5 Mev to 3.5 Mev. The scattered intensity was measured at fourteen angles of scattering, running from 22.5° to 164.5° in the center of gravity coordinate system. It is convenient, for the purposes of analysis, to represent this data by plotting $k^2\sigma(\theta)$ against $\cos\theta$, where θ is the angle of deflection of the proton in the center of gravity system, $\sigma(\theta)$ is the usual differential cross section, and

$$k=\frac{2\pi}{\lambda}=\frac{2}{3}\frac{Mv}{\hbar}=1.463(E_{\text{Mev}})^{\frac{1}{2}}\times10^{12}\ \text{cm}^{-1} \quad (1)$$

for protons of mass M and relative velocity v (energy E_{Mev} in the laboratory system). The experimental results are plotted in these terms in Fig. 1.

The experimental results are characterized by very strong scattering at small angles ($\cos\theta\simeq1$), i.e., in the forward direction of the protons, and this is an obvious effect of the Coulomb repulsion between the proton and the deuteron. The pure Coulomb field differential cross section (times k^2) is shown as a dotted curve in Fig. 1, for $E=2.53$ Mev, just for comparison. The more remarkable feature of the results is that the scattering at angles near 180°, i.e., in the backward direction, becomes very strong also, especially for the higher energies of bombardment.

Strong backward scattering, in the energy range concerned, has been found in the theoretical work of Buckingham and Massey[2] on the

* On summer leave from the University of Minnesota, Minneapolis, Minnesota.

[1] R. Sherr, J. M. Blair, H. R. Kratz, C. L. Bailey, and R. F. Taschek, Phys. Rev. **72**, 662 (1947).

[2] R. A. Buckingham and H. S. W. Massey, Proc. Roy. Soc. **A179**, 123 (1942); Phys. Rev. **71**, 558, 829 (1947).

scattering of *neutrons* by deuterium. These authors use the resonating group-structure theory of Wheeler[3] and thus allow for the possibility that the incoming neutron may form a new deuteron with the proton and liberate the neutron that was originally held by the proton. It is plausible, just from the persistence of momentum of the impinging neutron, that the newly formed deuteron will move predominantly in the forward direction so that the liberated neutron will fly backward. Greater detail in this mechanism can be followed through the integro-differential wave equation set up and solved in reference 2. The strong scattering near 180° is thus *not* direct evidence of the exchange nature of nuclear forces but rather arises as an exchange of partners for the proton in forming a deuteron. On the contrary, it was found that if the nuclear forces are of an exchange nature they partially defeat the exchange of partners so that ordinary forces should give much more backward scattering, in this energy range, than exchange forces.

The calculations of neutron-deuteron scattering were made on the basis of various assumptions concerning the nuclear forces. Since nuclear forces are believed to be the same between two protons as between two neutrons, the qualitative features of these calculations should be applicable also to the proton-deuteron scattering. Hence, in the present paper, we shall depend upon the calculations by Buckingham and Massey for guidance in reducing the proton-deuteron results in terms of phase shifts. The results of calculation and of experiment cannot be expected to be quantitatively exactly the same, however, since the Coulomb repulsion in the *p-d* case will affect the amplitudes of the waves to some extent and also the calculations have been made assuming central forces with rather arbitrarily chosen exchange characters. The actual forces between nucleons are known to be partly non-central and may have a somewhat different exchange nature than those in the particular examples taken for calculation. No attempt has been made to interpret the differences between *n-d* calculations and *p-d* experimental results, as found below, except that it appears that nuclear forces are certainly not purely ordinary forces. This fact is known already from the saturation character of forces in nuclei.

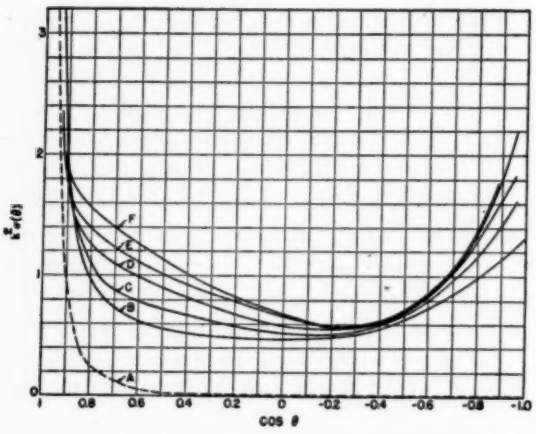

FIG. 1. Experimental results on angular distribution of protons scattered by deuterons.

A—Coulomb effect only ($E=2.53$)	*D*—2.53 Mev
B—1.51 Mev	*E*—3.00 Mev
C—2.08 Mev	*F*—3.49 Mev

In Fig. 2 is summarized the results of calculation for *S*-wave and *P*-wave phase shifts in quartet and doublet collisions of neutron and deuteron. For convenience, the phase shifts are represented in the first and fourth quadrants. Figure 2a is for ordinary forces and Fig 2b for a particular combination of exchange forces (and ordinary forces) as assumed in reference 2. It is evident from these figures that the *S*-wave shifts are practically independent of spin orientation.** Considering the very different nature of the *S*-wave solutions for quartet and doublet collisions (there is a region of repulsion in the quartet state, none in the doublet) it would seem that the independence of spin is accidental. In any case, for the analysis of the *p-d* results we shall assume that this feature of the *n-d* calculation carries over and adopt a single phase shift, K_0, for both *S*-waves. We assume also, of course, that this K_0 lies in the fourth quadrant.

Because of the effect of changing partners (in the *p-d* collisions the protons exchange) the higher partial waves, *P*, *D*, *F*, etc., may become affected when λ becomes of the order of the radius of the deuteron, i.e., at 2 Mev in the

[3] J. A. Wheeler, Phys. Rev. **52**, 1107 (1937).

** The calculations actually predict the quartet and doublet phase shifts to differ very nearly by 180°. Since, however, scattering experiments do not distinguish phase shifts differing by 180°, the two are plotted in the same quadrant.

center of gravity coordinates or 3 Mev in the laboratory system. Since the Coulomb repulsion at this radius is rather small compared with the bombarding energy, the extent to which the waves of higher orbital angular momenta, l, are affected will diminish rapidly with l, as in the collision of neutral particles. Hence, in the energy range of the experiments on p-d scattering we are justified in considering the S- and P-waves only as strongly shifted in phase with small shifts of diminishing importance in D and higher waves. The n-d results, Fig. 2, show that the P-waves are indeed strongly refracted and that there is a considerable difference in phase shift between ^2P and ^4P waves. For both ordinary and exchange forces, however, the ^4P phase shift lies above the ^2P and in the first quadrant. In analyzing the p-d data we shall assume, therefore, that the ^4P phase shift lies in the first quadrant.

The formula for $k^2\sigma(\theta)$, which forms the basis of the p-d analysis below, is written most conveniently for the simplified case of no spin-dependence of scattering

$$k^2\sigma(\theta)=\Big|-\frac{\eta}{1-\cos\theta}e^{i\eta\ \ln 2/1-\cos\theta}+e^{iK_0}\sin K_0 +3\cos\theta e^{i(\bar{K}_1+\phi_1)}\sin\bar{K}_1 +\frac{5}{2}(3\cos^2\theta-1)e^{i(\bar{K}_2+\phi_2)}\sin\bar{K}_2\cdots\Big|^2, \quad (2)$$

$$\eta=\frac{e^2}{\hbar v}, \quad \phi_s=\arg\frac{1+i\eta}{1-i\eta},$$

with K_0, $\bar{K}_1$, $\bar{K}_2$ the phase shifts in S, P, D, waves. In the energy range of interest, η is of the order 0.1, so that $\phi_1\simeq 2\eta$ and the $\bar{K}_2$ involved are so small that

$$e^{i(\bar{K}_2+\phi_2)}\sin\bar{K}_2\simeq\bar{K}_2. \quad (3)$$

II. ESTIMATES OF S- AND P-WAVE SHIFTS

The first step in a preliminary reduction of the experimental data is to estimate the phase shifts for the S-waves. As remarked above, we shall assume that D-waves and higher partial waves have very small phase shifts and also that the ^4S and ^2S waves have the same phase shift, K_0. We may then use Eq. (2), setting $\bar{K}_2$, $\cdots$ equal to zero, and avoid possible contributions of the

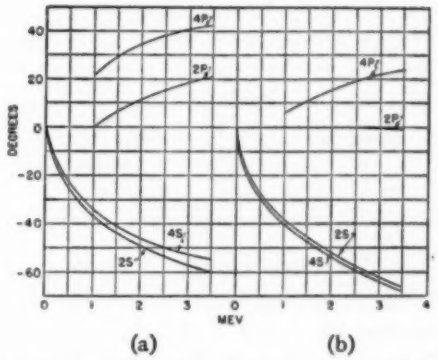

(a) (b)

FIG. 2. Calculated phase shifts of S-waves and P-waves in the scattering of neutrons by deuterons. (a) for ordinary forces; (b) for the "mixed exchange" forces of reference 2.

P-waves by using the experimental data at $\theta=90°$. The formula for $k^2\sigma(90°)$ then becomes

$$k^2\sigma(90°)=\eta^2-2\eta\sin K_0\cos(K_0-\eta\ln 2)+\sin^2K_0. \quad (4)$$

By the neglect of terms of the order η^3 (≤ 0.004 in the range of the experiments) Eq. (4) may be solved for $\cos(2K_0-2\eta)$ in terms of η and the measured values of $k^2\sigma(90°)$, *viz.*:

$$\cos(2K_0-2\eta)=\{1-2\eta^2(1-\ln 2)\}\{1-2k^2\sigma(90°)\}. \quad (5)$$

Equation (5) then leads to two possible values of K_0 for each energy represented in Fig. 1. In accordance with the n-d predictions we choose the solutions for K_0 that lie in the fourth quadrant. The deductions of K_0 from the experimental curves are given in Table I. Comparing these results with those in the n-d calculations, Fig. 2, we see that the p-d phase shifts are about $\frac{3}{4}$ those predicted for exchange forces and about $\frac{5}{6}$ those for ordinary forces. The smaller S-wave shift in p-d collisions may be due to the Coulomb repulsion, and it is not possible to conclude from this result alone whether ordinary or exchange forces are operative.

The second step is to estimate the P-wave

TABLE I. S-wave phase shifts.

E Mev	η	$k^2\sigma(90°)_{obs}$	K_0
1.51	0.129	0.48	−36.5°
2.08	0.110	0.54	−41.0°
2.53	0.100	0.58	−43.9°
3.00	0.092	0.64	−47.8°
3.49	0.085	0.68	−50.6°

TABLE II. *P*-wave phase shifts.

E	s	d	K_1	k_1
1.51	2.781	−0.054	15.2°	−6.0°
2.08	2.640	−0.147	16.9	−11.8
2.53	2.508	−0.139	17.2	−17.6
3.00	2.484	−0.098	16.1	−19.9
3.49	2.370	−0.064	17.2	−23.0

TABLE III. *D*-wave phase shifts.

E Mev	$5(\sin 2K_1 - \sin 2k_1)$	$\lvert\delta\rvert$	K_2 rad.	K_2 deg.	k_2 rad.	k_2 deg.
1.51	3.58	0.13	−0.036	−2.1	0.072	4.2
2.08	4.78	0.25	−0.052	−3.0	0.104	6.0
2.53	5.70	0.35	−0.061	−3.6	0.122	7.2
3.00	5.86	0.44	−0.075	−4.4	0.150	8.8
3.49	6.42	0.42	−0.065	−3.8	0.130	7.6

shifts. For the time being let us assume that there is no spin dependence, so that we may again use Eq. (2) with $\bar{K}_2=0$, etc., and substitute the values of K_0 already obtained. The formula for $k^2\sigma(\theta)$ then becomes:

$$\begin{aligned}k^2\sigma(\theta)=&\tfrac{1}{4}\eta^2\csc^4\tfrac{1}{2}\theta-\eta\csc^2\tfrac{1}{2}\theta[\sin K_0\cos(K_0-\beta)\\&+3\cos\theta\sin\bar{K}_1\cos(\bar{K}_1+\phi_1-\beta)]\\&+\sin^2K_0+9\cos^2\theta\sin^2\bar{K}_1\\&+6\cos\theta\sin K_0\sin\bar{K}_1\cos(K_0-\bar{K}_1-\phi_1),\end{aligned}$$

with

$$\beta=\eta\ln\frac{2}{1-\cos\theta}.$$

By the neglect of terms of the order η^3, this may be written in the approximate form:

$$\begin{aligned}k^2\sigma(\theta)=&\tfrac{1}{4}\eta^2\csc^4\tfrac{1}{2}\theta-\eta\csc^2\tfrac{1}{2}\theta[\sin K_0\cos K_0\\&+\beta\sin^2K_0+3\sin\bar{K}_1\cos\bar{K}_1\\&-3\sin^2\bar{K}_1(2\eta-\beta)]+6\eta\sin\bar{K}_1\\&\times\cos\bar{K}_1-6\eta(2\eta-\beta)\sin^2\bar{K}_1\\&+\sin^2K_0+9\cos^2\theta\sin^2\bar{K}_1\\&+6\cos\theta\sin K_0\sin\bar{K}_1[(1-2\eta^2)\\&\times\cos(K_0-\bar{K}_1)+2\eta\sin(K_0-\bar{K}_1)].\end{aligned}\tag{6}$$

In order to effect the best comparison of Eq. (6) with the experimental results we use the data (Fig. 1) for those angles θ_1 and θ_2 for which the *D*-wave vanishes, *viz.*,

$$\theta_1\equiv\cos^{-1}(3^{-\frac{1}{2}})=54.7°,\quad \theta_2\equiv\cos^{-1}(-3^{-\frac{1}{2}})=125.3°.$$

Then

$$\begin{aligned}k^2\sigma(\theta_{1,2})=&\tfrac{1}{4}\eta^2(12\pm6\sqrt{3})-\eta(3\pm\sqrt{3})\{\sin K_0\cos K_0\\&+\beta_{1,2}\sin^2K_0+3\sin\bar{K}_1\cos\bar{K}_1\\&-3(2\eta-\beta_{1,2})\sin^2\bar{K}_1\}+6\eta\sin\bar{K}_1\cos\bar{K}_1\\&-6\eta\sin^2\bar{K}_1(2\eta-\beta_{1,2})+\sin^2K_0\\&+3\sin^2\bar{K}_1\pm2\sqrt{3}\sin K_0\sin K_1[(1-2\eta^2)\\&\times\cos(K_0-K_1)+2\eta\sin(K_0-K_1)],\end{aligned}$$

the upper signs going with the subscripts 1 and the lower signs with the subscripts 2. It is convenient to take the sum and difference of $k^2\sigma(\theta)$ at θ_1 and θ_2. It is convenient also to approximate β_1 and β_2 in terms that neglect $\eta^2/10$ compared with unity, *viz.*,

$$\begin{aligned}\tfrac{1}{2}(\beta_1+\beta_2)&=0.90\eta\simeq\eta,\\\tfrac{1}{2}(\beta_1-\beta_2)&=0.66\eta\simeq3^{-\frac{1}{2}}\eta.\end{aligned}\tag{7}$$

Reducing the expression for

$$\Sigma\equiv k^2[\sigma(\theta_1)+\sigma(\theta_2)]$$

in a manner similar to that used previously for $k^2\sigma(90°)$, we find

$$\begin{aligned}&3\cos(2\bar{K}_1-\eta)+\cos(2K_0-3\eta)\\&\qquad=(1-\tfrac{1}{2}\eta^2)(4-\Sigma).\end{aligned}\tag{8}$$

An alternative method of determining $\bar{K}_1$ would be to calculate the formula for the difference

$$\Delta\equiv k^2[\sigma(\theta_1)-\sigma(\theta_2)],$$

which gives, to the same approximation, i.e., using (7),

$$\begin{aligned}3^{-\frac{1}{2}}\Delta=&[1+\tfrac{1}{2}\eta^2-\cos(2K_0-3\eta)]\\&\times[1+\tfrac{1}{2}\eta^2-\cos(2\bar{K}_1-\eta)]\\&+\sin(2K_0-3\eta)\sin(2\bar{K}_1-\eta).\end{aligned}\tag{9}$$

However, as anticipated in the introduction, there are no single values of $\bar{K}_1$ that satisfy (8) and (9) simultaneously, because there is a pronounced spin-dependence in the *P*-wave shifts.

To adapt the formulas just derived for Σ and Δ to the case of spin-dependence (in *P*-waves) we have to introduce a quartet *P*-wave shift, K_1, and a doublet *P*-wave shift, k_1, and replace $3\cos(2\bar{K}_1-\eta)$ by $2\cos(2K_1-\eta)+\cos(2k_1-\eta)$ and replace $3\sin(2\bar{K}_1-\eta)$ by $2\sin(2K_1-\eta)+\sin(2k_1-\eta)$. We may eliminate the cosine terms in Δ also, in terms of Σ, and arrive at the convenient relations for K_1 and k_1:

$$\begin{aligned}&2\cos(2K_1-\eta)+\cos(2k_1-\eta)\\&\quad=(1-\tfrac{1}{2}\eta^2)(4-\Sigma)-\cos(2K_0-3\eta)\equiv s,\\&2\sin(2K_1-\eta)+\sin(2k_1-\eta)\\&\quad=\{3^{\frac{1}{2}}\Delta-3[1+\tfrac{1}{2}\eta^2-\cos(2K_0-3\eta)]\\&\qquad\times[1+\tfrac{1}{2}\eta^2-(s/3)]\}\csc(2K_0-3\eta)\\&\qquad\equiv3d\csc(2K_0-3\eta).\end{aligned}\tag{10}$$

We now obtain the observed values of Σ and Δ from Fig. 1, use the previously determined values of K_0, and compute the quantities on the right-hand side of the two equations (10). These are then simultaneous equations for K_1 and k_1. Again, there will be two roots for each, but we choose that set of roots in which K_1 lies in the first quadrant as indicated by the *n-d* calculations. The results appear in Table II.

Comparing the values thus obtained with the *n-d* calculations, Fig. 2, we see that the ^4P-shift, K_1, is in general agreement with predictions for exchange forces but that the ^2P-shift is very different. Instead of remaining close to zero, the ^2P-shift grows rapidly negative. There is no clear indication of what this may mean, assuming the analysis is valid, in terms of the exchange character or of the non-central character of nuclear forces. This behavior, however, is so different from that of ordinary, central forces that it suggests very strongly that the nuclear forces are of an exchange nature.

III. EFFECT OF HIGHER ANGULAR MOMENTA

In Figs. 3, 4, 5, 6, and 7 are shown the departures of the experimentally determined cross sections (times k^2) from the calculations with formula (6), modified to take account of spin-dependence in the P collisions and using the values of K_0 from Table I and K_1, k_1 from Table II. By virtue of the method of estimating K_0, K_1, and k_1 these curves pass through zero at

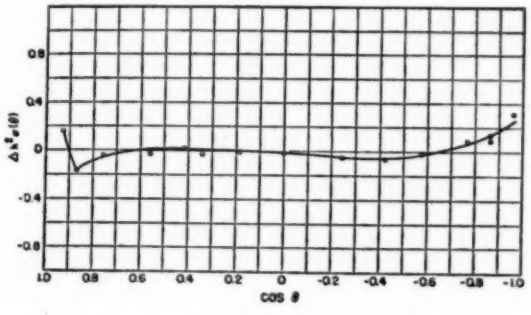

FIG. 3.

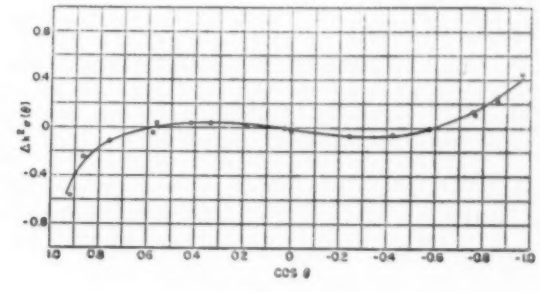

FIG. 4.

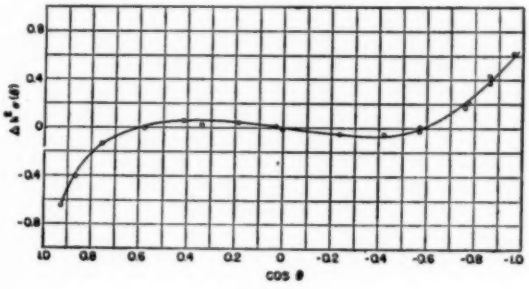

FIG. 5.

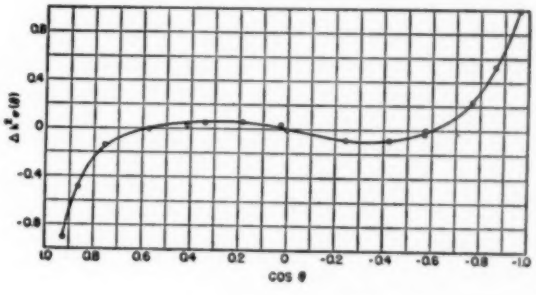

FIG. 6.

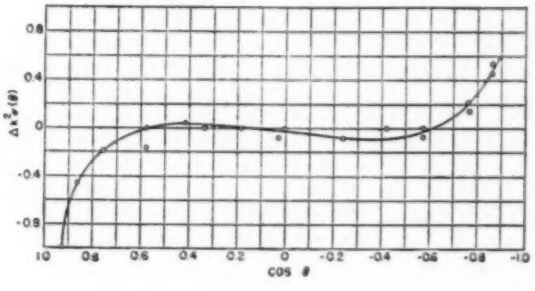

FIG. 7.

FIGS. 3–7. Deviations of experimental points (open circles) from angular distribution predicted on basis of *S*-wave and *P*-wave shifts alone. (Fig. 3, $E=1.51$ Mev; Fig. 4, $E=2.08$ Mev; Fig. 5, $E=2.52$ Mev; Fig. 6, $E=3.00$ Mev; Fig. 7, $E=3.49$ Mev.)

$\cos\theta=0.58, 0, -0.58$ (the agreement is not quite perfect for $E=3.49$ because the spread of the experimental points permitted a certain arbitrariness in selecting values for Σ and Δ). The curves in Figs. 3–7 are antisymmetrical about the origin, within the errors of experiment. This indicates that the departure contains very little S–D interference, and since the D-wave shifts, K_2 for the quartet and k_2 for the doublet, are expected to be small, we may deduce at once that

$$2K_2+k_2=0, \tag{11}$$

within the accuracy of the determinations. Condition (11) is based on the fact that the S–D interference would contribute to $k^2\sigma(\theta)$ a term (cf. Eq. (2))

$$\begin{aligned}5(3\cos^2\theta-1)\,&\sin K_0\{\tfrac{2}{3}\sin K_2\cos(K_0-K_2-\phi_2)\\&+\tfrac{1}{3}\sin k_2\cos(K_0-k_2-\phi_2)\}\\&\simeq\tfrac{5}{6}(3\cos^2\theta-1)\,\sin 2K_0(2K_2+k_2),\end{aligned}$$

and it simultaneously eliminates the D-Coulomb interference. It follows that the departures represented in Figs. 3, 4, 5, 6, and 7 are probably almost pure D–P interference effects. Again, from Eq. (2), and allowing for spin-dependence, the P–D interference term is of the form

$$\begin{aligned}\Delta k^2\sigma(\theta)&=5\cos\theta(3\cos^2\theta-1)\\&\times[2\sin K_1\sin K_2\cos(K_1-K_2-\eta)\\&+\sin k_1\sin k_2\cos(k_1-k_2-\eta)]\\&\simeq 5\cos\theta(3\cos^2\theta-1)K_2(\sin 2K_1-\sin 2k_1),\end{aligned}\tag{12}$$

using relation (11).

We shall use the mean departures at $\cos\theta=-0.852$ and $\cos\theta=0.852$, at which angles $\cos\theta(3\cos^2\theta-1)=\mp 1$, and call the average absolute values $|\delta|$. The phase shift K_2 is then determined by the relation

$$K_2=-\frac{|\delta|}{5(\sin 2K_1-\sin 2k_1)}.$$

The results for K_2 and k_2 (from Eq. (11)) are shown in Table III.

It is self-evident that using the values of K_2 and k_2 determined in this way will reproduce the curves in Figs. 3, 4, 5, 6, and 7 reasonably well. This comparison will not be carried out in detail as it appears to be pushing the data farther than justifiable. If further refinement were attempted, one should next include the possibility that the quartet and doublet S-waves are not shifted by exactly the same amount. This would lead principally to an antisymmetric contribution through interference with the P-waves (since these are of opposite sign). A further antisymmetric term that becomes of increasing importance as the energy increases will be the S–F interference. Refined analysis would also detect symmetrical contributions such as the S–D interference, the D^2-terms and, finally, the possibility of spin-orbit coupling which gives waves that do not interfere with the other partial waves. Thus, the estimates of D-wave shifts presented in Table III characterize the limits of the experimental data in yielding to phase-shift analysis rather better than a final analysis of the phase shifts in the proton-deuteron scattering.

This paper is based on work performed at Los Alamos Scientific Laboratory of the University of California under Government Contract No. W-7405-eng-36, and the information contained therein will appear in Division V of the National Nuclear Energy Series (Manhattan Project Technical Section), as part of the contribution of the Los Alamos Laboratory.

ACKNOWLEDGMENTS

I should like to thank Dr. Rubby Sherr of the P Division at Los Alamos for access to the experimental results before publication, and Dr. Bengt Carlson for the assistance by his group in computing the angular distributions on which Figs. 3, 4, 5, 6, and 7 are based, and Mr. Louis Jacot for preparation of the figures. I am indebted also to Professor Edward Teller for many interesting discussions of the exchange effects in this scattering problem.

Proton-Gamma-Ray Coincidence Counting with Cyclotron Bombardment*

BRUCE B. BENSON**
*Sloane Physics Laboratory, Yale University,*** *New Haven, Connecticut*
(Received September 18, 1947)

A technique is given for studying associations between protons and gamma-rays emitted when a target is bombarded with particles from the cyclotron. A description is included of the theoretical considerations involved and of the apparatus developed. The results on the $Al^{27}(\alpha, p)Si^{30}$ reaction indicate that no gamma-rays accompany the end group of protons, while other groups exhibit coincidences. The coincidence rate increases with excitation energy. This may be due to cascade transitions giving more quanta, or to increased sensitivity for higher energy quanta. The fourth group observed with zero-degree bombardment is shown to be a composite of knock-on protons and protons from the reaction. A brief proton group study is included with Q values in essential agreement with previous work.

1. INTRODUCTION

ONE method of studying nuclear energy levels is the observation of proton groups from (α, p) and (d, p) reactions. These groups are usually ascribed to the formation of the residual nuclei in various energy states, the end group corresponding to the ground state. The nuclei which are excited then revert to the ground state with the emission of gamma-rays. If this interpretation and the energy levels derived from proton data are correct, coincidences should occur between gamma-rays and appropriate proton groups.

Because of the intrinsic difficulties involved, relatively little has been done on the gamma-radiation produced in such bombardment. Still fewer experiments have been carried out on coincidences between particles and gamma-rays emitted in transmutation reactions. Bothe and v. Baeyer[1] first observed proton-gamma-coincidences in the bombardment of boron by polonium alpha-particles. They found no genuine coincidences with the end group of protons, while the next group exhibited coincidences. Maier-Leibnitz,[2] using a paraffin "proton radiator" for the neutrons, found neutron-gamma-coincidences in the $Be^9(\alpha, n)C^{12}$ reaction. He and Bothe[3] also repeated the boron experiment. In these experiments natural alpha-particle sources were used.

The purpose of the present work has been to develop a technique by which proton-gamma-coincidence work could be done with cyclotron bombardment. The instrumentation problems for coincidence work with cyclotron bombardment are considerable, primarily because of the background radiation from the machine and because of the limitations on possible solid angles for the counters with respect to the target. The apparatus developed to meet these difficulties is described below with the first results obtained in the study of the $Al^{27}(\alpha, p)Si^{30}$ reaction. This reaction was chosen for developing the technique for two reasons. First, aluminum is a single stable isotope for which the proton groups from alpha-particle bombardment are well known. Second, the background radiation problem is smaller with alpha-particles than with deuterons. Once established, the method may be applied to other reactions.

The general procedure employed consisted of bombarding a thin target with particles from the cyclotron. Proportional counters, of appropriate designs, were used to record emitted protons and gamma-rays, respectively. Pulses from each counter were fed to a preamplifier and then to a high gain video amplifier. The amplified pulses were mixed in a coincidence circuit of special design, and coincidence pulses were recorded on a mechanical recorder.

Proportional counters were chosen for three reasons. First, since in the proportional counter

* Part of a dissertation presented to the Graduate School of Yale University, in partial fulfillment of the requirements for the degree of Doctor of Philosophy.
** Now at Amherst College, Amherst, Massachusetts.
*** Assisted by the Office of Naval Research under contract N6ori-44.
[1] H. J. v. Baeyer, Zeits. f. Physik **95**, 417 (1935).
[2] H. Maier-Leibnitz, Zeits. f. Physik **101**, 478 (1936).
[3] W. Bothe and H. Maier-Leibnitz, Zeits. f. Physik **107**, 513 (1937).

the pulses depend primarily upon the collection of electrons, the time lag uncertainty between the formation of the primary ionization and the occurrence of the counter pulse is smaller than with Geiger-Müller counters. This makes possible the use of fast electronic circuits without loss of genuine coincidences. Second, the proportional counter and its preamplifier recover very rapidly. Third, with a proportional counter for protons it is possible to set the counting level so that only those protons near the ends of their ranges will produce sufficient ionization to record in the counting circuits and Bragg "peaking" results. This allows one to examine each group separately in coincidence counting.

2. NUMERICAL CONSIDERATIONS

Most of the basic ideas involved in coincidence counting may be found in v. Baeyer's original paper.[1] Dunworth[4] has treated the method in greater detail with special reference to radioactive decay schemes. Because of the occurrence of gamma-rays from the several competing reactions in target bombardment, and because peaking of the proton counter was employed, the equations which apply in the present case are somewhat different and more complicated.

Let N_p and N_γ be the counting rates per second in the two counters, C_g and C_c the genuine and chance coincidence rates per second, e_p and e_γ the intrinsic counter efficiencies, Ω_p and Ω_γ the counter-solid angles expressed as fractions of the total sphere about the target, B the beam in particles per second, k_p, k_n, and k_s the yields per bombarding particle for the production of protons, neutrons, and inelastically scattered alpha-particles. Then

$$N_p = \rho_i k_p B e_p \Omega_p, \tag{1}$$

where ρ_i represents the fraction of the total number of protons produced that occur in the ith proton group. This factor appears because of the use of peaking. With this type of operation cosmic rays, gamma-rays, and beta-particles do not record in the proton counter. The background arising from neutrons in the proton counter is negligible when an alpha-particle beam is used.

Representing by W_p the *average* number of gamma-rays emitted per proton (protons of all energies are considered here), and by W_n and W_s the average number of gamma-rays emitted per neutron and per inelastically scattered alpha-particle, respectively:

$$N_\gamma = W_p k_p B \bar{e}_{\gamma p} \Omega_\gamma + W_n k_n B \bar{e}_{\gamma n} \Omega_\gamma + W_s k_s B \bar{e}_{\gamma s} \Omega_\gamma + \bar{e}_{\gamma b} F(B), \tag{2}$$

where $F(B)$ is the number of gamma-rays or cosmic rays incident upon the gamma-counter per second from sources other than the target. It is obviously some increasing function of B. Because the gamma-counter efficiency is a function of the gamma-ray energy, the e_γ's in Eq. (2) must be interpreted as the weighted mean values of the efficiencies for *all* the different gamma-rays associated, respectively, with each type of particle. The additional subscript on the $\bar{e}$'s refers to the origin of the radiation, proton, neutron, etc. This expression obviously has too many unknowns to be of much value in itself. Its importance, however, lies in enabling one to write down the approximate Eq. (5).

If we assume that no *angular* correlation exists between associated protons and gamma-rays, the number of genuine proton-gamma-coincidences per second (corresponding to the ith proton group) is

$$C_g = (\rho_i k_p B e_p \Omega_p)\Omega_\gamma \sum_{j=1}^{n} w_{ij} e_{\gamma j} = N_p \Omega_\gamma \sum_{j=1}^{n} w_{ij} e_{\gamma j}, \tag{3}$$

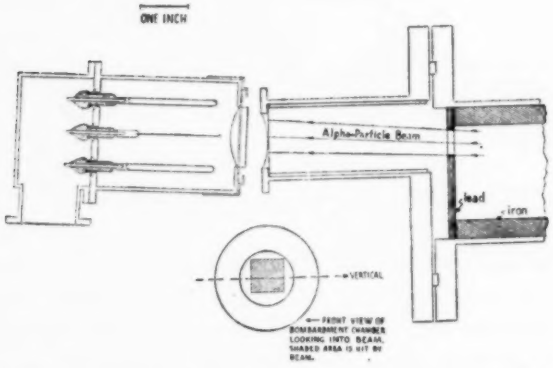

FIG. 1. Top view of the geometry for proton counting, showing, from right to left, the extension tube from the cyclotron, the rectangular limiting slit, the bombardment chamber and target, and the proton counter with its foil holder. The inset shows the target area hit by the beam.

[4] J. V. Dunworth, Rev. Sci. Inst. **11**, 167 (1940).

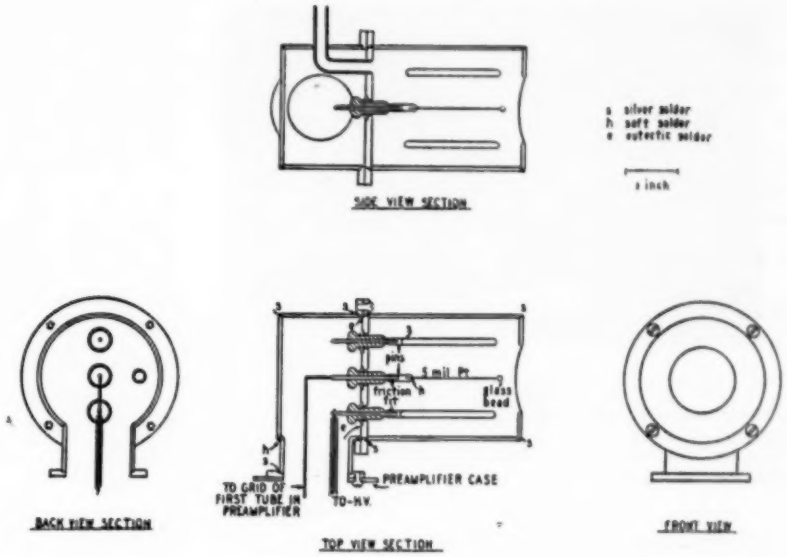

FIG. 2. Drawing of the details of the proton counter designed for large solid angle. The counter was connected directly to the preamplifier case.

where w_{ij} is the average number of gamma-rays of energy $h\nu_j$ associated with each proton in group i. Since "branching" may occur, w_{ij} may have any positive value, including fractional ones. The corresponding efficiency of the counting system for each gamma-ray is $e_{\gamma j}$. If branching does not occur, Eq. (3) becomes

$$C_g = N_p \Omega_\gamma w_i \bar{e}_\gamma, \tag{3a}$$

where w_i is the number of gamma-rays associated with each proton of the ith group, and $\bar{e}_\gamma$ is the average efficiency for the gamma-rays associated with these protons. For the number of chance coincidences per second we have

$$C_c = 2TN_pN_\gamma, \tag{4}$$

where T is the resolving time of the counting circuit. Substituting the expressions for N_p and N_γ from (1) and (2) into (4), and dividing the resulting expression by (3a), we obtain

$$\frac{C_c}{C_g} \cong \frac{2TB}{w_i}[W_pk_p + W_nk_n + W_sk_s] + \frac{2TF(B)}{w_i\Omega_\gamma}. \tag{5}$$

The simplest case has been taken, with $\bar{e}_\gamma = \bar{e}_{\gamma p} = \bar{e}_{\gamma n} = \bar{e}_{\gamma s} = \bar{e}_{\gamma b}$.

Equation (5) and either (3) or (3a) are very useful qualitatively in designing the apparatus. In order to make C_g large, while keeping C_c/C_g small, it is desirable to have Ω_p, Ω_γ, e_p, and e_γ as large as possible. On the other hand, T should be as small as possible, and the smallest beam intensity B consistent with yield is preferable. This minimizes not only the first term in (5) but also the second, since $F(B)$ is an increasing function of B. Good gamma-counter shielding is imperative to keep $F(B)$ small.

In a given experiment the total coincidence rate with the ith group of protons is measured, as well as N_p and N_γ. Since the proton counter is insensitive to cosmic rays, beta-particles, and gamma-rays, one needs only to calculate C_c from (4) and subtract this from the total coincidence rate to obtain C_g. Taking the ratio $C_g/(N_p\Omega_\gamma)$, one obtains a value for $\sum_j w_{ij}e_{\gamma j}$. This coupled with a knowledge of the proton group energy spacing, and the gamma-counter efficiency *vs.* $h\nu$ curve, enables one to clarify the level scheme.

3. EXPERIMENTAL APPARATUS

The apparatus designed and constructed to fulfill as well as possible the above criteria is described below. A zero-degree bombardment chamber, Figs. 1 and 3, was chosen because of the large proton solid angle possible. The circular brass flange, into which was silver soldered the cylindrical brass tube, was bolted through a rubber-gasket vacuum seal to the tube leading to the cyclotron "can." Insulating bushings were used for the bolts so that the beam intensity could be measured by simply clipping a galvanometer lead to the chamber flange. The

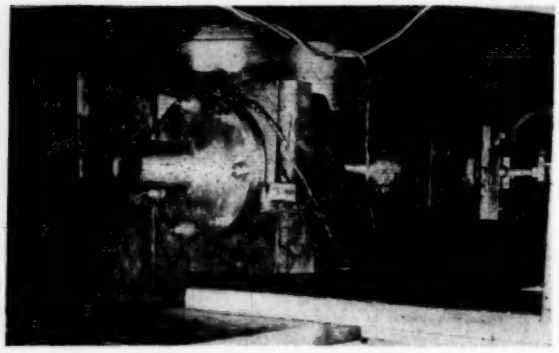

FIG. 3. Photograph showing the cyclotron magnet, with the extension tube leading out to the bombardment chamber. Part of the lead gamma-counter shielding is shown. The target was immediately behind the aluminum proton "window."

bombardment-chamber tube was made as small as possible to allow a large Ω_γ. An aluminum-foil (8.36-cm air—corrected for stretching under vacuum) proton window was waxed to the end of the chamber.

Immediately inside the window was placed a thin aluminum foil (1.01-cm air), backed by a gold foil of 8.60-cm air (stopping power taken as 5.20), which stopped the bombarding alpha-particles. These foils were carefully cleaned and were held in good metallic contact with the chamber by the inner friction tube shown in Fig. 1. The total bombardment chamber wall thickness through which gamma-rays had to pass was one-eighth inch. This will be reduced in future work to minimize absorption of weak gamma-rays. The beam passed through a lead plate with a rectangular hole in it, which limited the beam to hitting the target only. The iron tube acted as a partial magnetic shield in getting the beam away from the machine.

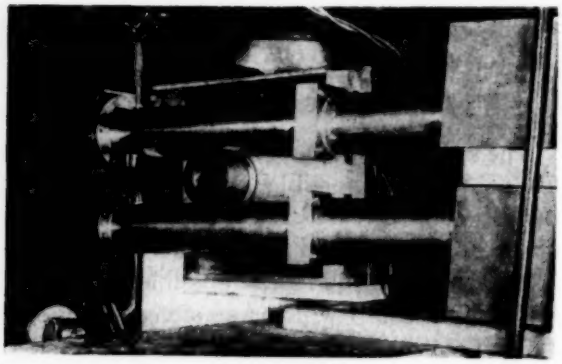

FIG. 4. Photograph of the gamma-counters in place above and below the bombardment chamber. A lead plate, for further shielding, was slipped over the nose of the bombardment chamber. The tube between each counter and its preamplifier was necessary to keep the latter out of the fringing field.

The proton proportional counter, Figs. 1 and 2, was especially designed to give a large proton solid angle. The wire was 5-mil platinum with the unattached end melted into a tiny platinum ball and then coated with glass. This made the counter effective over nearly its entire cathode diameter. The large window was a 4.54-cm air (corrected for stretching) aluminum foil. The L-shaped shield, connecting the counter to the preamplifier case, was necessary because of space limitations near the cyclotron magnet yoke. The axis of the counter was parallel to the center of the beam.

Pure argon at 20 cm of Hg was used, with cathode potentials ranging from 740 to 1000 volts. The depth (beyond the window) to which protons had to penetrate in order to count (biases set for peaking) was calculated from data taken with ThC′ alpha-particles to be approximately (0.6 ± 0.2) cm air. No attempt at great accuracy was made because of the poor proton-counting geometry necessary for the coincidence work. A foil holder was slipped over the nose of the counter so that carefully calibrated aluminum foils (1.518 mg/cm^2 equivalent to one cm air) could be placed between target and counter. The total basic absorption for the protons emitted at zero degrees was 25.1 cm air, subject, of course, to variation in stopping power with proton energy.

Because of the large collection angle for protons (the effective solid angle for coincidence counting was approximately 0.07) with the corresponding variation in both proton energies and basic absorption, extrapolated beam energies were used. Even then, how they should be extrapolated under the above conditions led to some uncertainty in measuring ranges. Clearly, this apparatus, designed for coincidence work, was not expected to give precision Q values. Those given below were obtained as a necessary by-product of the coincidence work.

The gamma-ray counter has been described in an earlier publication.[5] A photograph of it with

[5] B. B. Benson, Rev. Sci. Inst. **17**, 533 (1946).

its preamplifier is included in Fig. 4. The counter was long and large for large gamma-solid angle. Since the preamplifier did not operate properly in the fringing field of the cyclotron magnet coils, it was found necessary to build the intermediate cylindrical shield to bring the preamplifier further away from the magnet, where it operated satisfactorily. Pure argon at 50 cm of Hg, and a cathode potential of 1600 volts were used for the work reported here. This corresponded to operation in the transition region between true proportional counting and Geiger counting, and gave a reasonably high efficiency while still retaining the desirable features of a proportional counter. The average gamma-solid angle was approximately 0.08.

As shown in Figs. 3 and 4, between four and five inches of lead shielding was placed between all parts of the cyclotron acceleration chamber and the gamma-counter. This reduced the cyclotron gamma-background to the point of being negligible with an alpha-particle beam. The second gamma-counter, shown in Fig. 4, was built originally to increase the gamma-ray solid angle but was found more useful as a control unit, with the voltage turned down, to eliminate line disturbance which got past the voltage regulators. Any coincidence counts which occurred simultaneously with one from this counter were thrown out. Very few of these spurious counts occurred, however.

The circuit diagram for the counter preamplifiers[6] is given in Fig. 5. The variable capacitive feedback from the plate of the second tube to the control grid of the first tube made possible the neutralization of the capacity of the input part of the circuit, including the counter and its lead, almost to the point where self-oscillation set in. In this way very narrow pulses with a steep rate of rise were possible. The signal-to-noise ratio was still ample. The fourth tube acted as a cathode-follower impedance transformer, transferring pulses from a high impedance level to a low one, for transmission through 75-ohm terminated cable to an attenuator box on the video amplifier. This prevented r-f pick-up, as well as minimized pulse attenuation in going from the cyclotron room, where the preamplifiers were, to the control room, where the remainder of the circuits were located for easy adjustment while running. The video amplifiers and regulated power supplies have been reported previously.[5] The gain of the amplifiers was approximately 80 db, with a band width of four megacycles per second. The amplified counter pulses, as determined with a synchroscope, were about one microsecond in half-width and had a rate of rise of less than 10^{-7} sec.

The circuit diagram for the coincidence circuit is shown in Fig. 6. Each of the two channels contained, in order, a buffer stage, a diode discriminator with variable bias, and two stages of amplification, after which the pulses were fed into a blocking oscillator pulse-sharpening stage. The special feature of this arrangement was that a blocking oscillator pulse of constant shape and size was initiated by the *first* part of the leading edge of the amplified pulse coming in. Neglecting the delay of perhaps 10^{-7} sec., which was the same in both amplifier channels, the position in time of the front edge of the blocking oscillator pulse was essentially coincident with the first arrival of electrons on the counter wire. Therefore, since electron transit times are of the order of only 10^{-8} sec., the variation in the time correlation between the formation of the primary ionization and the initiation of the blocking-oscillator pulse was much less than the rate of rise, which was only 10^{-7} sec. Clearly, it was desirable to set the discriminator biases as near "noise" as possible. The resolving time was determined primarily by the width (about 0.3μ sec.) of the

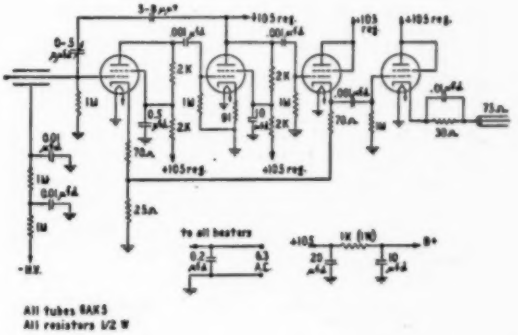

FIG. 5. 105-volt capacity-neutralized preamplifier for No. 2 γ-counter and for proton counter. The variable capacitive feedback from the plate of the second tube to the grid of the first made it possible to neutralize the input capacity of the system and thus attain a very rapid rate of rise.

[6] H. L. Schultz, Phys. Rev. 69, 689 (1946).

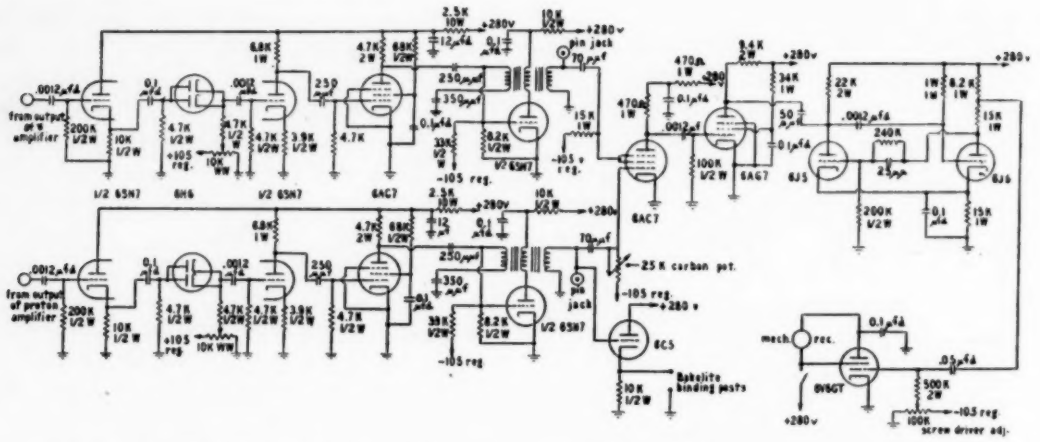

FIG. 6. Circuit diagram for the coincidence circuit, with a pulse-sharpening blocking-oscillator stage in each channel. The resolving time was 5×10^{-7} second.

blocking-oscillator pulses. This agreed with the value for T of approximately 5×10^{-7} sec. determined from Eq. (4).

The mixer tube was a 6AC7 pentode, with the grids biased below cut-off. A multivibrator output stage was used, with a 6V6 tube driving the recorder. Before the coincidence runs the pin jack on the output of the gamma-channel blocking oscillator was used with a counting rate meter to calibrate the gamma-counter rate as a function of beam intensity. During coincidence runs the protons were recorded by connecting a modified Higinbotham scaling circuit to the output of the buffer tube connected to the proton blocking oscillator. This prevented any possible interaction with the coincidence circuit proper because of loading of the blocking oscillator. The scaling circuit actuated a mechanical recorder.

The amplifier of the second gamma-counter, used as a control only, was connected separately to its own recording circuit.

TABLE I. Summary of the results of the proton counting on $Al^{27}(\alpha, p)Si^{30}$, with the Q values of Duncanson and Miller,[8] Haxel,[9] and Meerhaut[10] included for comparison.

Group	Extrapolated range (cm air)	Proton energy	Q-value (Mev)	Si^{30} excitation (Mev)	Q-values (Mev) Duncanson and Miller	Haxel	Meerhaut
1	101.6	9.34	2.22	0	2.26	2.3	2.25
2	60.8	6.98	−0.06	2.28	−0.02	0.0	+0.01
3	40.8	5.55	−1.44	3.66	−1.32	−1.1	−1.15
4	25–30	4.2–4.65	−2.63 to −2.20	about 4.6	−2.49	−2.6	—

4. DATA ON THE REACTION $Al^{27}(\alpha, p)Si^{30}$

1. The proton groups from this reaction have been studied by many workers. The work prior to 1937 accepted by Livingston and Bethe[7] as being the most authoritative is that of Duncanson and Miller,[8] and of Haxel.[9] Meerhaut[10] found essential agreement with them in 1940. Since all the previous studies were done with natural alpha-particles, the following data, obtained primarily as an aid in orientation in the coincidence work, are of some interest in themselves, despite the poor geometry necessary.

Figure 7 is a plot of the proton-yield *vs.* proton-absorption data. The proton counter was set for the best possible peaking. The "unit beam" was approximately 2.5×10^{-3} microampere of alpha-particles, and one-minute counts were taken. To obtain the actual number of counts per minute multiply ordinates by 0.7. The small dip in the peak of the second group is interesting in that it appeared in all of the single runs whose composite is shown.

Two auxiliary experiments were carried out on the fourth group, since both the fourth group observed by Duncanson and Miller[8] with right-angle bombardment and any knock-on protons from hydrogenous contamination were to be

[7] M. S. Livingston and H. A. Bethe, Rev. Mod. Phys. **9**, 301 (1937).
[8] W. E. Duncanson and H. Miller, Proc. Roy. Soc. **146**, 396 (1934).
[9] O. Haxel, Zeits. f. Physik **83**, 323 (1933); **88**, 346 (1934); **90**, 373 (1934).
[10] O. Meerhaut, Zeits. f. Physik **115**, 77 (1940).

expected here. A brief run was taken with the aluminum target removed, the beam hitting the gold backing. A proton yield was observed at an absorption corresponding to the fourth group and of the same order of yield. Another run was taken with a thin layer of vacuum grease smeared on the gold backing. A proton yield at the same absorption, but of approximately 100 times greater yield, was observed. The group consisted, therefore, at least largely of knock-on protons, although the coincidence work showed that some protons were truly associated with the aluminum reaction.

In Table I the extrapolated (and corrected) proton ranges, energies, and corresponding Q values from the present work are given, with the Si^{30} excitation levels derived therefrom. An extrapolated alpha-particle beam energy of 7.3 Mev was used. In addition, the Q values of Duncanson and Miller, Haxel, and Meerhaut are included.

II. In the coincidence work the voltage on the proton counter was set as high as possible (for high efficiency), subject to being somewhat below where beta-particles would record. The proton-yield curve with the counting system set as for coincidence counting is shown in Fig. 8. It should be noted that the groups were separated, a fact which is important in the interpretation below.

The method employed in the coincidence studies was to set the proton absorption at each of the values indicated on Fig. 8 by the abscissae of the five vertical lines shown, i.e., 25-, 33.8-, 50.6-, 78.0-, and 89.7-cm air, respectively. The proton absorption was also set at "infinity" by inserting a $\frac{1}{16}$-in. thick copper plate to stop all protons. This was a second control to check that the circuits were operating properly. At each of the absorptions the number of proton-gamma-coincidences per 1600 recorded protons was measured. The runs were taken in a random fashion so far as the value of the absorption was concerned, with an average of approximately 35–40 runs at each absorption. This method was chosen for three reasons: (1) Any slight fluctuations in counter efficiencies or cyclotron conditions canceled out. (2) The number of chance coincidences at each absorption was approximately the same, since although the proton counting rates at each absorption were different, those with low rates were counted on for longer times. (3) The number of genuine coincidences per proton allowed not only information on the gamma-counter efficiency to be found, but also

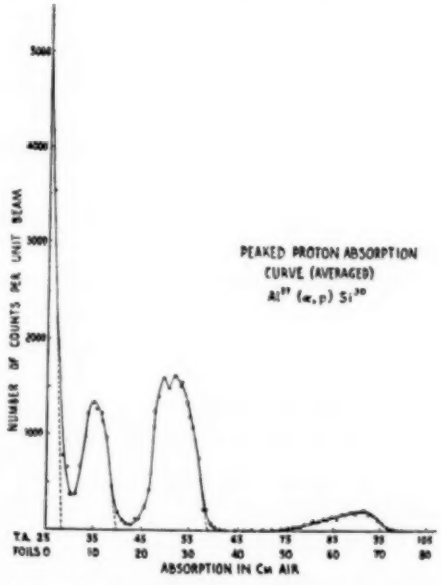

FIG. 7. Graph of the composite proton yield *vs.* absorption data, with biases set for the best possible peaking. The small dip in the second group occurred in each of the separate runs.

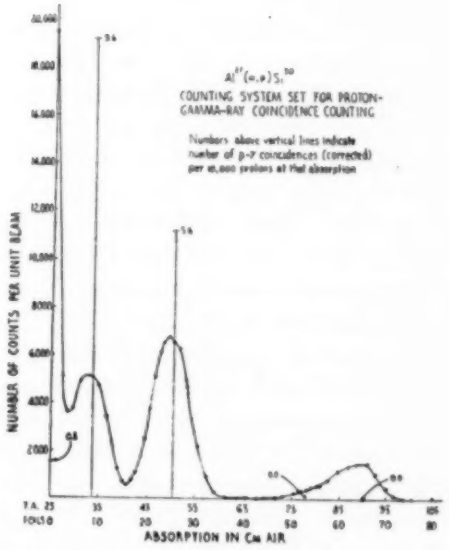

FIG. 8. Graph of the proton yield *vs.* absorption data, with biases set for coincidence counting. Compare the yields of Figs. 7 and 8. The numbers above the vertical lines indicate the number of genuine proton-gamma-coincidences per 10^4 protons at each of the five values of absorption.

TABLE II. Summary of the results of the proton-gamma-coincidence counting on the reaction $Al^{27}(\alpha, p)Si^{30}$.

Group	Absorption (cm air)	No. runs	No. protons	Approx. total time (min)	No. coinc. C_{total}	Expected chance coinc. C_c	Genuine coinc. C_g	Genuine coinc. per 10^4 proton	Probable error in $C_g/10^4$
1	89.7	32	51,200	64	3	3	0	0	—
1(a)	78.0	7	11,200	35	0	0.7	0	0	—
2	50.6	37	59,200	15	37	4	33	5.6	±0.7
3	33.8	39	62,400	20	64	4	60	9.6	±0.85
4	25.0	43	68,800	8	10	4.5	5.5	0.8	±0.3
∞	∞	16	—	32	0	—	0	—	—

yielded information concerning gamma-ray transitions. The beam intensity was recorded each time (so that a knowledge of an average N_γ was possible) as well as the length of time for each run. All circuits were allowed to come to equilibrium before use. Table II is a summary of the results of the coincidence experiment on the aluminum reaction. The approximate probable errors were calculated by taking

$$\frac{(C_T)^{\frac{1}{2}}}{C_g}\times\frac{C_g}{10^4}\times 0.67.$$

5. DISCUSSION AND INTERPRETATION

It should be noted that in approximately 32 minutes of running (interspersed among the other runs), with an infinite absorption for the protons, no "coincidence" pulses occurred, indicating the circuits were operating satisfactorily. The number of expected chance coincidences was calculated in each case from Eq. (4), using a resolving time T of 5×10^{-7} sec. and an average N_γ equal to 65 per second (determined from the gamma-rate *vs.* beam calibration). Instead of considering N_p as a counting *rate*, the *total number* of protons recorded was used, giving the number of chance coincidences directly.

The number of genuine gamma-ray coincidences observed with 51,200 protons in group one was zero, indicating that no gamma-rays are associated with the end group of protons. Because, however, of the much lower efficiency of a copper cathode gamma-counter for very low energy radiation,[11] one cannot exclude absolutely the possibility of a weak gamma-ray being associated with the end group. In addition to the much lower efficiency any weak radiation would have suffered greater absorption in the wall of the bombardment chamber and in the counter case. From the coincidence work alone, therefore, the possibility of the association of a weak gamma-ray with the end group cannot be ruled out, but it can be stated that (except for the existence of a long-lived metastable state) the Si^{30} level corresponding to the end group cannot be more than a few tenths of a Mev above ground, for the occurrence of an energetic gamma-ray or several low energy ones in cascade would show up clearly. One means of clearing up this uncertainty would be to use a gamma-counter with a lead cathode, since its efficiency would not drop so greatly for low energies.

As further evidence, the high pressure ionization chamber work of Savel[12] in 1934 may be cited. He found that two components existed (one of 0.55 Mev and one of 2.1 Mev) in the gamma-radiation excited by the bombardment of aluminum by polonium alpha-particles. The former was attributed to annihilation and the latter to the (α, p) reaction.

Since the coincidence work excludes the possibility of any gamma-rays of greater than a few tenths of a Mev being associated with the end group, while other work indicates that no radiation of this order of energy is present (except for pair annihilation radiation), the conclusion to be drawn is that the end group leaves the Si^{30} in its ground state, and mass values calculated on this basis are justifiable.

The second group at 50.6-cm air gave 5.6 genuine coincidences per 10^4 protons. For lack of evidence concerning any excitation level in Si^{30} between 0 and 2.28 Mev, it is reasonable to assume that only one gamma-ray accompanies each proton. In this case Eq. (3) reduces to $C_g/N_p=\Omega_\gamma e_\gamma$, and putting in $C_g/N_p=5.6\times10^{-4}$ and $\Omega_\gamma=0.08$, we obtain $e_\gamma=7\times10^{-3}$ for $h\nu=2.28$ Mev. The intrinsic efficiency of the gamma-counter at 1600 volts is therefore approximately half that of a Geiger-Müller counter. With higher voltages the efficiency increases, being about 8.5×10^{-3} at 1650 volts.

For the third group (assuming no intermediate levels between 2.28 and 3.66 Mev) three possi-

[11] H. Bradt, P. C. Gugelot, O. Huber, H. Medicus, P. Preiswerk, and P. Scherrer, Helv. Phys. Acta 19, 77 (1946).

[12] P. Savel, Comptes Rendus 198, 368 (1934).

bilities exist: (1) A direct transition to ground with one gamma-ray of 3.66 Mev for each proton; (2) a cascade transition with one 1.38- and one 2.28-Mev gamma-ray accompanying each proton; (3) branching, with both types of transitions occurring. The expected number of genuine coincidences per 10^4 protons for the first two cases, assuming that no angular correlation exists and that the proportional gamma-counter followed the efficiency curve of a Geiger-Müller counter, can be calculated.[11] With $e_{2.28}$ equal to 7×10^{-3}, we get from simple proportions that $e_{1.38}=4.1\times10^{-3}$ and $e_{3.66}=9\times10^{-3}$. The latter is obtained by extrapolating the brass curve.

Therefore, in case 1, $C_g/N_p=0.08\times9\times10^{-3}=7.2$ coincidences per 10^4 protons. In case 2, $C_g/N_p=0.08\times(7\times10^{-3}+4.1\times10^{-3})=8.9$ coincidences per 10^4 protons. The number of coincidences per 10^4 protons actually observed with the third group was 9.6 ± 0.85. The calculated value from case 1 thus lies outside the probable range of fluctuation, while that for case 2 lies within it. This may be taken as indication that the cascade transition is more likely than the direct transition to ground. Since this interpretation is based upon the assumptions above, and depends, further, upon how the efficiency curve is extrapolated out to 3.66 Mev, the efficiency curve for the proportional gamma-counter must be determined experimentally before a conclusive statement can be made.

Finally, the value of 0.8 coincidence per 10^4 protons for the fourth group indicates that while most of the protons in this group are not associated with gamma-rays and are therefore knock-on protons, it is still possible to detect the presence of those protons associated with the (α, p) reaction. The brief data at 78.0-cm air are insufficient to make any quantitative statement, but the indication is that the first group is a single one.

6. SUMMARY

The first results of the application of the coincidence method to the study of the $Al^{27}(\alpha, p)Si^{30}$ reaction show that to a high degree of probability the end group of protons leaves the Si^{30} in its ground state. The coincidences observed with the second group have been used to calculate the efficiency of the gamma-counter for 2.28-Mev radiation. Preliminary results indicate that a cascade gamma-ray transition from the second excited state in Si^{30} may be more probable than the direct one to ground. The presence of protons associated with the third excited state has been demonstrated, despite the high background of knock-on protons.

In considering further applications of the method to the study of nuclear transmutations, the following are possibilities: By producing the same residual nucleus in different ways, it is not only possible to see if the same levels occur in all cases, but also whether the same gamma-ray transitions occur. In this way information on any selection rules which may exist may be obtained. Further information may be obtained from the measurement of proton-gamma-coincidences per proton as a function of gamma-ray absorption, as well as from gamma-gamma-coincidence studies. The method should be applicable to the detection or examination of close nuclear "doublets" by measuring proton-gamma-coincidences per proton as a function of proton absorption. With variable delay techniques metastable levels may be looked for and studied. Reactions may be examined for angular correlations between protons and gamma-rays. The technique can be very useful in the interpretation of the proton groups obtained in the bombardment of multiple isotope elements.

7. ACKNOWLEDGMENTS

The author wishes to express his appreciation to Professor Ernest C. Pollard for his enthusiastic direction of this research. The designing of all the electronic circuits was done by Professor Howard L. Schultz. The author is also grateful for several valuable discussions on coincidence counting with Professor Schultz and Professor E. R. Beringer. Mr. Harry A. Schultz gave much technical advice and assistance.

The Limits of Beta-Stability

TRUMAN P. KOHMAN
Institute for Nuclear Studies, University of Chicago, Chicago, Illinois
(Received August 6, 1947)

The beta-stable nuclides are plotted in such a manner as to indicate the charge of maximum stability for odd mass numbers and the upper and lower limits of beta-stability for even mass and charge numbers. Curves representing these three quantities are drawn in following considerations based on the liquid-drop nuclear model, by which their positions can be determined fairly closely. The spacing between the curves is related to the parameters of the empirical mass equation of Bohr and Wheeler. The diagram is used to indicate the possibility of undetected natural radioactivities, and to suggest possible undiscovered or "missing" beta-stable nuclides.

I. INTRODUCTION: THE LIQUID-DROP NUCLEAR MODEL

MANY of the general properties of the atomic nucleus can be explained by the liquid-drop model proposed by Gamow[1] and developed by Heisenberg,[2] Wick,[3] Gamow,[4] Weizsäcker,[5] Bethe and Bacher,[6] Bohr and Kalckar,[7] Bohr and Wheeler,[8] and others. According to this model, which is applicable when the number of nucleons is sufficiently large ($\gtrsim$30), nuclear binding energies and atomic masses are smoothly varying functions of the numbers of constituent protons and neutrons. By treating the various nuclear forces in a statistical manner and estimating their magnitudes empirically, it is possible to reproduce the general trends of binding energies and masses. Superposed on these general trends are more rapid variations caused by quantum-mechanical effects not well understood, and alternations with even and odd character of the proton and neutron numbers caused by the pairing of like elementary particles with opposite spin in otherwise identical quantum states.

As a result of the latter effect, all nuclides[9] may be divided into three general classes, those of odd A, those of even A and even Z, and those of even A and odd Z, where A is the mass number and Z the charge number. For each class, the nuclidic mass[10] as a function of A and Z lies on a surface having the general shape of a valley. The three surfaces have nearly the same shapes but are displaced vertically with respect to one another, the even-A, even-Z surface lying lowest, the even-A, odd-Z highest, and the odd-A midway between. The cross sections of the surfaces are approximately symmetrical in the region of the valley.

Beta-transitions occur when a nuclide occupies a higher position than that of a neighboring isobar.[11] In beta-transitions all nuclides of odd A

[1] G. Gamow, Proc. Roy. Soc. (London) **A123**, 386 (1929), **A126**, 632 (1930); Physik Zeits. **30**, 717 (1929); *Constitution of Atomic Nuclei and Radioactivity* (Clarendon Press, Oxford, 1931), Chapter I.

[2] W. Heisenberg, Zeits. f. Physik **77**, 1 (1932), **78**, 156, **80**, 587 (1933); "Rapport du VIIième Congrès Solvay, Brussels, 1933," 289 (1934).

[3] G. C. Wick, Nuovo Cimento **11**, 227 (1934).

[4] G. Gamow, Zeits. f. Physik **89**, 592 (1934); *Structure of Atomic Nuclei and Nuclear Transformations* (Clarendon Press, Oxford, 1937), Chapter II.

[5] C. F. v. Weizsäcker, Zeits. f. Physik **96**, 431 (1935); *Die Atomkerne* (Akademische Verlagsgesellschaft, Leipzig, 1937), Chapter II.

[6] H. A. Bethe and R. F. Bacher, Rev. Mod. Phys. **8**, 82 (1936); H. A. Bethe, Rev. Mod. Phys. **9**, 69 (1937).

[7] N. Bohr and F. Kalckar, Kgl. Danske Vid. Sels. Math.-Fys. Medd. **14**, No. 10 (1937).

[8] N. Bohr and J. A. Wheeler, Phys. Rev. **56**, 426 (1939).

[9] The term *nuclide*, derived from *nucle-* (nuclear) and *εἶδος* (species), is used for "a species of atom characterized by the constitution of its nucleus, in particular by the numbers of protons and neutrons in its nucleus." T. P. Kohman, Am. J. Phys. **15**, 356 (1947).

[10] In this paper the masses considered are *atomic* rather then *nuclear* masses. Thus the energy release in a beta-transition (negatron emission, electron capture, or positron emission), being determined by the difference in mass between the initial and final *atom*, is given by the sum of the kinetic energies of the particles emitted, the rest-mass (if any) of the neutrino, and any quantum radiation accompanying the decay. The rest-masses of emitted or captured negative electrons are not included, but in the case of positron emission two election rest-masses must be included, since these are ultimately transformed to annihilation radiation.

[11] This is strictly true in all cases only if the rest-mass of the neutrino is zero, as is assumed for the present discussion. This is known to be at least very nearly true and is believed to be exactly true: E. Fermi, Zeits. f. Physik **88**, 161 (1934); H. A. Bethe and R. F. Bacher, Rev. Mod. Phys. **8**, 82 (1936); E. J. Konopinski, Rev. Mod. Phys. **15**, 209 (1943; W. E. Stephens, Rev. Mod. Phys. **19**, 19 (1947).

remain on the middle surface, while isobars of even A alternate between the upper and lower. The beta-stable nuclides are those having smaller masses than either of their neighboring isobars. For each odd A there is one and only one beta-stable isobar, for which Z is within one-half unit of Z_A, the coordinate of the bottom of the valley. For even A, in general, one, two or three isobars of even A are beta-stable and all others, including those of odd Z, are unstable. According to the statistical considerations on which the liquid-drop model is based, Z_A should be a smoothly varying function of A, and the region of stability for even-A, even-Z nuclides should be bounded by smoothly varying limits symmetrically disposed with respect to Z_A. This paper describes a method for evaluating these quantities by an examination of the distribution of the beta-stable nuclides.

II. DIAGRAMATIC REPRESENTATION OF THE BETA STABILITY LIMITS

Diagrams and plots of the stable nuclides too numerous to cite have been published in early demonstrations of regularities and irregularities in their pattern of distribution. Gamow[4] in 1934 used plots of the neutron-proton ratio *versus* A to locate Z_A as a function of A within narrow confines. Separate plots were made for even A and odd A, each plot revealing definite windings in the path of beta-stability. The accuracy was limited by the then incomplete knowledge of the beta-stable nuclides. Bohr and Wheeler[8] determined Z_A more accurately by plotting the beta-stable odd-A nuclides, each with a vertical line extending one-half charge unit above and below the stable charge number to indicate the confines of the curve. A similar plot was made by I. Joliot-Curie,[12] who used additional data from the beta-stable even-A nuclides and from beta-disintegration energies to assist in localizing the curve.

At the present time the isotopic constituents of the naturally occurring forms of the elements are known fairly completely.[13] By making use of the previously mentioned considerations based on the liquid-drop nuclear model, it is possible to determine the limits of beta-stability from a single plot in which both even-A and odd-A nuclides are represented.

In Fig. 1 the abscissa is A and the ordinate $U=Z-0.4\,A$. The latter function of the charge has been chosen instead of the charge itself to eliminate the main part of the variation of Z with A, represented approximately by the term $0.4\,A$. This allows all of the points of interest to be contained on one horizontal plot with large vertical separations. Thus, deviations from the general trend can be clearly seen, and a given change of A or of Z is represented similarly in any part of the chart. Values of Z are indicated at the top and by the sloping lines.

Beta-stable odd-A nuclides are plotted as solid circles and even-A ones as open circles. From each solid circle there has been drawn, following the method of Bohr and Wheeler,[8] a vertical line extending upward and downward by one-half unit. The curve representing Z_A as a function of A must cross each of these lines. From the open circle representing the lowest beta-stable charge for each even A there has been drawn a line extending downward by two units. The curve representing the lower limit for beta-stability must cross each of these lines. From the open circle representing the highest beta-stable charge for even A there has been drawn a line extending upward by two units. The curve representing the upper limit for beta-stability must cross each of these lines. Where an even A has only one beta-stable isobar, both lines originate from the same point.

The three curves are drawn in such a manner that each stays within its prescribed limits at all points, fluctuations are minimized, and the center line is vertically midway between the other two insofar as is possible. By this procedure the localization of each curve is influenced by the limits of the other two, and together their positions can be determined more closely than when each is considered separately. Only in the region $150<A<190$ is it impossible to keep the vertical spacings equal.

This procedure can be followed only up to the region of the heavy natural radioelements. Beyond lead, many of the beta-stable nuclides

[12] I. Joliot-Curie, J. de phys. et rad. [8] 6, 209 (1945).
[13] F. W. Aston, *Mass Spectra and Isotopes* (Edward Arnold and Company, London, 1942), second edition; J. Mattauch and S. Flügge, *Nuclear Physics Tables* (Verlag Julius Springer, Berlin, 1942—trans. Interscience Publishers, Inc., New York, 1946); G. T. Seaborg, Rev. Mod. Phys. 16, 1 (1944).

are missing because of alpha-instability, and the beta-stability or -lability of the short-lived alpha-emitters cannot be determined in all cases. Such of the heavy natural radionuclides as are fairly certainly beta-stable, and those of the heavy synthetic radionuclides for which information has been published,[14] are included in the plot, but the positions of the lines for $A>200$ are only rough approximations. The treatment for small values of A is described below.

Viewing Fig. 1 as a whole, it is seen that the beta-stable even-A even-Z nuclides occupy a definite path bounded by the upper and lower curves. In the center of this path is a narrower path occupied by the beta-stable odd-A nuclides. The boundaries of the latter path are two lines, respectively, one-half charge unit above and below the center line; these have been omitted from the diagram to avoid crowding. The curve of maximum stability shows definite wave-like variations superposed on the long-range variation, as was shown by Gamow.[4] The Z_A values of Bohr and Wheeler[8] follow those of Fig. 1 closely, especially in the region $97 \leqslant A \leqslant 145$ where their curve is shown in detail. The plot of Joliot-Curie,[12] when replotted on the coordinate system of Fig. 1, shows numerous irregular fluctuations about the position of the present curve.[15] It will be recalled that the latter was intentionally made as smooth as was consistent with the data used. Undoubtedly short-range fluctuations do occur, and the curves of Fig. 1 are, therefore, to be considered as mean positions only.

[14] G. T. Seaborg, E. M. McMillan, J. W. Kennedy, and A. C. Wahl, Phys. Rev. **69**, 366 (1946); G. T. Seaborg, A. C. Wahl, and J. W. Kennedy, Phys. Rev. **69**, 367 (1946); G. T. Seaborg, Chem. Eng. News **23**, 2190 (1945), **25**, 358 (1947), Science **104**, 379 (1946); G. T. Seaborg, J. W. Gofman, and R. W. Stoughton, Phys. Rev. **71**, 378 (1947); G. T. Seaborg, and others, reported by J. M. Cork, *Radioactivity and Nuclear Physics* (Edwards Brothers, Inc., Ann Arbor, 1946 and D. Van Nostrand Company, Inc., New York, 1947), Chapter XII; F. Hagemann, L. I. Katzin, M. H. Studier, A. Ghiorso, and G. T. Seaborg, Phys. Rev. **72**, 252 (1947); A. C. English, T. E. Cranshaw, P. Demers, J. A. Harvey, E. P. Hincks, J. V. Jelley, and A. N. May, Phys. Rev. **72**, 253 (1947).

[15] Joliot-Curie defined Z_A in terms of nuclear rather than atomic masses. Thus her curve of maximum stability is not centrally disposed with respect to the distribution of the stable nuclides, but lies above the present curve on the average by the electron rest-mass (0.51 Mev) divided by B_A (see next section), or a few tenths of a charge unit.

III. THE BETA-STABILITY LIMITS IN TERMS OF THE BOHR-WHEELER EMPIRICAL MASS EQUATION

Bohr and Wheeler[8] have shown that the semi-theoretical semi-empirical atomic-mass equation given by Bethe and Bacher[16] can be transposed into the following more convenient form:

$$M_{A,Z}=A(1+f_A)+\tfrac{1}{2}B_A(Z-Z_A)^2\pm\tfrac{1}{2}\delta_A \text{ or } 0.$$

Here $M_{A,Z}$ is the mass of a nuclide of mass number A and charge number Z, f_A is the packing fraction of the hypothetical odd-A isobar of greatest stability having charge Z_A (not necessarily integral), B_A represents the steepness of the walls of the valley of the mass surface, and δ_A is the apparent energy of pairing of nucleonic spins, the last term[17] being taken negative for even A and even Z, positive for even A and odd Z, and zero for odd A.

The parameters f_A, B_A, and Z_A can be expressed in terms of the more fundamental parameters representing the properties of the nuclear fluid. When the latter parameters are evaluated empirically, the Bohr-Wheeler equation correctly expresses the observed general trends of atomic masses. However, the short-period variations are not reproduced. Consequently, Bohr and Wheeler proposed to use their equation with its parameters determined empirically as functions of A, independently of the theory. They evaluated f_A from mass-spectrographic data and estimated Z_A from the values of Z for stable odd-A nuclides. In the absence of sufficient data on radioactive disintegration energies, B_A was calculated from Z_A according to a theoretical relationship. δ_A was then estimated from the limits of stable even-A nuclides and from some radioactive disintegration energies. Subsequently, Joliot-Curie[12] undertook a completely empirical evaluation of Z_A, B_A, and δ_A as functions of A. With the parameters so determined, the Bohr-Wheeler empirical equation, though divested of much of its theoretical significance, is quite useful in practical correlations of atomic masses and predictions of disintegration energies.

The beta-stability limits are readily expressed in terms of the parameters of the Bohr-Wheeler

[16] Equation (182) of reference 6, based on the liquid-drop nuclear model, and modified from Weizsäcker (reference 5).

[17] Added by Bohr and Wheeler following Heisenberg (reference 2).

equation. The equation yields for the energy, E_-, released by the emission of a negative beta-particle by an even-A even-Z nuclide of charge Z

$$E_- = B_A(Z_A - Z - \tfrac{1}{2}) - \delta_A.$$

For a hypothetical nuclide just at the lower limit of stability, whose charge is Z_A',

$$E_- = B_A(Z_A - Z_A' - \tfrac{1}{2}) - \delta_A = 0.$$

Consequently,

$$Z_A' = Z_A - \frac{\delta_A}{B_A} - \tfrac{1}{2} = Z_A - S_A,$$

where

$$S_A = \frac{\delta_A}{B_A} + \tfrac{1}{2}.$$

Similarly, the upper limit, Z_A'', is given by

$$Z_A'' = Z_A + S_A.$$

S_A is thus the vertical spacing between the curves of Fig. 1. The lower and upper stability limits for odd-A nuclides are $Z_A - \frac{1}{2}$ and $Z_A + \frac{1}{2}$, respectively.

Although the statistical treatment of the nucleus is not valid for small numbers of nucleons ($A \lesssim 30$), it is of interest that a slight modification allows the scheme of the diagram to be extended all the way down to $A = 1$. Throughout the region of validity of the statistical model, $B_A < 2\delta_A$, $S_A > 1$, and all even-A odd-Z nuclides are unstable. But if $B_A > 2\delta_A$, as is the case for $A \lesssim 30$, then $S_A < 1$; and if for a given A no even Z lies between the limits $Z_A \pm S_A$, the isobar of odd Z which does will be beta-stable. This may be considered to be the case for mass numbers 2, 6, 10, and 14; therefore, from the points in Fig. 1 representing $_1H^2$, $_3Li^6$, $_5B^{10}$, and $_7N^{14}$, a line is drawn extending one unit upward and one unit downward. The limiting even-A curves must cross these lines, which fix their positions fairly closely in this region. The curves as drawn correspond to such known facts as the small disintegration energies of H^3 and C^{14} and the approximate equality in mass of the ground states of He^5 and Li^5.

Figure 1 was constructed as a part of a plan

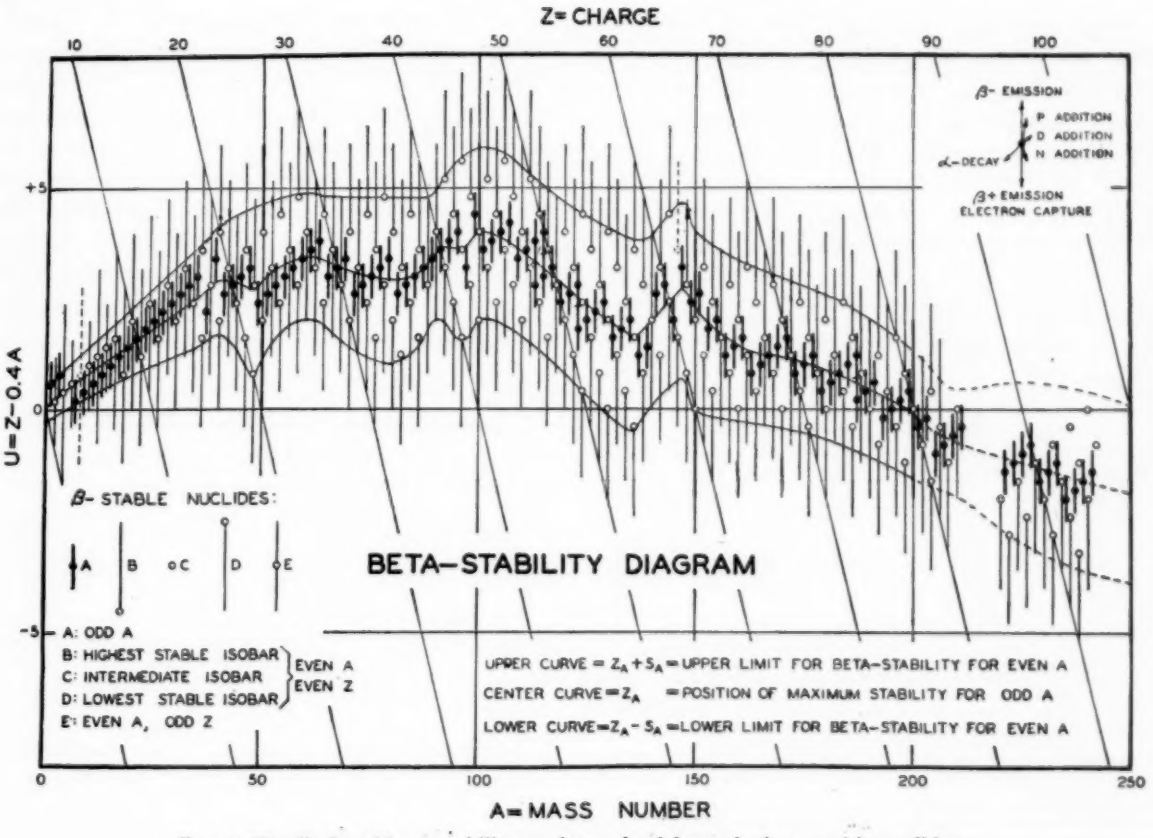

FIG. 1. The limits of beta-stability as determined from the beta-stable nuclides.

to determine the validity of the parabolic mass expression of Bohr and Wheeler and to evaluate the best empirical values of the parameters. However, this relation was not involved in the construction of the diagram. The curves can, of course, be placed more accurately by making use of disintegration energies, but for the present purpose only a few beta-disintegration energies were used as qualitative guides. It is evident that a knowledge of the beta-stable nuclides is by itself sufficient for a fairly close determination of the charge of maximum stability and the limits of beta-stability.

IV. APPLICATIONS OF THE BETA-STABILITY DIAGRAM

Besides clearly indicating the trends of nuclear stability, the beta-stability diagram has additional value, as may be demonstrated by several examples of its usefulness.

Relative Stability of Neighboring Odd-*A* Isobars

Four odd mass numbers, 113, 115, 123, and 187, have two neighboring apparently beta-stable isobars. In each case one should have a greater mass than the other and transform to it by a beta-transition.[11] From the position of the Z_A curve it can be predicted that Sn^{115} is probably unstable with respect to electron capture[11] to form In^{115}, and Sb^{123} is probably unstable with respect to negatron emission to form Te^{123}. For the other two pairs, Cd^{113}-In^{113} and Re^{187}-Os^{187}, no choice can be made. The reported[19] activity of Os^{187} has recently been questioned, with indications that Re^{187} instead is radioactive.[20] If this is the case, the point representing Re^{187} must be removed and the stability curves raised slightly in this region.

TABLE I.

A		B		C	
−	+	−*	+*	−*	+*
P^{33}	Mn^{53}	Si^{22}	Ti^{44}	Ca^{48}	Ni^{58}
A^{39}	Sb^{119}	Ti^{52}	Ge^{68}	Se^{82}	Kr^{78}
Ni^{63}	La^{127}	Cr^{56}	Zr^{88}	Kr^{86}	Mo^{92}
Se^{79}	61^{145}	Fe^{60}	Pd^{100}	Zr^{96}	Ru^{96}
Pd^{107}	Tb^{157}	Ni^{66}	Te^{118}	Mo^{100}	Cd^{106}
I^{129}	Ho^{163}	Cd^{118}	Nd^{140}	Sn^{124}	Sn^{112}
Cs^{135}	Ta^{179}	Dy^{166}	Gd^{150}	Te^{130}	Xe^{124}
Tm^{171}	Pt^{193}	Hf^{182}	Dy^{156}	Xe^{136}	Ba^{130}
	Pb^{205}		Hf^{172}	Nd^{150}	Ce^{136}
			W^{178}	Yb^{176}	Sm^{144}
			Pt^{190}	Hg^{204}	Er^{162}
			Pb^{202}		Yb^{168}
					Os^{184}
					Hg^{196}

A: unknown odd-*A* nuclides of low disintegration energy, some of which may be sufficiently long-lived to exist as natural radioactivities.
B: unknown even-*A*, even-*Z* nuclides on or near the limits of beta-stability, some of which may be beta-stable but undiscovered or missing in nature, and some of which may be sufficiently long-lived to exist as natural radioactivities.
C: apparently stable even-*A*, even-*Z* nuclides on or near the limits of beta-stability, some of which may be beta-labile with long lifetimes.
−: nuclides which if beta-labile would emit negative beta-particles.
+: nuclides which if beta-labile would capture electrons.
*: nuclides which if beta-active would be accompanied by daughters of large disintegration energies and relatively short lifetimes.

Odd-*A* Nuclides of Low Beta-Disintegration Energy

By inspection of the diagram it is possible to locate positions corresponding to odd-*A* nuclides of low beta-disintegration energy. Those whose radioactive properties are not known are listed in Table I-A. These should all be long-lived, and in some cases the long lifetimes have been the reason for their non-discovery.

If it is assumed that the universe is 3×10^9 years old and that at the time of its origin all stable and nearly stable isotopes of an element were present in comparable amounts, the half-life of a nuclide would, in general, have to be $\gtrsim1.5\times10^8$ years in order for detectable amounts to remain, $\lesssim4\times10^8$ years in order not to have been discovered mass spectrometrically, and $\lesssim2\times10^8$ years not to have been discovered radiometrically unless the radiations are extremely soft. There is thus a small but finite chance that traces of one or more of the nuclides of Table I-A may remain as natural radioactivities.[21]

Even-*A*, Even-*Z* Nuclides Possibly Beta-Stable and "Missing," or of Low Disintegration Energy

The position of Sm^{146} is well within the region of beta-stability, and its absence (at least in

[18] A similar prediction has been made by E. D. Eastman on the basis of atomic-mass calculations, Phys. Rev. **46**, 1 (1934), and of the common occurrence of indium in tin ores, Phys. Rev. **52**, 1226 (1937).
[19] E. T. Lougher and S. Rowlands, Nature **153**, 374 (1944).
[20] W. F. Libby and S. N. Naldrett, private communication.
[21] S. Katcoff, Phys. Rev. **71**, 826 (1947) has presented evidence for the possible presence of I^{129} to the extent of about one part per million in natural iodine, suggesting a minimum half-life of 10^8 years.

amounts sufficient to be detected mass spectrometrically[22]) is undoubtedly to be attributed to alpha-instability.[23] Positions of even A and Z which lie on or just outside of the stability limits as drawn are listed in Table I-B.[24] Some of these may actually be beta-stable and either completely "missing" in nature or present in such low abundance as to be still undiscovered. Considerations based on the liquid-drop nuclear model indicate that the lightest beta-stable isotopes of some of the heavy even elements may be alpha-unstable with cosmologically short lifetimes,[25] and some of the nuclides in the latter part of list I-B (+) may be missing in nature for that reason. Pt^{190} in particular seems to lie within the stability limits, and if the low energy electrons[26] emitted by Ir^{190} are actually negative beta-particles, Pt^{190} must owe its absence to alpha-decay.

On the other hand, any nuclide in Table I-B which is beta-labile will have a low disintegration energy and will be long-lived. If any should be present in nature it would be accompanied by a daughter of large disintegration energy and short lifetime. By chemical extraction of the active daughter the sensitivity of detection could be enormously enhanced, so that the half-life might be as low as $\sim 1.0 \times 10^8$ years, on the above assumption regarding the formation of the elements, and still permit detection in the presence of stable isotopes.

Naturally Occurring Even-A, Even-Z Nuclides Which May Possibly Be Beta-Labile

Apparently stable nuclides which lie on or just within the stability limits as drawn are listed in Table I-C. Some of these may actually be unstable but with lifetimes sufficiently long to have prevented appreciable decay since their formation. The absence of detectable radiations would indicate minimum lifetimes of about 10^{13} years for most of the nuclides listed. Any which are beta-active, however, would be accompanied by short-lived daughters with energetic radiations, so that by use of the active-daughter extraction technique it should be possible to detect activities with half-lives as great as $\sim 10^{19}$ years.

Ca^{48} is of particular interest, since it lies well below the main region of stability. Its natural occurrence, at least as a stable nuclide, has been doubted,[12, 27] but the mass-spectrometric[28] and nuclear-reaction[29, 30] evidence for its existence in natural calcium appears conclusive. It has been reported[30] that Sc^{48} apparently undergoes electron capture, in which case Ca^{48} would be stable. If, however, Ca^{48} is radioactive, the accumulation of Ti^{48} would make it a valuable geological and paleontological time index.

A natural radioactivity of neodymium has been reported[31] though never confirmed. If the activity actually belongs to this element, the isotope of mass 150 is probably responsible, since it seems to be outside the stability region, with Nd^{140} as an alternate possibility. If Nd^{150} is unstable, its daughter would be an active isotope of element 61, which element has not yet been found naturally in either stable or radioactive forms.[32] Similarly, if Sm^{144} undergoes electron capture, an element 61 activity would result. If Mo^{100} or Ru^{96} is unstable, an active isotope of technecium, the missing element 43, would be present naturally.

A search is being made for natural radioactivities such as those indicated as possibilities in this paper.

ACKNOWLEDGMENT

I wish to thank Mr. Anthony Van Zervic for his careful reproduction of the drawing for Fig. 1.

[22] F. W. Aston, Proc. Roy. Soc. (London) **A146**, 46 (1934).
[23] This has been suggested previously, for example, by Flügge (reference 12), p. 103.
[24] Several nuclides which an inspection of the chart would place in this group are known to be radioactive, being produced in fission (for example, Sr^{90}) or by alpha-decay (for example, Pb^{210}), and hence are not listed.
[25] T. P. Kohman, paper in preparation.
[26] L. J. Goodman and M. L. Pool, Phys. Rev. **71**, 288 (1947).
[27] M. N. Saha and A. K. Saha, Trans. Nat. Inst. Sci. India **2**, 193 (1946); Nature **158**, 6 (1946).
[28] A. O. Nier, Phys. Rev. **53**, 282 (1938); C. W. Sherwin and A. J. Dempster, Phys. Rev. **59**, 114 (1941).
[29] H. Walke, F. C. Thompson, and J. Holt, Phys. Rev. **57**, 177 (1940); H. Walke, Phys. Rev. **57**, 163 (1940).
[30] C. T. Hibdon and M. L. Pool, Phys. Rev. **67**, 313 (1945).
[31] W. F. Libby, Phys. Rev. **45**, 845 (1934); **46**, 196 (1934).
[32] D. M. Yost, H. Russell, Jr., and C. S. Garner, *The Rare-Earth Elements and their Compounds* (John Wiley and Sons, Inc., New York, 1947), Chapter 4. See, however, B. S. Hopkins, *Chapters in the Chemistry of the Less Familiar Elements* (Stipes Publishing Co., Champaign, 1938), Chapter 6.

The (H^3, p) Reaction in Rh and Co and Probable Evidence of the Di-Neutron

D. N. KUNDU AND M. L. POOL
Ohio State University, Columbus, Ohio

(Received September 24, 1947)

By H^3 bombardment, two neutrons have been introduced into Rh and Co nuclei according to reactions $Rh^{103}(H^3, p)Rh^{105}$ and $Co^{59}(H^3, p)Co^{61}$, with half-lives of 35 hours and 1.75 hours, respectively. The mechanism appears to be an Oppenheimer-Phillips process with H^3. The results are interpreted in the light of the di-neutron ($_0n^2$). It is believed that $_0n^2$ may exist under the physical conditions of the experiments reported.

1. INTRODUCTION

IN previous works,[1,2] H^3 was used as the bombarding particle for producing nuclear reactions in Ag leading to Pd^{107}. A series of investigations was undertaken with a view to introduce two neutrons into a nucleus. Considering the ease with which (d, p) reactions proceed according to the Oppenheimer-Phillips[3–6] process, the H^3 particle was regarded as suitable for the above purpose.

Two similar nucleons are known to have forces of attraction between them. It has, therefore, been speculated[7] that the so-called "di-neutron" ($_0n^2$) may exist. The di-neutron might be examined experimentally if by an Oppenheimer-Phillips process the proton could be separated from the H^3 nucleus and the remaining neutron pair could be observed to behave as a single group.

Bombardments with H^3, made with these aims in view, are mostly complicated by extraneous activities produced by deuterons, neutrons, etc., because the H^3 was produced, as in the previous works by bombarding Be with deuterons. These non-essential activities usually come in such great strength as to mask, in many cases, the H^3 activation, if there is any. However, in the case of Rh and Co the experimental results are sufficiently free from ambiguity and are therefore, reported in the present paper. The reactions observed are $Rh^{103}(H^3, p)Rh^{105}$ and $Co^{59}(H^3, p)Co^{61}$.

2. EXPERIMENTAL

Rhodium + H^3

A Be foil was bombarded with 10-Mev deuterons and the H^3 thus produced was made to bombard a number of Rh foils (each 1 or 2 mils thick), placed immediately behind the Be foil. Two thicknesses of Be (5 and 8 mils) were used in different experiments. After the bombardment* the foils were separately cut to very fine pieces, sealed into heavy-walled glass tubes with a mixture of HCl and $HClO_4$ (20:1) and heated to 300°C for 4 hours. The tubes were then cooled to liquid-air temperature and opened while cold. Ruthenium carrier and later sufficient $HClO_4$ was added to change the Ru to RuO_4. The mixture was distilled by bubbling air through it while heating with a microburner and the distillate was collected in very concentrated KOH kept in an ice bath as potassium perruthenate. The residue was evaporated nearly to dryness with concentrated H_2SO_4 till there was copious evolution of SO_3 fumes, distilled and the Rh precipitated by adding $TiCl_2$.

The decay curve of the Rh fraction of the first foil is shown in Fig. 1. The 35-hour Rh^{105} activity is seen above the long-period background which is mostly 210-day Rh^{102}. The strong 12.8-hour activity was suspected to be due to copper impurity in the Rh sample. This was confirmed by a spectro-chemical examination of the Rh sample. Repeated separations of

[1] D. N. Kundu and M. L. Pool, Phys. Rev. **71**, 467 (1947).
[2] D. N. Kundu and M. L. Pool, Phys. Rev. **72**, 101 (1947).
[3] J. R. Oppenheimer and M. Phillips, Phys. Rev. **48**, 500 (1935).
[4] H. A. Bethe, Rev. Mod. Phys. **9**, 201 (1937).
[5] H. A. Bethe, Phys. Rev. **53**, 39 (1938).
[6] H. A. Bethe, Phys. Rev. **53**, 205 (1938).
[7] M. Y. Colby and R. N. Little, Phys. Rev. **70**, 437 (1946).

* The Rh chemistry was kindly done by H. L. Finston and Ula M. Bigham of the Ohio State University.

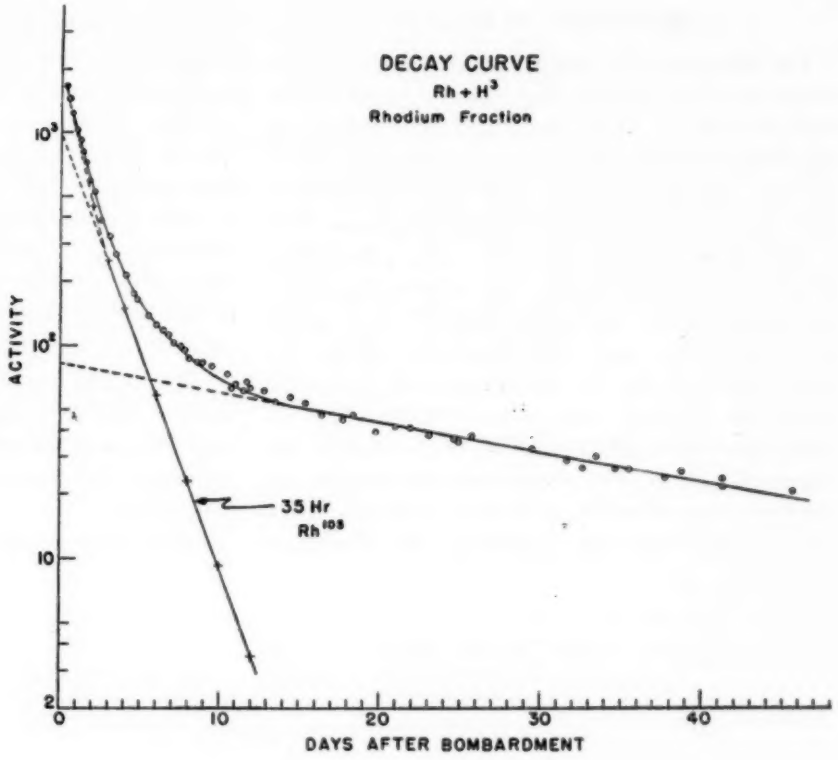

FIG. 1. Decay curve of the rhodium fraction after bombardment of rhodium with H^3 showing the 35-hour Rh^{105}. The crosses denote the points obtained by subtracting the base line from the earlier part of the decay curve

Cu from the Rh fraction removed a large fraction of this 12.8-hour activity. Beta-energy measurements of Rh final fraction by absorption in aluminum, gave 0.6 Mev which checks with accepted Rh^{105} value. No 35-hour activity was observed in the Rh fraction of the foils behind the first one. The Pd fraction of the first foil showed the 17-day Pd^{103} due to the reaction $Rh^{103}(d, 2n)Pd^{103}$, but no 13-hour activity was found.

Cobalt+H^3

Hilger Co metal was used in the form of a 40-mil thick block. After bombardment** with H^3, a few mils of the material from the front surface, which was hit by the H^3, were etched out with concentrated HNO_3. The sample on manufacturer's analysis contained less than 0.1, 0.01 percent of Ni and Cu, respectively, and spectroscopically just observable traces of Cr, Fe, and Ag. Carriers of Cu, Ni, and Mn were added and the Mn separated as MnO_2 with $KBrO_3$ from the 1–N solution in HNO_3. The Cu was then repeatedly precipitated with H_2S from the 3N HCl solution. The supernate was made basic with NH_4OH and NH_4Cl and, the Ni precipitated with alcoholic solution of dimethyl glyoxime. The Co was later precipitated from 1–N HCl medium with α-nitroso-β-naphthol solution. Initial tests with separation of Fe and Cr showed that these introduce no complications and were, therefore, eliminated from the general procedure.

Figure 2 shows the decay curve of the Co fraction. The 1.75-hour Co^{61} activity recently reported[8] is seen above the very long-period activity. The short length of the curve is due to the long time needed for the chemistry and the comparatively short half-life under study. The identification was substantiated by β-energy measurements which gave 1.1 Mev for the maximum value by absorption in aluminum. The 1.75-hour Co^{61} emits no γ-radiation as seen from the γ-decay curve.

** The Co chemistry was kindly done by J. M. Hollander of the Ohio State University.

[8] T. J. Parmley and B. J. Moyer, Phys. Rev. 72, 82 (1947).

3. DISCUSSION OF RESULTS

The elements Rh and Co were chosen as the target material because they have a single stable isotope (Fig. 3). This gives greater freedom in the interpretation of results. The 35-hour Rh^{105} activity can be produced only by the introduction of two neutrons into a Rh^{103} nucleus. This is not possible by activation with deuterons which have been used as the primary particles for producing H^3. Neither is it likely, on grounds of probability, that two neutrons which are available from the Be+d source, will enter the same Rh nucleus one after another. Experimentally, also, this possibility is excluded for the back foils of Rh, which were bombarded by neutrons only, showed no 35-hour activity under similar conditions of chemistry. All efforts to impute the 35-hour activity to impurities were unsuccessful. For example, a small amount of Pd as impurity in the Rh metal might produce the 35-hour activity by (n, p) or (d, $2p$) reaction. This is, however, contrary to observtions, for it is experimentally well known that the 13-hour Pd^{109} activity is produced in very high strength by deuteron and neutron activation of Pd. The absence of the 13-hour activity in the Pd fraction of the first foil is strong evidence that no observable Pd is present in the Rh sample. The absence of the 35-hour activity in the back foils also indicates that the same activity, as measured in the first foil, is not due to (n, p) reaction from Pd impurity. The reaction must, therefore, be Rh^{103} (H^3, p)Rh^{105}.

Essentially similar arguments hold in the case

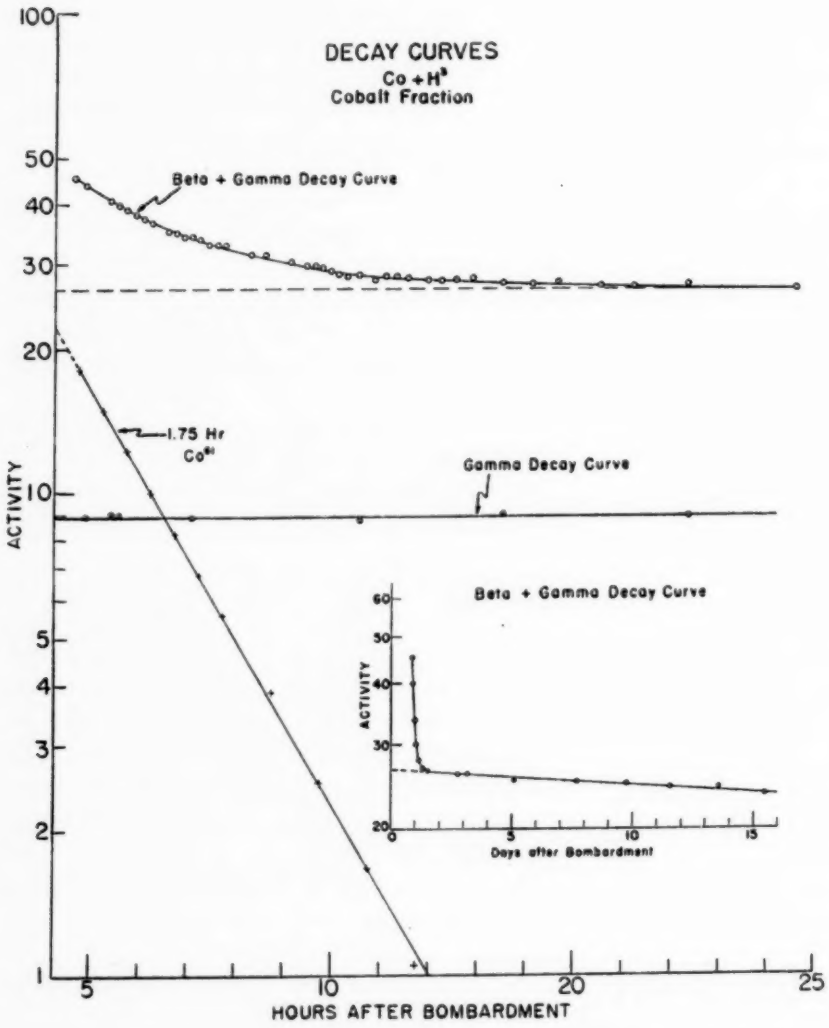

FIG. 2. Decay curve of the cobalt fraction after H^3 bombardment of cobalt showing the 1.75-hour Co^{61}. The crosses denote the points obtained by subtracting the base line from the earlier part of the beta- and gamma-decay curve.

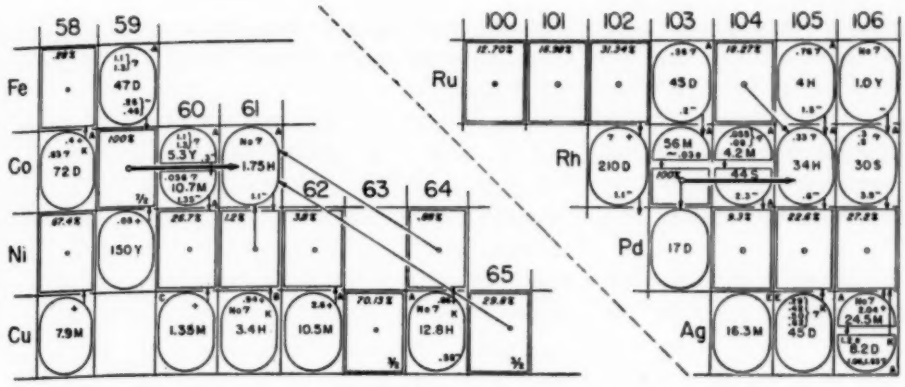

FIG. 3. Rhodium and cobalt regions in the chart of atomic nuclei. The heavy arrow indicates the formation of Rh^{106} and Co^{61} from Rh^{103} and Co^{59} respectively by the (H^3, p) reaction.

of the 1.75-hour Co^{61} activity which has been produced from the single stable Co^{59} isotope. In this case, the activity of the main block, after the etching out of the thin layer bombarded with H^3, was followed to check neutron activation. As seen from Fig. 3, Ni stands in the same relation to Co as Pd did to Rh. Though a minute trace of Ni is present in the Co Metal used, it is only less than 0.1 percent, and the percentage abundance of Ni^{61} from which Co^{61} might be produced by (n, p) or $(d, 2p)$ reaction is only 1.2. It would thus be impossible to detect any 1.75-hour activity produced from the Ni impurity. Moreover, the main block which was many times more active than the Co fraction showed no 1.75-hour period. The β-energy measurement was also an important help. Every test showed that the reaction is $Co^{59}(H^3, p)Co^{61}$.

H^3 has thus been instrumental for the simultaneous introduction of two neutrons into the nucleus of Rh^{103} and Co^{59}.

4. INTERPRETATION AND THE DI-NEUTRON HYPOTHESIS

Since H^3 is responsible for the introduction of the two neutrons into the Rh and Co nucleus, it is plausible, as indicated in the introduction, to assume that the mechanism involved is, in large part at least, the Oppenheimer-Phillips process with H^3 instead of with d as the bombarding particle. As the H^3 approaches the high potential barrier of the target nucleus, it is "polarized." The charged proton part of the polarized H^3 is strongly repelled. The two neutrons find no barrier in front and enter the target nucleus. As in the case of the deuteron, the formation of the compound nucleus, by Gamow-Condon-Gurney process, and then the ejection of the proton, would be less probable even for moderately heavy nuclei like Rh and Co. It was also experimentally noted by changing the thickness of the Be foil, that the yield of the 35-hour activity was not greatly sensitive to the energy of the H^3 particles as it should have been if the mechanism had been one in which a G–C–G compound nucleus was formed. The yield according to the O–P process, on the other hand, will not be strongly affected by small changes in the energy of the bombarding particle. Moreover, in the ordinary G–C–G scheme, the (H^3, p) reaction will probably have to compete with (H^3, n), $(H^3, 2n)$, and $(H^3, 3n)$ reactions whereas there will be no such competition in the O–P scheme. This is of special significance[5] because of the fact that the products of (H^3, n) and $(H^3, 2n)$ are each stable for Rh and Co while the product of (H^3, p) is β-active.

If, therefore, the phenomenon is mostly an Oppenheimer-Phillips process with H^3, as it is very likely to be, the next question that arises is whether the two neutrons are captured separately one after another or whether they are captured simultaneously as a group. Inside the H^3 nucleus, the two neutrons had been within the range of nuclear forces and there was a force of attraction between them. When the H^3 comes in the immediate vicinity of the target nucleus, though the proton momentarily stays at some distance away from it, the two neutrons which are practically on its surface may still be held to each other by mutual forces of attraction. In other words, in the absence of specific causes which would take the two neutrons apart, they would

hold together as a group and would be captured as such. This group would then be the di-neutron ($_0n^2$), but a di-neutron only under very peculiar physical conditions. It is being found in course of these (H^3, p) reactions only for a very short time, *viz.* the interval between the instant the H^3 begins to be polarized and the instant the capture takes place.

The di-neutron may be an extremely unstable particle and hence, the circumstances of the present investigations may be just the extreme physical conditions under which it may be observed.

The authors are grateful for the support received from the Ohio State University Development Fund. Thanks are also due the Watumull Foundation, Los Angeles, and the Ghosh Travelling Fellowship Board of the Calcutta University for their support to one of the authors.

PHYSICAL REVIEW VOLUME 73, NUMBER 1 JANUARY 1, 1948

On Infinities in Generalized Meson-Field Theory

ALEX E. S. GREEN
Department of Physics, University of Cincinnati, Cincinnati, Ohio
(Received September 24, 1947)

The results of an extension of Podolsky's generalized electrodynamics, corresponding to Proca's extension of Maxwellian electrodynamics, are presented. In this extension the Lagrangian is permitted to depend upon the field coordinates themselves, which is a major step in going from electrodynamics to meson-field theory.

The static interaction and static self-energy, derived by exact classical and quantum methods, as well as the dynamic interaction and dynamic self-energy, obtained by a quantum-mechanical perturbation method, are given. The complete interaction and self-energy are free from singularities and infinities. This is in contrast with the results of ordinary relativistic meson-field theory. It thus appears that these defects may be removed from meson theory, just as in electrodynamics, by going to a generalized field theory in which the Lagrangian contains the second derivatives of the field coordinates.

1. INTRODUCTION

IT is well known that the outstanding difficulty in the quantum theory of fields is the problem of infinite self-energies or inertia effects which arise in those theories which meet the requirement of relativistic invariance. In fact, most of the current research in field theory is directed at solving this problem.[1,2]

In a recent series of papers Podolsky,[3] Podolsky and Kikuchi,[4,5] Montgomery,[6] and Green[7] have developed a completely relativistic electrodynamics which appears to be free from the defect of infinite self-energies and which reduces to the Maxwell-Lorentz formulation for low energy phenomenon. In the present paper we extend this generalized field theory by allowing the Lagrangian to contain the field coordinates themselves. The corresponding extension of Maxwellian electrodynamics has been investigated by Proca[8] and others[9,10,11] and is considered to be among the more promising of meson-field theories.

In order to show the essential consequences of this generalization we shall consider only its simplest aspects. It is probable that modification of this theory by the inclusion of such concepts

[1] See G. Wentzel, Rev. Mod. Phys. **19**, 1 (1947).
[2] Also W. Pauli *Meson Theory of Nuclear Forces* (Interscience Publishers, Inc., New York, 1946).
[3] B. Podolsky, Phys. Rev. **62**, 68 (1942), to be referred to as GE I.
[4] B. Podolsky and C. Kikuchi, Phys. Rev. **65**, 228 (1944), to be referred to as GE II.
[5] B. Podolsky and C. Kikuchi, Phys. Rev. **67**, 184 (1945), to be referred to as GE III.
[6] D. J. Montgomery, Phys. Rev. **69**, 117 (1946), to be referred to as GE IV.
[7] A. E. S. Green, Phys. Rev. **72**, (1947), to be referred to as GE V.
This series of five papers will be called the GE S.
[8] A. Proca, J. Phys. Rad. (vii) **7**, 347 (1936).
[9] N. Kemmer, Proc. Roy. Soc. **A166**, 127 (1938).
[10] H. Frohlich, W. Heitler, and N. Kemmer, Proc. Roy. Soc. **A166**, 154 (1938).
[11] H. J. Bhabha, Proc. Roy. Soc. **A166**, 501 (1938).

as isotopic spin and symmetry requirements will be necessary to explain nuclear phenomenon. Nevertheless it seems worth while to present the consequences of a development which differs from Podolsky's generalized electrodynamics merely in two respects.

(1) The Lagrangian of the field depends quadratically upon the field coordinates which are components of a four vector $\varphi_\alpha=(\mathbf{A}, i\phi)$.

(2) The parameter coupling the field with a nucleon is a constant g instead of the charge e.

As the mathematical formalism used in this investigation parallels almost exactly that used in the GE S we shall present only the differences which arise as a result of the modification in assumptions. The reader should refer to the GE S for the steps of the calculations and for the notation, nomenclature, and references.

2. LAGRANGIAN, HAMILTONIAN, AND WAVE EQUATION

We choose as our basic Lagrangian of the field

$$L=-(1/2)[\mu^2\varphi_\alpha{}^2+\varphi_{\alpha,\beta}{}^2+a^2(\Box\varphi_\alpha)^2], \quad (2.1)$$

where μ is a constant having the dimension of reciprocal length and a is a constant with the dimension of length. The scalar counterpart of this equation has been suggested by Rayski.[12] The development leading to Eqs. Ge II (2.16) and Ge II (2.22) is altered but slightly by the additional term in the Lagrangian. The corresponding field equation is

$$a^2\Box\Box\varphi_\alpha-\Box\varphi_\alpha+\mu^2\varphi_\alpha=0, \quad (2.2)$$

which is a fourth-order generalization of the Klein-Jordan equation. The Hamiltonian is

$$H=(1/2)[\mu^2\varphi_\alpha{}^2+\varphi_{\alpha,\beta}{}^2+a^2(\Box\varphi_\alpha)^2]$$
$$-\varphi_{\alpha,4}(1-a^2\Box)\varphi_{\alpha,4}-a^2\varphi_{\alpha,44}\Box\varphi_{\alpha,4}. \quad (2.3)$$

3. CLASSICAL TREATMENT OF THE STATIC CASE

For the static case the field equation becomes

$$a^2\nabla^2\nabla^2\phi-\nabla^2\phi+\mu^2\phi=0. \quad (3.1)$$

If we consider the interaction of the field with a point nucleon at the origin then we must, as in GE I, place on the right the nucleon density

$$\rho=g\delta(\mathbf{R}). \quad (3.2)$$

A well behaved solution of (3.1) which gives rise to the delta-function is

$$\phi=(g/4\pi\gamma R)(e^{-\mu_0 R}-e^{-\mu_1 R}), \quad (3.3)$$

where

$$\mu_0=[(1+2a\mu)^{\frac{1}{2}}-(1-2a\mu)^{\frac{1}{2}}]/2a, \quad (3.4)$$

$$\mu_1=[(1+2a\mu)^{\frac{1}{2}}+(1-2a\mu)^{\frac{1}{2}}]/2a, \quad (3.5)$$

and

$$\gamma=a^2(\mu_1{}^2-\mu_0{}^2)=(1-4a^2\mu^2)^{\frac{1}{2}}. \quad (3.6)$$

The volume integral of the Hamiltonian (henceforth called simply the Hamiltonian) is

$$\bar{H}=\int H dV=(1/2)\int[\mu^2\phi^2+(\nabla\phi)^2$$
$$+a^2(\nabla^2\phi)^2]dV. \quad (3.7)$$

Using (3.3) we obtain for the energy of the field

$$\bar{H}=g^2/8\pi a(1+2a\mu)^{\frac{1}{2}}. \quad (3.8)$$

4. CLASSICAL SOLUTION OF THE GENERAL CASE

A general solution of the field equation (2.2), expressed in terms of Fourier integrals, is[13]

$$\varphi_\alpha(\mathbf{r}, t)=(1/2\pi)^{\frac{1}{2}}\int[\varphi_\alpha(\mathbf{k})\exp(-i\phi_0)$$
$$+\varphi_\alpha{}^*(\mathbf{k})\exp i\phi_0+\bar{\varphi}_\alpha(\mathbf{k})\exp(-i\phi_1)$$
$$+\bar{\varphi}_\alpha{}^*(\mathbf{k})\exp i\phi_1]d\mathbf{k}, \quad (4.1)$$

where

$$\phi_0=ck_0t-\mathbf{k}\cdot\mathbf{r}, \quad \phi_1=ck_1t-\mathbf{k}\cdot\mathbf{r}, \quad (4.2)$$

$$k_0{}^2=k^2+\mu_0{}^2, \quad \text{and} \quad k_1{}^2=k^2+\mu_1{}^2. \quad (4.3)$$

From the standpoint of quantum mechanics, Eqs. (4.3) indicate that our field is associated with particles having the masses

$$m_0=\hbar\mu_0/c \quad \text{and} \quad m_1=\hbar\mu_1/c. \quad (4.4)$$

To avoid particles of complex mass, Eqs. (3.4) and (3.5) require that

$$2a\mu\leq 1. \quad (4.5)$$

By expressing all the quantities in (2.3) in terms of Fourier amplitudes and carrying out the

[12] G. Rayski, Phys. Rev. **70**, 573 (1946).

[13] In this paper bars are used in place of tildas.

integrations over all space we obtain, after a tedious calculation, the Hamiltonian

$$\bar{H}=\gamma\int[k_0^2(\varphi_\alpha\varphi_\alpha^*+\varphi_\alpha^*\varphi_\alpha)$$
$$-k_1^2(\bar{\varphi}_\alpha\bar{\varphi}_\alpha^*+\bar{\varphi}_\alpha^*\bar{\varphi}_\alpha)]d\mathbf{k}. \quad (4.6)$$

5. QUANTIZATION AND AUXILIARY CONDITIONS

Accepting (4.6) as the quantum-mechanical Hamiltonian, we may obtain the commutation rules for amplitudes by requiring that

$$\dot{\varphi}_\alpha(\mathbf{r},t)=(i/\hbar)[\bar{H},\varphi_\alpha(\mathbf{r},t)]. \quad (5.1)$$

Expressing both sides in terms of Fourier integrals and equating coefficients of corresponding exponentials, gives

$$[\varphi_\alpha^*(\mathbf{k}),\varphi_\beta(\mathbf{k}')]=-\delta_{\alpha\beta}\delta(\mathbf{k}-\mathbf{k}')ch/2k_0\gamma, \quad (5.2)$$

and

$$[\bar{\varphi}_\alpha^*(\mathbf{k}),\bar{\varphi}_\beta(\mathbf{k}')]=\delta_{\alpha\beta}\delta(\mathbf{k}-\mathbf{k}')ch/2k_1\gamma. \quad (5.3)$$

To reduce the number of degrees of freedom of the field, we take as auxiliary conditions on our wave functional

$$C(\mathbf{k})\psi=[Q(\mathbf{k})-\phi(\mathbf{k})]\psi=0, \quad (5.4)$$

$$\bar{C}(\mathbf{k})\psi=[\bar{Q}(\mathbf{k})-\bar{\phi}(\mathbf{k})]\psi=0, \quad (5.5)$$

and their complex conjugates where

$$[Q^*(\mathbf{k}),Q(\mathbf{k}')]=-\delta(\mathbf{k}-\mathbf{k}')ch/2k_0\gamma, \quad (5.6)$$

and

$$[\bar{Q}^*(\mathbf{k}),\bar{Q}(\mathbf{k}')]=\delta(\mathbf{k}-\mathbf{k}')ch/2k_1\gamma. \quad (5.7)$$

This insures that $C(\mathbf{r},t)$ commutes with $C(\mathbf{r}',t')$ taken at another space-time point.

When nucleons are present in the field, the modified auxiliary conditions are

$$C(\mathbf{k})\psi=[Q(\mathbf{k})-\phi(\mathbf{k})+f(\mathbf{r}_s,t_s)/2k_0^2\gamma]\psi=0, \quad (5.8)$$

and

$$\bar{C}(\mathbf{k})\psi=[\bar{Q}(\mathbf{k})-\bar{\phi}(\mathbf{k})-\bar{f}(\mathbf{r}_s,t_s)/2k_1^2\gamma]\psi=0. \quad (5.9)$$

This modification is made so that $C(\mathbf{r},t)$ commutes with the operator $R_s-i\hbar\partial/\partial t_s$, where R_s, the sum of the relativistic Hamiltonian of the particle and the field-particle interaction, is given by

$$R_s=c\boldsymbol{\alpha}_s\cdot\mathbf{p}_s+m_sc^2\beta_s$$
$$+g_s\phi(\mathbf{r}_s,t_s)-g_s\boldsymbol{\alpha}_s\cdot\mathbf{A}(\mathbf{r}_s,t_s). \quad (5.10)$$

6. THE INTERACTION ENERGY

The extension of the mathematical formalism of Fock, given in GE III, may now be used to eliminate the scalar potential and part of the longitudinal component of the vector potential from the wave functional. We thus obtain for the static interaction of a system of particles

$$V=\sum'_{s,u}(g_sg_u/8\pi\gamma R)(e^{-\mu_0R}-e^{-\mu_1R}), \quad (6.1)$$

and the static self-energy of a single particle

$$V_s=g^2/8\pi a(1+2a\mu)^{\frac{1}{2}}. \quad (6.2)$$

These are in agreement with the results obtained classically. Applying the procedure given at the end of GE III and beginning of GE IV gives, as the wave equation for a system of particles,

$$\{\sum_s[c\boldsymbol{\alpha}_s\cdot\mathbf{p}_s-g_s\boldsymbol{\alpha}_s\cdot\mathbf{D}(\mathbf{r}_s,t)+m_sc^2\beta_s$$
$$+g_s^2/8\pi a(1+2a\mu)^{\frac{1}{2}}]+\sum'_{s,u}(g_sg_u/8\pi\gamma R)$$
$$\times(e^{-\mu_0R}-e^{-\mu_1R})\}\Omega=[i\hbar\partial/\partial t]\Omega, \quad (6.3)$$

where

$$\mathbf{D}(\mathbf{k})=\mathbf{A}(\mathbf{k})-\mathbf{k}Q(\mathbf{k})/k_0$$

and

$$\bar{\mathbf{D}}(\mathbf{k})=\bar{\mathbf{A}}(\mathbf{k})-\mathbf{k}\bar{Q}(\mathbf{k})/k_1 \quad (6.4)$$

To calculate the dynamic interaction we write the wave equation (6.3) as

$$[H-i\hbar\partial/\partial t]\Omega=[\sum_s g_s\boldsymbol{\alpha}_s\cdot\mathbf{D}(\mathbf{r}_s,t)]\Omega, \quad (6.5)$$

and treat the right-hand side as a perturbation.

An analysis corresponding to that given in GE V gives as a first-order approximation the perturbation energy

$$U_d=-\sum_{s,u}(g_sg_u/16\pi^3\gamma)$$
$$\times\Big[\int\boldsymbol{\alpha}_s\cdot\boldsymbol{\alpha}_u\exp i\mathbf{k}\cdot\mathbf{R}(1/k_0^2-1/k_1^2)d\mathbf{k}$$
$$-\int(\boldsymbol{\alpha}_s\cdot\mathbf{k}/k)(\boldsymbol{\alpha}_u\cdot\mathbf{k}/k)$$
$$\times\exp i\mathbf{k}\cdot\mathbf{R}(k^2/k_0^4-k^2/k_1^4)d\mathbf{k}\Big]. \quad (6.6)$$

After integration this becomes

$$U_d=-\sum_{s,u}(g_sg_u/16\pi\gamma)\times\{\boldsymbol{\alpha}_s\cdot\boldsymbol{\alpha}_u(e^{-\mu_0R}-e^{-\mu_1R})/R+(\boldsymbol{\alpha}_s\cdot\mathbf{R}/R)(\boldsymbol{\alpha}_u\cdot\mathbf{R}/R)\times[e^{-\mu_0R}(\mu_0+1/R)-e^{-\mu_1R}(\mu_1+1/R)]\}. \quad (6.7)$$

The dynamic self-energy of a single particle is thus

$$U_{ds}=-\boldsymbol{\alpha}\cdot\boldsymbol{\alpha}g^2/16\pi a(1+2a\mu)^{\frac{1}{2}}=-3g^2/16\pi a(1+2a\mu)^{\frac{1}{2}}. \quad (6.8)$$

Considering the static terms, we have for the complete interaction

$$U=\sum'_{s,u}(g_sg_u/8\pi\gamma)\times\{(1-\boldsymbol{\alpha}_s\cdot\boldsymbol{\alpha}_u/2)(e^{-\mu_0R}-e^{-\mu_1R})/R-(1/2)(\boldsymbol{\alpha}_s\cdot\mathbf{R}/R)(\boldsymbol{\alpha}_u\cdot\mathbf{R}/R)\times[e^{-\mu_0R}(\mu_0+1/R)-e^{-\mu_1R}(\mu_1+1/R)]\}. \quad (6.9)$$

This result resembles in its spatial and spin dependence the interaction function used in several of the "mixed" theories of meson forces.[14] An important difference is the fact that the present interaction function contains no singularities. We also do not have as a factor the isotopic spin operator, as the isotopic spin formalism,[15] which seems to be necessary in order to predict the correct sign for the interaction energy, is not considered in this paper.

An equivalent expression for the interaction energy is

$$U=\sum'_{s,u}(g_sg_u/16\pi a^2\eta)\times[(1-\boldsymbol{\alpha}_s\cdot\boldsymbol{\alpha}_u/2)e^{-\eta R}\sinh\xi R/\xi R-(1/2)(\boldsymbol{\alpha}_s\cdot\mathbf{R}/R)(\boldsymbol{\alpha}_u\cdot\mathbf{R}/R)e^{-\eta R}(\sinh\xi R/\xi R+\eta R\sinh\xi R/\xi R-\cosh\xi R)], \quad (6.10)$$

where

$$\eta=(1+2a\mu)^{\frac{1}{2}}/2a \quad \text{and} \quad \xi=(1-2a\mu)^{\frac{1}{2}}/2a. \quad (6.11)$$

The complete self-energy is finite in contrast with the results of most relativistic theories. It is given by

$$U_s=-g^2/16\pi a(1+2a\mu)^{\frac{1}{2}} \quad (6.12)$$

Generalized electrodynamics is now a special case in which $\mu=0$ and $g=e$. With these constants Eq. (6.9) reduces to GE V (4.1). Letting $a=0$, this further reduces to Breit's formula, a result of ordinary quantum electrodynamics.

Placing $a=0$ in (6.9) gives

$$U=\sum'_{s,u}(g_sg_u/8\pi)\times[(1-\boldsymbol{\alpha}_s\cdot\boldsymbol{\alpha}_u/2)e^{-\mu R}/R-(1/2)(\boldsymbol{\alpha}_s\cdot\mathbf{R}/R)\times(\boldsymbol{\alpha}_u\cdot\mathbf{R}/R)e^{-\mu R}(\mu+1/R)]. \quad (6.13)$$

As might be expected, this result, apart from a matter of constants, is the same as that obtained from the ordinary Proca equations.

7. CONCLUSION

It appears from the present investigation that infinities and singularities may be removed from meson theory, just as in the case of electrodynamics, by allowing the Lagrangian to contain the second derivatives of the field coordinates.

The writer wishes to acknowledge his indebtedness to Dr. Boris Podolsky for his valuable suggestions and criticism.

[14] See references 1 and 2.

[15] B. Cassen and E. U. Condon, Phys. Rev. **50**, 846 (1936).

The Gravitational, Electromagnetic, and Vector Meson Fields and the Similarity Geometry

BANESH HOFFMANN
*The Institute for Advanced Study, Princeton, New Jersey**

(Received August 21, 1947)

It is shown that a special case of the general conformal geometry, called here the similarity geometry, forms the basis for a unitary theory of the gravitational, electromagnetic, and vector meson fields. The field equations are obtained from a simple four-dimensional, gauge invariant variational principle involving the curvature scalar of a basic second rank symmetric similarity tensor $S_{\sigma\tau}$. Since $S_{\sigma\tau}$ is here specialized, there is the possibility of incorporating further fields when the restrictions are removed.

I. INTRODUCTION

IN a recent paper, "The vector meson field and projective relativity,"[1] it was shown that the general projective geometry could be regarded as appropriate for the unitary description of the gravitational and vector meson fields. Since the general projective geometry had hitherto been used as the basis for unitary theories of the gravitational and electromagnetic fields,[2] this raised the question of the place of the electromagnetic field in such unitary theories. It was indicated that a unitary theory of the gravitational, electromagnetic, and vector meson fields might be constructed in terms of the general conformal geometry.

In the present paper it is shown that one can construct a unitary theory of the gravitational, electromagnetic, and vector meson fields in terms of a special case of the general conformal geometry. The field equations are obtained from a variational principle based on the curvature scalar formed from a fundamental symmetric second-rank tensor belonging to this geometry. Since this is done without exploiting the full resources residing in the tensor in question, the present paper is more an exploration than a complete discussion of the possibilities residing in the similarity geometry.

II. THE SIMILARITY GEOMETRY

The general conformal geometry treats of those geometrical objects which are invariant under transformations of the type

$$g_{ab}(x^c) \rightarrow \bar{g}_{ab}(x^c) = \rho^2(x^c) g_{ab}(x^c), \qquad (1)$$

where $g_{ab}(x^c)$ is the metrical tensor, and $\rho(x^c)$ is an arbitrary, non-zero function of position. The subject has been developed in some detail, the modern theory being attributable to E. Cartan, H. Weyl, J. M. Thomas, T. Y. Thomas, and others.[3] It has been found that the general conformal geometry of an n-dimensional space is concerned with the theory of projective tangent spaces of $(n+1)$ dimensions, in each of which lies an invariant n-dimensional quadric surface called a conformal tangent space.

The tensorial treatment employs entities, called conformal tensors, which have $(n+2)^k$ components. We are here concerned with the case $n=4$, and shall use the following conventions as to indices:

(a) Latin indices take on the range 1, 2, 3, 4, these pertaining to space-time.
(b) Greek indices from the beginning of the alphabet, as α, β, γ, δ, $\cdots$, take on the range 0, 1, 2, 3, 4, as in the projective theory of relativity.
(c) Greek indices from the later part of the alphabet, as π, ρ, σ, τ, $\cdots$, take on the range 0, 1, 2, 3, 4, 5. (We use 5 where the geometers, who deal with spaces of an arbitrary number of dimensions, n, use either the symbol $n+1$ or the symbol ∞.)

* On leave from Queens College, Flushing, New York.

[1] B. Hoffmann, Phys. Rev. 72, 458 (1947). This paper will be referred to as V.M.P.R.

[2] References to the work of Kaluza, Klein, Veblen, Hoffmann, Van Dantzig, Schouten, Einstein, Mayer, and Pauli are given in V.M.P.R.

[3] The present paper starts out from the treatment given by O. Veblen in his paper "Formalism for conformal geometry," Proc. Nat. Acad. Sci. 21, 168 (1935), which will be referred to as F.C.G. For a bibliography of papers on the subject, see, for example, the paper by K. Yano, "Sur la théorie des espaces à connexion conforme," J. Fac. Sci. Tokyo 4, 1 (1939).

A conformal tensor has components $K_\tau{}^{\sigma\cdots}{}_{\cdots}$ which, under a transformation of the space-time coordinates, x^a, and the gauge variable x^0, of the type

$$x^a \to \bar{x}^a = \bar{x}^a(x^b), \quad x^0 \to \bar{x}^0 = x^0 + \log\rho(x^a), \tag{2}$$

transform according to the law

$$K_\tau{}^{\sigma\cdots}{}_{\cdots}(x^a) \to \bar{K}_\tau{}^{\sigma\cdots}{}_{\cdots}(\bar{x}^a) = K_\rho{}^{\pi\cdots}{}_{\cdots}(\bar{x}^a(x^b))\, U_\tau{}^\rho \cdots V_\sigma{}^\pi \cdots, \tag{3}$$

where[4]

$$U_\tau{}^\sigma = \begin{array}{|c|c|c|} \hline \rho & \dfrac{\partial\rho}{\partial\bar{x}^b} & \tfrac{1}{2}\bar{g}^{ab}\rho\dfrac{\partial\log\rho}{\partial\bar{x}^a}\dfrac{\partial\log\rho}{\partial\bar{x}^b} \\ \hline O & \dfrac{\partial x^a}{\rho\,\partial\bar{x}^b} & \bar{g}^{bc}\dfrac{\partial x^a}{\partial\bar{x}^b}\dfrac{\partial\rho}{\partial\bar{x}^c} \\ \hline O & O & \dfrac{1}{\rho} \\ \hline \end{array}, \tag{4}$$

and

$$U_\rho{}^\pi V_\sigma{}^\rho = \delta_\sigma{}^\pi. \tag{5}$$

If, instead of (1), we consider the more restricted group of transformations

$$g_{ab}(x^c) \to \bar{g}_{ab}(x^c) = k^2 g_{ab}(x^c), \tag{6}$$

where k is independent of the coordinates, we have a special case of the general conformal geometry. Since the transformation (6) makes similar figures equivalent, we shall call this the similarity geometry, and shall use the term similarity tensor to denote a restricted type of conformal tensor subject to the above similarity transformations rather than to the full conformal group.

Setting $\rho = k$ in (2), (3), and (4), and making appropriate changes in the notation, we see that under a transformation of the coordinates x^a and the gauge variable x^0, of the type

$$x^a \to \bar{x}^a = \bar{x}^a(x^b), \quad x^0 \to \bar{x}^0 = x^0 + \log k, \tag{7}$$

the components, $S_\tau{}^{\sigma\cdots}{}_{\cdots}$, of a similarity tensor transform according to the law

$$S_\tau{}^{\sigma\cdots}{}_{\cdots}(x^a) \to \bar{S}_\tau{}^{\sigma\cdots}{}_{\cdots}(\bar{x}^a) = S_\rho{}^{\pi\cdots}{}_{\cdots}(\bar{x}^a(x^b))\, \tilde{U}_\tau{}^\rho \cdots \tilde{V}_\sigma{}^\pi \cdots, \tag{8}$$

where

$$\tilde{U}_\tau{}^\sigma = \begin{array}{|c|c|c|} \hline k & O & O \\ \hline O & k\dfrac{\partial x^a}{\partial\bar{x}^b} & O \\ \hline O & O & \dfrac{1}{k} \\ \hline \end{array}, \tag{9}$$

and

$$\tilde{U}_\rho{}^\pi \tilde{V}_\sigma{}^\rho = \delta_\sigma{}^\pi. \tag{10}$$

Introducing a new variable, x^5, we can now write

$$\tilde{U}_\tau{}^\sigma = k\frac{\partial x^\sigma}{\partial\bar{x}^\tau}, \tag{11}$$

where the six variables x^σ undergo transformations of the following type:

$$x^0 \to \bar{x}^0 = x^0 + \log k, \quad x^a \to \bar{x}^a = \bar{x}^a(x^b), \quad x^5 \to \bar{x}^5 = \frac{1}{k}x^5. \tag{12}$$

The introduction of a new variable in this way is not possible in the general conformal geometry.

Since the tangent spaces are projective in character, we may assign an index, as in the general projective theory, to each similarity tensor.[5] This allows us to use, instead of the matrix $\tilde{U}_\tau{}^\sigma$ given in (11), the simple Jacobian matrix

$$U_\tau{}^\sigma = \frac{\partial x^\sigma}{\partial\bar{x}^\tau}. \tag{13}$$

To conform with our previous equations we must make the index of a similarity tensor depend on the number of its covariant and the number of its contravariant indices.[6] Thus if

[4] F.C.G. pp. 169–70. We are writing ρ for the quantity there denoted by $U_0{}^0$.

[5] The idea of using an index in the general conformal geometry occurs explicitly in unpublished notes of O. Veblen.

[6] It is possible to generalize by relinquishing this requirement. In fact, it appears reasonable to introduce two different indices, the second one having to do with

$S_\tau\ldots^{\sigma\cdots}$ has p covariant and q contravariant indices, the index will be $(p-q)N$, where N is a fixed constant. The transformations (12) pertain to the case $N=1$. It is convenient, however, to have N explicitly present. Therefore we shall not take $N=1$ here, but shall instead make the appropriate modification by replacing (12) by

$$x^0\to\bar{x}^0=x^0+\frac{1}{N}\log k,\quad x^a\to\bar{x}^a=\bar{x}^a(x^b),$$
$$x^5\to\bar{x}^5=\frac{1}{k^2}x^5. \tag{14}$$

Thus the components of a similarity tensor $S_\tau\ldots^{\sigma\cdots}$ now are to have the form

$$e^{(p-q)Nx^0}\bar{S}_\tau\ldots^{\sigma\cdots}(x^a).$$

Under the transformation (14) they will transform according to the law

$$S_\tau\ldots^{\sigma\cdots}(x^a)\to\bar{S}_\tau\ldots^{\sigma\cdots}(\bar{x}^a)$$
$$=S_\rho\ldots^{\pi\cdots}(\bar{x}^a(x^\beta))\frac{\partial\bar{x}^\sigma}{\partial x^\pi}\cdots\frac{\partial x^\rho}{\partial\bar{x}^\tau}\cdots. \tag{15}$$

The part, $\bar{S}_\tau\ldots^{\sigma\cdots}$, of $S_\tau\ldots^{\sigma\cdots}$ which does not contain x^0 now behaves as if it transformed by means of the matrix in (9).

III. FIELD EQUATIONS FOR A SPECIAL CASE

Let $S_{\sigma\tau}$ be a second rank, symmetric similarity tensor of index $2N$, and let $S^{\sigma\tau}$ be defined by

$$S^{\sigma\pi}S_{\pi\tau}=\delta_\tau{}^\sigma. \tag{16}$$

We wish to consider the curvature scalar formed from $S_{\sigma\tau}$; but first we have to investigate the properties of the components of $S_{\sigma\tau}$.

Because, by (14),

$$\frac{\partial x^\sigma}{\partial\bar{x}^\tau}=\left|\begin{array}{c|c}\dfrac{\partial x^\alpha}{\partial\bar{x}^\beta} & O\\ \hline O & \dfrac{1}{k^2}\end{array}\right|, \tag{17}$$

the components $S_{\alpha\beta}$ of $S_{\sigma\tau}$ form a projective tensor of index $2N$, but of a restricted type in that the gauge transformations (14) do not involve the coordinates x^a. Also, S_{a5} and S_{55} transform according to the laws

$$S_{a5}(x^\gamma)\to\bar{S}_{a5}(\bar{x}^\gamma)=\frac{1}{k^2}S_{\beta5}(\bar{x}^\gamma(x^\delta))\frac{\partial x^\beta}{\partial\bar{x}^a}, \tag{18}$$

and

$$S_{55}(x^a)\to\bar{S}_{55}(\bar{x}^a)=\frac{1}{k^4}S_{55}(\bar{x}^a(x^\beta)). \tag{19}$$

We now specialize $S_{\sigma\tau}$ by requiring that

$$S_{05}=0, \tag{20}$$

and that

$$S_{55}/S_{00}\text{ be independent of }x^a. \tag{21}$$

Because of (14), (17), (18), and (19), these are invariant requirements. They are imposed here for the sake of simplicity. Removing these restrictions makes available two further field functions which we purposely ignore in this paper. We are here concerned with obtaining a quick result rather than with formulating a complete theory.

Write

$$s_{\sigma\tau}=S_{\sigma\tau}/S_{00}, \tag{22}$$

so that $s_{\sigma\tau}$ is of zero index, and $s_{00}=1$. Now write

$$\gamma_{\sigma\tau}=s_{\sigma\tau}-s_{\sigma5}s_{\tau5}/s_{55}, \tag{23}$$

so that $\gamma_{\sigma5}=0$, and $\gamma_{\alpha\beta}$ is a projective tensor, of zero index, such that $\gamma_{00}=1$. We identify this with the $\gamma_{\alpha\beta}$ in V.M.P.R. Thus γ_{a0} is the φ_a that forms part of the θ_a representing the vector meson field, and $(\gamma_{ab}-\varphi_a\varphi_b)$ is the gravitational metric g_{ab}.

Next we write

$$\psi_\sigma=s_{\sigma5}/(s_{55})^{\frac{1}{2}}, \tag{24}$$

so that by our specializing assumptions (20), (21),

$$\psi_0=0 \tag{25}$$

and, since $\psi_5=(s_{55})^{\frac{1}{2}}=(S_{55}/S_{00})^{\frac{1}{2}}$,

$$\psi_5\text{ is independent of }x^a. \tag{26}$$

Then ψ_a behaves like an affine vector while ψ_5 acquires a multiplying factor $1/k^2$ under the transformation (14).

the x^5 transformations. Since the index is related to the mass of the particle aspect of the field, this may be of importance in view of the different masses of the fundamental particles.

We may now express (23) in the form

$$s_{\sigma\tau}=\gamma_{\sigma\tau}+\psi_\sigma\psi_\tau, \tag{27}$$

or, more specifically,

$$s_{\alpha\beta}=\gamma_{\alpha\beta}+\psi_\alpha\psi_\beta, \quad s_{\alpha 5}=\psi_\alpha\psi_5, \quad s_{05}=\psi_0\psi_5=0. \tag{28}$$

Let $z_{\rho\sigma\tau}{}^\pi$ be the curvature tensor formed from $s_{\sigma\tau}$ according to the usual formula, and let $z_{\rho\tau}$ and z be its contractions. Then, since z is of zero index and a scalar, it must be gauge invariant.[7] Therefore we may compute z for a particular gauge. We choose the gauge so that ψ_5, which is independent of x^σ, shall have the value unity.

With $\psi_5=1$, the relation (27) between $s_{\sigma\tau}$, $\gamma_{\sigma\tau}$, and ψ_σ is of the same form as that between $\gamma_{\alpha\beta}$, $g_{\alpha\beta}$, and φ_α in the projective theory of relativity. In the projective theory, the curvature scalar B formed from $\gamma_{\alpha\beta}$ has the value

$$B=R-\varphi_b{}^a\varphi_a{}^b, \tag{29}$$

where R is the curvature scalar formed from g_{ab}. Therefore we may infer that the curvature scalar z formed from $s_{\sigma\tau}$ has the value

$$z=B-\psi_\beta{}^\alpha\psi_\alpha{}^\beta, \tag{30}$$

where

$$\psi_{\alpha\beta}=\frac{1}{2}\left(\frac{\partial\psi_\alpha}{\partial x^\beta}-\frac{\partial\psi_\beta}{\partial x^\alpha}\right), \tag{31}$$

and

$$\psi_\beta{}^\alpha=\gamma^{\alpha\gamma}\psi_{\gamma\beta}. \tag{32}$$

By (25), and the fact that ψ_σ is of index zero, we see that

$$\psi_{\alpha 0}=0. \tag{33}$$

So, since

$$\psi_\beta{}^\alpha\psi_\alpha{}^\beta=\psi^{\alpha\beta}\psi_{\beta\alpha},$$

we have

$$\psi_\beta{}^\alpha\psi_\alpha{}^\beta=\psi_b{}^a\psi_a{}^b. \tag{34}$$

Hence

$$z=B-\psi_b{}^a\psi_a{}^b, \tag{35}$$

or, using (29),

$$z=R-\varphi_b{}^a\varphi_a{}^b-\psi_b{}^a\psi_a{}^b. \tag{36}$$

Now let $Z_{\rho\sigma\tau}{}^\pi$ be the curvature tensor formed from $S_{\sigma\tau}$, let $Z_{\rho\tau}$ be the result of contracting with respect to the indices π and σ, and let Z be the curvature scalar formed by contracting again, this time by means of $S^{\rho\tau}$.

The relation (22) between $s_{\sigma\tau}$ and $S_{\sigma\tau}$ is of the same form as that between $\gamma_{\alpha\beta}$ and $G_{\alpha\beta}$ in the projective theory of relativity. In the projective theory the curvature scalar[8] $\bar{P}$ formed from $G_{\alpha\beta}$ has the value[9]

$$\bar{P}=\Phi^{-2}(B+2Nn\Phi^\alpha{}_{;\alpha}+N^2n(n-1)\Phi^\alpha\Phi_\alpha),$$

for the case $n=4$, (37)

where the semicolon denotes the covariant derivative with respect to $\gamma_{\alpha\beta}$, and indices are raised by means of $\gamma^{\alpha\beta}$. Therefore we may infer that the curvature scalar Z formed from $S_{\sigma\tau}$ has the value

$$Z=\Psi^{-2}(z+2Nn\Psi^\sigma{}_{/\sigma}+N^2n(n-1)\Psi^\sigma\Psi_\sigma),$$

for the case $n=5$, (38)

where

$$\Psi^2=S_{00}, \tag{39}$$

$$\Psi_\sigma=\frac{1}{N}\frac{\partial\log\Psi}{\partial x^\sigma}, \tag{40}$$

the solidus "/" denotes the covariant derivative with respect to $s_{\sigma\tau}$, and indices are raised by means of $s^{\sigma\tau}$.

Setting $n=5$ in (38), we have

$$Z=\Psi^{-2}(z+10N\Psi^\sigma{}_{/\sigma}+20N^2\Psi^\sigma\Psi_\sigma). \tag{41}$$

Since Ψ does not contain x^5, $\Psi_5=0$ and so

$$\Psi^\sigma\Psi_\sigma=\Psi^\alpha\Psi_\alpha. \tag{42}$$

And because Ψ corresponds to the quantity Φ of the projective theory, we have[10]

$$\Psi^\sigma\Psi_\sigma=\Psi^\alpha\Psi_\alpha=\Phi^\alpha\Phi_\alpha=1+\theta^a\theta_a, \tag{43}$$

where θ_a has the same significance as in V.M.P.R.

In order to simplify the quantity $\Psi^\sigma{}_{/\sigma}$ entering (41), we first calculate the value of the determinant s of $s_{\sigma\tau}$. By (24) and (27) we have

$$s=\begin{vmatrix}\gamma_{\alpha\beta}+\psi_\alpha\psi_\beta & \psi_5\psi_\alpha\\ \psi_5\psi_\beta & (\psi_5)^2\end{vmatrix}=\begin{vmatrix}\gamma_{\alpha\beta} & \psi_5\psi_\alpha\\ O & (\psi_5)^2\end{vmatrix}$$

$$=(\psi_5)^2\gamma=(\psi_5)^2g, \tag{44}$$

[7] Though multiplying factors involving k are brought in by changes of the variable x^5, the fact that z is a scalar and does not contain x^5 will make these factors cancel automatically.

[8] For the distinction between $\bar{P}$ and P, see V.M.P.R., Eqs. (18) and (19).

[9] We use the value of $P_{\alpha\beta}$ given by Veblen, Quart. J. Math. (Oxford) **1**, 60 (1930), Eq. (5.16), contracted by means of $G^{\alpha\beta}$.

[10] Cf. reference 9, Eqs. (5.3) and (5.8).

since $\gamma = g$. Thus, because of (26), and since neither s nor Ψ^σ contains x^0 or x^5,

$$\Psi^\sigma{}_{/\sigma} = \frac{1}{(s)^{\frac{1}{2}}} \frac{\partial((s)^{\frac{1}{2}}\Psi^\sigma)}{\partial x^\sigma} = \frac{1}{(g)^{\frac{1}{2}}} \frac{\partial((g)^{\frac{1}{2}}\Psi^a)}{\partial x^a}. \quad (45)$$

Again, by (22), the determinant S of $S_{\sigma\tau}$ is given by

$$S = (S_{00})^6 s = \Psi^{12} s. \quad (12)$$

Following the same general procedure as in V.M.P.R., we set up a four-dimensional, gauge-invariant variational principle containing the curvature scalar Z. Since $Z_{\sigma\tau}$ is of zero index, Z is of index $-2N$. By (46), $(S)^{\frac{1}{2}}$ is of index $6N$. Hence the quantity $Z(S)^{\frac{1}{2}}$ is of index $4N$. To obtain a quantity of index zero we divide by an appropriate power of Ψ, which is a part of the fundamental tensor $S_{\sigma\tau}$. Thus we consider the quantity $Z(S)^{\frac{1}{2}}/\psi_5\Psi^4$, which, being of index zero, is an affine scalar density, by (44).

We now write the four-dimensional, affine variational principle

$$\delta \int (Z(S)^{\frac{1}{2}}/\psi_5\Psi^4) dx^1 dx^2 dx^3 dx^4 = 0, \quad (47)$$

for variations of either $S_{\sigma\tau}$ or $s_{\sigma\tau}$.

Writing $\hat{Z}$ for the affine quantity $\Psi^2 Z$, we may express (47) in the form

$$\delta \int \hat{Z}(g)^{\frac{1}{2}} dx^1 dx^2 dx^3 dx^4 = 0. \quad (48)$$

Later, as in the corresponding situation in V.M.P.R., we shall introduce a slight modification of this variational principle.

Since lemmas analogous to those in V.M.P.R. are valid here, we shall merely perform the variation of g_{ab}, φ_a, ψ_a. Because of the restrictions imposed on $S_{\sigma\tau}$ in the present paper, these variations suffice to give the essential field equations in their affine groups.

By (41), (44), and (46), we may write (47) in the form

$$\delta \int (z + 10N\Psi^\sigma{}_{/\sigma} + 20N^2\Psi^\sigma\Psi_\sigma)(g)^{\frac{1}{2}} \times dx^1 dx^2 dx^3 dx^4 = 0, \quad (49)$$

and, using the explicit values in (36), (43), and (45), we have

$$\delta \int \left\{ R - \varphi_b{}^a\varphi_a{}^b - \psi_b{}^a\psi_a{}^b + 10N \frac{1}{(g)^{\frac{1}{2}}} \frac{\partial((g)^{\frac{1}{2}}\Psi^a)}{\partial x^a} + 20N^2(1 + \theta^a\theta_a) \right\} (g)^{\frac{1}{2}} dx^1 dx^2 dx^3 dx^4 = 0. \quad (50)$$

Since variations vanish at the boundary, it follows from Green's theorem that the term $10N\partial((g)^{\frac{1}{2}}\Psi^a)/\partial x^a$ in the integrand of (50) will contribute nothing to the field equations. As for the other terms, they are all of familiar types for which the results of the variations are already known. Thus the term $R(g)^{\frac{1}{2}}$ is the Lagrangian density for the gravitational field in general relativity, the term $(-\psi_b{}^a\psi_a{}^b)(g)^{\frac{1}{2}}$ is the Lagrangian density for the electromagnetic field, the terms $(-\varphi_b{}^a\varphi_a{}^b + 20N^2\theta^a\theta_a)(g)^{\frac{1}{2}}$ constitute the Lagrangian density for the vector meson field, and the term $20N^2(g)^{\frac{1}{2}}$ corresponds to the term $12N^2(g)^{\frac{1}{2}}$ in Eq. (42) of V.M.P.R. and has the same general significance. As in V.M.P.R., we can remove this term by replacing the variational principle in the form (48) by

$$\delta \int (\hat{Z} - 20N^2)(g)^{\frac{1}{2}} dx^1 dx^2 dx^3 dx^4 = 0. \quad (51)$$

By use of the known results[11] of the variations for the individual terms, and introducing the quantity θ_{ab} defined in Eq. (53) of V.M.P.R., we see that the field equations arising from (51) may be grouped into the following affine sets:

$$(R^{ab} - \tfrac{1}{2}g^{ab}R) + 2(g^{cd}\psi_c{}^a\psi_d{}^b + \tfrac{1}{4}g^{ab}\psi_d{}^c\psi_c{}^d) + \{\tfrac{1}{2}(g^{cd}\theta_c{}^a\theta_d{}^b + \tfrac{1}{4}g^{ab}\theta_d{}^c\theta_c{}^d) - 20N^2(\theta^a\theta^b - \tfrac{1}{2}g^{ab}\theta^c\theta_c)\} = 0, \quad (52)$$

$$\psi^{ab}{}_{,b} = 0, \quad (53)$$

and

$$\theta^{ab}{}_{,b} + 20N^2\theta^a = 0, \quad (54)$$

the commas denoting covariant derivatives with respect to g_{ab}.

Equations (53) are the Maxwell field equations in general relativity in the absence of matter, Eqs. (54) are the vector meson field equations in general relativity in the absence of matter, and Eqs. (52) are the field equations of general relativity linking additively the stress-energy-momentum tensors of the gravitational, electromagnetic, and vector meson fields. Thus we have shown that three physically identifiable fields

[11] Cf. V.M.P.R. Section 4.

are contained in the specialized similarity tensor $S_{\sigma\tau}$, and that their field equations are obtainable in a unitary manner from a simple variational principle based on the curvature scalar of $S_{\sigma\tau}$. Though the Lagrangian of the total field turns out to be the sum of the Lagrangians of the three constituent fields, there has here been no arbitrary addition of three partial Lagrangians to form this total Lagrangian.

It is natural to ask what could happen if the restrictions on $S_{\sigma\tau}$ were removed. It is clear that new field quantities would appear, but whether these would prove to have physical significance recognizable in the present state of theoretical physics cannot be decided without further investigation. One would expect to obtain field equations of which those of the present paper are a special case. Yet relinquishing the present restriction that S_{05} be zero greatly increases the difficulty of making a proper dissection and physical interpretation of the constituents of $S_{\sigma\tau}$, not to mention of calculating its curvature scalar, and it is possible that the physical identifications of the present paper might need to be modified. On the geometrical side, one can see the key role of the component S_{05}, for when this component is zero one cannot directly set up a $g_{\sigma\tau}$ of the sort found in the conformal geometry, namely,

$$g_{\sigma\tau} = \begin{vmatrix} 0 & 0 & -1 \\ 0 & g_{ab} & 0 \\ -1 & 0 & 0 \end{vmatrix}. \qquad (55)$$

One could imagine that in the present paper there is a vestigial field having the constant value $+1$ which just cancels the -1's that occur in $g_{\sigma\tau}$. But when S_{05} does not vanish we are able to normalize $S_{\sigma\tau}$ by dividing through by $-S_{05}$, thus obtaining the -1's in a natural manner not available to us here. If it should turn out that this was the proper way to normalize $S_{\sigma\tau}$, the vanishing of S_{05} would imply that we had here a non-trivially degenerate theory, and it might be this fact that lay behind the appearance of well-known infinities in solutions of the present equations.

The idea of treating the conformal geometry of n dimensions by means of conformal tensors having $(n+2)^k$ components arose naturally from the character of the conformal group itself and was developed by the geometers without reference to physical theory. Moreover, there is a close connection between the conformal geometry and the similarity geometry, on the one hand, and the geometry of spinors and the Lorentz group on the other.[12] On the physical side, the gravitational, electromagnetic, and vector meson fields entered physical theory by widely separated paths. The present confluence of such diverse mathematical and physical concepts may well be more than a coincidence.

I wish to thank Professor O. Veblen for many stimulating discussions.

[12] See O. Veblen, Proc. Nat. Acad. Sci. **19**, 503 (1933), and F.C.G. Section 5. Also P. A. M. Dirac, Proc. Roy. Irish Acad. **50**, 261 (1945). In all cases one finds the geometrical picture of an invariant four-dimensional quadric surface in a five-dimensional projective space.

The Energy Levels of Sodium Chloride

E. FISHER
University of Wyoming, Laramie, Wyoming
(Received April 7, 1947)

An energy-level scheme is given for sodium chloride. Its predictions are compared with observations in the ultraviolet and x-ray regions and color-center phenomena.

WAVE-MECHANICAL calculations[1] have fallen far short of even a consistent qualitative explanation of the data on the energy levels of sodium chloride. And NaCl models[2] set up to interpret individual experiments fail to explain other results. For the present work all the experimental results available were subjected to a consistent wave-mechanical interpretation. This led to the energy-level scheme of Figs. 1–3.

A lattice of Na^+ ions and Cl atoms is assumed. The Cl $3p$ band contains only the five $3p$ electrons of a Cl atom, the valence electron being in a higher band. Compared to the Cl $3p$ electrons, the valence electron is relatively free, and its wave function near a Na^+ ion much larger. The energy-level density of the Cl $3p$ band has two sharp maxima, the $^2P_{3/2}$ and $^2P_{1/2}$ peaks. Similar peaks of atomic Cl and Na origin are in the first Cl conduction band. The levels and peaks of atomic Na, Cl, and Na^+ origin are not displaced.[3] Allowed energy levels,[4] bound levels,[5] and two effects of temperature are used. In the energy effect, the allowed energy of a discrete level whose wave function is of small radius depends on boundary conditions that are sensitive to the thermal motion of neighboring atoms. The momentum effect enables an electron trapped as a standing wave at one lattice point to escape, as a running wave, to another. Transition probabilities for the peaks of the Cl $3p$ and conduction bands are much greater than for their other levels. Transitions involving the bound levels are strong, and the valence levels—of wave-mechanical origin—very weak. Selection rules are carried over from the atomic Na, Na^+, and Cl spectra. Cross transitions are appreciable, being especially strong from the Cl to the low Na $3s$ levels.

The reasoning by which the energy-level scheme was derived is omitted for brevity. Instead, the predictions of the model are checked against observation. The number in each level of Figs. 1 to 3 is its energy in ev above or below the weighted mean of the $^2P_{3/2,1/2}$ peaks.

The edges of the Cl conduction band are fixed by photo-conductivity and photoelectric data[6]—the edges vary (dashed lines, Fig. 1) with lattice direction. Transitions from the $^2P_{3/2,1/2}$ peaks to Cl peaks in the conduction band explain the low energy fine structure observed[6] in the photoelectric current; but numerical agreement fails because of complexity in the atomic Cl levels,[3] overlapping of bound levels for other lattice directions into the band, and actual uncertainty in the data. Owing to transitions to the Na $4s$, $3d$, $5s$, and $4d$ peaks, structure is expected[3] at 11.04 ev, 11.47 ev, 11.97 ev, and 12.13 ev, and is observed[6] at 11.07 ev, 11.45 ev, 11.86 ev, and 12.02 ev. At shorter wave-lengths a sharp fall is predicted in photoelectric current because transitions are then to higher Na and Cl levels; this is observed[6] exactly. Structure is neither observed nor expected from the Na $3p$ and $4p$ peaks because of their large transition probability to the Na $3s$ level. Similar secondary effects greatly distort the photo-conductive current.

Three strong absorption bands are expected, due to transitions from the $^2P_{3/2,1/2}$ peaks to the Na $3s$ level, to the bound levels below the Cl conduction band and the Cl levels in the band, and to the Na $4s$ and higher peaks. The first two

[1] J. C. Slater and W. Shockley, Phys. Rev. **50**, 705 (1936); S. R. Tibbs, Trans. Faraday Soc. **35**, 1471 (1939).
[2] N. F. Mott, Trans. Faraday Soc. **34**, 500 (1938); H. M. O'Bryan and H. W. B. Skinner, Proc. Roy. Soc. **176**, 229 (1940).
[3] R. F. Bacher and S. Goudsmit, *Atomic Energy States* (McGraw-Hill Book Company, Inc., New York, 1932).
[4] A. Sokolow, Zeits. f. Physik **90**, 520 (1934).
[5] J. Frenkel, Physik. Zeits. Sowjetunion **9**, 158 (1936).
[6] J. N. Ferguson, Phys. Rev. **66**, 220 (1944).

are observed[7] at 1580A and 1280A, but data are not available to test the third. The width of the 1580A band results from the energy effect of temperature on the Na 3*s* level; transitions to this level in its lowest position (dashed line, Fig. 1) start strong absorption. A sharp drop in absorption is expected at 1000A because of much weaker transitions to higher levels; a decrease "below 1100A" has been reported.[8] Structure in the bands is also expected, and there is evidence[2] that the 1580A peak is a doublet due to the $^2P_{3/2,1/2}$ peaks.

Similarly, there are three types of weak optical transition: from valence band to Na 3*s* level, to bound levels, and to Na peaks. The first, however, is impossible because the Na 3*s* level bound to a Na^+ lattice point does not remain an allowed level when a positive hole is added to the point. Absorption of the second type should start at 5.5 ev; this agrees with the long-wave-length limit observed[9] for the weak "tail" in absorption. The third type is hidden under strong absorption from the $^2P_{3/2,1/2}$ peaks. Negligible primary photo-conductivity is expected, and none is observed.[6]

Ultra-soft x-ray absorption is predicted by transitions from the Na^+ 2*p* band to higher levels: the strongest line at 33.3 ev, due to the Na^+ 3*s* level, two lines at 35.1 ev and 36.8 ev, due to the Na 3*s* level and to the bound levels of the Cl conduction band, respectively, a weaker line at 38.7 ev, due to the Na peaks of the Cl band, and a wide band from about 41 ev to 47 ev, due to the Na^+ conduction band.[3] These are observed[8] exactly, except for the weak 38.7 ev line lost in the very strong background.

Transitions to the Cl *K* level from the $^2P_{3/2,1/2}$ peaks produce the x-ray Cl $K\beta_1$ line. Other *K* emission lines are predicted, due to transitions from the Na 2*p* level and the middles of the Na^+ 2*p* and valence bands; these are observed[10] as the $K\beta_1$, η, and β_x lines, respectively. Also ob-

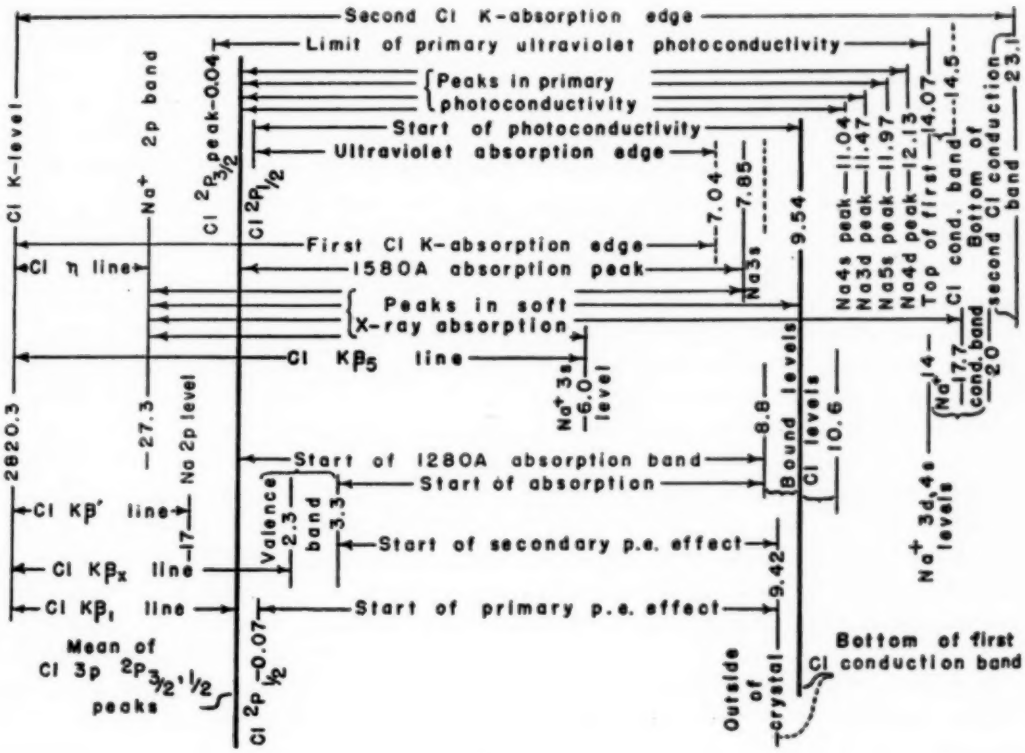

FIG. 1.

[7] E. G. Schneider and H. M. O'Bryan, Phys. Rev. **51**, 293 (1937).
[8] H. M. O'Bryan, Phys. Rev. **57**, 995 (1940).
[9] A. L. Hughes, Rev. Mod. Phys. **8**, 294 (1936).
[10] J. Valasek, Phys. Rev. **53**, 274 (1938).

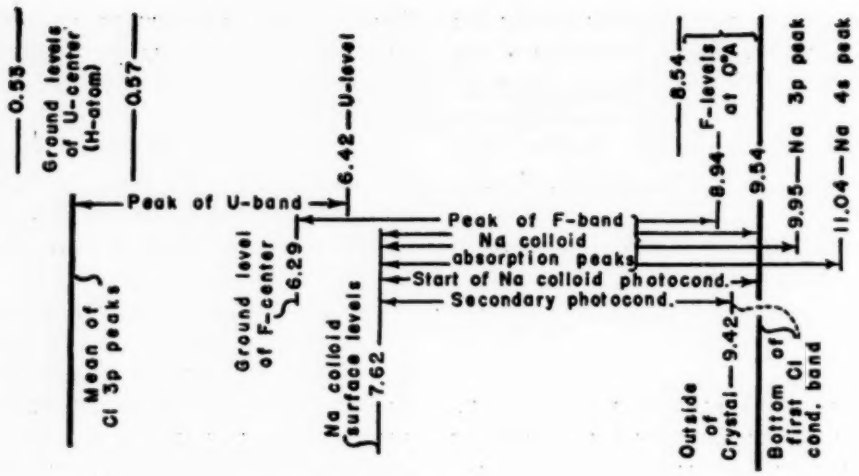

FIG. 2.

served is a $K\beta_5$ line, 6.0 ev higher than the $K\beta_1$: the model can explain this by Na^+ electrons raised to the Na^+ 3*s* level during excitation. There are no more lines like the $K\beta_5$ because they would lie inside the Cl *K* edge and be strongly absorbed.

Strong x-ray absorption from the Cl *K* level starts with transitions to the Na 3*s* level. So, the *K* edge is 7.04 ev above the $K\beta_1$ line; this agrees with the observation[11] of 7.06 ev. A second observation,[12] 0.4 ev higher, is explained as follows: temperature widening of the Na 3*s* level causes absorption in the *K* edge to increase rapidly over 0.8 ev, and low resolving power in the second observation placed the *K* edge at the middle of this range. Strong absorption is expected up to the top of the first Cl conduction band, that is, for 7.0 ev, taking account of all lattice directions (dashed line, Fig. 1). Then comes weak absorption to the Na^+ band because of Na^{++} ions. Experiment[12] confirms this. Also, it shows a second *K* edge,[12] which is the basis for the second Cl conduction band. Fine structure is predicted in the first *K* edge, due to Na 3*s* level, bound levels, and Cl conduction-band peaks; there are no data on this.

There is evidence[13] that in sodium the unallowed range between the first and second Brillouin zones, as well as the overlap of occupied levels from first zone to second, are both about 0.1 ev. This means a range of bound levels[5] and surface levels[14] of width less than 0.1 ev, that are occupied by electrons. Transitions from these bound levels are assumed much stronger than from zone levels. Application to bulk sodium, e.g., the absorption edge[15] at 2100A, is omitted for brevity. For violet rocksalt, colored by Na colloids, the bound Na levels—their width is neglected—are fixed by the start of photo-conductivity observed[16] at 1.92 ev. Then absorption bands are predicted because of transitions from these Na levels to the Na 3*s* level at 0.23 ev, to bound levels of the Cl conduction band at 1.92 ev, and to the Na 3*p*, 4*s*, etc., peaks at 2.33 ev, 3.42 ev, etc. Also, since the colloids originate from the diffusion of Na^+ ions and *F* centers to lattice flaws, the *F* band at 2.65 ev[9] is expected. There are no data in the infra-red. Absorption peaks are observed[16] at 1.92 ev, 2.35 ev, 2.80 ev, and 3.36 ev. Since *F* and Na-peak bands are widened toward each other, and resolving power is insufficient to separate the higher Na peaks, the agreement is satisfactory. Structure in photo-conductivity at 1.92 ev and 2.33 ev is neither observed[16] nor expected, because transitions in the 1.92-ev band are predominantly to bound levels, and secondary transitions from Na 3*p* peak to Na 3*s* level are very strong.

An *F* center[17] in the present model is an elec-

[11] O. Stelling, Zeits. f. Physik **50**, 506 (1928).
[12] A. E. Lindh, Physik. Zeits. **28**, 93 (1927).
[13] H. W. B. Skinner, Phil. Trans. Roy. Soc. **239**, 95 (1940).
[14] E. T. Goodwin, Proc. Camb. Phil. Soc. **35**, 205 (1939).
[15] R. W. Wood, Phys. Rev. **44**, 353 (1933).
[16] Z. Gyulai, Zeits. f. Physik **35**, 411 (1926).
[17] J. H. deBoer, Rec. Trav. Chim. Pays-Bas **56**, 301 (1937).

tron bound at a lattice point where a Cl atom is missing, and a U center[18] is a hydrogen atom at such a point. The ground state of the U center is widened by interaction with Cl atoms. The F and U levels and absorption peaks in Fig. 2 are fixed by experiment.[9,19] Then the yield of F centers from U centers by U band absorption should decrease at higher temperatures, and heat alone should reproduce U centers from such F centers. This is observed[20]—at too high temperatures the hydrogen escapes to lattice flaws. F center photo-conductivity[9] below the Cl conduction band is due to the very large radius of the wave function (loose binding) of an electron in an F center. The momentum effect of temperature explains the decrease observed at low temperatures in F center photo-conductivity,[21] and in the yield of F centers from ultraviolet absorption[22] and U band absorption.[20]

Secondary photo-conductivity has been attributed[23] to metallic filaments. Assuming that these are strings of Na colloids, then electrons move in the empty valence levels of the colloids which start at 1.80 ev below the outside of the crystal. This agrees with the observation[24] of currents in levels down to 1.8 ev below the outside. Surface polarization is assumed to strengthen the transitions of valence electrons at the surface; so a secondary photoelectric effect is expected to start at 6.1 ev. This has been observed,[25] starting at 6 ev.

Adjacent vacant Cl lattice points afford a means of dielectric breakdown at 0°A. A very wide, shallow, potential valley is at each flaw. An electric field narrows and lowers the potential hill between them, and lowers the energy levels of the second below the first. For a lowering of 2.25 ev an electron in the ground F level of the

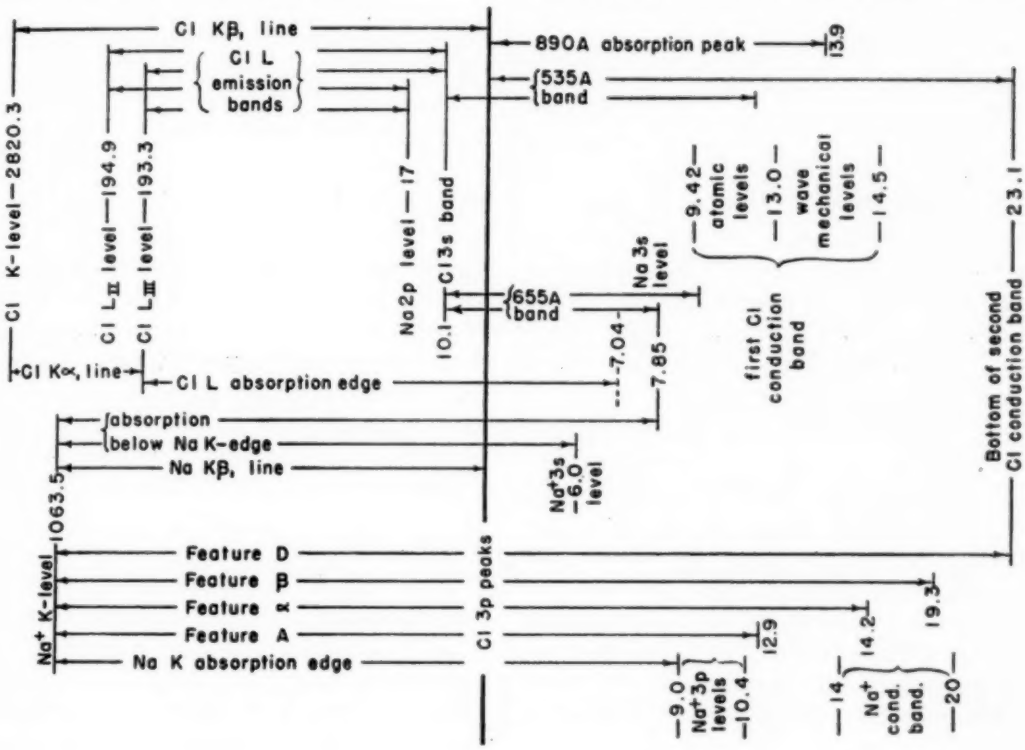

FIG. 3.

[18] R. Hilsch and R. W. Pohl, Göttinger Nachrichten **2**, 139 (1936).
[19] E. Mollwo, Göttinger Nachrichten **254** (1932).
[20] R. Hilsch and R. W. Pohl, Göttinger Nachrichten 322 (1933) and **1**, 115 (1934).
[21] R. W. Pohl, Proc. Phys. Soc. **49**, 3 (1937).
[22] R. Hilsch and R. W. Pohl, Göttinger Nachrichten 406 (1933).
[23] A. L. Hughes and L. A. Dubridge, *Photoelectric Phenomena* (McGraw-Hill Book Company, Inc., New York, 1932), Chapter 8.
[24] N. Kalabuchow, Zeits. f. Physik. **92**, 143 (1934).
[25] P. Lukirsky, N. Gudris and L. Kulikowa, Zeits. f. Physik **37**, 308 (1926).

first gets into the upper F levels of the second, from which it gets to conduction levels by repeating the process or by other means.[26] Although this reasoning neglects the effect of excess charge on the field, and of the field on the F levels, a simple calculation strongly confirms it. For an average separation between lattice points based on a density of 10^{16}/cc (obtained from F band measurements[9]), a minimum field of 4.8×10^5 volt/cm is needed, while extrapolation to 0°A of observed breakdown strength[26] gives 4.6×10^5 volt/cm.

Addendum. Figure 3 resulted from additional observations on x-ray emission[27] and ultraviolet absorption,[28] and from the suggestion[29] that the model be applied to data on x-ray absorption[30] and emission[31] by Na in NaCl.

The Cl L_{III} level was determined from the Cl $K\beta_1$ line[10] and the Cl $K\alpha_1$ line.[32] The L_{II} level and middle of Cl $3s$ band were then obtained from the Cl L emission bands observed[27] for LiCl and KCl, the structure common to both being assumed also for NaCl. The model then predicts the weak band observed[27] at about 177 ev by transitions to the Cl $L_{II,III}$ levels from the Na $2p$ level (produced by absorption in the Cl L edge). The separation of Cl $3p$ and Cl $3s$ is 2 ev less than that calculated by wave mechanics.[1]

Absorption bands have been observed[28] with maxima at 350A, 535A, 655A, and 890A. These data were discredited[7] because the absorption below 1000A was greater than that above. However, the 350A band coincides with the soft x-ray absorption peaks of Fig. 2. Therefore, it is assumed that only the intensity scale of these data is wrong, which leaves the structure approximately unchanged. Then the model also predicts the other three bands. The levels of atomic Na and Cl origin in the first Cl conduction band end[3] at 13.0 ev. Weak transitions from the Cl $^2P_{3/2,1/2}$ peaks to still higher levels—of wave-mechanical origin—produce the 890A band. A corresponding band, distorted by secondary effects, is expected in the photoelectric current, and is observed.[6] Other weak transitions expected are: from Cl $3s$ band to Na $3s$ level, to bound levels and Cl peaks of the first Cl conduction band, to Na peaks and higher levels of this band; from Cl $3p$ peaks to the second Cl conduction band, and from Cl $3s$ to this band. Of these five transitions, the first two generate the 655A band, so that it should be resolvable into a doublet, and the next two make up the 535A band. The fifth is hidden under stronger absorption from the Na^+ $2p$ band (Fig. 2).

The strongest x-ray absorption from the Na^+ K level starts with transitions to the Na^+ $3p$ levels. This interpretation requires that the observed[30] Na K edge be reduced by 3.0 ev, so that it will lie at the peak of the photometer curve.[30] Considerable structure is observed[30] above the Na K edge, the "features" of which are explained by the model. Strong absorption from the Na K edge to feature A is associated with strong transitions from the Na^+ K level to Na^+ $3p$ levels and Na peaks of the Cl conduction band, weaker absorption from A to α, with the wave-mechanical levels of the Cl band, absorption from α to β—first increasing, and then decreasing—with the Na^+ conduction-band levels, and the maximum at D, with transitions to the bottom of the second Cl band. The structure between β and γ is explained by additional levels, of wave-mechanical origin, on top of the Na^+ band, and the lowering of α from 14.5 to 14.2 ev, by overlapping of Cl and Na^+ bands. Transitions from the Na^+ K level to Na $3s$ and Na^+ $3s$ contribute to the weak absorption[30] just below the K edge. The Na $K\beta_1$ line, due to transitions to the Na^+ K level from Cl $3p$, is expected 12.0 ev below the uncorrected Na K-edge, and this is observed[31] exactly. A weaker line is also expected from the valence band.

Finally, the wave-mechanical evidence[5] for bound levels at the bottom of the first Cl conduction band is completely satisfactory only for levels bound to large lattice flaws[33]—e.g., Na colloids. The levels bound to Cl and Na^+ centers are better assumed of atomic origin, starting[3] at 8.88 ev and 9.03 ev above the Cl $^2P_{3/2,1/2}$ mean, respectively.

[26] A. v. Hippel and G. M. Lee, Phys. Rev. **59**, 824 (1941).
[27] H. M. O'Bryan and H. W. B. Skinner, Proc. Roy. Soc. **176**, 229 (1940).
[28] A. Smith, Phys. Rev. **44**, 520 (1933).
[29] The author takes pleasure in thanking Prof. J. Valasek for this suggestion.
[30] K. C. Rule, Phys. Rev. **66**, 199 (1944).
[31] T. Wetterblad, Zeits. f. Physik **42**, 603 (1927).
[32] A. H. Compton and S. K. Allison, *X-Rays in Theory and Experiment* (D. Van Nostrand Company, Inc., New York, 1935), Appendix V, Table II.
[33] A. Sokolow and N. Machalowa, Zeits. f. Physik **99**, 503 (1936).

Penetrating Showers in Lead*

W. B. FRETTER
Department of Physics, University of California, Berkeley, California
(Received September 16, 1947)

Production of penetrating showers in lead has been observed in a cloud chamber containing eight ½-inch thick lead plates. In over half of the 53 examples of penetrating showers photographed high, energy electronic radiation was simultaneously produced. Many examples of mesons accompanying air showers were observed, but no production of penetrating particles in lead by electronic radiation was observed. The pictures taken give general support to recent theoretical speculations that the primary radiation produces penetrating particles and electronic radiation in the same event.

I. INTRODUCTION

THE production of penetrating showers by cosmic rays has been observed by means of counters[1–9] and cloud chambers.[10–31] Only with a cloud chamber can any identification of individual particles be made. Since the processes involved in penetrating showers in lead may be similar to those occurring in the production of penetrating particles such as mesons in the upper atmosphere, it is of considerable interest to make some attempt at identification and analysis. Protons and mesons can be distinguished if they are near the end of their range, while high energy electrons make cascade showers in lead. Protons and mesons of high energy may act differently in one respect: Protons may make meson showers.

It is desirable to be able to trace the shower of penetrating particles from the beginning to the end, and observe the entire event in a cloud chamber. In practice, the high energies of the particles created make this impossible in many cases. The present experiment was designed for observation of the initial event, with as much lead as possible in the cloud chamber for identification of the particles. All pictures were taken at sea level with only a thin roof of sheet metal and wood over the cloud chamber.

II. APPARATUS

The cloud chamber was 16 inches in diameter, 9 inches deep, and contained eight ½-inch thick lead plates, 8 inches wide. These were supported from ½-inch slabs of Lucite and were tilted so that the camera viewed them all end-on. One of the difficulties with multi-plate cloud chambers has been the lateral displacement of tracks in the chamber because of irregular motion of the gas during expansion. The Lucite side plates seemed to prevent this effect, and removed one source of confusion in the analysis of showers. The plates

* This work was supported in part by the Office of Naval Research.

[1] L. Janossy and P. Ingleby, Nature **145**, 511 (1940).
[2] G. Wataghin, M. D. de Souza Santos, and P. A. Pompeia, Phys. Rev. **57**, 61 (1940).
[3] M. D. de Souza Santos, P. A. Pompeia, and G. Wataghin, Phys. Rev. **59**, 902 (1941).
[4] L. Janossy, Proc. Roy. Soc. **A179**, 361 (1942).
[5] P. Auger and J. Daudin, Phys. Rev. **61**, 549 (1942).
[6] L. Janossy and G. D. Rochester, Nature **150**, 633 (1942).
[7] L. Janossy, Phys. Rev. **64**, 345 (1943).
[8] L. Janossy and G. D. Rochester, Proc. Roy. Soc. **A182**, 180 (1943).
[9] L. Janossy and G. D. Rochester, Proc. Roy. Soc. **A183**, 181 (1944).
[10] H. J. J. Braddick and G. S. Hensby, Nature **144**, 1012 (1939).
[11] W. Powell, Phys. Rev. **58**, 474 (1940).
[12] J. G. Wilson, Proc. Roy. Soc. **A174**, 73 (1940).
[13] L. Janossy, C. B. McCusker, and G. D. Rochester, Nature **148**, 660 (1941).
[14] G. Herzog and W. H. Bostick, Phys. Rev. **59**, 122 (1941).
[15] D. J. Hughes, Phys. Rev. **60**, 414 (1941).
[16] W. Powell, Phys. Rev. **60**, 413 (1941).
[17] E. O. Wollan, Phys. Rev. **60**, 532 (1941).
[18] W. H. Bostick, Phys. Rev. **61**, 557 (1942).
[19] L. Seren, Phys. Rev. **62**, 204 (1942).
[20] W. E. Hazen, Phys. Rev. **64**, 257 (1943).
[21] W. E. Hazen, Phys. Rev. **63**, 213 (1943).
[22] J. Daudin, Ann. de physique **18**, 217 (1943).
[23] D. M. Bose, B. Choudhuri, and M. Sinha, Phys. Rev. **65**, 341 (1944).
[24] J. Daudin, Ann. de physique **19**, 10 (1944).
[25] W. E. Hazen, Phys. Rev. **65**, 67 (1944).
[26] L. Janossy, G. D. Rochester, and D. Broadbent, Nature **155**, 142 (1945).
[27] W. Powell, Phys. Rev. **69**, 385 (1946).
[28] R. P. Shutt, Phys. Rev. **69**, 261 (1946).
[29] G. D. Rochester, Proc. Roy. Soc. **A187**, 464 (1946).
[30] W. B. Fretter and W. E. Hazen, Phys. Rev. **70**, 230 (1946).
[31] G. D. Rochester, C. C. Butler, and S. K. Runcorn, Nature **159**, 227 (1947).

were covered with very thin aluminum foil for reflection of light. The light for photography was at right angles to the line of sight and was provided by G.E. flash tubes FT-422 flashed on 220 mfd, 1700 volts. The illuminated depth was five inches. The chamber was counter-controlled with various arrangements of counters, but was always selective for showers.

Several different counter arrangements were used during the course of the experiment. In order to increase the yield of usable pictures there was always a counter below the cloud chamber. Since it was necessarily some distance below the lowest lead plate and no other lead shielding was used, low density side showers often tripped the counters and were not recorded in the cloud chamber. Most of the pictures were taken with one of the following arrangements: (1) Selective for air showers. Counters in triple coincidence, one above the chamber, one below, and one at a distance of one meter horizontally from the upper chamber. (2) Selective for narrow air showers. Same as (1) except the distance was 20 cm. (3) Selective for showers produced in the chamber. Counters in triple coincidence, two side by side just below the chamber, with the third 18 inches below these two.

With arrangements (1) and (2) most of the pictures showing counter-controlled tracks were those of electron air showers. With arrangement (3) a large fraction of the pictures with counter-controlled tracks showed single penetrating particles making knock-on electrons in the last lead plate.

III. THE ELECTRON SHOWERS

Approximately 1000 pictures of electron showers were obtained, the particles of which penetrated three or more lead plates. Over 500 more were observed penetrating two plates or less, the identification being uncertain because of the low particle density in low energy air showers. The total number of electron showers incident on the apparatus was probably about 2000. One hundred and one of these penetrated all of the eight lead plates. An example of a high energy electron shower, several particles of which penetrated the eighth plate, is shown in Fig. 1a.

In 52 pictures of electron showers, penetrating particles associated with the shower (tracks of about the same age) and moving parallel to it were observed. This amounts to 2.5 percent of the pictures of air showers showing parallel penetrating particles. The counter experiments of Cocconi, Loverdo, and Tongiorgi[32] on penetrating particles in air showers are thus supported by cloud-chamber observations of air showers.

In no case were penetrating particles observed produced in an air shower by electronic radiation. Production of penetrating particles by electronic radiation would, of course, be of great interest, and the electron showers were examined carefully for evidence of this type of reaction. Penetrating particles made in high energy electron showers might be masked by the high density of particles, and there were many pictures in which the existence of penetrating particles could not have been observed. There were a great many more favorable cases, however, and the usually large angle of deviation of penetrating particles in the true penetrating showers (see below) makes detection of these particles fairly easy.

Heavy tracks, presumably protons, were observed in only 24 electron showers. Thus, it seems that the cross sections for production of penetrating particles (mesons or fast protons) and slow protons by electrons or γ-rays must be extremely small.

IV. ELECTRON BURST PRODUCTION BY PENETRATING PARTICLES

In 93 pictures an ionizing particle, after traversing three or more of the lead plates without any interaction, created an electron shower that penetrated at least two plates. These are probably mostly examples of radiation by mesons, with the γ-ray creating an electron shower. Seventy-five percent of these occurred with counter set-up 3) which was, of course, more favorable to this sort of event. Twenty-two of the bursts penetrated four or more of the lead plates, indicating that the energies involved in such electron showers may be 500–1000 Mev, and might have been a considerable fraction of the energy of the incident meson.

[32] G. Cocconi, A. Loverdo, and V. Tongiorgi, Phys. Rev. 70, 852 (1946).

V. THE PENETRATING SHOWERS

Fifty-three pictures were obtained in which one or more penetrating particles were produced in the cloud chamber. The energy released in these events varied widely, from low energy events in which a penetrating particle created one or two other penetrating particles and usually a few heavy tracks, to extremely high energy

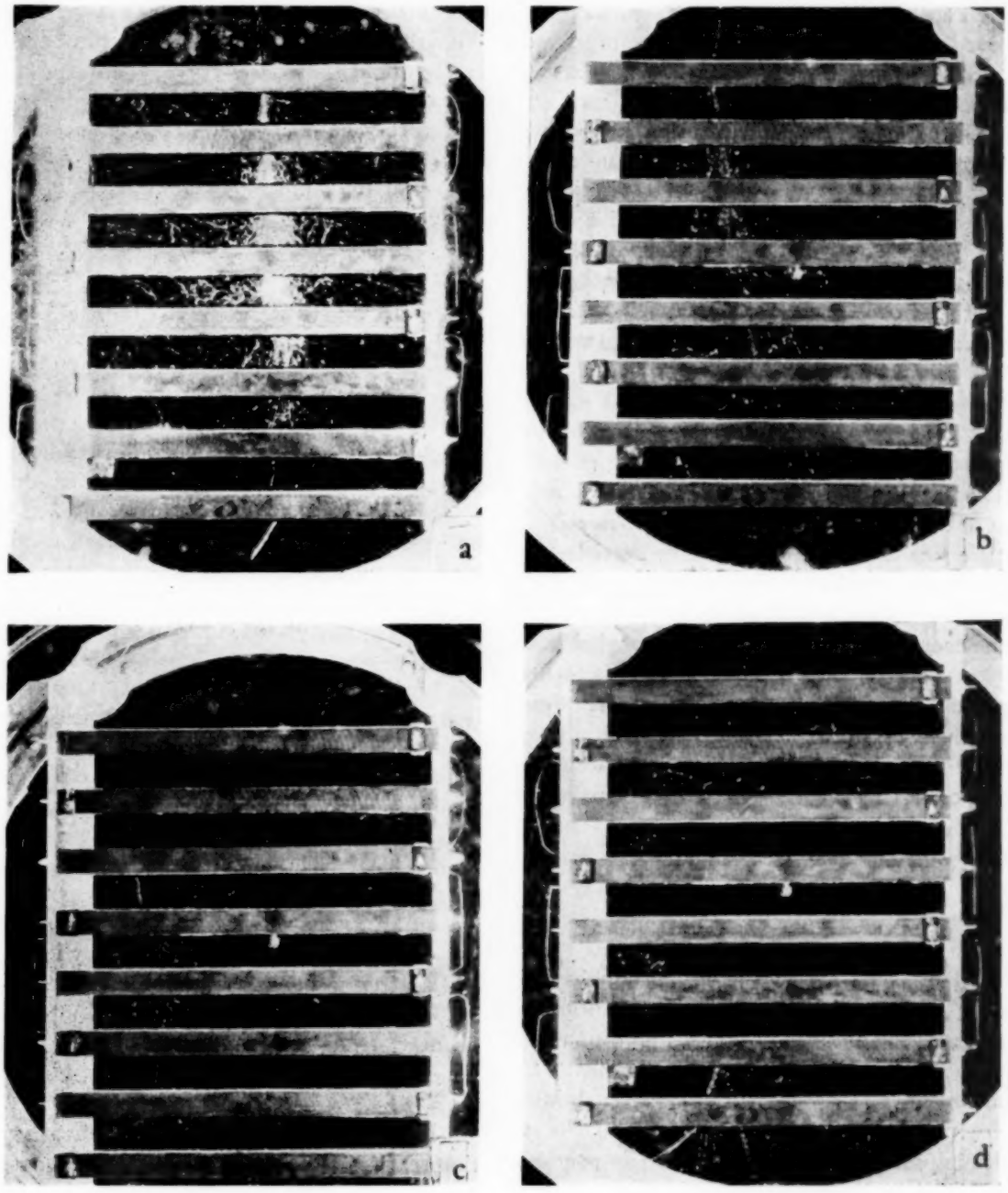

FIG. 1. a. Electron shower penetrates 10 cm of lead. b. Penetrating shower possibly made by neutral radiation. Conservation of momentum in such a high energy event makes it unlikely that the heavy track above the top plate produced the shower. The particle making this heavy track was probably a slow particle produced in the event. c. An air shower of five penetrating particles is incident on chamber, with penetrating particles produced in the fourth and possibly the seventh plate. d. An air shower with a penetrating particle that produces a penetrating shower in the seventh plate.

events in which many penetrating particles and electrons were created. Analysis of the pictures reveals several characteristic properties of penetrating showers.

(1) Many of them are created by ionizing penetrating particles. Thirty such showers were observed, with 7 others created in the top plate by ionizing particles so that the penetrating power could not be observed. Six showers were believed to be initiated by neutral radiation, and in 10 others the initiating particle was uncertain. It seems clear, however, that neutral radiation can create penetrating showers, but the selectivity of the first two counter arrangements for ionizing particles excluded neutral radiation for part of the time. One could not say that the results of this experiment were in disagreement with Janossy and Rochester,[8] who found that the penetrating showers are produced almost equally by ionizing and nonionizing particles. In 60 percent of the showers the initiating particle was not accompanied by other particles, but in most of the very high energy events the initiating particle was accompanied by other particles.

(2) Heavy tracks of protons or slow mesons were observed in 70 percent of the pictures, and often several were seen scattered throughout the shower. The presence of heavy tracks is in distinct contrast to the case of electron showers, where heavy tracks were relatively rare, and may be due to neutrons produced in the initial event or accompanying the shower-producing radiation. In the high energy events heavy tracks were almost always produced in the initial event, sometimes upwards, and may have been the debris from the original nuclear explosion.

(3) The penetrating particles produced had usually a rather wide angular deviation from the direction of the initiating particle, and the shower continued to fan out from the initial point. This is in contrast to the behavior of electron showers where the angular spread is due primarily to multiple scattering and the wide-angle particles do not usually penetrate the next plate.

(4) The number of identifiable penetrating particles produced in a given event varied from 1 to 15, according to the energies involved. The multiplicity in the high energy events may have been even higher, but the particles could not be counted in the core of the shower.

(5) Showers started with almost equal probability in any one of the lead plates, except the seventh plate, in which almost twice as many were observed as in any other. This is very likely due to the geometry of the counter set-up which would be selective for showers produced near the bottom of the chamber. The amount of lead in the chamber would have to be increased considerably in order to measure an absorption coefficient by counting events occurring in each plate.

(6) In three pictures successive production of penetrating particles was observed. This indicates that some particle like a negative proton or antimatter is not responsible for the event, for if an explosive action such as an annihilation of a negative proton had to occur to make a penetrating shower, it could only occur once, and successive events such as observed here and in a previous experiment[30] would not occur.

(7) Sixty percent of the pictures showed clear evidence that electronic radiation was simultaneously produced having energies large enough to create an electron shower. In many of the high energy events the electron shower produced was very large and made observation of the penetrating component difficult. One shower (Fig. 2d), although obviously a nuclear event because of the multiple production of heavy tracks in the initial event, contained no identifiable penetrating particles, although it is possible that the core of the shower consists of both electrons and penetrating particles.

(8) In only six pictures was it possible to identify any one of the penetrating particles as mesons, although the identification by ionization and scattering in these cases was quite clear.

(9) The frequency of penetrating showers with counter arrangement (3) was 0.035 per hour.

VI. DISCUSSION

Events in which high energy penetrating particles and high energy electrons occur simultaneously have been observed in cloud chambers by Rochester[29] and Daudin,[24] although the initial event was not seen in these cases. Rochester shows that the electrons cannot have been produced by knock-ons or decay electrons of

ordinary mesons, but that if they are decay products, the lifetime of the mesons producing them must be extremely small. Recently J. R. Oppenheimer has suggested that in these nuclear events not only charged mesons may be produced, but also uncharged mesons. The neutral mesons are calculated to have an extremely short life ($\sim 10^{-15}$ sec.). Thus, even if the neutral

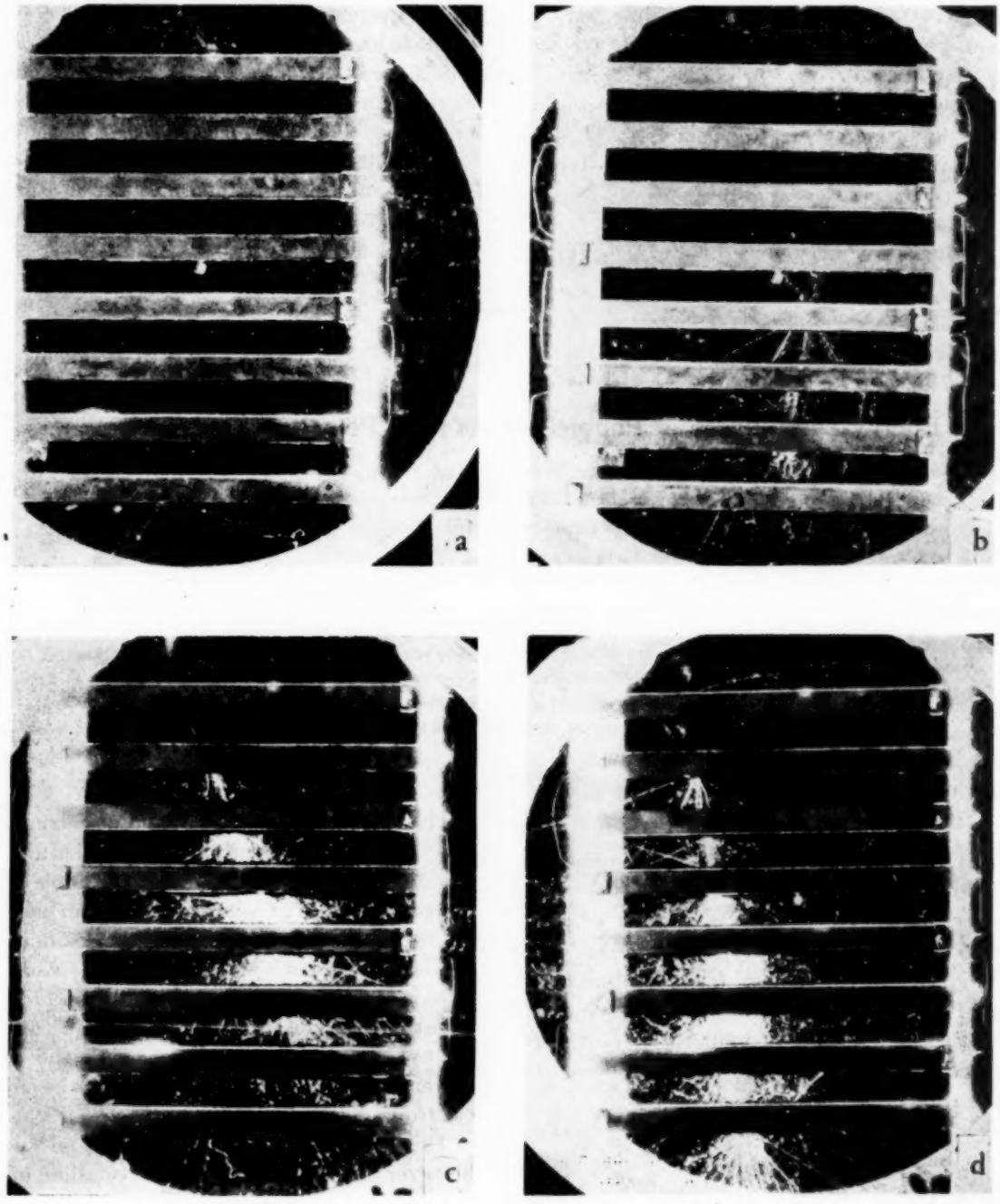

FIG. 2. a. Penetrating shower in which mesons can be identified by scattering and ionization. b. Penetrating particle makes a shower of electrons, slow heavy particles, and fast penetrating particles. c. High energy event with many high energy electrons and penetrating particles. d. Nuclear event in which seven slow heavy particles and high energy electrons are produced. Continued production of heavy tracks throughout the chamber is characteristic of penetrating showers, but no penetrating tracks are observed.

mesons were given a large amount of energy in the initial event they would decay almost immediately and produce a pair of γ-rays, which would then create the electron shower. Recent calculations by Heitler and Power[33] indicate that "transverse" mesons of short lifetime may be responsible for the production of electron showers.

Whatever the actual mechanism for production of high energy electrons may be, it seems clear that they are produced simultaneously with penetrating particles and may absorb enough of the primary energy to account for the very energetic electron air showers observed by Auger and others. It seems likely that primary particles and possibly high energy neutrons created by them are responsible for the showers observed. The frequency of events observed is not inconsistent with the number of primaries expected at sea level as estimated from the somewhat uncertain values of primary intensity and absorption in the atmosphere.

I am indebted to Professor R. B. Brode for his friendly interest in this experiment and to Professor J. R. Oppenheimer and Professor W. E. Hazen for stimulating discussions.

[33] W. Heitler and S. Power, Phys. Rev. **72**, 266 (1947).

PHYSICAL REVIEW VOLUME 73, NUMBER 1 JANUARY 1, 1948

Energy Distribution of Photoelectrons from Polycrystalline Tungsten*

L. APKER, E. TAFT, AND J. DICKEY
General Electric Research Laboratory, Schenectady, New York

(Received September 19, 1947)

Total-energy distributions of the photoelectrons from aged polycrystalline tungsten ribbons, with the usual rolling texture, were determined by applying retarding potentials to spherical collectors. Particular attention was paid to the region of low energy. When stray fields were eliminated, energy-distribution functions rose linearly with energy. The average work function was determined by extrapolation of (current)$^{\frac{1}{2}}$-voltage curves to the saturation line. The result agreed with the value 4.49 ev determined both from the spectral distribution and from the temperature variation of the photo-current. Application of spherical photo-cells to investigations of semiconductors is discussed briefly.

1. INTRODUCTION

USING simple assumptions about photoelectric emission from a Sommerfeld metal, Fowler[1] and DuBridge[2] developed graphical methods for analyzing photoelectric data. These techniques are convenient for determining the work functions of metals used as reference surfaces in studies of semiconductors.[3] This paper reports work done in preparation for such investigations.

The general theory of the photoelectric effect[4] has justified the assumptions of Fowler and DuBridge for a uniform, ideal metal surface with a potential barrier rounded by an image field. Faces of metallic single crystals approximate this ideal case. For such surfaces, Fowler's work provides a simple interpretation of the spectral distribution near the threshold. DuBridge's analysis treats the temperature variation of the photocurrent and the energy distribution of the emitted electrons.

These techniques had their original success, however, when applied to polycrystalline metals.

* Presented in part at the meeting of the American Physical Society, New York, New York, January, 1947.

[1] R. H. Fowler, Phys. Rev. **38**, 45 (1931).

[2] L. A. DuBridge, Phys. Rev. **39**, 108 (1932); **43**, 727 (1933); *New Theories of the Photoelectric Effect* (Hermann and Cie, Paris, 1935).

[3] R. A. Millikan, Phys. Rev. **18**, 236 (1921); E. U. Condon, Phys. Rev. **54**, 1089 (1938).

[4] K. Mitchell, Proc. Camb. Phil. Soc. **31**, 416 (1935); L. I. Schiff and L. H. Thomas, Phys. Rev. **47**, 860 (1935); R. D. Myers, Phys. Rev. **49**, 938 (1936); A. G. Hill, Phys. Rev. **53**, 184 (1938); R. E. B. Makinson, Proc. Roy. Soc. **A162**, 367 (1937); H. Y. Fan, Phys. Rev. **68**, 43 (1945).

In such cases, work functions may vary from point to point by several tenths of a volt. Empirical values are more or less complicated averages, the exact magnitudes of which depend on the particular methods of determination. Simple interpretations of such results may give rise to discrepancies, as careful investigations in thermionics have shown so clearly in the past ten years.[5]

The work reported here was done to test the agreement of three useful photoelectric methods in determining the "average work function" of polycrystalline ribbons. The spectral distribution of the photoelectric yield was analyzed by Fowler's method. The temperature variation of the yield was treated by DuBridge's method. Current-voltage data were compared with DuBridge's analysis of the total-energy distribution of the photoelectrons, and the work function was determined from the emission energies. Particular attention was given the region of low energies, in which results for other materials do not agree.[6]

Work functions determined by the three methods agreed to within a few hundredths of a volt. Fowler plots gave the value 4.49 ev. The energy-distribution function rose linearly with energy at low energies.

The new features of the photo-cells are described in Section 2. The results are given in Section 3 and are discussed in Section 4.

2. EXPERIMENTAL DETAILS

Figure 1 shows the construction of the two photo-cells used. They were like those previously used by Roehr,[7] except that the emitter supports were covered with nickel sleeves. These sleeves were held at various potentials with respect to the tungsten-ribbon emitters. Unavoidable contact-potential differences between the emitter and the supports were thus compensated.

The emitters were 99.9+ percent pure tungsten ribbons, 0.25 cm wide, 2.5 cm long, and 0.0025 cm thick. The aging treatment after assembly of the photo-cells was such that the original rolling texture was almost, but not quite, preserved. Most of the crystallites were oriented

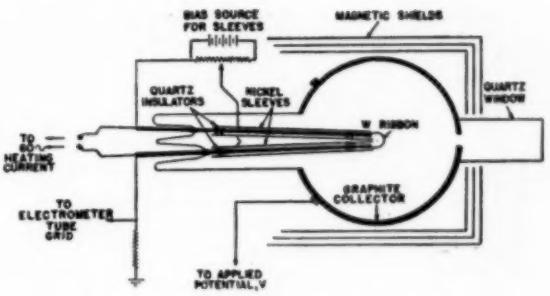

FIG. 1. Schematic diagram of photo-cell.

with (100) directions within 10° of the perpendicular to the ribbon surface.[8,9] The average crystal diameter was about 0.005 cm. At the grain boundaries there were barely detectable grooves, apparently due to preferential thermal etching. The rest of the surface appeared smooth when magnified 500 diameters.

Pressure in the tube after the seal-off was 2.10^{-8} mm Hg as indicated by an ionization gauge calibrated for air.[10] The active gas pressure was such that the work function of the clean ribbon increased by about 0.5 ev to an equilibrium value in 4 days. The transient pressure increase caused by flashing the ribbon showed that there was roughly 20 percent of a monolayer of adsorbed gas on the contaminated tungsten. Most of this could be removed by a 10-sec. flash at 1100°K; the remainder came off at 2100°K. Before each photoelectric measurement, the ribbon was flashed at 2900°K. Spectral data could be taken in 20 seconds, current-voltage curves in three minutes.[11]

Radiation sources for energy measurements were low pressure Zn, Cd, or Hg discharges in rare gas. The desired spectral lines were isolated with a Bausch and Lomb quartz monochromator.[12] No background radiation could be detected

[5] M. H. Nichols, Phys. Rev. **57**, 297 (1940); **59**, 944A (1941); W. B. Nottingham, Bull. Am. Phys. Soc. **22**, 14 (1947).

[6] E. Rudberg, Phys. Rev. **48**, 811 (1935). For a discussion, see A. G. Hill, Phys. Rev. **53**, 184 (1938).

[7] W. W. Roehr, Phys. Rev. **44**, 866 (1933).

[8] W. G. Burgers and J. J. A. Ploos van Amstel, Physica **3**, 1064 (1936); J. F. H. Custers and J. C. Riemersma, Physica **12**, 195 (1946).

[9] Mr. Eric Asp kindly took x-ray diffraction photographs of the ribbons.

[10] For the type of evacuation schedule used, see W. B. Nottingham, Phys. Rev. **55**, 203 (1939); J. App. Phys. **8**, 762 (1939).

[11] The initial contamination rate after a flash caused the saturation photo-current for $h\nu = 4.89$ ev to decrease by 0.1 to 0.4 percent per min. When necessary, plots of current *vs.* time were extrapolated back to the time zero. No effects due to contamination were found. See C. E. Mendenhall and C. F. DeVoe, Phys. Rev. **51**, 346 (1937).

[12] We are indebted to the University of Rochester Physics Department for the loan of this instrument.

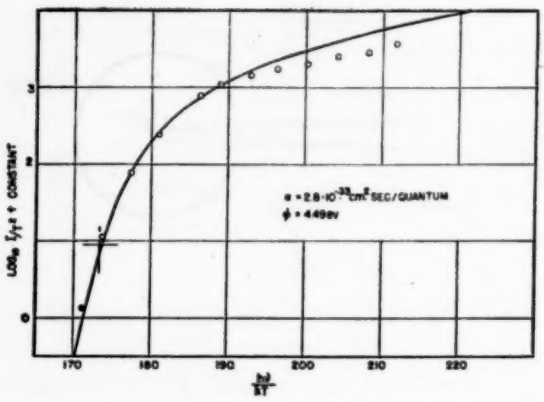

FIG. 2. Fowler plot for normal incidence and for $T=300°K$. The point at the extreme left is an upper limit set by the sensitivities of the thermocouple and the current detector. For currents measured in electrons/quantum, the additive constant on the ordinate scale is -7.765.

between lines. Intensities were constant to 0.2 percent. On the emitter, the area illuminated varied from 0.5 to 1.0 mm². The angle of incidence could be changed by moving this spot over the surface. For spectral measurements, Hg arcs operating at 2 atmospheres served as sources. In this case, intensities were constant to 1 percent, and corrections for background were made when necessary.

Intensities were determined with a compensated vacuum thermocouple[13] calibrated against a standard radiation source from the Bureau of Standards. Currents were measured with a split FP-54 electrometer tube[14] using a $5.10^{10}\Omega$ grid resistor and a sensitivity of 50,000 mm/volt.

3. RESULTS

Figure 2 is a Fowler plot for the clean ribbon. The parameter α in Fowler's equation, $I=\alpha A T^2 \bar{\phi}(h\nu/kT)$, rose from $2.8\cdot10^{-33}$ cm² sec./quantum at $\theta=0°$ to $14\cdot10^{-33}$ cm² sec./quantum at $\theta=45°$, where θ is the angle of incidence of the radiation. The variation was roughly parabolic near $\theta=0$. The work function determined was $\varphi=4.49\pm0.02$ ev.[15]

In Fig. 3 are DuBridge isochromatic plots showing the temperature variation of the photoelectric yield for $h\nu=4.42$, 4.49, and 4.59 ev. The temperature was changed from 300°K to 1040°K, the latter value being determined with an optical pyrometer. The work function determined was $\varphi=4.49\pm0.02$ ev. Values of α varied by a factor of 2.

Figure 4 shows the interesting portions of current-voltage curves for $h\nu=4.89$ and 5.80 ev. Data were taken in the range $-10<V<180$ volts. Ordinates in Fig. 4 are normalized at $V=+10$ volts. The dashed curves show the effects of the sleeve potentials. The work function of the sleeves as determined from photoelectric measurements was 5 volts. The resultant 0.5-volt contact-potential difference between the sleeves and the ribbon was thus compensated by a +0.5-volt sleeve potential. Reverse currents were present for $h\nu=5.80$ volts. Corrections were made by extrapolation of the reverse current line in the usual way.[16] This was checked by repeating the process with the ribbon contaminated, in which

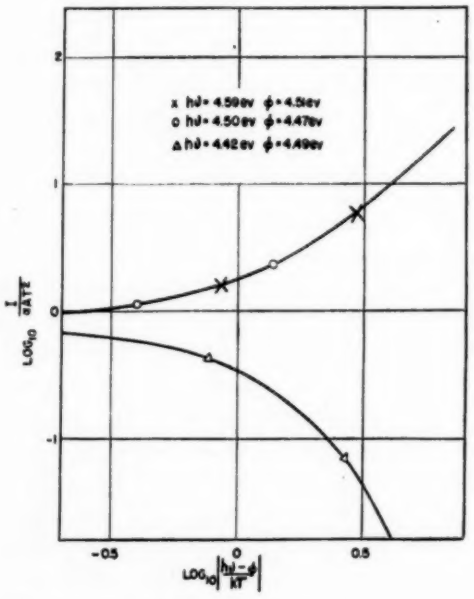

FIG. 3. Typical DuBridge plot for the temperature variation of the photoelectric yield between 300°K and 1040°K. For each value of $h\nu$, the corresponding value found for φ is shown.

[13] Kindly made for us by Dr. C. H. Cartwright.

[14] J. M. Lafferty and K. H. Kingdon, J. App. Phys. **17**, 894 (1946).

[15] The data of Fig. 2 fall below the Fowler curve for $h\nu/kT>190$. This is difficult to understand, since a non-uniform surface should produce deviations in the other direction. This discrepancy, however, has no important effect on the value of the work function determined from the Fowler plot. Mendenhall and DeVoe[11] found that data for the faces of a single tungsten crystal fitted Fowler plots for a range of $h\nu/kT$ equal to 40 when the surfaces were clean.

[16] P. Lukirsky and S. Prilezaev, Zeits. f. Physik **49**, 236 (1928); S. Prilezaev, J. Tech.Phys. U.S. S.R. **9**, 1439 (1939).

case the reverse current was a larger fraction of the total.

Figure 5 shows a DuBridge plot for $T=300°K$ and $h\nu=4.89$ ev. Values of $eV_0=h\nu-\varphi_c$, where φ_c is the work function of the collector, could be determined from these plots to within ± 0.01 volt. Points so determined are marked with arrows in Fig. 4.

Figure 6 shows the current-voltage curves plotted on a parabolic scale. Currents were normalized at $V=+0.7$ volt, a point definitely on the saturation line. The plots were insensitive to the particular value of V selected for normalization. Saturation points determined by this extrapolation process were $V_s=+0.62\pm 0.02$ volt. The extreme range of these values is shown by the brackets above the arrows in Figs. 4 and 6. The value of φ determined from Einstein's relation, $\varphi=h\nu-e(V_s-V_0)$, was 4.48 ± 0.03 ev.

The saturation lines in Fig. 4 were clearly not horizontal. Between $V=10$ and $V=180$ volts the photo-current increased 4.5 percent for

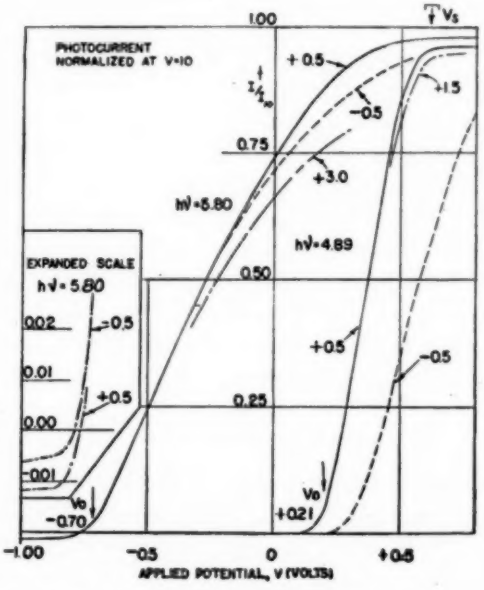

FIG. 4. Portions of typical current-voltage curves for $h\nu=4.89$ and 5.80 ev; $T=300°K$. Complete curves extended from $V=-10$ to $+180$ volts. The photo-current at $V=+10$ is set equal to 1. The ordinates for $h\nu=5.80$ ev are expanded by a factor of ten in the inset to show the behavior of the exponential temperature "tails" in the presence of reverse currents. Sleeve potentials in volts are written next to the curves; a value of $+0.5$ compensates for the effect of stray fields. Experimental points were taken at intervals of 0.02 volt near the tails and near the saturation points. Their deviation from the curves is not visible on this scale. Arrows mark the values of V_0 and V_s determined from Figs. 5 and 6, respectively.

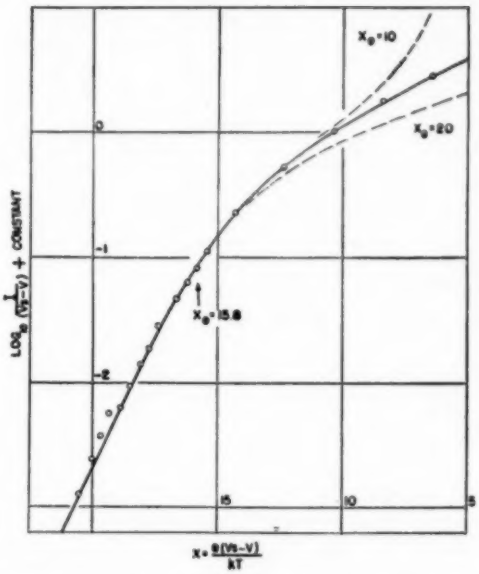

FIG. 5. Typical DuBridge plot for total-energy distribution. $T=300°K$; $h\nu=4.89$ ev. The theoretical curve for $x_0=(h\nu-\varphi)/kT=15.8$ is shown as a solid line; curves for $x_0=10$ and 20 are dashed. The value of V_0 determined from this plot is $+0.21$ volts. It shows a negligible dependence on the value of V_s used in evaluating x. In this case, $V_s=+0.62$ volt was taken from Fig. 6.

$h\nu=4.89$ ev and 1.8 percent for $h\nu=5.80$ ev. From the geometry, rough estimates were made of the field F at the emitting area.[17] Plots of I *vs.* $F^{\frac{1}{2}}$ had roughly 5 times greater slope at $F=1$-volt cm^{-1} than that calculated from Fowler's equation and Schottky's relation, $\Delta\varphi=(eF)^{\frac{1}{2}}$; at $F=100$-volt cm^{-1} the experimental slope was less than 2 times the theoretical value.

4. DISCUSSION

The results in Section 3 show that the methods of Fowler and DuBridge gave consistent values for the work function of two polycrystalline tungsten ribbons. The slopes of the saturation lines in Fig. 4 indicate that there were surface non-uniformities with a patch spacing larger than those normally found in thermionic work.[18] The three methods used for determining work functions represent quite different kinds of averaging over these patches, but the results differed by only a few hundredths of a volt. A similar result

[17] We are indebted to Mr. R. N. Hall for the results of his calculation of the field in a spherical condenser with a radial support.

[18] J. A. Becker, Rev. Mod. Phys. **7**, 95 (1935); C. Herring, private communication.

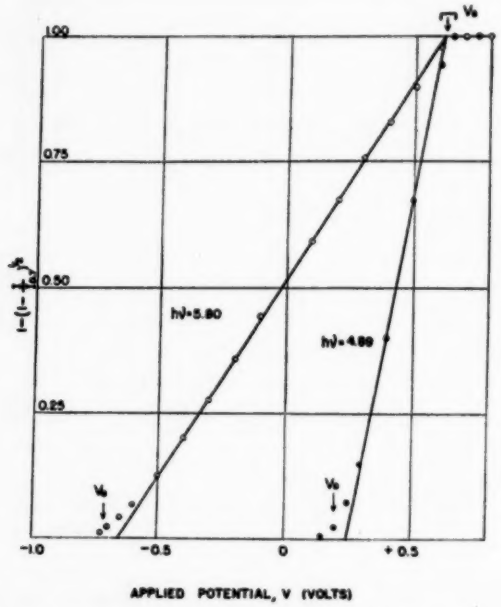

FIG. 6. Current-voltage data for $h\nu=4.89$ and 5.80 ev plotted on a parabolic scale. The extreme range over which V_s varied for six sets of data is shown by the bracket over the upper arrow. The lower arrows show values of V_0 determined from Fig. 5. DuBridge's analysis gives a straight line passing through V_0 and V_s at 0°K.

has been obtained in early work on the equality of the photoelectric and thermionic work functions for other metals.[2,19] An emitter with a small fraction of its area occupied by patches of higher work function than the rest would behave in this manner. It is of interest in this connection that the average work function of the tungsten ribbons used here is close to Nichol's value of 4.56 ev for the thermionic work function associated with the (100) direction in single-crystal tungsten wire.[5,20]

In the low energy region, the current-voltage characteristics of Fig. 4 are parabolic, corresponding to a total-energy distribution function rising linearly with energy. This point has been the subject of previous discussion.[2,6,21] Henshaw has obtained an analogous result in work on the normal-energy distribution of photoelectrons from potassium films.[22]

The surface properties of semiconductors can be investigated with particular convenience in spherical photo-cells with interchangeable emitters.[3] Work functions of metals used for purposes of comparison can be found by the methods of Fowler and DuBridge, but for semiconductors this is not the case. Prilezaev in work on $SbCs_3$, a non-metallic material, has used the saturation point of current-voltage curves to determine contact-potential differences.[16] Since the collector work function was known, the emitter work function could be obtained. The results in Section 3 show that this procedure is sensitive to stray fields. Where these are compensated, however, work functions so determined for tungsten agree with those found by the two other methods used.

Current-voltage curves for metallic emitters fall to zero exponentially when V is of the order of 0.1 volt more negative than $V_0=(h\nu-\varphi_c)/e$. For ideal semiconductors they approach zero in a different way at values of V several tenths of a volt more positive. Inspection of Fig. 4 shows that such an effect is also found for metals if stray retarding fields are present. The region near the saturation point is even more easily distorted. Retarding-potential measurements, especially at low energies, are obviously not reliable unless these fields are eliminated.

ACKNOWLEDGMENTS

We are indebted to Dr. C. Herring and Dr. J. A. Burton for helpful discussions of this work.

Dr. A. W. Hull has given us the benefit of his interest and advice.

[19] Interpretation of such comparisons is complicated by the wide difference between the temperatures at which photoelectric and thermionic phenomena are observed. For discussions see F. Seitz, *The Modern Theory of Solids* (McGraw-Hill Book Company, Inc., New York, 1940); C. Herring Phys. Rev. **59**, 879 (1941).

[20] Dr. Nichols has kindly informed us that his published value, 4.53 ev, is 0.03 ev too low because of a computational error.

[21] I. Liben, Phys. Rev. **51**, 642 (1937).

[22] C. L. Henshaw, Phys. Rev. **52**, 854 (1937).

On the Magnetic Field of a Rotating Molecule

G. C. Wick
University of Notre Dame, Notre Dame, Indiana
(Received September 22, 1947)

The space distribution and magnitude of electronic currents in a rotating molecule with a $^1\Sigma$ ground state are re-examined. An evaluation of the magnetic field set up by the rotation is attempted, and the results are used to interpret the width of radiofrequency resonance lines of some alkali halides.

I. INTRODUCTION

THE study of radiofrequency spectra of molecules in a strong magnetic field has shown that the resonance lines associated with nuclear magnetic moments are often quite wide, indicating the presence of relatively strong interactions within the molecule. In many cases the magnitude of the effect has been satisfactorily explained on the assumption that the nucleus possesses a quadrupole moment.[1] This explanation, however, does not apply to the resonance associated with the F^{19} nucleus in alkali fluorides (4000 cycles/gauss sec.), as the nucleus has spin $\frac{1}{2}$ and cannot have a quadrupole moment. The widths at half-value of the resonance line are given in the second column of Table I[2]. The remaining columns in the table will be explained later. In two out of the three molecules studied so far the width was felt to be surprisingly large, considering that it could only be due to magnetic interactions. An admittedly somewhat naive evaluation of the magnitude of the interactions leads one to expect much smaller widths than found, see below. The problem, therefore, seemed to deserve further consideration.

The measurements are performed in a strong magnetic field, so that both nuclear spins in the molecule, as well as the molecular rotation, are quantized in the direction of the field; in the transitions studied here the alkali nucleus does not flip over, so that only the two following interactions are of real importance: (a) interaction between the magnetic moments of the two nuclei, and (b), interaction between the moment of the F^{19} nucleus and the molecular rotation. Interaction (a), however, is much too small to account for the effects observed and will be neglected. We are left with (b). The broadening of the line is then due to the fact that the rotation of the molecule causes a magnetic field at the nucleus, which is proportional to the component m_J of the rotational momentum along the axis of quantization. Hence molecules with different m_J's will have different frequencies, the shift being

$$\delta\nu = 4000 H_r m_J, \tag{1}$$

where H_r is the rotational magnetic field per unit rotational quantum number.

As the observed shape of the resonance line seems to fit the statistical distribution of m_J values (that follows from Boltzmann's law), one may confidently use the width at half-value of the line to compute the "experimental" value of H_r. A simple statistical consideration shows that one-half of the molecules must have an $|m_J|$ smaller than $0.674(kT/2B)^{\frac{1}{2}}$. This is listed as $m_J(\frac{1}{2})$ in the table. B is the rotational constant of the molecule $\hbar^2/2I$. Its value is not known from direct spectroscopic data;[3] it is known, however, for other alkali halides, and it is found that the internuclear distance in the molecule is from 0.1 to 0.3A smaller than the sum of the ionic radii. The internuclear distances listed in the table are derived from this rule, the uncertainty being of the order ± 0.1A, which is quite accurate for our purpose. Inserting the value of $m_J(\frac{1}{2})$ in Eq. (1) and comparing the shift with the half-width of the line, the values of H_r listed in the table have been obtained.

These values are remarkable both as regards

[1] B. T. Feld and W. E. Lamb, Phys. Rev. **67**, 15 (1944); W. A. Nierenberg, N. F. Ramsey, and S. B. Brody, Phys. Rev. **70**, 773 (1946).

[2] I am indebted to Drs. Rabi, Ramsey, and Nierenberg for communicating to me these as yet unpublished data.

[3] For CsF see, however, H. K. Hughes, Phys. Rev. **70**, 570 (1946); **72**, 614 (1947).

TABLE I. Magnitude of the magnetic field at the nucleus caused by molecular rotation computed from the width of the resonance line.

Molecule	Width of resonance line (Mc/sec.)	Internuclear distance r (A)	B (10^{-16} erg)(cm^{-1})		$m_J(\frac{1}{2})$	H_r (gauss)
LiF	0.5	1.8	2.0	1.0	13.1	±4.8
NaF	0.08	2.1	0.73	0.37	21.8	±0.46
CsF	0.5	2.6	0.3	0.15	34	±1.85

the magnitude and the trend with increasing mass of the alkali. A naive estimate of the magnitude of H_r could be made on the assumption that the magnetic field is simply caused by the rotation of the alkali ion relative to the F nucleus. One should have $H_r=2Be/\hbar cr$, since $2B/\hbar$ is the angular velocity of the rotation per unit rotational quantum number. For LiF one finds $H_r=0.33$ gauss, a value 14 times smaller than observed. In CsF the discrepancy is by a factor 50. As the mass of the alkali is varied, one might expect H_r to vary roughly proportionally to the angular velocity, i.e., to B. Instead, H_r drops to a very low value for NaF and rises again to a high value for CsF.

Another naive way of estimating H_r consists in the assumption that the electron cloud rotates rigidly with the molecule. The field estimated in this way[4] is indeed of the order of magnitude required by experiment. Unfortunately, the assumption of a rigid rotation of the electron cloud is wholly unjustified. Because of the slip phenomenon that was first observed and understood in the case of the H_2 molecule,[5] a rotation of the spherically symmetrical shells of the F^- ion can be induced only insofar as these shells are polarized by the neighboring ion; we shall see in Section V that the rotation of the 1s and 2s shells is quite negligible, and even the 2p shell can only yield a very small field.

[4] The main contribution comes from the electron shells of the F^- ion itself. In the evaluation one may assume (see Section II) that the rotation takes place around the F nucleus. A spherically symmetrical shell containing z electrons rotating with an angular velocity $2B/\hbar$ causes a field at the center: $H_r=(4zeB/3\hbar c)(\overline{1/r})$. For the 2$p$ shell of F^-, $z=6$, and the average reciprocal distance $\overline{1/r}$ is about 2.10^8 cm^{-1}. The contribution of the 2p shell alone is $4.8B$ with B in cm^{-1}, or about the field observed in LiF. In CsF one ought to assume a partial rotation also of the inner 1s and 2s shells.

[5] R. Frisch and O. Stern, Zeits. f. Physik **85**, 4 (1933); G. C. Wick, Zeits. f. Physik **85**, 25 (1933) and Nuovo Cimento **10**, 118 (1933); N. F. Ramsey, Phys. Rev. **58**, 226 (1940).

It will also appear from the following discussion that the distribution of the currents induced by the rotation within the molecule is, in general, quite different from the distribution corresponding to a rigid rotation. In the next section the general formulae for these currents will be developed, and later various models will be examined.

II. GENERAL FORMULAE

For simplicity, we shall treat the rotation of the molecule classically. We consider a system of axes rigidly connected to the molecule, the z axis being the line that joins the nuclei. We assume that the rotation takes place around the x axis. One can then write, first of all, the time-dependent Schrödinger equation for the electrons, referred to non-rotating axes (one must use the time-dependent equation because the potential is time dependent). Assuming a solution that is stationary with respect to the rotating axes, and transforming the equation to these axes, one finds:

$$E\psi=H_0\psi-\omega\hbar L_x\psi, \tag{2}$$

where H_0 is the Hamiltonian, such as it would be if the system were not rotating. The perturbation term caused by the rotation contains ω, the angular velocity, and the x component of the total orbital momentum of the electrons: $\hbar L_x$.[6] We may write: $\hbar\omega=2BJ$, where J is the rotational quantum number. We see, therefore, that all first-order effects caused by the rotation will be proportional to J. We shall henceforth refer all such effects to unit rotational quantum number.

A simple perturbation calculation shows that the electronic current j induced by the rotation is

$$\mathbf{j}=2B\sum_n{}'\frac{1}{E_n-E_0}[L_{0n}\mathbf{j}_{n0}+\mathbf{j}_{0n}L_{n0}], \tag{3}$$

where L stands for L_x, and $\mathbf{j}_{0n}$ is a matrix element of the unperturbed current density, for example, in the case of one electron only: $\mathbf{j}_{0n}=(ie\hbar/2m)(\psi_0^*\,\mathrm{grad}\psi_n-\psi_n\,\mathrm{grad}\psi_0^*)$. Moreover, E_0 is the energy of the electronic ground state of

[6] We neglect the interaction of the rotation with the electronic spins. This is permissible in light molecules in a singlet state. Inclusion of that interaction would lead to only slightly more complicated formulae, while leaving the main conclusions unchanged.

the molecule, and E_n is the energy of an excited state. Only Π-states contribute to the sum in (3) if the ground state is of the Σ type. From Eq. (3) it is found that the magnetic moment caused by the rotation, see also reference 5, is

$$M=-4B\sum_n{}'|L_{0n}|^2/(E_n-E_0)$$

Bohr magnetons. (4)

It may be noticed that this moment has the sign that one would expect from a rigid rotation of the electron cloud together with the nuclei; the magnitude, however, may be entirely different, as we know from the case of the molecule H_2.

From Eq. (3) it is also possible to derive an expression for the average magnetic field H_r at any point within the molecule. If $\mathbf{r}$ is the radius vector from the field point to an unspecified integration point, and setting

$$H_{0n}=c^{-1}\int \mathbf{r}\times\mathbf{j}_{0n}d\tau/r^3,$$

we have

$$H_r=2B\sum_n{}'\frac{1}{E_n-E_0}\{H_{0n}L_{n0}+L_{0n}H_{n0}\}. \quad (5)$$

Let us assume for a moment that the point at which we want the field is on the rotation axis; then the integral that yields H_{0n} is seen to be the same that yields L_{0n}, but for the presence of an additional factor r^{-3}. The value of (5) is then of the order of (4) divided by the cube of a distance, which is an average distance of the electrons from the point under question. The value of the field found by Rabi and collaborators is in accord with this evaluation in the case of the hydrogen molecule, but we shall see that the evaluation of that average distance may be quite critical.

Actually, the molecule rotates about a point which does not coincide with the F nucleus, but it can be shown that this is immaterial. In fact, the difference between the perturbation operators corresponding to two different rotation axes parallel to one another, is seen to be the operator corresponding to a uniform translation of the molecule; the magnetic field produced by this translation at a given point is related by a Lorentz transformation to the average electric field at the same point when the molecule is at rest. Now precisely at the position of a nucleus the average electric field caused by the remaining particles is zero, and the magnetic field caused by a uniform translation is also zero, as one should indeed expect.

One further remark is necessary before we proceed. If the field (5) is multiplied into the magnetic moment of the nucleus, we obtain the perturbation of the energy levels that is caused by the interaction between rotation and the magnetic moment. This formula could also be arrived at from an analogous formula derived by Hebb[7] for the interaction between the rotation and the electronic spin when this is not zero. This incidentally shows that the μ-term in Hebb's paper is exactly equivalent to the magnetic coupling between the spin of the molecule and the magnetic field set up by the molecular rotation considered by Kramers,[8] and this explains why the two computations give formulae of the same structure.

III. ORDERS OF MAGNITUDE

It is rather difficult to estimate the sums in Eqs. (4) and (5). The difficulty is best illustrated by the fact, to be discussed later, that also very high excited states may give a strong contribution to the sums. On the other hand, it is also clear that owing to the denominator E_n-E_0 the lowest excited states will be quite important. One can, however, proceed a little farther on the assumption that the various electron shells in the two ions contribute independently to the sums. The most appropriate approximation may then be applied to each shell. For the outer shells we may replace in the sums the denominator E_n-E_0 by a suitable average value, which will not be much larger than the excitation energy of the lowest Π-states. The spectroscopic evidence indicates[9] that the energy curves of these states are practically horizontal so that the minimum value of E_n-E_0 is of the order of the dissociation energy D of the molecule, or about $(1-n^{-1})e^2/r$, where n is of the order of 8 or 9. Approximate values of D for the three molecules, LiF, NaF, CsF are $D=7$ ev, 6 ev, and 5 ev,

[7] M. H. Hebb, Phys. Rev. **49**, 610 (1936), see especially Eq. (12).
[8] Kramers, Zeits. f. Physik **53**, 422 (1929).
[9] See R. S. Mulliken, Phys. Rev. **50**, 1017 (1936) and **51**, 310 (1936).

respectively. From the structure of H_{0n} we may expect it to be of the order of the magnetic field at the nucleus caused by a $2p$ electron, when L_{0n} is of order unity, and proportionately smaller if L_{0n} is small. The field caused by a $2p$ electron in fluorine is of the order of 6.10^5 gauss.[10] Collecting all these factors together, and noticing that there are two terms in Eq. (5) that are equivalent, we get for the contribution of the outer shells the evaluation:

$$H_r \sim 4(B/D)\sum_n |L_{0n}|^2 \times 6.10^5 = 2.4\times 10^6 (B/D)(L_x^2)_{00}. \quad (6)$$

It will now be noticed at once that the values of $(L_x^2)_{00}$ that will make the field (6) equal to the experimentally observed field in Table I are fairly low (0.11, 0.03, and 0.2, respectively) and should not be very hard to explain on almost any model. But it must be pointed out that a really crucial *assumption* about the space distribution of the current $\mathbf{j}_{0n}$ has been made in estimating H_{0n} from L_{0n}.[11] Before we examine these points in more detail, let us settle a minor question.

IV. EFFECT OF THE INNER SHELLS

Some simple remarks will clarify the discussion of the inner shells. In the isolated ion these shells have spherical symmetry; because of the strong binding, the inner shells probably preserve a high degree of symmetry even in the molecule. Let us first consider a spherically symmetrical shell of the F ion; the operator L_x of Eq. (3) applied to the wave function of this shell yields zero, hence there is no perturbation, the slip is 100 percent. This result is trivial, as it is clear that a rotation of the shell will take place only as a consequence of the asymmetrical perturbation of the shell caused by the neighboring ion. Let us now consider a shell in the alkali ion; taking into account the fact that the rotation is assumed to take place with the F ion as a center (and that consequently L_x is referred to this point) it is again easy to see that the shell does not rotate about its own center, but is, of course, affected by a translational motion with a speed equal to that of the alkali nucleus. This type of velocity distribution in the shell will set up a magnetic field which outside the shell will be equivalent to the field one would obtain if the charge of the shell were concentrated at its center. We thus see that the main effect of the inner shells of the alkali ion will be to screen a large fraction of the magnetic field produced by the motion of the alkali nucleus. The value of this field is

$$H_{rn} = 2ZeB/hcr \quad (7)$$

for unit J (Z is nuclear charge of alkali). To be consistent we have, of course, assumed that the rotation takes place about the F nucleus. The field (7) should of course be added to (5) to get the complete field. It is, however, rather small compared to the observed H_r in LiF; in CsF, with $Z=55$, $H_{rn}=1.9$ gauss, which is nearly equal to the field observed. As soon as a large fraction of it is screened by the inner shells it will be negligible. This shows that we may simply omit the field (7) if at the same time we omit in the sum (5) the terms corresponding to the excitation of the inner shells of the alkali. At the same time this remark substantiates a previous statement, namely, that in the sum (5) the contribution from very high electronic levels is far from small.

V. ROTATIONAL PROPERTIES OF A FEW SIMPLE MODELS

In Section III we found that the experimental data could be explained by making some not too unreasonable assumptions about the order of magnitude of certain matrix elements. Our knowledge of the wave functions and states of the molecule is not, of course, sufficient to permit a real test of these assumptions. But a closer examination of a few strongly schematized models may perhaps contribute to a better understanding of the phenomenon. Although all the calculations may be based on the general formulae (3), (4), (5), the following remark may be useful. Since the unperturbed non-relativistic Hamiltonian H_0 is real and L_x is imaginary,

[10] This being an average over the $P_{\frac{1}{2}}$ and the $P_{3/2}$ states estimated from the fine structure of the ground state of the F atom.

[11] Namely, in the current distribution for a p electron, the angular velocity varies as the inverse square of the distance from the rotation axis. This type of current distribution yields a much stronger field at the center than a rigid rotation, the resultant magnetic moment being the same.

the unperturbed wave function u for the Σ ground state may be assumed to be real, and the perturbed wave function, neglecting second-order terms in $\omega=2B/h$, will be of the form: $u+i\omega v$, where v is also a real function. From this it follows that the electronic density distribution relative to the nuclei is unaffected by the rotation, again neglecting second-order terms. Therefore, the time derivative of the electronic density, $\partial\rho/\partial t$, *at a space-fixed point* will be the same as for a rigidly rotating electron cloud: $\partial\rho/\partial t=-\omega\partial\rho/\partial\vartheta$, ϑ being the azimuth about the rotation axis. The electronic current induced by the rotation must hence satisfy the continuity equation

$$\mathrm{div}\mathbf{j}=\omega\partial\rho/\partial\vartheta=\mathrm{div}(\rho\boldsymbol{\omega}\times\mathbf{r}), \tag{8}$$

from which it does *not* follow, however, that j coincides with the current $\rho\boldsymbol{\omega}\times\mathbf{r}$ corresponding to a rigid rotation. This may be seen most simply for a one-electron system. One has then, with $\psi=u+i\omega v$,

$$\mathbf{j}=(ihe/2m)\{\psi^*\,\mathrm{grad}\psi-\psi\,\mathrm{grad}\psi^*\}=(2B/m)\rho\,\mathrm{grad}(v/u), \tag{9}$$

since $\rho=-eu^2$. For the ground state of a one-particle system u has no nodes, so that v/u is regular everywhere. Equation (9) then shows that the current is obtained by impressing on the density ρ a velocity $(2B/m)\,\mathrm{grad}(v/u)$, i.e., *an irrotational velocity field*. This condition together with (8) determines $\mathbf{j}$ completely and may be used instead of Eq. (3). The velocity field for rigid rotation $\boldsymbol{\omega}\times\mathbf{r}$ is not, of course, irrotational: $\mathrm{curl}(\boldsymbol{\omega}\times\mathbf{r})=2\boldsymbol{\omega}$. The actual field may be regarded as the superposition of a rigid rotation plus a velocity field $\mathbf{w}$ such that: $\mathrm{div}.\rho\mathbf{w}=0$, and $\mathrm{curl}\mathbf{w}=-2\boldsymbol{\omega}$. *As the circulation of this field is contrary to the rotation, it is clear that it will lead in general to a lowering of the magnetic moment.*

An especially simple example is afforded by a one-dimensional model. An electron is constrained to move on a circle under the action of a potential $V(\vartheta-\vartheta_0)$, ϑ being the azimuth of the particle and ϑ_0 the azimuth of a massive particle symbolizing the nuclei in the actual case of a molecule. If the heavy particle rotates with an angular velocity ω, the average rotation of the light particle may be computed as follows. Equations (8) now takes the form: $\partial j/\partial\vartheta=\omega\partial\rho/\partial\vartheta$, or $j=\omega\rho-j_0$. The additive constant j_0 may be determined from condition (9) or $j=(2B/m)\rho(\partial/\partial\vartheta)(v/u)$, remembering that v/u must be a periodic function of ϑ. This gives $j_0\int d\vartheta/\rho=4\pi B/h=2\pi\omega$, or

$$j=\omega\rho-j_0=\omega\rho-\omega/\overline{\rho^{-1}}. \tag{10}$$

This shows that on the current there is superimposed a constant slip term representing a current contrary to the rotation. If the potential $V(\vartheta-\vartheta_0)$ is weak, so that ρ is nearly constant on the circle, $j_0\approx\omega\rho$; the rigid rotation, therefore, is completely cancelled by the additive term; the slip is almost 100 percent. On the other hand, if the potential is very strong so that ρ is very unevenly distributed, j_0 is much smaller than the average of $\omega\rho$, and the slip is almost negligible. This example simply illustrates the need for an asymmetry in the electron cloud in order to have an induced rotational moment.

In the actual physical case, a certain amount of asymmetry may be produced in the shells of the F^- ion by the field of the neighboring alkali ion. It is essential to ascertain not only the average amount of rotation, or the average magnetic moment induced in each shell, but also the actual distribution of the rotational currents; because of the r^{-3} factor, the field H_r depends quite strongly on the distribution (compare reference 11).

In an admittedly rough way, the electric field of the neighboring ion may be replaced by the Coulomb field of a point charge $+e$ at the center of the alkali. Considering that the distance r between the nuclei is fairly large, we may develop the potential

$$e/R=e/r+ez/r^2+e(2z^2-x^2-y^2)/2r^3+\cdots \tag{11}$$

and consider the polarization of the F^- ion by the various terms. For a simple evaluation we have used a crude model in which the electrons are treated as isotropically bound oscillators, with a suitable frequency for each shell. For the $2p$ shell of the F^- ion, a value of the frequency $\tilde{\omega}=4.10^{16}$ or $\hbar\tilde{\omega}=26$ ev may be estimated from the polarizability $\alpha=Ze^2/m\tilde{\omega}^2$, Z being now the number of electrons in the shell. The polarizability is about 10^{-24} cm^3. A lower limit for $\hbar\tilde{\omega}$ is certainly 5 ev.

Now consider first the second term in (11),

representing a constant field $\mathcal{E}=e/r^2$. The effect of this is merely to shift the center of a shell with respect to the F nucleus by a small amount $\alpha\mathcal{E}/Ze$. The shell remains spherically symmetrical around the new center. When the system rotates about the F nucleus, the ensuing motion of the shell will be of the same type as that described in Section IV for the inner shells of the alkali. It is quite easy to compute the magnetic moment and field. The magnetic moment is, rather obviously, the same as one would find in a purely classical treatment of the elastically bound electrons:

$$M=-\omega(\alpha\mathcal{E})^2/2Zec=-\omega(Ze/2c)(e\mathcal{E}/m\tilde{\omega}^2)^2. \quad (12)$$

This gives for the outer shell $(2s+2p)$ in the case of LiF, a value between 0.001 and 0.6 nuclear magneton as $\tilde{\omega}$ is varied between the limits indicated above.[12] The magnetic field generated at the F nucleus depends on the charge distribution in the shell. For a shell consisting of s electrons, the field is obtained on multiplying the moment (12) by $(8/3\sqrt{\pi})(m\tilde{\omega}/\hbar)^{3/2}$. The net result is a field proportional to $\tilde{\omega}^{-5/2}$, so that *the contribution of the inner shells is negligible compared to that of the outer shells*, as we stated before. On the other hand, it is found that for a $2p$ shell the field at the center is much weaker than for $2s$ electrons, because of the lower density at the center. Assuming for an optimistic evaluation the formula for s electrons and applying it also to the $2p$ electrons, the ensuing field is still uncomfortably small. It may be pushed up to 2.5 gauss in LiF, or one-half the experimental value, by assuming for $\tilde{\omega}$ the lower limit indicated above, but this is already an extreme assumption; since we are dealing with the perturbation caused by a homogeneous field, the higher value of $\tilde{\omega}$ indicated by the polarizability should be much nearer to the truth.

Considering now the third term in Eq. (11), we may have the advantage that for this type of perturbation the average excitation energy may be closer to the lower limit of 5 ev. On the other hand, the result will be smaller by a factor $(r_0/r)^2$, r_0 being an average radius of the F^- ion. This is confirmed by the detailed computation in the case of the elastically bound electrons. The effect of the perturbation is to make the frequency $\tilde{\omega}_1$ in the direction of the line joining the nuclei lower than the frequency $\tilde{\omega}_2$ in a perpendicular direction. We do not give the details of the calculation, which is quite elementary, as all the matrix elements needed for Eqs. (3) and (4) are known. For s electrons the result is quite simple; the stream lines instead of being circles, are equilateral hyperbolae $y^2-z^2=$const. The magnetic moment is $[(\tilde{\omega}_2-\tilde{\omega}_1)/(\tilde{\omega}_2+\tilde{\omega}_1)]^2$ times the moment for rigid rotation. This factor turns out to be 0.3. The field at the center is only 0.12 of the field for rigid rotation, assuming an optimistic value $\tilde{\omega}=10^{16}$. All these data refer to LiF; in CsF the disagreement with experiment is stronger, because of the larger internuclear distance. We have also examined the case of p electrons; the current distribution is then so unfavorable that the field in the center becomes quite negligible.

The conclusion to be drawn from all this is that the polarized-ion model does not give a very satisfactory representation of the facts, although by some stretching it can be made to yield fields that are not much smaller than those observed.

It may be pointed out that the models we have considered so far do not clearly exhibit one feature that may be of importance. Let us first consider the extreme case of a molecule with a very low excited Π-state, connected to the Σ ground state by a strong L_{n0} matrix element. This will obviously make the induced momentum, Eq. (4), very strong. Physically, this means that the molecule has a nearly free angular momentum that tends to set itself parallel to the rotation axis. Now, although the alkali halides certainly do not approach this extreme case, it is clear that the kind of gyroscope-like distortion of the electronic motion we have just described will be present to a certain extent. In particular it may be noticed[13]

[12] It may be pointed out that this result is not really dependent on the special assumption of elastically bound electrons. One may arrive at a formula perfectly similar to Eq. (12), with the sole difference that $\hbar\tilde{\omega}$ is replaced by an average excitation energy of the electrons, if one replaces in Eq. (4) the energy difference in the denominator by an average value, thus expressing the magnetic moment in a form similar to Eq. (6). The average value of L_z^2 for the shell, when it is polarized by the homogeneous field, may be evaluated by perturbation theory, again introducing a suitable average value for the excitation energy.

[13] H. M. Foley, in the press. I wish to thank Dr. Foley for allowing me to see his manuscript before publication.

that the partially non-ionic character of the ground state will endow the molecule with a small component of orbital angular momentum precessing about the internuclear axis (this momentum being due to the hole in the $2p$ shell of the F atom, when it is in the neutral state). What is more important, it is not difficult to see that the currents induced by the rotation under these circumstances have just the type of space distribution that is most favorable to a strong field in the center,[11] so that the assumption made at the end of Section III about the connection between L_{n0} and H_{n0} is in this case well justified. It seems, therefore, that this model may give a satisfactory account of the data.

I wish to thank Dr. Rabi for attracting my attention to the large width of the resonance lines in LiF, CsF. Dr. Van Vleck kindly made available to me an early evaluation he had made independently by means of Hebb's formulae (unpublished). I am deeply indebted especially to Dr. Teller for his friendly interest and much helpful advice.

This work was partly supported under Contract N6-ori-83 with the Office of Naval Research.

PHYSICAL REVIEW VOLUME 73, NUMBER 1 JANUARY 1, 1948

Note on the Dirac Character Operators

E. M. CORSON
Institute for Advanced Study, Princeton, New Jersey

(Received July 7, 1947)

The Dirac character operators are evaluated for the classes of the symmetric group consisting of the triad, double interchange, tetrad, and pentad, and the corresponding group-theoretical primitive characters are listed for comparison. It is also shown that the evaluation of these and similar character operators is all that is required for the solution of the standard molecular problems in the spirit of Dirac's original program which avoids appeal to formal group theory.

I. INTRODUCTION

SOME years ago Dirac[1] established the remarkable exchange-spin identity

$$\mathbf{P}_{ij}=-\tfrac{1}{2}(1+\boldsymbol{\sigma}_i\cdot\boldsymbol{\sigma}_j), \tag{1}$$

which expresses the simple interchanges of electron orbits in terms of the associated vector-spin operators. In the discussion of the classification of multiplets he introduced the character (class) operators

$$\chi_c=\frac{1}{n_c}\sum_{\text{class}}\mathbf{P}_c, \tag{2}$$

defined as the average of all similar permutations, and showed that the *almost* exclusive states are characterized by the different sets of eigenvalues of these operators. These operators commute with all permutations so that in an irreducible representation of the symmetric group their matrices are scalar (Schur's lemma),[2] and it follows that the eigenvalues of the χ's are simply the corresponding primitive group characters divided by the dimension of the representation;[3] *viz.*,

$$\chi'[2^{\alpha_2}\cdots n^{\alpha_n}]=[2^{\alpha_2}\cdots n^{\alpha_n}]/[I], \tag{3}$$

where $\{2^{\alpha_2}\cdots n^{\alpha_n}\}$ is the usual group exponent notation (omitting unary cycles) for the partition[4] of n defining the class of permutations, and the square brackets indicate the associated primitive characters; $[I]$ being that of the unit class. From the result (1) and the expression

$$\sum_{i<j}(\boldsymbol{\sigma}_i\cdot\boldsymbol{\sigma}_j)=\tfrac{1}{2}[4\mathbf{S}(\mathbf{S}+1)-3n]=\mathfrak{p} \tag{4}$$

[1] Cf. P. A. M. Dirac, *Quantum Mechanics* (Clarendon Press, Oxford, 1935).

[2] Cf. F. D. Murnaghan, *Theory of Group Representations* (The Johns Hopkins University Press, Baltimore, 1938).

[3] This may be easily seen by operating on a degenerate set of eigenstates (symbolic $|>$'s) with the χ's and taking the spur, the degree of degeneracy being, of course, the dimension of the representation.

[4] $\alpha_1+2\alpha_2+\cdots n\alpha_n=n$.

defining the spin magnitude variable **S**, Dirac obtains the character variable of the class of interchanges in the form

$$\chi[2]=\frac{2}{n(n-1)}\sum_{i<j}\mathbf{P}_{ij}$$
$$=-\frac{2}{2n(n-1)}\sum_{i<j}(1+\boldsymbol{\sigma}_i\cdot\boldsymbol{\sigma}_j) \quad \text{(A)}$$
$$=-\frac{2}{2n(n-1)}\left\{\frac{n(n-1)}{2}+\mathfrak{y}\right\},$$

so that the exclusive sets of states are defined by the eigenvalues of **S**.[5]

For many purposes this result is essentially all that is required as regards group theory, e.g., the calculation of atomic term energies (without resolution of coincident terms).[6]

II.

It is not our purpose to consider here the details of these calculations for the atomic case and the modifications required in the case of coincident orbits. These may be found in the references of the preceding footnote. We wish to consider here the evaluation of some of the character variables of higher order, which is per se not entirely trivial; and moreover these more general variables are essentially all that is required in order to solve the 4–8 electron problems,[7] for example, in accord with Dirac's original program of avoiding appeal to formal group theory.

The characters considered here as examples are $\chi[3]$, $\chi[2^2]$, $\chi[4]$, $\chi[5]$, and we may merely list some easily verified aids to computation, *viz.*,

$$\mathfrak{y}^2=\frac{3n(n-1)}{2}+2(n-3)\mathfrak{y}$$
$$+\sum_{i<j}\sum_{\substack{k<l\\ \neq i,j}}(\boldsymbol{\sigma}_i\cdot\boldsymbol{\sigma}_j)(\boldsymbol{\sigma}_k\cdot\boldsymbol{\sigma}_l), \quad \text{(5a)}$$

$$(\boldsymbol{\sigma}_i\cdot\boldsymbol{\sigma}_j)(\boldsymbol{\sigma}_i\cdot\boldsymbol{\sigma}_k)=(\boldsymbol{\sigma}_j\cdot\boldsymbol{\sigma}_k)+i\boldsymbol{\sigma}_i\cdot\boldsymbol{\sigma}_j\times\boldsymbol{\sigma}_k, \quad \text{(5b)}[8]$$

$$(\boldsymbol{\sigma}_i\cdot\boldsymbol{\sigma}_j)(\boldsymbol{\sigma}_i\cdot\boldsymbol{\sigma}_k)+(\boldsymbol{\sigma}_j\cdot\boldsymbol{\sigma}_i)(\boldsymbol{\sigma}_j\cdot\boldsymbol{\sigma}_k)$$
$$=(\boldsymbol{\sigma}_j\cdot\boldsymbol{\sigma}_k)+(\boldsymbol{\sigma}_i\cdot\boldsymbol{\sigma}_k), \quad \text{(5c)}$$

$$(\boldsymbol{\sigma}_i\cdot\boldsymbol{\sigma}_j)(\boldsymbol{\sigma}_i\cdot\boldsymbol{\sigma}_k)+(\boldsymbol{\sigma}_k\cdot\boldsymbol{\sigma}_j)(\boldsymbol{\sigma}_k\cdot\boldsymbol{\sigma}_i)$$
$$=(\boldsymbol{\sigma}_j\cdot\boldsymbol{\sigma}_k)+(\boldsymbol{\sigma}_j\cdot\boldsymbol{\sigma}_i), \quad \text{(5d)}$$

and as a special case of these when $j=k$,

$$(\boldsymbol{\sigma}_i\cdot\boldsymbol{\sigma}_j)^2=3-2(\boldsymbol{\sigma}_i\cdot\boldsymbol{\sigma}_j). \quad \text{(5e)}$$

The class $\{3\}$. Here one readily obtains

$$\chi[3]=\frac{3}{4n(n-1)(n-2)}$$
$$\times\sum_{i=1}^{n-2}\sum_{j>i}^{n}\sum_{\substack{k>i\\ \neq j}}\{(1+\boldsymbol{\sigma}_i\cdot\boldsymbol{\sigma}_j)(1+\boldsymbol{\sigma}_j\cdot\boldsymbol{\sigma}_k)\} \quad \text{(B)}$$
$$=\frac{3}{4n(n-1)(n-2)}$$
$$\times\left\{\frac{n(n-1)(n-2)}{3}+2(n-2)\mathfrak{y}\right\},$$

and we leave the result in unsimplified form here, as in later cases, to show more clearly the origin of the various terms in the final expression.

The class $\{2^2\}$.

$$\chi[2^2]=\frac{8}{4n(n-1)(n-2)(n-3)}\sum_{i=1}^{n-3}\sum_{j>i}\sum_{\substack{k>i\\ \neq j}}\sum_{\substack{l>k\\ \neq j}}$$
$$\times\{(1+\boldsymbol{\sigma}_i\cdot\boldsymbol{\sigma}_j)(1+\boldsymbol{\sigma}_k\cdot\boldsymbol{\sigma}_l)\}$$
$$=\frac{8}{4n(n-1)(n-2)(n-3)}$$
$$\left\{\frac{n(n-1)(n-2)(n-3)}{8}+\frac{\mathfrak{y}^2}{2}\right. \quad \text{(C)}$$
$$\left.+\frac{(n-3)(n-4)}{2}\mathfrak{y}-\frac{3n(n-1)}{4}\right\}.$$

The class $\{4\}$.

$$\chi[4]=\frac{-4}{8n(n-1)(n-2)(n-3)}\sum_{i}^{n-3}\sum_{j>i}\sum_{\substack{k>i\\ \neq j}}\sum_{\substack{l>i\\ \neq j,k}}$$
$$\times\{(1+\boldsymbol{\sigma}_i\cdot\boldsymbol{\sigma}_j)(1+\boldsymbol{\sigma}_i\cdot\boldsymbol{\sigma}_k)(1+\boldsymbol{\sigma}_i\cdot\boldsymbol{\sigma}_l)\}$$
$$=\frac{-4}{8n(n-1)(n-2)(n-3)} \quad \text{(D)}$$
$$\left\{\frac{n(n-1)(n-2)(n-3)}{4}+\mathfrak{y}^2\right.$$
$$\left.+(n-3)(3n-8)\mathfrak{y}-\tfrac{3}{2}n(n-1)\right\}.$$

---

[5] Equivalently, the eigenvalues of **S** define the permissible eigenvalues of the χ, and hence the particular irreducible representations allowed by the exclusion principle.

[6] Cf. P. A. M. Dirac, see reference 1; J. H. Van Vleck, Phys. Rev. **45**, 405 (1934); R. Serber, Phys. Rev. **45**, 461 (1934).

[7] Including non-orthogonality correction, if desired.

[8] Dirac, see reference 1.

The class $\{5\}$.

$$\chi[5]=\frac{5}{16n(n-1)(n-2)(n-3)(n-4)}\times\sum_{i}^{n-4}\sum_{j>i}\sum_{k>i,\neq j}\sum_{l>i,\neq j,k}\sum_{m>i,\neq j,k,l}\{(1+\sigma_i\cdot\sigma_j)(1+\sigma_i\cdot\sigma_k)(1+\sigma_i\cdot\sigma_l)(1+\sigma_i\cdot\sigma_m)\}$$

$$=\frac{5}{16n(n-1)(n-2)(n-3)(n-4)}\times\left\{\frac{n(n-1)(n-2)(n-3)(n-4)}{5}+4(n-4)\mathfrak{y}^2+4(n-3)(n-4)^2\mathfrak{y}-6n(n-1)(n-4)\right\}. \quad (E)$$

These may be compared with the corresponding group-theoretical results

$$[2]=-\binom{n-2}{k}+\binom{n-2}{k-1}-\binom{n-2}{k-2}+\binom{n-2}{k-3}, \quad (A')$$

$$[3]=\binom{n-3}{k}-\binom{n-3}{k-1}+\binom{n-3}{k-3}-\binom{n-3}{k-4}, \quad (B')$$

$$[2^2]=\binom{n-4}{k}-\binom{n-4}{k-1}+2\binom{n-4}{k-2}-2\binom{n-4}{k-3}+\binom{n-4}{k-4}-\binom{n-4}{k-5}, \quad (C')$$

$$[4]=-\binom{n-4}{k}+\binom{n-4}{k-1}-\binom{n-4}{k-4}+\binom{n-4}{k-5}, \quad (D')$$

$$[5]=\binom{n-5}{k}-\binom{n-5}{k-1}+\binom{n-5}{k-5}-\binom{n-5}{k-6}, \quad (E')$$

$$k=\frac{n}{2}-S,$$

$$[I]=\binom{n}{k}-\binom{n}{k-1}$$

$=$dimension of representation.

These are obtained from the general expression given by Wigner,[9] namely, that within the restriction imposed by the exclusion principle the primitive character of the class of permutations of ρ cycles, with cycle lengths $\lambda_1, \lambda_2, \cdots \lambda_\rho$ is the coefficient of x^k in

$$(-)^{n-\rho}(1-x)(1+x^{\lambda_1})(1+x^{\lambda_2})\cdots(1+x^{\lambda_\rho}). \quad (6)$$

It does not appear to be possible to obtain a corresponding general result from the present primitive method because of the requirement of explicit resolution into products of interchanges, although the signature $(-)^{n-\rho}$ is a trivial consequence of the relation (1) and a cycle of length λ is resolvable into a product of $\lambda-1$ interchanges.

The application of the results (A–E) to the afore-mentioned molecular problems derives basically from Dirac's result that the average eigenvalue of $\mathbf{V}$ (for the states of a given multiplicity) is given by

$$\langle V'\rangle=\sum_P\langle P\alpha|\mathbf{V}|\alpha\rangle\chi'[P]=\sum_P V_P\chi'[P], \quad (7)$$

where $\mathbf{V}=\sum_P V_P\mathbf{P}$ represents the perturbation energy *or* the Hamiltonian, depending on the choice of the unperturbed functions $\langle x|P\alpha\rangle=\Pi_j\langle x_j'|P\alpha_j\rangle$ over which the matrix of $\mathbf{V}$ is defined. Correspondingly, as Dirac notes, the average eigenvalue of any function of $\mathbf{V}$ may be evaluated in similar fashion. Hence we need only evaluate the iterated quantities $\mathbf{V}$, $\mathbf{V}^2$, $\mathbf{V}^3$, $\cdots$ etc., the number of iterations depending on the number of states of a given multiplicity involved, and substitute the appropriate character eigenvalues as obtained from (A–E) to calculate the levels for various multiplicities. Thus, with (A) alone London's equation for 4 electrons follows in trivial fashion from the evaluation of $\langle V'\rangle$, $\langle V'^2\rangle$, and the generalization, including non-

[9] E. P. Wigner, *Gruppentheorie* (F. Vieweg und Sohn, Braunschweig, 1931), pp. 149, 196.

orthogonality correction, may be readily obtained by using the results (A–D). The calculations for the 6- and 8-electron problems are, of course, more tedious, but proceed along similar lines[10] after calculation of the additional requisite character operators for the higher order classes.

In this more physical approach the presence of additional elements of (space) symmetry in a given problem is also recognized by noting that **V** commutes with a certain *subgroup* of the symmetric group involved, the character operators of which therefore furnish additional commuting constants of the motion whose values may be simultaneously assigned, leading to a further significant classification of energy levels and a simplification of the problem. Group-theoretically this, of course, corresponds to recognizing that the rotation-reflection group of **V** (under which **V** is invariant) in such cases is realizable in terms of an appropriate subgroup of the symmetric group, i.e., with which it is abstractly identical. Thus, one finds *six* additional commuting constants of the motion in the 6-electron problem with hexagonal symmetry, *five* for octahedral symmetry, *ten* in the 8-electron problem with (extended) cubic symmetry, etc.[11] Needless to say, the more formal treatment, as given by Serber, is in many respects simpler since it is guided by the more definite prescription of group theory proper, but the present viewpoint shows again that following Dirac's program the formal group methods can, in effect, be avoided.

[10] This method may be compared with the equivalent treatment given by R. Serber, J. Chem. Phys. **2**, 697 (1934), along more matrical (group-theoretical) lines, which comparison also serves to show the relation between the symbolic and formal group methods. It may be mentioned that the iterations in the latter method give sums of eigenvalues rather than averages, for obvious reasons. Cf. Eq. (3).

[11] R. Serber, see reference 10.

PHYSICAL REVIEW VOLUME 73, NUMBER 1 JANUARY 1, 1948

On the Rydberg-Ritz Formula in Quantum Mechanics

ROBERT JASTROW
Columbia University, New York, New York

(Received September 22, 1947)

A derivation is given of the Rydberg-Ritz formula for series spectra. Simple expressions are obtained for the Rydberg and Ritz coefficients. It is shown that the Ritz coefficient is proportional to the difference between the radial period of the electron and the period of the hypothetical orbit, with the same energy which would exist if the atomic core were to contract to zero radius.

The derivation necessitates a study of the confluent hypergeometric function. An expansion in powers of the energy is obtained for this function. The coefficients in the expansion are found to be simple combinations of Bessel functions.

Calculations of the Rydberg and Ritz coefficients are carried out for the *S* series of Na, K, and Cs and show satisfactory agreement with observation. The comparison with experiment yields information concerning the relative accuracy of different types of central fields employed to approximate the effect of the atomic core upon the valence electron. It is concluded that the Hartree-Fock field is not a convenient starting point for this purpose.

1. INTRODUCTION

IT is known that in many cases the terms of series spectra obey the empirical Rydberg-Ritz formula,

$$E=-\frac{1}{2}\frac{1}{(n+\alpha+\beta E)^2}, \tag{1.1}$$

where E is the energy expressed in atomic units, n is the principal quantum number, and α and β are the Rydberg and Ritz coefficients, respectively. For a given atom these coefficients depend only upon l, the azimuthal quantum number.

Bohr, considering the electron as moving in the static central field arising from the nucleus and the core electrons, gave an ingenious derivation of (1.1) on the basis of the old quantum

theory.[1] Bohr's theory contained an interesting physical interpretation for the Ritz coefficient, β. He found that β should be proportional to the difference between the actual radial period of the electron and the period of the hypothetical orbit, with the same energy, which the electron would traverse if the core were to shrink to zero radius. Calling these periods t and t^*, Bohr's formula runs

$$\beta = R(t - t^*).$$

In a series of papers on atoms with non-Coulomb central fields,[2] Hartree showed that wave mechanics leads naturally to the following general expression for the effective quantum number, n,

$$n = (-2E)^{-\frac{1}{2}} = \mathfrak{n} + \alpha + \beta E + \gamma E^2 + \cdots, \quad (1.2)$$

which is identical with (1.1) if the development is broken off after the second term. Some formulae pertaining to the calculation of the Ritz coefficient were subsequently derived by Hargreaves[3] but no applications were given.

In the present paper we will investigate in detail the nature of the Rydberg and Ritz coefficients. Particular attention will be paid to the latter, since it offers the problem of determining the wave mechanical justification for the formula of Bohr. It will be shown that our expression can be brought into a form which corresponds to the Bohr interpretation.

The formula will be applied to the calculation of β for the S series of Na, K, and Cs. The agreement with experiment is satisfactory.

The numerical results depend upon the type of central field used in the calculation. Comparison of these results with experiment thus gives information concerning the validity, for use in a central field approximation, of various methods for finding the effective core distribution. The matter is discussed in Section 4, but we note here the conclusion that the Hartree-Fock field does not seem to be suitable for this purpose.

The general energy level formula is determined by the condition that the wave function inside the atomic core must join smoothly, at some intermediate point, with the wave function valid at large distances from the nucleus. The latter function satisfies the hydrogen wave equation, since a Coulomb field prevails outside the core.

For this hydrogenic solution, known to be the confluent hypergeometric function, an expansion in powers of the energy will be required. The problem of obtaining this expansion in a simple way has been partially treated by Wannier.[4] The complete expansion is obtained in Section 2 of this paper, and is of some interest apart from its application to our problem. As will be seen, the coefficients in the expansion are simple combinations of Bessel functions.

Notation

In what follows we will use Hartree atomic units. If R is the radial part of the wave function for the valence electron, we define P by

$$P = rR.$$

P satisfies the equation

$$P'' + 2\left(E - V - \frac{l(l+1)}{2r^2}\right)P = 0. \quad (1.3)$$

Here E is the energy of the electron, $V(r)$ is the central field in which it is assumed to move, and l is the azimuthal quantum number. The effective quantum number, n, and the energy parameter, ϵ, are defined by: $\epsilon = 1/n^2 = -2E$.

All quantities which refer to the region of the atomic core will be distinguished by a superscript "i" standing for interior, while quantities referring to the region exterior to the core will have attached a superscript "e." E.g., the radial solution valid inside the core will be denoted by ${}^iP$ and the exterior solution in the Coulomb region by ${}^eP$.

2. THE EXTERIOR SOLUTION (COULOMB REGION)

An Integral Representation

The solution of the hydrogenic wave equation which vanishes at infinity is a confluent hypergeometric function, $W_{n,l+\frac{1}{2}}(2r/n)$, in the nota-

[1] M. Born, *Vorlesungen Über Atommechanik* (Verlag Julius Springer, Berlin, 1925), pp. 185–187.
[2] D. R. Hartree, Proc. Camb. Phil. Soc., **24**, 426 (1928); **25**, 310 (1929).
[3] J. Hargreaves, Proc. Camb. Phil. Soc. **25**, 315 (1929).
[4] G. H. Wannier, Phys. Rev. **64**, 358 (1943).

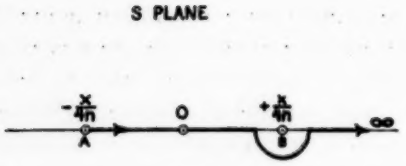

FIG. 1. The contour C which defines ${}^{e}P$, the confluent hypergeometric function vanishing at infinity.

tion of Whittaker and Watson.[5] We rewrite (1.3) for a Coulomb field,

$$ {}^{e}P''+\left(-\frac{1}{n^2}+\frac{2}{r}-\frac{l(l+1)}{r^2}\right){}^{e}P=0. \quad (2.1) $$

It is possible to write the required solution to (2.1) in the form of the following integral,

$$ {}^{e}P(x)=x^{-2l-1} $$

$$ \times Re\left\{\frac{1}{2\pi i}\int_{c} e^{-\frac{1}{2}xs}\frac{\left(1+\dfrac{4ns}{x}\right)^{n-l-1}}{\left(1-\dfrac{4ns}{x}\right)^{n+l+1}}ds\right\}, \quad (2.2) $$

where the independent variable is now $x=(8r)^{\frac{1}{2}}$. Constant multiplicative factors have been disregarded.

The left side of (2.2) satisfies (2.1) if the contour C fulfills the following condition:

$$ \frac{e^{-\frac{1}{2}xs}}{x^2}\left(\frac{1+\dfrac{4ns}{x}}{1-\dfrac{4ns}{x}}\right)^{n}\Bigg|_{c}^{f}=0 \quad (2.3) $$

The integrand in (2.2) has branch points at $s=\pm x/4n$, consequently a cut is drawn between these two points.

In Fig. 1 is shown a contour which satisfies (2.3). The arguments of both $[1+(4ns/x)]$ and $[1-(4ns/x)]$ are zero along the stretch AB. Therefore the part of the integral from the negative half of the s plane, which becomes infinite as x approaches infinity, is purely real and does not contribute to ${}^{e}P$. The remainder goes to zero as $x\to\infty$, hence ${}^{e}P$ vanishes at infinity. Thus (2.2) gives the desired solution.

[5] Whittaker and Watson, *Modern Analysis* (The Cambridge University Press, 1927), §16.12 (example).

In the region $B\to\infty$ the argument of $[1+(4ns/x)]$ remains zero, but that of $[1-(4ns/x)]$ has increased to πi. We may therefore write (2.2) in the form

$$ {}^{e}P=Re\left\{\frac{e^{-n\pi i}}{2\pi i}\int_{c} e^{-\frac{1}{2}xs}\frac{\left(1+\dfrac{4ns}{x}\right)^{n-l-1}}{\left(1-\dfrac{4ns}{x}\right)^{n+l+1}}s^{-2l-2}ds\right\}, \quad (2.4) $$

provided the arguments of both $[1+(4ns/x)]$ and $[1-(4ns/x)]$ are taken as zero along $B\to\infty$. This form is convenient for comparison with the Bessel functions, since for $n\to\infty$ the integral in (2.4) will converge to the well known Schläfli representation for the Hankel function of the first kind.

We denote the integral in (2.4) by H_l^n, and its real and imaginary parts by J_l^n and N_l^n, so that

$$ H_l^n=J_l^n+iN_l^n. $$

Using these definitions,[6]

$$ {}^{e}P=xRe\{e^{-n\pi i}H_l^n\} $$

$$ =xJ_l^n\cos\pi n+xN_l^n\sin\pi n. \quad (2.5) $$

The integral in (2.4) has been labeled H_l^n with the intention of indicating that it has the nature of an extended Hankel function. Similarly, J_l^n and N_l^n are related to the Bessel and Neumann functions. It will be shown below that H_l^n may be expanded in powers of the energy, i.e., of $1/n^2$, the coefficients in the expansion being linear combinations of Hankel functions.

We note that the approximately sinusoidal dependence upon n, expressed in (2.5), agrees with the results of Hartree and of Wannier.

[6] It is of interest to note that as n approaches infinity the solution to the limiting form of the equation for ${}^{e}P$ differs from the limiting form of the solution, since the latter never loses its sinusoidal dependence upon n. This anomaly arises from the fact that ${}^{e}P$ is subject to a boundary condition at infinity. The effect of the infinite interval of integration is clarified by making the transformation, $r=1/u$ upon the independent variable in (2.1). The transformed equation is

$$ \frac{d^2{}^{e}P}{du^2}+\frac{2}{u}\frac{d{}^{e}P}{du}+\left(-\frac{1}{n^2u}+\frac{2}{u^2}-l(l+1)\right){}^{e}P=0. $$

We see from this equation that in the neighborhood of $u=0$, i.e., for large r, the term involving n becomes important no matter how large n may be. We are indebted to Professor F. J. Murray for this point.

Expansion in Powers of the Energy

We wish to show the relation of H_l^n to the ordinary Hankel function of the first kind, defined by

$$H_l^{(1)}(x)=(-1)^{l+1}\frac{1}{\pi i}\int_0^\infty e^{-\frac{1}{2}x(s-1/s)}s^{-l-1}ds, \quad (2.6)$$

where the contour is as in Fig. 2. To do this we write the integrand in (2.4) in the form[7]

$$e^{-\frac{1}{2}x(s-1/s)}s^{-2l-2}a\left(\frac{x}{4ns}\right), \quad (2.7)$$

where

$$\begin{aligned}a(v)&=e^{-2vn}\left(\frac{1+v}{1-v}\right)^n(1-v^2)^{-l-1}\\&=1+(l+1)v^2+\tfrac{2}{3}nv^3+\cdots\\&=1+\left[(l+1)\frac{x^2}{16s^2}+\frac{2}{3}\frac{x^3}{64s^3}\right]\frac{1}{n^2}+\cdots. \quad (2.8)\end{aligned}$$

The expansion of $a(v)$ in powers of v or of $1/s$ is possible if s is always large enough so that $|v|=|x/4ns|<1$. In Fig. 3 we have redrawn the contour of Fig. 1 so as to satisfy this condition.

If the result of the expansion of $a(v)$ is substituted in (2.7), the latter becomes a series each of whose terms has the form of the integrand in (2.6). More important, it is readily seen from (2.8) that $a(v)$ contains n only in powers of $1/n^2$. Hence the expansion of $a(v)$ is a power series in ϵ.

Substituting the expansion of (2.7) into (2.4), we obtain the desired formal expansion of H_l^n in powers of ϵ. The functions which constitute the expansion coefficients are integrals whose integrands are identical with those defining the Hankel functions, but whose contours differ from the Hankel contours in that one terminus is at $s=-x/4n$, rather than at $s=0$. (Compare Figs. 2 and 3.) However, this difference is not an essential one, because the contour in Fig. 3 may be broken into two parts,

$$\int_{-x/4n}^{\infty}=\int_0^\infty-\int_0^{-x/4n},$$

of which the first is the Hankel contour, and the second, from $s=0$ to $s=-x/4n$, may easily be shown to behave as e^{-2n} and consequently may be neglected beside any power of $1/n^2$.

Using (2.6), (2.7), and (2.8) together with the definition of H_l^n in (2.4), and neglecting the terms behaving as e^{-2n}, we have

$$\begin{aligned}&H_l^n=F_0+F_1\epsilon+F_2\epsilon^2+\cdots;\\&F_0=xH^{(1)}{}_{2l+1},\\&F_1=\left[(l+1)\frac{x^3}{16}H^{(1)}{}_{2l+3}-\frac{x^4}{96}H^{(1)}{}_{2l+4}\right], \text{ etc.}\end{aligned} \quad (2.9)$$

For reference below we combine (2.5) and (2.9) into the final result for the series expansion of ${}^eP$,

$${}^eP=Re\left\{e^{-n\pi i}\left[xH^{(1)}{}_{2l+1}+\left((l+1)\frac{x^3}{16}H^{(1)}{}_{2l+3}-\frac{x^4}{96}H^{(1)}{}_{2l+4}\right)\epsilon+\cdots\right]\right\}. \quad (2.10)$$

3. THE INTERIOR WAVE FUNCTION

In the preceding section we have determined the dependence upon n of the exterior solution to the radial wave equation in a Coulomb field. We will now consider certain features of the solution which obtains in the neighborhood of the nucleus. We assume for this solution an expansion in powers of $\epsilon=1/n^2$. Let

$${}^iP={}^iP_0+{}^iP_1\epsilon+{}^iP_2\epsilon^2+\cdots={}^iP_0(1+{}^iT_\epsilon). \quad (3.1)$$

${}^iT$ is defined by the two relations in (3.1).

In order that the interior and exterior solutions should join smoothly, their logarithmic derivatives must be equal at any intermediate point. Consequently, it is the energy dependence of $\varphi=P'/P$ in which we are interested, rather than in that of P itself. We have, using (3.1),

$${}^i\varphi={}^i\varphi_0+{}^i\varphi_1\epsilon;\ {}^i\varphi_0={}^iP_0'/{}^iP_0,\ {}^i\varphi_1={}^iT'. \quad (3.2)$$

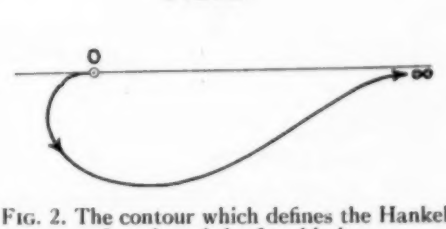

FIG. 2. The contour which defines the Hankel function of the first kind.

[7] The manipulation of the integrand herein performed is identical with that carried out by Wannier for J_l^n.

We now determine ${}^iT'$ from the differential equation satisfied by P. Let ${}^iP_0$ be a solution of the equation

$$ {}^iP_0''+\left(-2V-\frac{l(l+1)}{r^2}\right){}^iP_0=0, \qquad (3.3) $$

and let ${}^iP$ be a solution of

$$ {}^iP''+\left(-\epsilon-2V-\frac{l(l+1)}{r^2}\right){}^iP=0. \qquad (3.4) $$

Substituting (3.1) into (3.4) and making use of (3.3), we obtain

$$ 2{}^iP_0{}^iT'+{}^iP_0T''={}^iP. $$

Integrating,

$$ {}^iP_0{}^2{}^iT')_r-{}^iP_0{}^2{}^iT')_a=\int_a^r {}^iP_0{}^2dr+0(\epsilon). $$

For the interior wave function, $P_0{}^2T'$ is clearly zero at the origin. Hence

$$ {}^iT'(r)=\frac{1}{{}^iP_0{}^2}\int_0^r {}^iP_0{}^2dr. \qquad (3.5) $$

It is clear that a similar analysis can be applied to the exterior wave function, so that writing

$$ {}^eP={}^eP_0(1+{}^eT\epsilon), $$

one has, in analogy with (5),

$$ {}^eT'(r)=\frac{1}{{}^eP_0{}^2}\int_{r_p}^r {}^eP_0{}^2dr. \qquad (3.6) $$

Here the lower limit, r_p, is the value of r for which ${}^eT'$ vanishes. It may be shown, by using the formulae of Section 2, that ${}^eT'$ changes sign in the neighborhood of the classical perihelion of the electron's orbit. Hence, r_p is approximately equal to the perihelion distance.

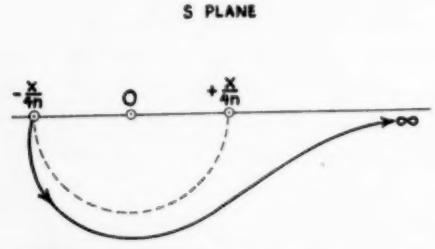

FIG. 3. The contour of Fig. 1 has here been redrawn so as to have $|s|>x/4n$. This is necessary for the expansion of the integrand in powers of $x/4ns$.

4. THE ENERGY LEVEL FORMULA

The matching condition determining the energy levels is

$$ {}^i\varphi={}^e\varphi, $$

or

$$ {}^i\varphi=\frac{F'+G'\tan\pi n}{F+G\tan\pi n}, \quad \left\{\begin{matrix}F=xJ_l{}^n\\ G=xN_l{}^n\end{matrix}\right\}, \qquad (4.1) $$

where (2.5) has been substituted for ${}^e\varphi$. Solving for n,

$$ \pi n=\pi\mathbf{n}-\tan^{-1}\gamma; \quad (\mathbf{n}=\text{positive integer}) \qquad (4.2) $$

$$ \gamma=\frac{F'-{}^i\varphi F}{G'-{}^i\varphi G}. $$

The Rydberg Coefficient

The Rydberg and Ritz coefficients, α and β, respectively, are defined by the expansion of the effective quantum number in powers of ϵ,

$$ n=\mathbf{n}+\alpha+\beta\epsilon+\cdots. \qquad (4.3) $$

From (4.2) and (4.3) we have for α,

$$ \alpha=\frac{1}{\pi}\tan^{-1}\gamma\Big)_{\epsilon=0} $$

$$ =\frac{1}{\pi}\tan^{-1}\gamma_0, \quad \gamma_0=\frac{F_0'-{}^i\varphi_0F_0}{G_0'-{}^i\varphi_0G_0}. \qquad (4.4) $$

The quantity γ_0 is to be evaluated at any point sufficiently far outside the core so that the field is Coulombian.

The expression for α becomes particularly simple if the matching is effected at a zero of ${}^iP_0$. Then

$$ \gamma_0=\frac{F_0}{G_0}=\frac{J_{2l+1}(x)}{N_{2l+1}(x)}. \qquad (4.5) $$

The matching condition expressed by (4.1) must be imposed well outside the atomic core. It was found that at any such point x is large enough to justify the use of the asymptotic expressions for the Bessel functions,

$$ J_{2l+1}=\left(\frac{2}{\pi x}\right)^{\frac{1}{2}}\left\{\cos\left[x-(2l+\tfrac{3}{2})\frac{\pi}{2}\right]+0\left(\frac{1}{x}\right)\right\}, \qquad (4.6) $$

$$N_{2l+1}=\left(\frac{2}{\pi x}\right)^{\frac{1}{2}}\left\{\sin\left[x-(2l+\tfrac{3}{2})\frac{\pi}{2}\right]+0\left(\frac{1}{x}\right)\right\}. \quad (4.7)$$

Combining (4.4), (4.5), (4.6), and (4.7), we arrive at the simple result

$$\alpha)_{ni}=\frac{x_0)_{ni}}{\pi}-\tfrac{1}{4}, \quad (4.8)$$

where x_0 is any zero of ${}^1P_0$ outside the core, and the subscript "*ni*" means "non-integral part of."

The Ritz Coefficient

From (4.3) we see that the Ritz coefficient is determined by

$$\beta=\frac{dn}{d\epsilon}\Big)_{\epsilon=0}. \quad (4.9)$$

Inserting (4.2) in (4.9),

$$\pi\beta=-\frac{1}{(1+\gamma_0^2)}\frac{d\gamma}{d\epsilon}\Big)_{\epsilon=0}$$

$$=-\frac{1}{1+\gamma_0^2}\left[\frac{F_0{}^1\varphi_1+F_1{}^1\varphi_0-F_1'}{G_0{}^1\varphi_0-G_0'}\right.$$

$$\left.-\frac{G_0{}^1\varphi_1+G_1{}^1\varphi_0-G_1'}{(G_0{}^1\varphi_0-G_0')^2}(F_0{}^1\varphi_0-F_0')\right]. \quad (4.10)$$

As with α, this expression may be made to assume a simple and rather elegant form at a zero of ${}^1P_0$. At such a point, using (3.2) and (3.5), (4.10) becomes

$$\pi\beta=\frac{1}{1+(F_0/G_0)^2}$$

$$\times\left[\frac{d}{d\epsilon}\left(\frac{G}{F}\right)_{\epsilon=0}+\frac{{}^1\varphi_1}{{}^1\varphi_0{}^2}\frac{d}{dr}\left(\frac{G_0}{F_0}\right)\right]. \quad (4.11)$$

It is clearly indicated by (4.11) that in place of F and G we should define two new variables, θ and ρ:

$$\theta=\tan^{-1}(G/F), \quad \rho=(F^2+G^2)^{\frac{1}{2}}. \quad (4.12)$$

When stated in terms of θ and ρ, the wave function is

$${}^eP=F\cos\pi n+G\sin\pi n=\rho\cos(\pi n-\theta). \quad (4.13)$$

From (4.11), (4.12), and (3.5), the Ritz coefficient is now given by

$$\pi\beta=d\theta/d\epsilon)_{\epsilon=0}+\frac{\theta_0'}{{}^1P_0'^2}\int_0^r {}^1P_0{}^2dr, \quad (4.14)$$

where θ_0 indicates θ evaluated at $\epsilon=0$.

The Bohr Formula

We show next that

$$\frac{d\theta}{d\epsilon}\Big)_{\epsilon=0}\propto {}^eP_0{}^2{}^eT'=-\int_{r_p}^r {}^eP_0{}^2dr. \quad (4.15)$$

This result will lead us to our desired interpretation of β as a certain difference in orbital periods, since

$$\int_{r_1}^{r_2} P^2dr$$

is proportional to the time the electron spends in the region between r_1 and r_2.

To achieve this we recall first from Section 3 that if ${}^e\varphi$ is written in the form

$${}^e\varphi={}^e\varphi_0+{}^e\varphi_1\epsilon,$$

then ${}^e\varphi_1={}^eT'$. For our purposes we need ${}^e\varphi$ in terms of θ and ρ rather than F and G. Using (4.13),

$${}^e\varphi={}^eP'/{}^eP=\eta+\theta'\tan(\pi n-\theta); \quad (\eta=\rho'/\rho)$$

$${}^e\varphi_1=d\varphi/d\epsilon)_{\epsilon=0}=d\eta/d\epsilon)_{\epsilon=0}+d\theta'/d\epsilon)_{\epsilon=0}$$

$$\times\tan(\pi n-\theta_0)-\theta_0'\frac{d\theta}{d\epsilon}\Big)_{\epsilon=0}\sec^2(\pi n-\theta_0).$$

We remember that the matching point has been assumed to be a zero of P_0[8] and therefore of $\cos(\pi n-\theta_0)$. Hence the last term in the expression above dominates the others and we have

$${}^e\varphi_1=-\frac{\theta_0'\dfrac{d\theta}{d\epsilon}\Big)_{\epsilon=0}}{\cos^2(\pi n-\theta_0)}. \quad (4.16)$$

The various derivatives of θ occurring in (4.14) and (4.16) may be expressed in terms of x by referring to (2.10) in order to determine the relation of θ to the Bessel functions, and then employing the asymptotic formulae (4.6) and

[8] The superscripts may be dropped outside the core since the two functions are identical in that region.

(4.7). We also use the following expression for P_0 which is obtained from (4.13) by means of (4.6) and (4.7):

$$ {}^{\epsilon}P_0 = x^{\frac{1}{2}} \cos(\pi n - \theta_0). \tag{4.17} $$

It is found in this way that (4.16) reduces to

$$ {}^{\epsilon}\varphi_1 = -\frac{4}{{}^{\epsilon}P_0^2}\frac{d\theta}{d\epsilon}\Big)_{\epsilon=0}. $$

Hence, since ${}^{\epsilon}\varphi_1 = {}^{\epsilon}T'$,

$$ d\theta/d\epsilon)_0 = -\tfrac{1}{4}P_0^2 T' = -\frac{1}{4}\int_{r_p}^{r} {}^{\epsilon}P_0^2 dr. $$

Referring again to (4.14), we find by a similar procedure that the coefficient therein occurring is given by

$$ \theta_0'/{}^{i}P_0'^2 = 1/4. $$

Substituting these results in (4.14), the Ritz coefficient becomes

$$ \pi\beta = \frac{1}{4}\left\{\int_0^r {}^{i}P_0^2 dr - \int_{r_p}^r {}^{\epsilon}P_0^2 dr\right\}. \tag{4.18} $$

The first integral on the right in (4.18) represents the time t which the electron spends within the radius r.[9] The second integral represents the time which the electron would spend in this region if it were traversing a hypothetical orbit with the same energy, but in a field which was Coulombian all the way down to the nucleus, i.e., assuming the radius of the core were to shrink to zero. Calling this hypothetical time t^*, we have from (4.18),

$$ \beta = (1/4\pi)(t - t^*). \tag{4.19} $$

The time in (4.18) is expressed in atomic units. (A.u./sec. $= h^3/8\pi^2 me^4$.) If t and t^* are expressed in seconds, we arrive at precisely the formula of Bohr,

$$ \beta = R(t - t^*). $$

TABLE I. Sodium.

	α	β	Ionization pot'l.
Observed	0.652	−0.07	4.145×10^4 cm^{-1}
Effective field	0.648	−0.06	4.155
Hartree-Fock field	0.780	−0.05	3.387

TABLE II. Potassium.

	α	β	Ionization pot'l.
Observed	0.822	−0.16	3.501×10^4 cm^{-1}
Hartree-Fock field	1.020	−0.11	2.766
Hartree-Fock field expanded 20%	0.860	−0.13	3.309

TABLE III. Casium.

	α	β	Ionization pot'l.
Observed	0.953	−0.29	3.114×10^4 cm^{-1}
Effective field	0.940	−0.27	3.162
Bohr Theory		−0.18	

5. COMPARISON WITH EXPERIMENT

The application of the formulae (4.8) and (4.14) for α and β requires a knowledge of ${}^{i}P_0$, the unbound or zero energy solution to the wave equation in the core region. This solution is obtained by numerical integration[10] of (3.4) out from the origin past the core, using a suitable potential $V(r)$.

In the course of carrying out these integrations, it was found that all factors which would be expected to affect ${}^{i}P_0$, such as small numerical errors, refinement of interval of integration, etc., left unchanged the positions of the zeros of ${}^{i}P_0$ although they did alter its amplitude. Now this means that the calculated value of α is largely independent of minor numerical mistakes or poor integration techniques, since (3.7) indicates that α depends only upon the position of these zeros. Unfortunately, β depends upon the amplitude of ${}^{i}P_0$ as well as upon the location of its zeros and consequently will be affected by integration errors.

In order to determine ${}^{i}P_0$ one must have a central field, $V(r)$, to use in the integration of the wave equation. One possible field for this purpose is the Hartree-Fock field of the core combined with the Coulomb field of the nucleus. Another possibility is an effective field so constructed to have the x-ray levels of an electron in this field match the observed levels, to a WKB approximation, for about twenty levels beginning with the K shell. For purposes of

[9] We have $t/T = \int_0^r p^2 dr / \int_0^\infty p^2 dr$, where T is the radial period of the electron. But when P is so normalized as to fit the relation (4.17), then it is found that $T = \int_0^\infty p^2 dr$. Hence directly $t = \int_0^r p^2 dr$.

[10] The integration method employed is described by L. Feinstein and M. Schwarzschild, Rev. Sci. Inst. 12, 405 (1941), although carried out by hand rather than with the punched card methods therein reported.

comparison, calculations were carried out for Na both with the Hartree-Fock field[11] and with an effective field determined in the second manner by Prokofjew.[12] Potassium was treated with a Hartree-Fock field,[13] and also with the same field after it had been uniformly expanded by 20 percent. Caesium was calculated with an effective field.[14] The Ritz coefficient for Cs was also computed from Bohr's formula directly as a difference in times, using half-integral angular momentum on the orbital model. The latter calculation is of interest because of the demonstration by Kramers[15] that the Bohr theory with half-integral angular momentum should provide a good approximation to the central field problem.

The results of these calculations are compared with the experimental values of α and β in Tables I, II, and III and are discussed below. The observed and calculated values for the first ionization potential are also included.

Comparison of the Two Types of Central Fields

The results for K and Na indicate that the uncorrected Hartree-Fock field does not provide a good approximation to a central field for the motion of the valence electron. From Table II it may be seen that a uniform expansion of the Hartree core distribution by 20 percent almost suffices to remove the discrepancy. A field expanded by 25 percent probably would produce quite good results.

The unsuitability of the unadjusted Hartree-Fock field for calculating optical energy levels also indicates that it should not be used for determining the valence electron wave functions. One may, of course, modify the field by adding to it fictitious polarization potentials, etc.,[16] and then adjusting various parameters in these added terms so as to have the calculated energy levels agree with the observed values. Biermann[16] has calculated the intensities of certain lines in the alkali spectra, using a Hartree field so modified by the introduction of fictitious potentials. He finds that the results show good agreement with the experimental values. However, even assuming one has available the Hartree-Fock field for a given atom, the additional labor required for the modification of this field to obtain good energy levels, and therefore good wave functions, is of the same order as the labor necessary for the entire construction of the effective field. For the heavier atoms the latter field is the only one possible since the Hartree-Fock calculations for these atoms are prohibitively long.

Tables I and III show good agreement between the experimental values of α and β and the values calculated from the effective fields on our theory. Because of the nature of the effective field, agreement as regards α is probably to be expected. However, our interest in the calculation was directed primarily toward the Ritz coefficient.

It is also indicated by Table III that the calculation based upon the Bohr theory, while of the right order of magnitude, compares rather unfavorably with the more exact result.

ACKNOWLEDGMENTS

The author is deeply indebted to Professor H. A. Kramers, who suggested this investigation and gave generously of his time in valuable discussions throughout its course. He wishes also to express his thanks to Professor L. H. Thomas, Dr. H. M. Foley, and Professor W. E. Lamb, Jr., for helpful suggestions and criticism.

[11] V. Fock and M. Petrashen, Phys. Zeit. d. USSR **6**, 368 (1934).
[12] E. U. Condon and G. H. Shortley, *The Theory of Atomic Spectra* (The Cambridge University Press, 1935), p. 343.
[13] D. R. Hartree, Proc. Roy. Soc. **166**, 450 (1938).
[14] H. C. Urey and Y. Sugiura, Kgl. Danske Vid. Sels. Math.-Fys. Medd **7**, no. 13 (1926).
[15] H. A. Kramers, Zeits. f. Physik **39**, 828 (1926).
[16] L. Biermann, Zeits. f. Astrophys. **22**, 157 (1943).

Vortices and Streams Caused by Sound Waves*

CARL ECKART
University of California, Marine Physical Laboratory, San Diego, California
(Received August 28, 1947)

As shown by Rayleigh, a considerable number of acoustic phenomena are known which involve the viscosity of the medium and require the solution of the hydrodynamic equations to a higher degree of approximation than is customary in elementary treatments of the theory of sound. Among these are the fluid streams that occur near intense sources of sound (e.g.: the "quartz wind").

The general equations of these second-order acoustic phenomena are developed in a systematic manner. When viscous forces are neglected, the effects are of three kinds: (1) those that can be ascribed to the inertia of acoustic energy, (2) those arising from radiation pressure, and (3) those caused by the variable compressibility of the medium. All of them result in the production of overtones of the fundamental vibration. In certain cases, this distortion can become very large, being unlimited except by the viscous forces. However, even when the average value of the gradient of the radiation pressure does not vanish, it does not, on the average, cause an acceleration of the fluid. Such gradients are balanced by the elastic rather than by the viscous forces.

When the latter are introduced into the calculation, a fourth effect appears: the irrotational motion in the sound wave generates vorticity as a second-order effect. This vortex motion will ultimately approach a steady state, being generated and resisted by forces that are independent of the time. Both generating and resisting forces are viscous, and consequently the steady motion is independent of the magnitude of the coefficient of viscosity. However, the resisting forces depend only on the shear viscosity of the medium, while the generating forces depend also on the bulk viscosity. It is suggested that the ratio of the bulk and shear coefficients of viscosity can be determined by studying these phenomena.

Calculations of the velocity of the stream generated by a beam of sound show that it is proportional (1) to $b=(4/3)+(\nu'/\nu)$, where ν' and ν are the bulk and shear viscosities, (2) to the power being radiated in the beam, (3) inversely to the square of the wave-length, and (4) inversely to ρ^2c^3, where ρ is the density and c the sound velocity of the medium. The maximum value of the steady-streaming velocity depends on the resistance offered by the walls of the vessel or room in which the experiment is performed. The time required to set up the steady state is, of course, inversely proportional to this resistance, and the flow is apt to become turbulent when the resistance is low.

INTRODUCTION

THE subject matter of this paper cannot be outlined more clearly than by quoting from the first paragraphs of Lord Rayleigh's paper[1] "On the circulation of air observed in Kundt's tubes, and on some allied acoustical problems":

> Experimenters in acoustics have discovered more than one set of phenomena, apparently depending for their explanation upon the existence of regular currents of air resulting from vibratory motion . . . such currents, involving as they do *circulation* of the fluid, could not arise in the absence of friction. . . . And even when we are prepared to include the influence of friction, we have no chance of reaching an explanation if, as usual, we limit ourselves to the supposition of infinitely small motion and neglect the squares and higher powers [of the velocity]. . . . The more important of the problems relates to the currents generated over a vibrating plate, arranged as in Chladni's experiments. It was discovered by Savart that very fine powder does not collect itself at the nodal lines, as does sand in the production of Chladni's figures, but gathers itself into a cloud which, after hovering for a time, settles itself over the places of maximum vibration. This was traced by Faraday[2] to the action of currents of air, rising from the plate at the place of maximum vibration, and falling back to it at the nodes. In a vacuum the phenomena observed by Savart do not take place, all kinds of powder collecting at the nodes. . . . [Another] problem relates to the air currents observed by Dvorak in a Kundt's tube, to which is apparently due the formation of the dust figures.

With the advant of piezoelectric generators of sound, these effects were rediscovered. Strong currents of air ("quartz wind") or liquid appear in front of the vibrating surface of the crystal. In the case of liquids, these currents are frequently great enough to disturb its free surface. Unless great care is exercised, they may vitiate intensity measurements with a Rayleigh disk. It is possible that this effect was actually discovered by Rayleigh, who performed the following experi-

* This work represents one of the results of research carried out under contract with the Bureau of Ships and Office of Naval Research, Navy Department.

[1] Lord Rayleigh, *Scientific Papers* (Cambridge University Press, Teddington, England), No. 108, p. 239; Phil. Trans. **175**, 1 (1883).

[2] Michael Faraday, Phil. Trans. 299 (1831).

ment: ". . . when the corresponding fork, strongly excited, was held to the mouth [of the Helmholtz resonator] a wind of considerable force issued from the nipple at the opposite side. This effect may rise to such intensity as to blow out a candle upon whose wick the stream is directed. . . . Closer examination revealed the fact that at the sides of the nipple the outward flowing stream was replaced by one in the opposite direction, so that a tongue of flame from a suitable placed candle appeared to enter the nipple at the same time that another candle situated immediately in front was blown away."[3]

Although Rayleigh summarized his calculations in *Theory of Sound*,[4] his results appear to be virtually unknown. At lest two different and incorrect explanations of the quartz wind can be found in recent literature, while the correct explanation appears to be virtually unknown to the experimenter. It is even possible that Rayleigh himself gave an incorrect explanation of the resonator experiment just described. Without giving adequate reasons, he says: "The two effects [flow and counter-flow] are of course in reality alternating, and only appear to be simultaneous in consequence of the inability of the eye to follow such rapid changes." It is at least possible that the streams are steady and that this is an effect similar to the others described above.

In the following pages, a systematic account of the theory of second-order acoustic effects will be developed. In the first part, acoustic radiation pressure and the inertia of acoustic energy will be considered. It will be shown that, as Rayleigh knew, these cannot cause the phenomena described above. However, the structure of this mathematical theory will be useful in the second part, where the second-order viscous forces will be considered, and in the third, where a calculation will be given of the steady flow produced by a sound beam of circular cross section. The remarkable fact will appear that the steady flow "is *independent of the value of the coefficient of viscosity*. We cannot, therefore, avoid considering this motion by supposing the coefficient of viscosity to be very small, the maintenance of the vortices becoming easier in the same proportion as the forces tending to produce the vortical motion diminish."[5]

[3] Rayleigh, *Theory of Sound* (MacMillan Company, Ltd., London, 1896), Vol. II, p. 217.
[4] Reference 3, Vol. II, p. 333.

PART I. ACOUSTIC RADIATION PRESSURE AND THE INERTIA OF ACOUSTIC ENERGY

The question is sometimes asked, why the velocity of sound does not function in acoustic theory in the same way that the velocity of light functions in relativity theory. From the standpoint of the latter, the question is foolish, for the velocity of light is both that, and also the maximum velocity with which any kind of signal or object can be transmitted. The velocity of sound is not maximal in the same sense. Still, the principle of the inertia of energy is not very directly connected with the principle of maximal velocity, but rather with the equations of motion of matter. Consequently, it would be expected that acoustic energy will display an inertia that is much greater than the inertia of electromagnetic radiation, in the inverse ratio of the squares of their velocities of propagation. It will be shown that this expectation is correct, provided the proposition be given a suitable interpretation.

The First- and Second-Order Equations of Acoustics

The general equations of hydrodynamics for a non-viscous fluid are

$$(\partial\rho/\partial t)+\nabla\cdot(\rho\boldsymbol{u})=0, \tag{1}$$

$$[\partial(\rho\boldsymbol{u})/\partial t]+\rho\boldsymbol{u}\cdot\nabla\boldsymbol{u}+\boldsymbol{u}\nabla\cdot(\rho\boldsymbol{u})=-\nabla p, \tag{2}$$

where ρ is the density, p the pressure, and $\boldsymbol{u}$ the velocity of the fluid. For the present purposes, it will be supposed that p is a function of ρ only; then

$$\nabla p=C^2\nabla\rho, \tag{3}$$

where C is a function of ρ which has the units of a velocity. This presupposes that the motion is isentropic.

The essential idea of Rayleigh's treatment of the problems discussed in the introduction, is that some of the terms in Eqs. (1) and (2) are sometimes much less important than others. In different circumstances, different terms will be

[5] Reference 1, p. 246.

negligible and others will be important. Thus, in acoustics, the terms $\partial\rho/\partial t$ and $\nabla\rho$ are important; in hydraulics, the term $\nabla\cdot(\rho\boldsymbol{u})$ becomes more important than $\partial\rho/\partial t$, but $\nabla\rho$ retains its importance. In order to bring the relative importance of the terms clearly to the attention, it is useful to depart from the c.g.s. system of units and to introduce one that is specially adapted to the problems under consideration.

In such a system, let the unit of length be X cm; of time, T sec.; of velocity, U cm sec.$^{-1}$. The unit of density is immaterial, since the equations are essentially homogeneous in ρ. In these units the equations become

$$(\partial\rho/\partial t)+N\nabla\cdot(\rho\boldsymbol{u})=0, \tag{4}$$

$$[\partial(\rho\boldsymbol{u})/\partial t]+N[\rho\boldsymbol{u}\cdot\nabla\boldsymbol{u}+\boldsymbol{u}\nabla\cdot(\rho\boldsymbol{u})] = -(NC^2/U^2)\nabla\rho, \tag{5}$$

where the numeric

$$N=UT/X. \tag{6}$$

To insure that the system of units will serve its purpose, the units X and T are to be chosen so that $\partial f/\partial t$ and $\partial f/\partial x$ are of the same order of magnitude, f being any of the functions ρ, $\boldsymbol{u}$. The unit U could be chosen in any of a number of ways: so that $N=1$, or so that $C/U\sim 1$, or so that $u/U\sim 1$. The third is the choice appropriate for most problems. Having thus defined the units, acoustics may be defined as consisting of those hydrodynamic problems for which $N\ll 1$ and $NC/U\sim 1$. (Hydraulics is apparently those hydrodynamic problems for which $N\gg 1$ and $NU^2/C^2\sim 1$.)

Introducing the quantity

$$c(\rho)=NC(\rho)/U,$$

Eq. (5) becomes

$$N[\partial(\rho\boldsymbol{u})/\partial t]+N^2[\boldsymbol{u}\nabla\cdot(\rho\boldsymbol{u})+\rho\boldsymbol{u}\cdot\nabla\boldsymbol{u}] = -c^2\nabla\rho. \tag{7}$$

The numeric N is now to be treated as a perturbation parameter,** and the expansions

$$\rho=\rho_0+N\rho_1+N^2\rho_2+\cdots, \tag{4.0}$$

$$u+u_0+Nu_1+N^2u_2+\cdots \tag{7.0}$$

are introduced. The zero-order equations are then

$$\partial\rho_0/\partial t=0, \tag{4.0}$$

$$c_0^2\nabla\rho_0=0, \tag{7.0}$$

where $c_0=c(\rho_0)$. Hence, ρ_0 is a constant, which fact may be used to simplify the first- and second-order equations:

$$(\partial\rho_1/\partial t)+\rho_0\nabla\cdot\boldsymbol{u}_0=0, \tag{4.1}$$

$$\rho_0(\partial\boldsymbol{u}_0/\partial t)=-c_0^2\nabla\rho_1; \tag{7.1}$$

$$(\partial\rho_2/\partial t)+\rho_0\nabla\cdot\boldsymbol{u}_1+\nabla\cdot(\rho_1\boldsymbol{u}_0)=0, \tag{4.2}$$

$$\rho_0(\partial\boldsymbol{u}_1/\partial t)+(\partial/\partial t)(\rho_1\boldsymbol{u}_0)+\rho_0(\boldsymbol{u}_0\cdot\nabla\boldsymbol{u}_0+\boldsymbol{u}_0\nabla\cdot\boldsymbol{u}_0) = -c_0^2\nabla\rho_2+c_0(dc_0/d\rho_0)\nabla\rho_1^2. \tag{7.2}$$

The Eqs. (4.1) and (7.1) are the equations of elementary acoustic theory, while Eqs. (4.2) and (7.2) are less familiar.

Integrals of the First-Order Equations

The equation expressing the conservation of acoustic energy is derived by multiplying Eq. (4.1) by $c_0^2\rho_1/\rho_0$, and Eq. (7.1) by $\boldsymbol{u}_0$, and adding. The result is

$$(\partial W/\partial t)+\nabla\cdot J=0. \tag{8}$$

The quantity

$$W=\tfrac{1}{2}\rho_0u_0^2+\tfrac{1}{2}c_0^2\rho_1^2/\rho_0 \tag{9}$$

is the acoustic energy density, while

$$J=c_0^2\rho_1\boldsymbol{u}_0 \tag{10}$$

is the acoustic energy flow.

The conservation law of acoustic "momentum" is obtained by multiplying Eq. (4.1) by $\boldsymbol{u}_0$, and Eq. (7.1) by ρ_1/ρ_0 and adding: the result is

$$\frac{1}{c_0^2}\frac{\partial J}{\partial t}+\rho_0(\boldsymbol{u}_0\cdot\nabla\boldsymbol{u}_0+\boldsymbol{u}_0\nabla\cdot\boldsymbol{u}_0) -\nabla(W-\rho_0u_0^2)+\rho_0\boldsymbol{u}_0\nabla\times(\nabla\times\boldsymbol{u}_0)=0. \tag{11}$$

It will be noted that the time derivative of J/c_0^2 appears in Eq. (11). Thus the acoustic momentum is related to acoustic energy flow in the same manner as the corresponding electromagnetic quantities. Also that, instead of the total energy density, W, Eq. (11) contains the Lagrangian difference between the potential and kinetic energy densities.

The last term in Eq. (11) usually vanishes,

** After the special units have served their purpose of providing a perturbation parameter, one may always return to the c.g.s. system, for which $N=1$, $C=c$. This will be done in the following pages.

since only solutions for which $\nabla \times \boldsymbol{u}_0 = 0$ are of interest. This will be assumed in the following.

Simplification of the Second-Order Equations

The second-order equations are seen to contain several combinations of terms that also appear in the conservation laws. The former can therefore be simplified by introducing a quantity ρ_{II}, defined by

$$\rho_2 = \rho_{II} + W/c_0^2. \tag{12}$$

The quantity ρ_{II} obeys equations that are much simpler than those for ρ_2, and much more analogous to the first-order equations:

$$(\partial \rho_{II}/\partial t) + \rho_0 \nabla \cdot \boldsymbol{u}_1 = 0, \tag{4-II}$$

$$\rho_0(\partial \boldsymbol{u}_1/\partial t) = -c_0^2 \nabla \rho_{II} - \nabla[\rho_0 u_0^2 + c_0(dc_0/d\rho_0)\rho_1^2]. \tag{7-II}$$

The term in $dc_0/d\rho_0$ would disappear if the medium obeyed Hooke's law. Thus, only the term in $\rho_0 u_0^2$ needs discussion. This functions like an additional (known) pressure, and may therefor be called the acoustic radiation pressure:

$$P = \rho_0 u_0^2, \tag{13}$$

which is thus given by twice the kinetic energy density. In gases, the term

$$H = c_0(dc_0/d\rho_0)\rho_1^2 \tag{14}$$

will be of the same order of magnitude as P. In liquids, H will be much less than P.

Because of the similarity between the equations for ρ_{II} and ρ_1, physicists will find it easier to think about ρ_{II} than about ρ_2. In particular, propositions arrived at intuitively (that is, derived from experience with elementary acoustic problems) will usually apply to ρ_{II} and not to ρ_2. Fortunately, the necessary correction is simple: it is only necessary to take the "inertia" of acoustic energy into account and add W/c_0^2 to ρ_{II} in order to obtain ρ_2.

The Solution of the Second-Order Equations

Certain general conclusions can be reached about the second-order effects in simple harmonic sound fields. In these cases, neither P nor H will contain terms of the fundamental frequency, but both will contain constant terms and terms with the double frequency. The latter will result in the generation of the second harmonic in the sound field—a phenomenon that has been observed at even moderate sound intensities. In certain cases, notably that of the plane wave, the amplitude of these harmonics will increase until they are limited by the viscous forces which have thus far been omitted.

Because of interference and the divergence of sound rays, the time-constant terms in P and H will, in general, depend on position. Thus, there will be a constant pressure gradient, and one might expect that this constant gradient will produce a constant acceleration of the fluid, whose velocity would thus increase until the viscous forces balance the pressure gradient. The end result would be fluid streaming at a constant velocity, proportional to the acoustic energy-gradient and inversely proportional to the coefficient of viscosity. These might account for the phenomena described in the Introduction. Unfortunately, however, this reasoning is faulty. The constant part of the gradient of $P+H$ is balanced, not by the viscosity of the fluid, but by its elasticity. Thus neither P nor H cause streaming of the fluid.

This is very simply proven: ρ_{II} may be eliminated between Eqs. (4-II) and (7-II) by taking the gradient of the former and the time derivative of the latter; the result is

$$\rho_0(\partial^2 \boldsymbol{u}_1/\partial t^2) - \rho_0 c_0^2 \nabla \nabla \cdot \boldsymbol{u}_0 = -(\partial/\partial t)[\nabla(P+H)]. \tag{15}$$

Since only the time derivatives of ∇P and ∇H appear, the first-order velocity $\boldsymbol{u}_1$ is independent of the constant parts of these gradients. This result would not be essentially altered by introducing the viscous terms. On the other hand, if $\boldsymbol{u}_1$ is eliminated from the equations, the result is

$$\rho_0(\partial^2 \rho_{II}/\partial t^2) - \rho_0 c_0^2 \nabla^2 \rho_{II} = \nabla^2(P+H). \tag{16}$$

Thus the constant parts of gradients will produce a constant part of ρ_{II}.

Consequently, neither radiation pressure nor the failure of Hooke's law can be invoked to explain the fluid streams mentioned above, and it becomes necessary to proceed to a study of the viscous forces.

PART II. THE EFFECTS OF VISCOSITY

When the viscous forces are included, the equations become (in the X, T, U system of

units):

$$(\partial\rho/\partial t)+N\nabla\cdot(\rho\boldsymbol{u})=0, \tag{17}$$

$$N[\partial(\rho\boldsymbol{u})/\partial t]+N^2[\boldsymbol{u}\nabla\cdot(\rho\boldsymbol{u})+\rho\boldsymbol{u}\cdot\nabla\boldsymbol{u}] = -c^2\nabla\rho+(NT/X^2)[((4/3)\nu+\nu')\rho\nabla\nabla\cdot\boldsymbol{u} - \nu\rho\times(\nabla\times\boldsymbol{u})]. \tag{18}$$

The quantity $\nu\rho$ is the ordinary coefficient of shear viscosity, so that ν is measured in cm²/sec. For an ideal gas, the bulk viscosity, ν', is zero; for liquids it is presumably different from zero, although no measurements or calculations of its magnitude have been made.[6] For convenience the abbreviation

$$b=4/3+\nu'/\nu \tag{19}$$

will be used: it is a numerical characteristic of the fluid, and its value will presumably be somewhere between 2 and 10 for liquids, and near 4/3 for gases.

For simplicity, it will be assumed that both b and the product $\nu\rho=\nu_0\rho_0$ are independent of the density of the liquid; effects due to their variation may be of importance, but will not be treated here. The coefficient of the viscous forces may be written

$$NT\nu_0/X^2=N^2/R,$$

where

$$R=UX/\nu_0$$

is the Reynold's number, calculated for the unit of velocity and the unit of length. The values of N and U have above been fixed with respect to the problem, but the value of X has not yet been specified. This freedom could be utilized to assign any desired order of magnitude to the viscous forces; however, there appear to be good physical reasons for supposing them to be of first order. This determines X by means of the equation $N=R$. The unit of length thus calculated has a simple physical significance in the case of gases: it is the mean-free path of their molecules. Since the viscous terms are introduced into the equations in order to take approximate account of molecular processes, this is a very appropriate unit.

It is then obvious that the zero-order equations will be unaffected by the viscous terms, and that the first-order equations are

$$(\partial\rho_1/\partial t)+\rho_0\nabla\cdot\boldsymbol{u}_0=0, \tag{17.1}$$

$$\rho_0(\partial\boldsymbol{u}_0/\partial t)=-c_0^2\nabla\rho_1+\rho_0\nu_0 b\nabla\nabla\cdot\boldsymbol{u}_0 - \rho_0\nu_0\nabla\times(\nabla\times\boldsymbol{u}_0), \tag{18.1}$$

and the second-order equations are

$$(\partial\rho_2/\partial t)+\rho_0\nabla\cdot\boldsymbol{u}_1+\nabla\cdot(\rho_1\boldsymbol{u}_0)=0, \tag{17.2}$$

$$\rho_0(\partial\boldsymbol{u}_1/\partial t)+(\partial/\partial t)(\rho_1\boldsymbol{u}_0) +\rho_0[\boldsymbol{u}_0-\nabla\boldsymbol{u}_0+\boldsymbol{u}_0\nabla\cdot\boldsymbol{u}_0]=-c_0^2\nabla\rho_2 +\rho_0\nu_0 b\nabla\nabla\cdot\boldsymbol{u}_0-\rho_0\nu_0\nabla\times(\nabla\times\boldsymbol{u}_0). \tag{18.2}$$

Effects due to the failure of Hooke's law have been omitted, although they may be of importance in problems involving distortion.

The conservation (or better, the dissipation) of acoustic energy is then derivable from the first-order equations as before, and results in the equation

$$(\partial W/\partial t)+\nabla\cdot\boldsymbol{J}=\rho_0\nu_0[b\boldsymbol{u}_0\cdot\nabla\boldsymbol{u}_0 - \boldsymbol{u}_0\cdot\nabla\times(\nabla\times\boldsymbol{u}_0)]. \tag{20}$$

Similarly, the dissipation of acoustic momentum is expressed by

$$\tfrac{1}{2}c_0^2(\partial\boldsymbol{J}/\partial t)+\rho_0[\boldsymbol{u}_0\cdot\nabla\boldsymbol{u}_0+\boldsymbol{u}_0\nabla\cdot\boldsymbol{u}_0] +\nabla(W-\rho_0u_0^2)+\rho_0\boldsymbol{u}_0\times(\nabla\times\boldsymbol{u}_0) =\nu_0 b\rho_1\nabla\nabla\cdot\boldsymbol{u}_0-\nu_0\rho_1\nabla\times(\nabla\times\boldsymbol{u}_0). \tag{21}$$

Setting $\nabla\times\boldsymbol{u}_0=0$, and introducing ρ_{II} as before, Eqs. (17.2) and (18.2) are seen to be equivalent to

$$(\partial\rho_{II}/\partial t)+\rho_0\nabla\cdot\boldsymbol{u}_1=(\nu_0 b/c_0^2)\boldsymbol{u}_0\cdot\nabla(\partial\rho_1/\partial t), \tag{17-II}$$

$$\rho_0(\partial\boldsymbol{u}_1/\partial t)=-c_0^2\nabla\rho_{II}-\nabla(\rho_0u_0^2) +\rho_0\nu_0 b\nabla\nabla\cdot\boldsymbol{u}_1-\rho_0\nu_0\nabla\times(\nabla\times\boldsymbol{u}_1) -\rho_1\nu_0 b\nabla\nabla\cdot\boldsymbol{u}_0. \tag{18-II}$$

Equations (17.2) and (17-II) show that neither ρ_2 nor ρ_{II} are conserved. In the previous part, it was noted that ρ_{II} obeyed laws that would be expected by physicists who rely on physical intuition, while ρ_2 did not. The reason that ρ_{II} is no longer conserved is clearly to be found in the dissipation of acoustic energy by the viscous forces. There appears to be no convenient way of introducing a relevant quantity that is conserved.

The Second-Order Motion of the Fluid

Elimination of ρ_{II} between the Eqs. (17-II) and (18-II) results in the equation

[6] H. Lamb, *Hydrodynamics* (Cambridge University Press, Teddington, England), sixth edition, pp. 573, 645; Reference 3, Vol II, pp. 314, 320; G. Kirchhoff, Pogg. Ann. **134**, 177 (1868).

$$\rho_0(\partial^2\boldsymbol{u}_1/\partial t^2)-\rho_0 c_0^2\nabla\nabla\cdot\boldsymbol{u}_1 +\rho_0\nu_0 b\nabla(\partial/\partial t)(\nabla\cdot\boldsymbol{u}_1) -\rho_0\nu_0(\partial/\partial t)\cdot\nabla\times(\nabla\times\boldsymbol{u}_1) =-\nabla(\partial/\partial t)(\rho_0 u_0^2)-b\nu_0(\partial/\partial t)[\rho_1\nabla\nabla\cdot\boldsymbol{u}_0] -b\nu_0\nabla[\boldsymbol{u}_0\cdot\nabla(\partial\rho_1/\partial t)]. \quad (22)$$

This equation can be simplified by introducing the divergence and rotation of the velocity

$$D=\nabla\cdot\boldsymbol{u}, \quad \boldsymbol{R}=\nabla\times\boldsymbol{u}. \quad (23)$$

Taking the divergence of Eq. (22), the rotation $\boldsymbol{R}_1$ is eliminated:

$$\partial^2 D_1/\partial t^2-c_0^2\nabla^2 D_1-\nu_0 b\nabla^2(\partial D_1/\partial t) =-\nabla^2(\partial u_0^2/\partial t)-(b\nu_0/\rho_0)\nabla\cdot[(\partial/\partial t)(\rho_1\nabla D_0)] -(b\nu_0/\rho_0)\nabla^2[\boldsymbol{u}_0\cdot\nabla(\partial\rho_1/\partial t)]. \quad (24)$$

Taking the rotation of Eq. (18-II) similarly eliminates D_1:

$$(\partial\boldsymbol{R}_1/\partial t)-\nu_0\nabla^2\boldsymbol{R}_1=(b\nu_0/\rho_0^2)\nabla\rho_1\times\nabla(\partial\rho_1/\partial t). \quad (25)$$

It is worth noting in more detail than above that when the first-order quantities are simple harmonic functions of the time, the right side of Eq. (25) is independent of the time. For, let

$$p_1=\rho_1 c_0^2=P'\cos nt+P''\sin nt,$$

where P and P'' are functions of the space coordinates only; then

$$c_0^2\nabla\rho_1=\nabla P'\cos nt+\nabla P''\sin nt,$$
$$(c_0^2/n)\nabla(\partial\rho_1/\partial t)=-\nabla P'\sin nt+\nabla P''\cos nt,$$

whence

$$\nabla\rho_1\times\nabla(\partial\rho_1/\partial t)=(n/c_0^4)\nabla P'\times\nabla P''.$$

This is perhaps the first indication that the theory of the fluid streams generated by sound sources is governed by Eq. (25). It also indicates that the vorticity generated by a sound wave will approach a steady value after a sufficiently long time. The length of this time depends on the value of the viscosity coefficient ν_0, but the steady state itself does not: it is determined by the equation

$$-\nabla^2\boldsymbol{R}_1=(b/\rho_0^2)\nabla\rho_1\times\nabla(\partial\rho_1/\partial t). \quad (25a)$$

The general procedure to obtain the velocity $\boldsymbol{u}_1$ will involve two steps, the first being the solution of Eqs. (24) and (25). Then $\boldsymbol{u}_1$ itself can be obtained from D_1 and $\boldsymbol{R}_1$ because of the vector identity

$$\nabla^2\boldsymbol{u}_1=\nabla D_1-\nabla\times\boldsymbol{R}_1.$$

This equation is most conveniently handled by introducing the scalar and vector potentials defined by

$$\nabla^2\phi_1=-D_1, \quad (26)$$

$$\nabla^2\boldsymbol{A}_1=-\boldsymbol{R}_1, \quad (27)$$

in terms of which

$$\boldsymbol{u}_1=-\nabla\phi_1+\nabla\times\boldsymbol{A}_1. \quad (28)$$

Equation (28) indicates that the irrotational and incompressible parts of the motion can be treated independently. Only the steady state of the latter will be considered further, the discussion being based on Eq. (25a).

The Diffusion of Vorticity

This equation has the general form of Fourier's equation for the conduction of heat or the diffusion of matter. Hence vorticity is generated in those regions where its right side is different from zero, and diffuses into other regions. However, the analogy to heat conduction and diffusion is not complete.

Being a partial differential equation, Eq. (25) has many solutions, and that solution appropriate to the given problem is determined by the boundary condition. In the case of heat flow, this is usually one of two: if the boundaries are thermally insulated, the normal component of the temperature gradient will be zero on them; if the boundaries are kept at a fixed temperature, this fact serves to determine the special solution.

Neither of these boundary conditions applies to vorticity. This is perhaps to be expected, since vorticity is a vector rather than a scalar. In fact, the accepted boundary condition is not formulated in terms of $\boldsymbol{R}_1$ but in terms of $\boldsymbol{u}_1$, and requires that all components of the latter vanish on the walls of the container.

For simplicity, let it be supposed that there is no free surface, so that $\boldsymbol{u}_1$ vanishes at all boundaries of the fluid. Then an easy application of Stokes' theorem shows that

$$\boldsymbol{n}\cdot\boldsymbol{R}_1=0, \quad (29)$$

$\boldsymbol{n}$ being the unit normal at the boundary, while the divergence theorem results in

$$\int\int\int R_1 dv=0. \quad (30)$$

These are the only conditions restricting the solutions of Eq. (25) that can be formulated in terms of $\boldsymbol{R}_1$ *alone*. They are very weak conditions, and do not suffice to determine the solution uniquely. This latter step must be postponed until $\boldsymbol{u}_1$ has been found from Eqs. (27) and (28).

Because of this difference in the boundary conditions, vorticity may be generated at the walls of the containing vessel in a manner that is quite different from the influx (or efflux) of heat in the thermal analogy. Consequently also, the steady states of vortex distribution will be quite different from those familiar in the theory of heat. If these general considerations are not kept in mind, the reader may be surprised at some of the results obtained when the above equations are applied to a special case.

PART III. THE FLOW CAUSED BY A BEAM OF SOUND

In order to simplify the calculations, consider a long tube of radius r_0, whose walls are rigid, and whose ends are closed by some material that permits an axial sound beam to enter and leave the tube without reflection. These ends prevent fluid from entering or leaving the tube; the latter is long enough so that at its center all effects due to the ends may be neglected, except that the total flow through any cross section must be zero.

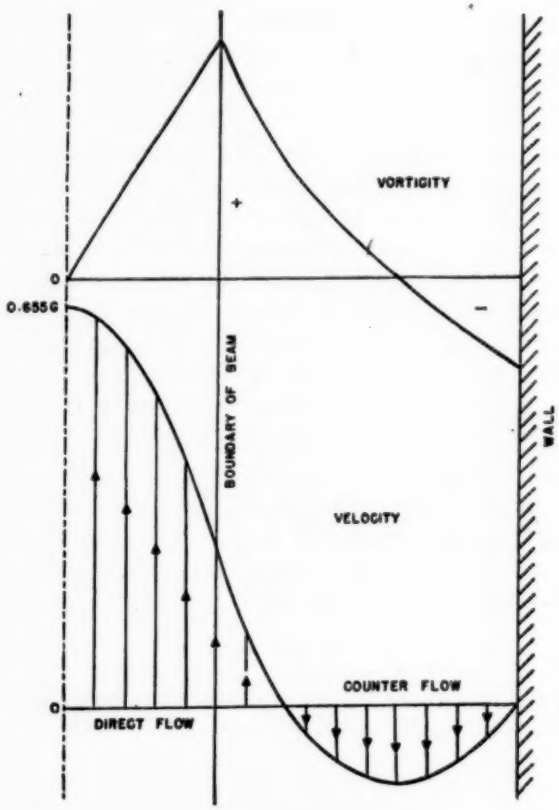

FIG. 1.

If the axis of the tube is the z axis and r the perpendicular distance from the axis, the pressure variations in the sound beam will be assumed to be

$$p_1 = \rho_1 c_0^2 = P(r)\sin(kz - nt). \tag{31}$$

This requires some justification, since it neglects both the divergence and the attenuation of the beam. The former is justified if the wave-length ($=2\pi/k$) is very small compared to the diameter of the beam. The latter would not be justified except that only the ultimate steady state is to be investigated here, and by Eq. (25a), this is independent of the viscosity except as the latter enters into ρ_1. It is thus permissible to consider first the case of negligible attenuation, and to reserve until later the complications resulting from attenuation of the sound beam.

Using Eq. (31), Eq. (25a) reduces to

$$-\nabla^2 \boldsymbol{R}_1 = K(d^2P/dr^2)(-\mathbf{i}\sin\phi + \mathbf{j}\cos\phi), \tag{32}$$

where

$$K = bk/2\rho_0^2 c_0^3, \tag{33}$$

and ϕ is the azimuthal coordinate. This equation has the special solution

$$\boldsymbol{R}_1 = f(r)(-\mathbf{i}\sin\phi + \mathbf{j}\cos\phi), \tag{34}$$

where

$$f(r) = (K/r)\int_0^r rP^2 dr + 2\beta r + \gamma/r, \tag{35}$$

β and γ being constants of integration. The value of γ must be zero, since infinite values of the vorticity are impossible; the value of β remains indeterminate, since both Eq. (29) and Eq. (30) are satisfied for any value of β.

The calculation of the vector potential $\boldsymbol{A}_1$ can be avoided by noting that if $u_{1x} = u_{1y} = 0$, $u_{1z} = g(r)$, then

$$\boldsymbol{R}_1 = -(dg/dr)(-\mathbf{i}\sin\phi + \mathbf{j}\cos\phi),$$

so that

$$dg/dr = -f(r). \tag{36}$$

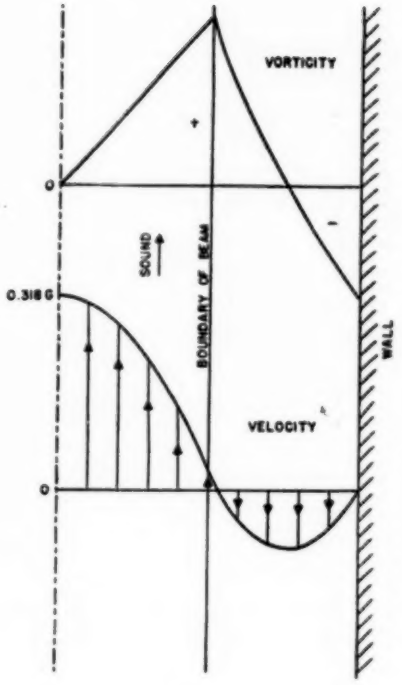

FIG. 2.

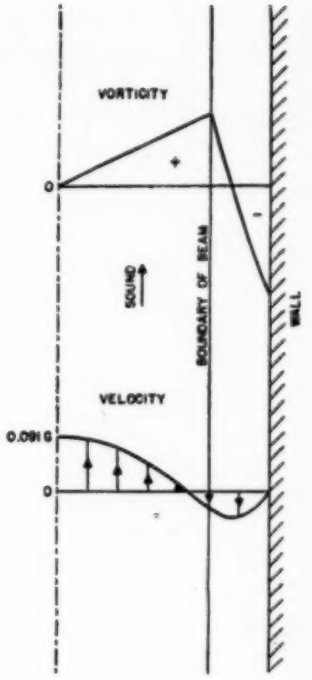

FIG. 3.

That solution of this equation is required which makes $g(r_0)=0$, since u_1 must vanish on the wall of the tube; this is given by

$$g(r)=\int_r^{r_0} f(r)dr$$

$$=K\int_0^{r_0}\Gamma(s,r)P^2(s)ds+\beta(r_0^2-r^2), \quad (37)$$

where

$$\begin{aligned}\Gamma(s,r)&=s\log(r_0/r) \quad \text{when} \quad s\leqslant r,\\ &=s\log(r_0/s) \quad \text{when} \quad s\geqslant r.\end{aligned} \quad (38)$$

Until this place, it has not been possible to assign a value to the constant of integration, β. The condition that there be no net flow through the tube can now be imposed:

$$\int_0^{r_0} rg(r)dr=0,$$

which is equivalent to

$$\beta=(K/r_0^4)\int_0^{r_0}(rr_0^2-r^3)P^2(r)dr. \quad (39)$$

This completes the formal solution of the problem; it remains to consider the numerical relations.

In order to carry the calculations further, suppose that the sound beam has the radius r_1, and a constant intensity throughout; then

$$\begin{aligned}P(r)&=P_0, \quad r\leqslant r_1;\\ &=0, \quad r>r_1.\end{aligned} \quad (40)$$

It will be found that the velocity of the stream is proportional to

$$G=\tfrac{1}{2}KP_0^2r_1^2, \quad (41)$$

so that it is convenient to calculate this quantity for several special cases.

First, suppose that the medium is water, that the beam has a radius $r_1=1.5$ cm, while $P_0=10^6\mu b$ ($=0.1$ atmos.). Since $c_0=1.5\times10^5$ cm/sec.

$$G=\tfrac{1}{6}bk^2\times10^{-5} \text{ cm/sec. (water).}$$

If the frequency of the sound is 24 megacycles, $k=10^8$, and hence $G=1.57b$ cm/sec. It will be expected, therefore, that these streams will become appreciable only at frequencies above 1 megacycle, and have a negligible velocity at lower frequencies. This is in agreement with observation.

If the medium is air, the value of K is much larger because it is inversely proportional to the square of the density and the cube of the sound velocity. Supposing the sound beam to have the same radius and intensity, it is found that

$$G=95.0bk^2 \text{ cm/sec. (air)}.$$

For a frequency of 1 kilocycle, $k=0.19$, and hence $G=3.4b$ cm/sec. Consequently, these streams should become important in air at frequencies above several hundred cycles. This is perhaps in agreement with Rayleigh's resonator experiment mentioned above, which was performed at 256 cycles per second.

While the velocity of the stream is proportional to G, its value will vary across the section of the tube which confines it. The direction of flow will coincide with that of the acoustic energy on the axis of the beam, and will be compensated by a counter-flow near the walls of the tube. The complete expression for the velocity is most conveniently written in terms of the ratios

$$x=r/r_0, \quad y=r_1/r_0,$$

and is

$$\begin{aligned} g&=G\{\tfrac{1}{2}(1-x^2/y^2)-(1-\tfrac{1}{2}y^2)(1-x^2)-\log y\}, \\ &\qquad\qquad 0\leqslant x\leqslant y; \quad (42) \\ &=-G\{(1-\tfrac{1}{2}y^2)(1-x^2)+\log x\}, \quad y\leqslant x\leqslant 1. \end{aligned}$$

Graphs of g as a function of x, are given, for various values of y, in Figs. 1, 2, and 3.

The maximum value of g occurs on the axis and depends on the resistance offered to the flow by the confining tube. When the radius of the latter is infinite, the maximum value of g becomes logarithmically infinite. On the other hand, when the sound beam fills the whole of the tube, the flow stalls and $g=0$ everywhere.

Experimental Determination of b

The experimental determination of the numerical constant b has eluded three generations of physicists. Stokes argued that its value must be $4/3$—i.e., that the bulk viscosity must be zero. This hypothesis has been theoretically verified for an ideal gas. Stokes' arguments do not appear to be convincing in the case of liquids, and there is a growing belief (based on discrepancies between the observed absorption of high frequency sound and that calculated on the assumption that $b=4/3$) that it may have larger values. It is hoped that these calculations may suggest methods for its experimental measurement.

It will be noted, however, that the above discussion shows that the streaming velocity is very sensitive to the geometry of the experiment, and will readily become turbulent. Consequently, the experimental measurement of b may not be easy.

Letters to the Editor

PUBLICATION of brief reports of important discoveries in physics may be secured by addressing them to this department. The closing date for this department is, for the issue of the 1st of the month, the 8th of the preceding month and for the issue of the 15th, the 23rd of the preceding month. No proof will be sent to the authors. The Board of Editors does not hold itself responsible for the opinions expressed by the correspondents. Communications should not exceed 600 words in length.

On the Measurement of Ionospheric Virtual Height at 100 Kilocycles*

R. A. HELLIWELL
Department of Electrical Engineering, Stanford University, California
November 20, 1947

STUDIES of the reflection of atmospherics by the ionosphere[1,2] have indicated that the effective height of the reflecting region lies between about 60 and 90 kilometers at very low frequencies. Continuous wave interference measurements[3] made at 16 kilocycles at oblique incidence have been interpreted to indicate that the effective height of the reflecting layer rises from 70 or 75 kilometers by about 12 kilometers at the time of sunset.

Further evidence on the height of the ionosphere at low frequencies has been obtained with a pulse technique applied at vertical incidence at a frequency of 100 kilocycles. The method is similar to that used at high frequencies where virtual height is determined from the time required for a pulse of radio energy to travel to the ionosphere and back. A pulse of approximately exponential decay is produced every second by allowing an antenna which is charged to a potential of about 100 kilovolts to discharge to ground through a sphere gap. This pulse, which has a time constant of about 200 microseconds, travels by way of the ground and the ionosphere to the receiver located 2.7 kilometers away. The peak power radiated vertically is about 500 watts.

The receiving antenna is a forty-foot dipole whose directional characteristic is used to discriminate against the ground pulse which would otherwise override the relatively weak ionospheric reflections. It is possible by this means to reduce the dipole response to the ground pulse to about sixty decibels below the maximum response. Discrimination of the same order of magnitude is obtained against most of the interfering signals and atmospherics which are present. The over-all band width of the receiving system is eighteen kilocycles. Results are displayed on a five-inch oscilloscope and recorded photographically. The sweep is triggered by the ground pulse picked up on a separate receiver having a shorter time delay than that used to receive the sky-wave signals.

Measurements made on the night of October 13 showed virtual heights ranging from about 91 to 98 kilometers in a group of thirty-three records. A sample of the records is shown in Fig. 1. The negative pips are timing markers spaced 167 microseconds apart corresponding to a virtual height of twenty-five kilometers. A reflected pulse is observed at about 95 kilometers and a first multiple at about 190 kilometers. These values are corrected for the time required for the ground pulse to travel over the 2.7-kilometer base line. The virtual heights measured from the multiple reflections, which were observed on a majority of the records, were in good agreement with those measured from the first reflections except in two or three cases.

On several occasions a characteristic effect which has been noted at high frequencies was observed on 100 kilocycles; namely, the amplitude of the first-order multiple was often greater than that of the first reflection. This is evidence of horizontal ion gradients such as might result from the action of winds in the ionosphere.

FIG. 1. Photograph of single sweep showing receiver-limited ground pulse followed by ionospheric reflections at virtual heights of 95 and 190 kilometers. Heights are measured with aid of the negative pips spaced 25 kilometers apart.

The ionosphere sounding technique described above should make it possible to fill an important gap in existing information on the ionosphere and to obtain a better understanding of the effect of the ionosphere on the propagation of low frequency waves.

* This work was sponsored by the National Bureau of Standards.
[1] Schonland, *et al.*, "Reflection of atmospherics from the ionosphere," Nature, May, 893 (1939).
[2] Laby, *et al.*, Nature 142, 353 (1938).
[3] J. E. Best, J. A. Ratcliffe, and M. V. Wilkes, Proc. Roy. Soc. 156, 614 (1936).

The Crystal Counter

W. JENTSCHKE
August 22, 1947

RECENTLY the problem of a crystal counter has been discussed.[1] The following remarks may be of interest: In order to detect single α-particles by means of a crystal counter alkali halides, sulfur, zincblende, and diamond crystals were investigated by G. Stetter, K. Huber, and the author, in 1940.[2] As expected, the alkali halides and the sulfur failed. The available zinc-sulfide crystal too was not useful, probably because of impurities.

Two chips of white diamonds, 0.4 mm thick, had a high photo-conductivity. We observed with them pulses produced by α-particles in a device similar to that mentioned by Wooldridge, Ahearn, and Burton,[1] using cathode sputtered gold electrodes. In the absence of light the insulation was perfect. An electric field strength of 3000 volts per

cm being applied, the pulses produced by α-rays of polonium or thorium were very sharp. The time constant of the amplifier was 10^{-3} sec.

The number of ions was generally of the same order as measured in an ordinary gas chamber; the number of registered pulses was smaller than the number of the absorbed α-particles.

In spite of the homogenous energy of the α-particles the magnitudes of the single pulses were very different from one another. Special experiments proved that the reason for this result was not the difference in pathway between the place of origin of the electrons and the anode.

Alpha-particles penetrating the crystal either at the anode or at the cathode side produced about the same distribution of pulses.

Single outstanding values of pulses of higher energy than that of a single α-particle were sometimes registered. The same field strength being applied saturation in photoconductivity was measured as expected.

For the explanation of the results the following may be pertinent: The α-particles penetrate only the surface layer of the crystal. Further the density of ionization by light is quite different from the ionization by α-rays which produce local lattice disturbances because of their high ionization density.

A sudden discharge of [the produced] space charge may be considered as an explanation of some of the pulses, especially the larger ones.

Regarding the experiments mentioned above, it is believed that a quantitative measurement of the number and energy of the single α-particles was not achieved.

The diamond crystals investigated up to now for crystal counters have very different properties, although all of them possess photoelectric saturation.

Some of the diamonds are quite insensitive to α-rays (P. J. Van Heerden; Wooldridge, Ahearn, and Burton).

Other crystals show the inhomogenous pulses mentioned above. It is of interest to note from the investigations of Wooldridge, Ahearn, and Burton that diamonds exist which possess the qualities necessary for a quantitative measurement of single α-particles.

[1] P. J. Van Heerden, *The Crystal Counter*, Dissertation, Utrecht 1945; D. E. Wooldridge, A. J. Ahearn, and J. A. Burton, Phys. Rev. **71**, 913 (1947); Robert Hofstadter, Bull. Am. Phys. Soc. **22**, No. 4 (1947).
[2] G. Stetter, Verh. d. D. Phys. Ges. **22**, 13 (1941).

Note on Gamma-Radiation from Europium

J. M. Cork, R. G. Shreffler, and C. M. Fowler
Department of Physics, University of Michigan, Ann Arbor, Michigan
November 19, 1947

On reporting the energies of the gamma-rays emitted by radioactive europium 154 it was noted that two spectral lines had the expected relative intensity and exactly the energy difference to be expected for conversion K and L electrons in the element of atomic number 61. This was interpreted as possibly indicating an impurity of neodymium in the bombarded specimen of europium, although no long half-lived isotope of neodymium is known. Continued observation has shown that this agreement with the K–L difference in element 61 is purely fortuitous and that these two lines have the same half-life as the other europium lines, namely, about 6 years. They are therefore K conversion lines in gadolinium, of energy 197.0 and 235.7 kev derived from gamma-rays of energy 247.3 and 286.0 kev. These new energies lead to an interesting combination as part of a level diagram since the 286 kev added to the previously reported 122.1 kev gives 408.1 kev, which is very close to the previously reported gamma-ray at 407.8 kev.

On Magnetism of Celestial Bodies

Jean Mariani
Institute for Advanced Study, Princeton, New Jersey
November 12, 1947

The proportionality between the magnetic moment and the angular moment of celestial bodies in the case of 78 Virginis has recently been verified by Mr. H. Babcock.[1] It seems possible to give a theoretical interpretation of that new natural law in the following way.[2]

The motion of a continuous, perfect fluid, without internal pressure, in an electromagnetic field not sensibly perturbed by it, is given by the ordinary Lorentz force, which yields the equations:

$$du_i/ds = (\sigma_0/\rho_0 c^2) F_{ij} u^j = w_{ij} u^j, \tag{1}$$

σ_0 being the proper charge density of the fluid, ρ_0 its proper mass density, $u^i = dx^i/ds$ its four-dimensional velocity at each point, $F_{ij} = \varphi_{i,j} - \varphi_{j,i}$ the external electromagnetic field (the gravitation effects being neglected). When $\sigma_0/\rho_0 c^2$ is constant in the domain occupied by the fluid, we easily get:

$$w_{ij} = u_{i,j} - u_{j,i} = (\sigma_0/\rho_0 c^2) F_{ij}, \tag{2}$$

from analytical dynamics, by writing (1) in canonical form; consequently,

$$u_i = (\sigma_0/\rho_0 c^2)\varphi_i + \partial F/\partial x^i. \tag{3}$$

Thus, u_i may be regarded as a determination of φ_i, which seems to furnish a very natural geometrization of electromagnetic field, but, in classical electromagnetism, we are dealing in this way with several difficulties.

First, in the general case of a fluid charged in the Maxwellian sense $\sigma_0/\rho_0 c^2$ has an arbitrary value; second, the φ_i are defined in the whole region occupied by the field and the u_i only interior to a certain light cone and require the presence of matter (from a remark of Professor Einstein), but we must notice that electromagnetic field has no existence "in self," contrarily to the classical assumption. For its determination at each point, we need at these points a fluid composed of test particles whose motion is governed by (1), otherwise the field remains indetermined.

In a peculiar case, we may determine uniquely $\sigma_0/\rho_0 c^2$, in order to satisfy the theory. If we suppose that rotation and electromagnetic field are uniquely associated, when a fluid regarded as neutral in classical theory is in rotational

motion, it must produce an electromagnetic field, acting on each particle of the fluid; in the Newtonian approximation of relativity, we get:

$$\tfrac{1}{2}\Delta g_{44}\simeq\Delta u_4=\frac{4\pi k\rho_0}{c^2}=\frac{\sigma_0}{\rho_0 c^2}\Delta\varphi_4=\frac{4\pi\sigma_0^2}{\rho_0 c^2}$$

with the help of (2); therefore: $\sigma_0=\pm k^{\frac{1}{2}}\rho_0$. This electrical density is precisely of the order assumed for producing cosmic magnetism;[3] conversely from this relation and relativistic symmetry (2) and (1) are easily deduced. We must also remark that from $e=\pm k^{\frac{1}{2}}m$, where e is a charge associated with the mass m, we deduce, in the Schwarzschild interior problem for an homogeneous sphere of radius a and classical mass m_0 where $m=m_0+3km_0^2/5c^2a$, $e'=\pm 3k^{\frac{1}{2}}m_0^2/5c^2a$; e' is the charge associated with the gravitational field energy $3km_0^2/5a$; it is of the same order as the negative charge at the surface of the earth.

[1] H. W. Babcock, Phys. Rev. **72**, 83 (1947).
[2] Comptes Rendus Ac. Sc. Paris **218**, 417, 585 (1944).
[3] Blackett, Nature **159**, 658 (1947).

On the Formation of Chemical Elements Inside the Stars

GLEB WATAGHIN
Department of Physics, University of Sao Paulo, Sao Paulo, Brasil
September 15, 1947

RECENT calculations have shown the possibility of relating the observed abundances of nuclei in the universe to the process of formation of nuclei in an early state of matter under conditions not far from thermal equilibrium.[1] The temperature and density of this primitive assembly of elementary particles at the moment of formation of nuclei were:

$$kT\sim 4\times 10^7 \text{ ev}, \quad \rho\sim 10^{13} \text{ g/cm}^3. \tag{1}$$

Important supplementary information about the origin of nuclei can be derived from the study of interaction between gravitational and thermal energies. Let us apply the following well-known formula of Jeans theory of gravitational instability to a fluid of density $\sim 10^{13}$ or $\sim 10^{14}$ g/cm^3: $\lambda_0^2=(\pi/G\rho)(dp/d\rho)$, where λ_0 indicates the linear dimensions of a star which can be formed, and $dp/d\rho\sim\langle v^2\rangle_{Av}/3$ for a gas of nucleons, or $\sim\frac{1}{3}c^2$ for a gas of photons and electron pairs of $kT>Mc^2$. One finds values for λ_0: $\sim 10^6$ or $\sim 10^7$ cm, and for masses M of the star, between 10^{33} g and 10^{36} g (depending on the values of ρ and of kT).

Further limitations arise from the conservation law of energy and from general theorems about the gravitational energy (e.g., the Perry-Ritter relation). The gravitational energy of a sphere of average density $\sim 10^{14}$ g/cm^3: $E_G\cong 3GM^2/5R$ becomes of the order of Mc^2, for $M\sim 10^{36}$ g, and $\gg Mc^2$ for the mass of a galaxy. We can deduce, therefore, that the energy of the particles should be too great to permit the formation of nuclei inside a mass $\gtrsim 10^{34}$ g. And thus the nuclei were probably formed inside the stars.[2] Indeed, writing the conservation law

$$E_{\text{rad}}+E_{\text{electrons}}+\Sigma\, n_{Z,A}E_{Z,A}-E_G=Mc^2,$$

where $\Sigma\, n_{Z,A}E_{Z,A}$ is the energy of the nuclei (including the rest energy) one can see that the energy of the particles + radiation must be $>E_G$ and $\sim 2Mc^2$ in the case $M\sim 10^{36}$ g.

Elementary calculations show that if the star is constituted of a neutron core of density 10^{14} g/cm^3, the neutrons will be in a degenerate state with critical value of energy

$$E_{cr}=\frac{h^2}{2M_N}\left(\frac{3n_N}{8\pi}\right)^{\frac{1}{3}}\sim 3\times 10^7 \text{ ev}.$$

Comparison with (1) shows that the temperature required for formation of nuclei is of the order of the critical temperature of degeneracy of neutrons.

If one applies to a star having $\rho\sim 10^{14}$ g/cm^3 and $M\sim 10^{36}$ g, the well-known formulae of a "standard model," one finds for the central pressure and central temperature values:

$$p_c\sim 11\times GM^2/R^4\sim 10^{36} \text{ erg/cm}^3;$$

$$kT_c\sim\beta GM\times M_N/R\sim\beta\times 10^9 \text{ ev},$$

where β is the ratio between the pressure resulting from nuclei and the total pressure. We see that these values are too high for a thermodynamical equilibrium which could give rise to the formation of nuclei and that further expansion and cooling are to be expected. The production of electron pairs and the blackbody radiation should play an important part in this process.[3] But a rapid expansion (perhaps of duration of few seconds[4]) would reduce the central temperature and density and permit the formation of the whole variety of nuclei in conditions near those indicated by (1).

Another possibility is given by the model of a quasi-degenerate neutron core. The value of p_c in this case is given by $[2E_{cr}/5+\pi^2(kT)^2/3E_{cr}]n_N$ and is of an order of magnitude sufficient to equilibrate the central gravitational pressure [if $10^{33}<M<10^{36}$ g and $n_N\sim 6\times 10^{37}$].

[1] P. Saraive de Toledo and G. Wataghin, Phys. Rev. **72** (1947).
[2] G. Wataghin, Phys. Rev. **70**, 430 (1946).
[3] G. Wataghin, Phys. Rev. **66**, 149 (1944).
[4] G. Gamow, Phys. Rev. **70**, 572 (1946).

On the Relative Abundances of Nuclei in the Universe

PAULO SARAIVA DE TOLEDO AND GLEB WATAGHIN
Department of Physics, University of Sao Paulo, Sao Paulo, Brazil
September 15, 1947

PREVIOUS attempts[1] to find conditions of thermodynamical equilibrium between nuclei, elementary particles, and radiation, corresponding to the observed distribution of nuclei in the universe, could not explain the

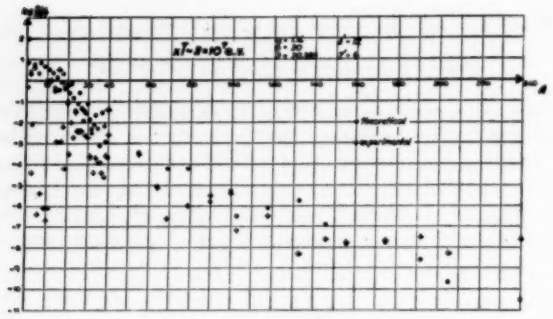

FIG. 1.

relative abundances of all nuclei, especially the approximate constance of abundance of heavy nuclei ($A>100$).[2] Working with a method proposed by one of us[3] we made an attempt to obtain the general law of distribution for the whole periodic system, looking for the average variation of abundances, without paying attention to the details of the distribution.[4]

The results for two temperatures are reproduced in the following Figs. 1 and 2, where experimental abundances are indicated following the data of Goldschmidt, and theoretical values were obtained by means of the formula:

$$\log\frac{n_{ZA}}{n_{Z'A'}}=a\times(Z-Z')+D\times(A-A')$$
$$-B\times(M_{ZA}-M_{Z'A'})+\tfrac{3}{2}\log\frac{M_{ZA}}{M_{Z'A'}}$$

already used in previous papers.[5] Here n_{ZA} and $n_{Z'A'}$ indicate number of nuclei per cm³; a, B, and D are parameters of the distribution. We neglected the factors representing the multiplicity of nuclear states and admitted that for $kT\gtrsim 10^7$ ev the contributions of excited states to the statistics of nuclei could be taken into account writing for the average energy E of nucleus: $E\cong Mc^2+kT$. We found by trial that for the temperatures of the order of 20 or 40 Mev ($B\sim 20$ or $B\sim 10$) the calculated abundances fit roughly the experimental curve, and we reproduce here two typical results between many possible ones corresponding to nearly the same parameters. The results obtained with $kT\sim 40\times 10^6$ ev ($B\sim 10$) are more satisfactory and give for U^{238} a theoretical abundance -6.95 compared with the observed -7.6 (whereas the other choice of parameter gives: -10.5). The total density of nuclei can be calculated using the general laws of equilibrium between nuclei, photons, and electrons,[3] (disregarding the eventual production of mesons) and assuming that initially the total charge is 0. In this way one obtains densities $\sim 10^{13}$ g/cm³ for light nuclei, $\sim 10^8$ g/cm³ for heavy nuclei. For protons one has: 1.7×10^{13} g/cm³ or 3.6×10^{12} g/cm³, at $kT\sim 40$ Mev or 20 Mev, respectively.

From the general satisfactory agreement between the calculated and observed points in Fig. 1, we deduce that nuclei were probably formed at conditions not very far away from those of thermal equilibrium. The high rate of nuclear reactions makes this assumption acceptable even if the phase of expansion at which nuclei were formed lasted only few seconds.[6]

A further inspection shows that there is no close correspondence between the relative abundances of isotopes in the two series of data (theoretical and observed ones). Obviously one should expect a change of relative abundances during the following cooling processes and, for radioactive nuclei or for nuclei formed in the known thermonuclear processes (H, Li, Be, B), continuous change with the time. We are inclined to admit that the observed ratios between the abundances of isotopic nuclei were established during the successive stages of cooling and expansion of matter, at lower temperatures: $kT\sim 10^6$ ev. Indeed previous calculations[1] show a close agreement between the theoretical and observed relative abundances of some isotopes at this temperature.

[1] C. F. v. Weizsaecker, Phys. Zeits. **39**, 633 (1938); S. Chandrasekhar and L. R. Henrich, Astrophys. J. **95**, 288 (1942); O. Klein, G. Bescow, and L. Treffenberg, Arkiv. f. Mat. Astr. Fysik. **33**, 1 (1946); C. Lattes and G. Wataghin, Phys. Rev. **69**, 237 (1946); **70**, 430 (1946).
[2] V. M. Goldschmidt, Geochem. Vert. d. El., (Oslo), **9** (1938).
[3] G. Wataghin, Comptes Rendus, **203**, 909 (1935); Phys. Rev. **66**, 149 (1944).
[4] G. Gamow, J. Washington Acad. Sci. **32**, 353 (1942).
[5] C. Lattes and G. Wataghin, Phys. Rev. **69**, 237 (1946); Phys. Rev. **70**, 430 (1946). Klein, Bescow, and Treffenberg used an equivalent formula (Eq. (1), loc. cit.) deduced with Gibbs thermodynamical method.
[6] G. Gamow, Phys. Rev. **70**, 572 (1946).

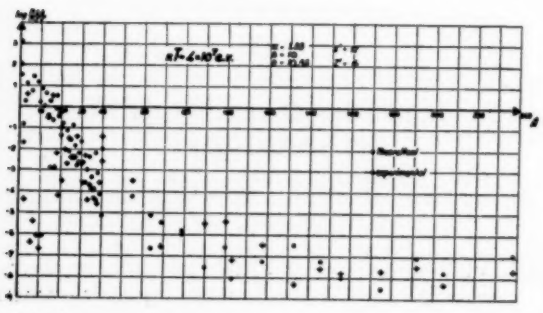

FIG. 2.

Absolute Cross Section for the Reaction $C^{12}(p, pn)C^{11}$ at High Energy

EDWIN M. MCMILLAN AND RICHARD D. MILLER
Radiation Laboratory, Department of Physics, University of California, Berkeley, California
November 21, 1947

RECENT measurements by Chupp and McMillan[1] have shown that the cross section for producing C^{11} from C^{12} by proton impact is independent of energy from 60 Mev up to at least 140 Mev; to find the absolute cross section for this process, it was only necessary to measure

the activity produced in carbon by a known proton current. The source of protons was the same as described in reference 1, using a ½-in. thick Be target. In a position corresponding about to that marked B in Fig. 1 of this reference was placed a lead box having a 1-in. round hole in one side to admit protons. The protons coming through the hole passed through ⅛ in. of copper to stop any slow particles, then through the sample to be activated (sheets of 5-mil polystyrene), then were collected in a thick insulated lead block. No defining slits other than the hole were used since other experiments showed that the action of the magnetic field gave ample collimation for this purpose; in fact, an excitation curve taken with a bare stack of carbon plates was reasonably accurate except for some loss of definition near the end of the range. Secondary emission from the collector block is known to be negligible from the fact that very little current is collected by the thin cyclotron targets when traversed by the deuteron beam. The energy of the protons going through the sample was equal to the mean proton energy (½ deuteron energy − ¾ energy loss in traversing Be target = 80 Mev) less the 18-Mev loss in the ⅛ in. of copper, or 62 Mev, which is on the flat part of the excitation curve.

The activity measurements were made by comparing the counting rates of the activated polystyrene sheets with a calibrated uranium standard; absorption corrections were small and back-scattering was minimized by mounting the sheets with no backing material. Three sheets were used in each run, and the individual counts agreed excellently. Another sheet behind the collector block served to evaluate the neutron background which gave a 1 percent correction. The proton-induced activity in sheets of 13.9 mg/cm² surface density (6.44×10^{20} carbon atoms/cm²), expressed as the saturation activity at the end of a very long bombardment, was found to be 5950 disintegrations/sec. in the first run and 6010 disintegrations/sec. in the second run.

In order to measure the current, a lead was brought out from the collector to a vacuum-tube electrometer outside the cyclotron shield. This circuit used a Victoreen VX-32 tube as an inverted triode, i.e., the input was connected to the plate, while the grid current was observed. The potential of the cathode was varied manually so as to keep the grid current constant, thus maintaining constant potential differences between the electrodes, and the cathode potential was read. Under ideal circumstances this method would give directly the integrated current during the exposure; in practice, it was found that the cable insulation became very leaky when the cyclotron was running. To minimize this effect, vacuum-insulated cable was used from the center of the cyclotron to a point 12 feet outside the vacuum chamber, the remaining 60 feet of cable being RG-62. A lead shutter in front of the sample box could be closed to make leakage measurements without exposing the sample. With the cyclotron running, it was found that the leakage current varied with collector potential in an ohmic fashion, with an effective resistance of about 2×10^{11} ohms; also, the potential of zero leakage was determined. Then extra capacitance was added, the collector potential was set at 1.5 volts below the point of zero leakage, the shutter was opened, and the cyclotron was run steadily until the collector potential had risen 3 volts. Voltage readings were made at 1-minute intervals during the run. The collected current I is then given by:

$$I=(\Delta V/2R)\,\mathrm{ctnh}(\Delta t/2RC)$$
$$\sim(C\Delta V/\Delta t)[1+(1/12)(\Delta t/RC)^2],$$

where ΔV = total voltage rise, Δt = time of exposure, R = leakage resistance, and C = capacitance. R can be evaluated from the shape of the voltage-time curve; if v represents the deviation of the curve from a straight line at the time mid-point, then:

$$IR=(\Delta V)^2/8v+\tfrac{1}{2}v.$$

In the first run, $\Delta V=3$ volts, $\Delta t=24$ min., $C=9120$ μμfd., and $v=0.25$ volt, from which $R=2.3\times10^{11}$ ohms, $RC=36$ min., and $I=1.97\times10^{-11}$ ampere. In the second run, $R=2.2\times10^{11}$ ohms, and $I=2.09\times10^{-11}$ ampere.

The above activity and current measurements can now be combined to get the activation cross section. Thus we get for the two runs $\sigma_a=0.075\times10^{-24}$ and 0.071×10^{-24} cm², respectively. Allowing for possible systematic errors, the result is given as 0.073 ± 0.010 barn.

An estimate of the total proton current is of some interest; from the area and position of the 1-in. hole and the theoretical energy and angle distributions this is estimated to be about 1/40 microampere, which agrees with the theoretical proton yield of 2 percent and the estimated deuteron current of about 1 microampere.

Also of interest is a determination of the relative yields of C^{11} from C, N(Be_3N_2), and O(BeO) samples bombarded simultaneously in a 60-Mev proton beam. The yields per atom were in the ratio C:N:O = 1:0.28:0.36.

The authors wish to thank Mr. Warren W. Chupp for his assistance in these measurements. This work was done under the auspices of the Atomic Energy Commission, under Contract No. W-7405-eng-48.

[1] W. W. Chupp and E. M. McMillan, Phys. Rev. **72**, 873 (1947).

The Mean Life of Negative Mesotrons in Sodium Fluoride*

HAROLD K. TICHO AND MARCEL SCHEIN
Department of Physics, University of Chicago, Chicago, Illinois
November 21, 1947

LAST year Conversi, Pancini, and Piccioni[1] showed that negative mesotrons, stopping in carbon, do disintegrate. This result seemed to indicate that the interaction of mesotrons with nucleons was much smaller than postulated in meson theories.[2,3] Since it seemed essential to prove that disintegration and nuclear capture are actually competitive

processes for every mesotron stopped, and since it appeared probable that the disintegration of negative mesotrons might have some bearing on the lower value of the mean life obtained in aluminum by one of us,[4] we carried out an experiment to determine the mean life of positive and negative mesotrons separately. The absorber chosen was NaF because the results of Sigurgeirsson and Yamakawa[5] indicated that for $Z \approx 10$ the effect should be easily detectable.

The counter arrangement is shown in Fig. 1. Anticoincidences (C_A, C_B, C_C, $-A$) actuated the timing circuit, and time intervals between the firing of counter S and any of the counters D were recorded. The linear sweep used in the timing circuit was automatically calibrated every hour by means of a 1-megacycle crystal oscillator. The iron bars, similar to the ones used by the Rome group,[1] were operated at magnetic saturation (15,000 gauss) and when collecting mesotrons of one polarity rejected all those of the opposite polarity whose energy was smaller than 160 Mev upon leaving the iron. The 16.2 g/cm² of NaF stopped mesotrons with energies smaller than 56 Mev. To check the separation of positive and negative mesotrons the NaF absorber was replaced by an equivalent amount of lead in which no negative mesotrons disintegrate. The effectiveness of the magnetic lens in barring mesotrons of the "wrong" polarity is at least 93 percent. The error in the time measurement

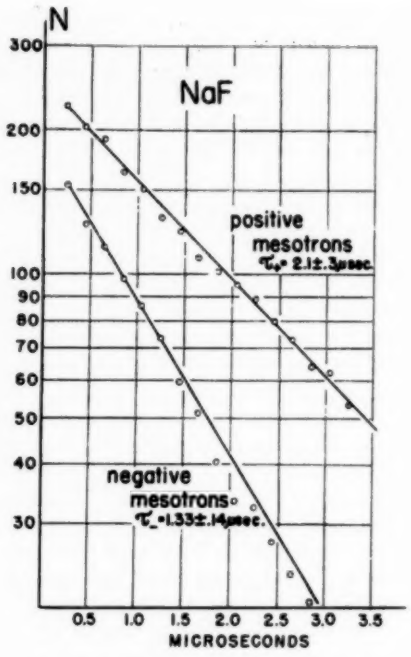

FIG. 2. Results of experiment with NaF.

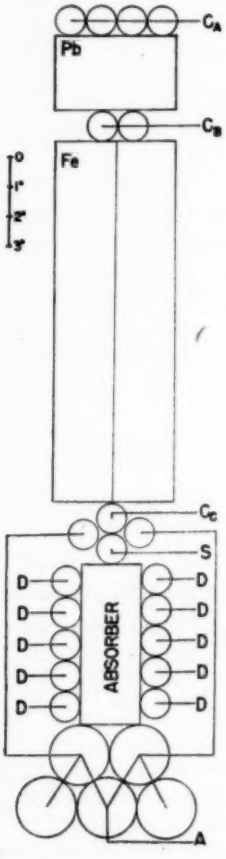

FIG 1. Counter arrangement.

for each individual disintegration, due mainly to the spontaneous lags in the counter tubes, is ± 0.05 μsec.

The results of the experiment with NaF are plotted in Fig. 2. The curve for *negative* mesotrons was plotted *accurately* and yields a mean life of $\tau_- = 1.33 \pm 0.14$ μsec; the curve for positive mesotrons is normalized with the curve for negative ones in such a way that both represent equal numbers of mesotrons stopped in the absorber. The mean life of positive mesotrons obtained from this curve is in agreement with the value of 2.15 μsec obtained by Nereson and Rossi.[6] Considerations published earlier[7] showed that the ratio τ_-/τ_+ may be obtained from the counting rates of disintegrations of positive and negative mesotrons. Using the actual counting rates of this experiment, and an excess of positive mesotrons of 20 percent, one obtains the ratio $\tau_-/\tau_+ = 0.73 \pm 0.10$, which is in satisfactory agreement with the ratio $\tau_-/\tau_+ = 0.62$ derived from the slopes of the disintegration curves of Fig. 2.

Assuming with Wheeler[3] that the probability for capture Λ is equal to kZ^4 (Z = atomic number), one obtains from the here determined mean life of negative mesotrons, $k = 29 \pm 3$. Furthermore, if this Z dependence should be correct, mesotrons, stopping in aluminum, should have a mean life of approximately 0.8 μsec, which would give a satisfactory explanation for the change in the mean life of all positive and negative mesotrons from 2.15 to 1.78 μsec observed in aluminum.[4] Further experiments are now in progress.

* The research described in this paper was supported in part by Contract N6ori-20, U. S. Navy Department.

[1] M. Conversi, E. Pancini, and O. Piccioni, Phys. Rev. 71, 209 (1947).
[2] E. Fermi and E. Teller, Phys. Rev. 72, 399 (1947).
[3] John A. Wheeler, Phys. Rev. 71, 320 (1947).
[4] H. K. Ticho, Phys. Rev. 72, 255 (1947).
[5] T. Sigurgeirsson and A. Yamakawa, Phys. Rev. 71, 319 (1947).
[6] N. Nereson and B. Rossi, Phys. Rev. 64, 199 (1943).
[7] H. K. Ticho and Marcel Schein, Phys. Rev. 72, 248 (1947).

Radiofrequency Conductivity of Gas-Discharge Plasmas in the Microwave Region

LADISLAS GOLDSTEIN AND NATHANIEL L. COHEN
Federal Telecommunication Laboratories, Inc., New York, New York
November 10, 1947

IN connection with a specific application, we have been investigating the conductivity of gas discharges in the microwave region. The problem involves the transmission of low power, very high frequency signals through a coaxial transmission line containing part of a gas-discharge tube as a dielectric gap in the center conductor.[1] The length of this gap is so determined that the radiofrequency signal normally is attenuated at least 40 decibels when the discharge is off.

The conditions established with respect to the signal level are: (1) that the radiofrequency energy be insufficient to accelerate electrons produced in the discharge to inelastic collision levels, and (2) the mean free path of electrons in the discharge be large compared to the amplitude of possible electronic oscillations in the radiofrequency field. Simple theoretical considerations lead, in the steady state, (1) to the use of non-electronegative gases, and particularly to the heavier rare gases such as argon, neon, krypton, or appropriate mixtures of them, and (2) to pressures such that the electronic mean free time be of the order of the period of the incident waves.[2]

The most significant results are presented here. The data shown below are for measurements made with signals of 2000 megacycles per second and power levels below about 1 milliwatt. For these conditions, pressure below 10 millimeters of mercury of the gases cited above gave best results in accordance with the tentative theory. Some typical characteristics of radiofrequency signal attenuation as a function of discharge direct current are shown in Fig. 1. The discharge tubes were so constructed relative to the coaxial line that discharge plasma fills the region of the dielectric gap. For relatively low current discharges, with either normal glow or arc conditions, the attenuation of the incident signal increases beyond the attenuation of the gap in the absence of a discharge. With further increases in discharge current, the attenuation is seen to fall sharply to a low value. This rapidly rising characteristic is suggestive of a resonance phenomenon. This appears to be related to the high frequency electronic plasmoidal oscillations.[3,4] The frequencies of such oscillations are given by $\nu=(Ne^2/\pi m)^{\frac{1}{2}}$, where N is the electron density in the discharge plasma, e, and m are the electronic charge and mass, respectively. Hence, in a discharge plasma one might expect a continuous spectrum of oscillation frequencies limited at the high frequency side by the value of ν corresponding to the maximum electron density. The maximum electron densities deduced from the discharge direct currents at conditions of minimum attenuation of radiofrequency signal (order of 3 decibels) were found to correspond to values of N which, when inserted in the above equation, yield a value of ν approximating the frequency of the radiofrequency signal. It appears that for conditions of maximum conductivity of a radiofrequency signal of frequency ν_s, an oscillation close to that frequency would exist in the conducting plasma

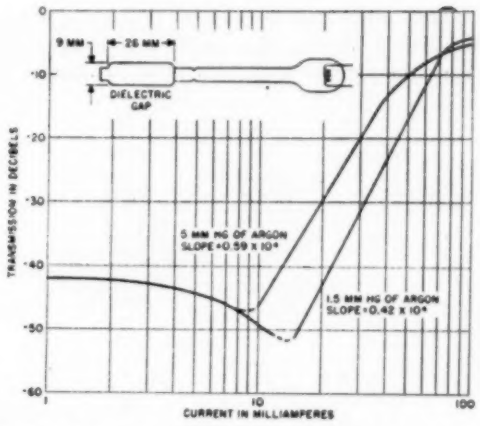

FIG. 1. Typical characteristics of radiofrequency signal attenuation as a function of discharge direct current.

even in the absence of the radiofrequency signal. This led us to investigate the radiofrequency oscillations produced in a direct current gas discharge in the absence of any external radiofrequency fields.

The results of this investigation indicate that such high frequency oscillations do exist in the discharge and have increasing amplitudes with increasing direct currents. In addition to these high frequency oscillations, we observed low frequency oscillations similar to those previously reported.[5,6] These oscillations are classified here, along with random oscillations, as noise. For conditions of minimum attenuation, this noise power was found to be of the order 2×10^{-19} watts/cycle at 2000 megacycles per second.

It may be indicated that this method may be used in the study of the properties of the gas discharge plasma. In particular, information concerning electron densities, electronic mean-free path, and in the disintegrating plasma, the electron distribution functions may be obtained.

[1] D. E. Kerr, S. C. Brown, and W. P. Kern, Bull. Am. Phys. Soc. 22, 28 (1947).
[2] H. Margenau, Phys. Rev. 69, 608 (1946).
[3] L. Tonks and I. Langmuir, Phys. Rev. 33, 195 (1929).
[4] I. Langmuir, Proc. Nat. Acad. Sci. 14, 627 (1928).
[5] J. D. Cobine and C. J. Gallagher, J. Franklin Inst. 243, 41 (1947) and the references included therein.
[6] B. Granovsky and L. Bykhovskaya, J. Phys. U.S.S.R. X, 351 (1946).

The Radiations from 2.70-Day Au^{198}

PAUL W. LEVY AND E. GREULING
Clinton National Laboratory, Oak Ridge, Tennessee
November 21, 1947

THE radiations from 2.70-day Au^{198} have been investigated with photographic and counter recording spectrometers of 10-cm radius. Sources were prepared by irradiating gold foil in the Clinton pile. Kurie plots, made from sources of various thicknesses, all indicate that the maximum energy of the continuous spectrum is 0.970

±0.010 Mev. Also, these plots are linear for energies greater than 0.6 Mev, but below this energy the points gradually rise above the straight line. This effect is observed even with the thinnest source used, 0.25 mg/cm², and consequently it is felt that it is not due to back-scattering or self-absorption. Superimposed on the continuous spectrum are prominent K, L, and M conversion lines from a gamma-ray of 0.408 Mev, and several weak lines from lower energy gamma-rays. The decay of these lines and the continuous spectrum was followed with the spectrometer, and they were found to have the same half-life. The conversion lines were studied with the photographically recording spectrograph, and the results are summarized in Table I.

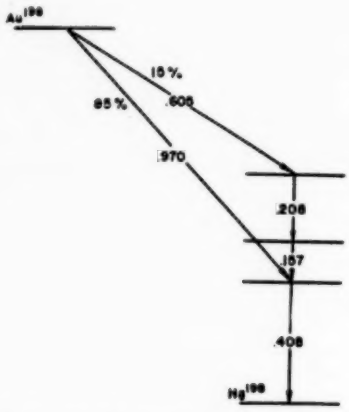

FIG. 1. Suggested decay scheme for 2.70-day Au¹⁹⁸.

TABLE I. Gamma-rays and conversion lines in Au¹⁹⁸.

Gamma-ray	Conversion lines observed	Estimated intensity of conversion lines	Energy of conversion lines (Mev)	Energy of gamma-rays (Mev)
1	K	Medium	0.074	0.157
	L_{I+II}	Weak	0.144	0.158
	L_{III}	Very weak	0.146	0.158
	M	Faint	0.155	0.157
2	K	Weak	0.125	0.208
	L	Very faint	0.193	0.207
3	K	Very strong	0.326	0.409
	L	Strong	0.395	0.407
	M	Strong	0.407	0.409

The conversion lines of the 0.408-Mev gamma-ray have been observed by several investigators,[1-3] and some of the other lines by Plesset.[2] The value obtained for the maximum energy of the beta-spectrum is considerably higher than the 0.92±0.01 Mev given by Siegbahn.[3] However, he used a very thick source and, as he states, the spectrum he obtained could be considerably distorted.

The gamma-ray data, together with the apparent inflection in the Kurie plot, support the decay scheme shown in Fig. 1. The maximum energies of the two components of the continuous spectrum are 0.970±0.010 Mev and 0.605 ±0.014 Mev. The end point of the low energy component was obtained by subtracting the sum of the energies of the low intensity gamma-rays from the maximum energy of the high energy beta-component. From the position of the inflection point in the Kurie plot we obtained a value for the low energy end point that agrees with, but is less accurate than, the value given above. The intensity of the low energy component is 15 percent, or less. The uncertainty in this figure is difficult to estimate since, in determining it, we had to assume that the back-scattering and absorption in the thinnest source was negligible.

A paper giving full details of this investigation and a discussion of the beta-ray theory involved is in preparation.

[1] J. L. Lawson and J. M. Cork, Phys. Rev. **58**, 580 (1940).
[2] E. H. Plesset, Phys. Rev. **62**, 181 (1942).
[3] K. Siegbahn, Proc. Roy. Soc. **189**, 527 (1947).

Spark Breakdown at Atmospheric Pressure and Above in Relation to Paschen's Law

CHARLES G. MILLER AND LEONARD B. LOEB
Department of Physics, University of California, Berkeley, California
November 22, 1947

THE streamer theory of the spark was developed independently by Loeb and Meek[1] and by Raether[2] from 1939–40 and is applicable to sparks at pressures of about atmospheric and above; it depends on ion concentrations. In consequence, as Varney and later Loeb and Meek[1] have indicated, Paschen's law observed for lower pressures and classically accepted as universally applicable, no longer holds. Proof of its failure in spark breakdown studies at higher pressures had been lacking because of inadequacy in range of the past observations until the recent work of Howell, of Trump, Safford, and Cloud, and of Skilling and Brenner at higher pressures and potentials.[4] The semi-quantitative theory of Meek, also set up independently by Raether, was admittedly incomplete in that it was based solely on field distortion produced by the positive ion

TABLE I.

	p (mm)	(cm)	V_s (Trump) in KV	V_s (Meek) in KV
p=200 lb./in. =26250 mm ×cm	7000	3.74	830	773.9
	8550	3.075	813	773.2
	10100	2.60	785	772.7
p=120 lb./in. =15760 mm ×cm	3878	4.064	528	487.3
	5430	2.896	515	486.6
	6981	2.261	502	486.0
	8532	1.849	487	485.6
	10084	1.565	473	485.2
p=20 lb./in. =2627 mm ×cm	775.7	3.378	95	94.3
	2327	1.130	90	93.9
	3878	0.676	87	93.8
	5430	0.485	87	93.6
	6981	0.373	84	93.5
	8532	0.307	82	93.4
	10084	0.260	81	93.4

space charge density which was created. It neglected the *high energy* photon production, absorption, and ionization in the gas. In a recent paper submitted for a special forthcoming issue of *Reviews of Modern Physics*, Loeb has arrived at a more nearly proper approach to the equation for the streamer advance.[5] This enables photon production and photoelectric ionization in the gas to be included, retaining as well the Meek-Raether criterion. It is there predicted that, owing to the pressure dependence of the absorption coefficient for ionizing photons, this will have the effect of emphasizing pressure variation in the sparking equation in a still higher degree than does the Meek-Raether criterion. Thus departures from Paschen's law should be even greater than calculated by the Meek equation. One of us has just computed a number of the characteristic curves between sparking potential V_s and gap length for three values of p (pressure p is in mm of Hg, δ-gap length in cm), experimentally observed by Trump, Safford, and Cloud[4] in a region where field emission cannot distort their curves as it might have in Howell's work. The data and results are shown in Table I, for plane-parallel electrodes in air. It is seen at once that while the Meek equation yields a small variation of V_s with δ for constant p which is of the correct form, it is less than the actually observed change by a factor of from 40 to 14. This is just the sort of departure to be expected by neglect of the absorption coefficient. Thus one must conclude that: (1) Paschen's law does not hold in this region in air, (2) that the departure is what one would expect from the streamer mechanism, and (3) that the Meek-Raether criterion requires amplification to include the photoelectric absorption. More theoretical work is needed along the line indicated by Loeb[5] to arrive at a correct and useful equation. Much more experimental work is needed further to confirm the departure and to determine where the streamer mechanism and failure of the law give way to the Townsend mechanism and Paschen's law as a function of gap length and pressure.

[1] L. B. Loeb, *Fundamental Processes of Electrical Discharge in Gases* (John Wiley and Sons, Inc., New York, 1939), p. 426 ff.; J. M. Meek, Phys. Rev. **57**, 722 (1940); L. B. Loeb and J. M. Meek, J. App. Phys. **11**, 438, 459 (1940); L. B. Loeb and J. M. Meek, *Mechanism of the Electric Spark* (Stanford University Press, Stanford University, California, 1941).
[2] H. Raether, Zeits. f. Physik **110**, 611 (1938); **117**, 386, 524 (1941); Archiv. f. Elektrotechnik **34**, 49 (1940).
[3] R. N. Varney, L. B. Loeb, H. J. White, and D. Q. Posin, Phys. Rev. **48**, 818 (1935).
[4] A. H. Howell, Trans. Am. Inst. Elec. Eng. **58**, 193 (1939); Skilling and Brenner, Trans. Am. Inst. Elec. Eng. **60**, 112 (1941); Trump, Safford, and Cloud, Trans. Am. Inst. Elec. Eng. **60**, 132 (1941).
[5] L. B. Loeb, Rev. Mod. Phys. (to be published).

The Disintegration Energy of $N^{14}(n, p)C^{14}$

P. Huber and A. Stebler
Physics Department, University of Basle, Switzerland
November 10, 1947

THE energy of reaction of the (n, p) disintegration of N^{14} was measured with an ionization chamber and a linear amplifier. The evaluation of the energies from the charges measured with this standard method is possible in two ways:

1. By direct calibration of the arrangement with α-particles of known energy.
2. By using the ionization energy for the calculation of the energies of reaction.

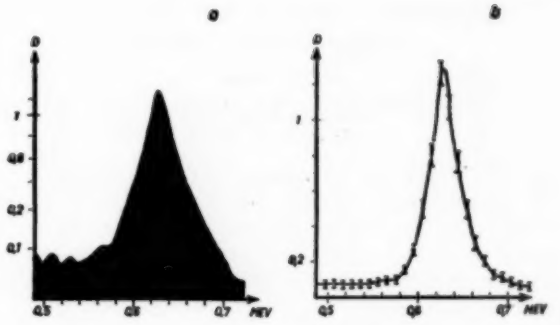

FIG. 1(a) Printed record of 1500 pulses >0.45 Mev of the (n, p) disintegration photographed with the "pulse spectrograph." D = relative number of pulses per energy interval. (b) Conversion to a linear scale of D.

The latter method has been used here with the value of 36.3 ev for the ionization energy of nitrogen measured by Alder, Huber, and Metzger.[1]

The (n, p) disintegrations in N^{14} are excited with slow neutrons from a *d-d* source. A total number of 5600 disintegrations were recorded with the "pulse spectrograph."[2] Figure 1a shows a record taken with 1500 pulses which is converted to a linear scale in Fig. 1b. The energy of reaction corresponds with the maximum of the pulse spectrum.

The width of the completely symmetrical distribution curve is caused by the noise of the apparatus.[3] The mean value of the maximum in five independent records is equal to $2.78 \cdot 10^{-13}$ coulomb, the deviations being smaller than 0.4 percent. This corresponds to an energy of reaction of 0.63 ± 0.01 Mev if the energy of ionization is taken equal to 36.3 ev. This calculation was done under the assumption that the energy of ionization is independent from the energy of the particles. The results of this and earlier papers are collected in Table I.

TABLE I.

Barschall and Battat	0.710	Mev[4]
Bonner und Brubaker	0.620	Mev[4]
Boggild	0.60	Mev[5]
Huber, Huber, and Scherrer	0.57 ± 0.04	Mev[6]
Computed from masses	0.60	Mev[7]
Present measurements	0.63 ± 0.01	Mev

[1] Alder, Huber, and Metzger, Helv. Phys. Acta **XX**, 234 (1947).
[2] D. Maeder, Helv. Phys. Acta **XX**, 139 (1947); D. Maeder, P. Huber, and A. Stebler, Helv. Phys. Acta **XX**, 230 (1947).
[3] E. Baldinger, Helv. Phys. Acta **XIX**, 423 (1946).
[4] H. H. Barschall and M. E. Battat, Phys. Rev. **70**, 245 (1946).
[5] T. K. Boggild, Kgl. Danske Vid. Sels. Math.-Phys. Medd. **23**, 23 (1945).
[6] Huber, Huber, and Scherrer, Helv. Phys. Acta **XIII**, 209 (1940), corrected with 36.3 ev as value of energy of ionization.
[7] P. W. Levy, Phys. Rev. **72**, 248 (1947).

Photoelectric Effect in Self-Quenching Geiger-Mueller Counters*

M. V. SCHERB
Bartol Research Foundation of the Franklin Institute
Swarthmore, Pennsylvania
November 22, 1947

A METHOD has been discovered for treatment of a Geiger-Mueller counter which produces a marked change in its photoelectric properties. By means of a discharge treatment at liquid-air temperatures, the results shown in Figs. 1 and 2 were obtained with the following experimental set-up.

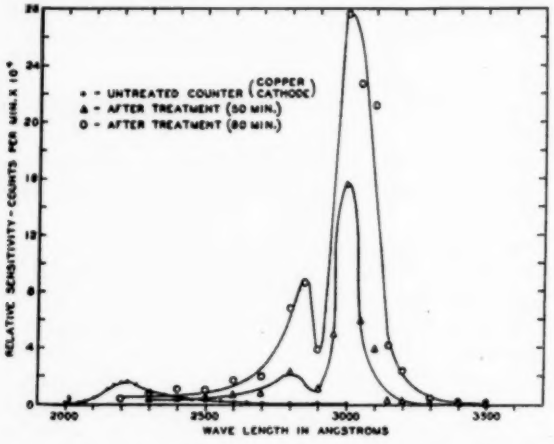

FIG. 1. Spectral distribution curves showing the effect produced by a prolonged discharge of a self-quenching Geiger-Mueller counter at liquid-air temperatures.

A glass wall counter, having a copper cathode 3 cm in length and 1 cm in diameter, was used. Light was transmitted along the counter axis through a Nonex glass bubble window, 0.01 mm thick, at one end of the tube. The counter was chemically washed, rinsed in distilled water, and vacuum baked at 420°C for 2 hours before a 12-cm Hg argon-butane filling was made. The discharge treatment was carried on by immersing the counter in liquid air and connecting to it a suitable voltage supply. To determine the spectral response, the discharge was terminated and the counter allowed to return to room temperature.

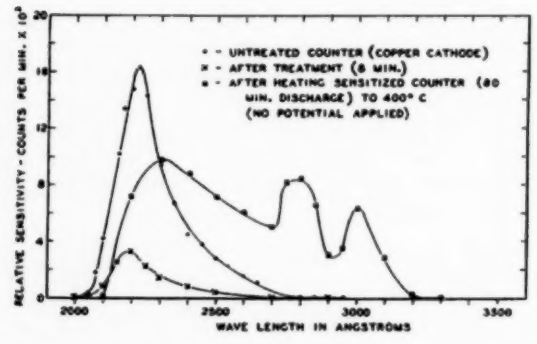
• - UNTREATED COUNTER (COPPER CATHODE)
× - AFTER TREATMENT (8 MIN.)
▪ - AFTER HEATING SENSITIZED COUNTER (80 MIN. DISCHARGE) TO 400° C (NO POTENTIAL APPLIED)
RELATIVE SENSITIVITY - COUNTS PER MIN. X 10³
WAVE LENGTH IN ANGSTROMS
2000
2500
3000
3500

FIG. 2. Spectral distribution curves showing the effect produced by the initial discharge and by heating the sensitized counter.

Spectral response curves were obtained by the use of a quartz monochromatic illuminator, a suitable radiation source, a quartz condensing lens, a slit system, a scale of 256, and a mechanical recorder. In this preliminary investigation, no corrections were made for counter losses, scaling circuit losses, or stray light effects in the illuminator.

The spectral response curve of the counter before treatment is plotted in Fig. 1, and to an enlarged scale in Fig. 2. It can be seen that the peak response is at 2250A, and the photoelectric threshold is roughly at 2900A which is in agreement with published results[1] considering the possible contamination of the cathode surface by the quenching gas. After discharging the counter for 8 minutes, the spectral response curve obtained (Fig. 2) indicated a sharp drop in the peak sensitivity. Response curves taken after 50- and 80-minute treatments are shown in Fig. 1.

These results indicate that the prolonged discharge (1) shifted the spectral distribution curve toward the longer wave-lengths, and (2) increased the sensitivity of the counter by a factor of 15 at the peak response. No decrease in sensitivity was observed 24 hours after treatment. Changes in Geiger-counter properties such as useful life, background, pulse shape, starting voltage, and plateau characteristics have not been observed. A counter treated in this manner 8 months ago has shown no long-term photoelectric fatigue to date.

A similar photoelectric effect has been observed for the argon-butane mixture using cathodes of nickel, silver, and Aquadag. Preliminary results obtained with an argon-ether mixture indicate that sensitivities many times greater than previously mentioned can be obtained in the same spectral range.

To check the indications that the photoelectric effect was a cathode-surface phenomena, the sensitized counter was heated to 400°C and allowed to cool to room temperature. The resultant spectral response curve (Fig. 2) shows that most of the assumed cathode deposit had been driven off although the peaks at 2850A and 3000A still persist. With further heating, it is expected that the response curve would revert to the original. The dip in the curve at 2900A may be due to absorption by some gaseous component after treatment.[2]

Spatz[3] and Bergstrand[4] have reported on the photosensitivity of argon-alcohol counters after long use. Similar effects, particularly after high speed counting, have been observed at this laboratory for various hydrocarbon quenching mixtures. The decomposition of the hydrocarbons in the discharge quenching mechanism is accompanied by the deposit of polymers on the cathode surface.[5,6] After being built up through counter use, it is likely that this deposited layer is responsible for the observed photo-sensitivity. Discharging a Geiger-Mueller counter at liquid-air temperatures would seem to be a

similar process[7] although the layer deposited and the gas disintegration products may very well be different.

While photon counters have been compared favorably with certain types of photo-multipliers, they have had few applications because of lack of reliability or limited spectral response.[8] A reliable photon counter of high surface quantum efficiency in the near ultraviolet or visible light region could find important uses in spectroscopy, as a Čerenkov radiation detector,[9] and possibly as an alpha-particle and low energy β-ray detector without thin-window techniques by the use of suitable phosphors.

Work is proceeding on the investigation of the reported photoelectric effect for various gases and cathode materials.

The author wishes to express his appreciation to Mr. W. E. Ramsey for many stimulating discussions and to Dr. W. F. G. Swann for his interest in this investigation.

* Supported by the Office of Naval Research.
[1] A. L. Hughes and L. A. DuBridge, *Photoelectric Phenomena* (McGraw-Hill Book Company, Inc., New York, 1932), p. 75.
[2] W. A. Noyes and P. A. Leighton, *The Photochemistry of Gases* (Reinhold Publishing Corporation, New York, 1941), Chapter VII.
[3] W. D. B. Spatz, Phys. Rev. **64**, 236 (1943).
[4] E. Bergstrand, Ark. iv. f. Mat. Astr. Fysik. **29A**, 4 (1943).
[5] Paul B. Weisz, "Radiation chemistry of the Geiger-Mueller discharge," to be published in J. of Phys. Coll. Chem.
[6] E. W. R. Steacie, *Atomic and Free Radical Reactions* (Reinhold Publishing Corporation, New York, 1946), Chapter VI.
[7] L. M. Yeddanapalli, J. Chem. Phys. **10**, 249 (1943).
[8] O. S. Duffendack and W. E. Morris, J. Opt. Soc. Am. **32**, 8 (1942).
[9] Paul B. Weisz and B. L. Anderson, Phys. Rev. **72**, 431 (1947).

Cosmic-Ray Bursts in the Upper Atmosphere*

H. E. Tatel** and J. A. Van Allen
Applied Physics Laboratory, Johns Hopkins University, Silver Spring, Maryland
November 10, 1947

ON July 29 a successful V-2 rocket carried a bundle of four automatically calibrated pulse ionization chambers mounted in the rocket nose (Fig. 1) to an altitude of 100 miles. During the flight there were recorded 150 seconds of good quality telemetered data above 180,000 ft.

The ionization chambers were similar to those used by Bridge and Rossi,[1] 20 in. long and 3 in. in diameter filled with 5 atmospheres of purified argon. Calibration was achieved by periodically sliding tubes internal to the chambers by means of external solenoids, thereby uncovering fairly thin polonium sources. There were 11 Po α-particle pulses per second during calibrations compared to a high altitude cosmic-ray counting rate of 4 per second (mostly smaller pulses). The pulses of 10-μsec. duration were amplified by a feed-back type pulse amplifier with 2-μsec. rise time. These pulses were shaped by an artificial line, amplified, lengthened by an integrating circuit, and then transmitted to the ground by the 23-channel radio telemetering system of the Naval Research Laboratory. Before firing, an artificial pulser was used to establish the amplitude calibration of the over-all amplifier, telemetering, and recording system. The system was linear and the scale and reliability were assured by the six Po-α-calibration periods of two-second length each at 27-second intervals during flight.

The results of three of the chambers are concordant and yield the distribution of pulse height shown in Fig. 2. The

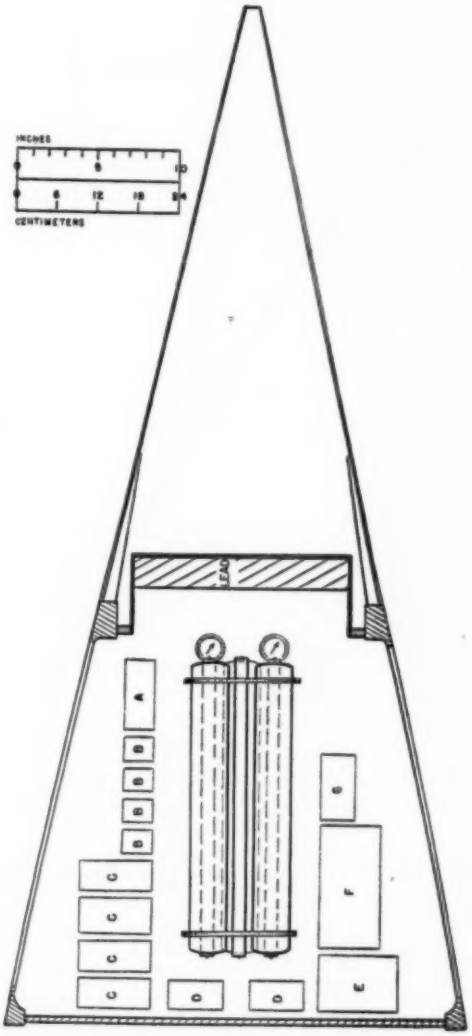

FIG. 1. Schematic diagram of ionization chambers in V-2 instrument cone. *A*, *B*, *C*, etc. represent electronic chasses. Remainder of rocket extends 40′ below.

data from the fourth chamber are in disagreement with these three, and by examining the distribution, we have deduced that there were 24 spurious large pulses, and so we have not used the data from this chamber although the distribution of smaller pulses is in complete agreement with the group of three.

Selecting the pulses with amplitude greater than 1.5 and 2.5 times the extrapolated integral pulse amplitude of a

Po-α, comparison can be made with the results of Bridge and Rossi taken up to 35,000 ft. (Fig. 3). It is not entirely clear whether our data should be considered an extension of their results taken in the case with 1 in. of lead surrounding the chamber or in the case without lead. In order to ballast the rocket, 250 pounds of lead were placed above the chamber, as shown in Fig. 1; however, the solid angle of this lead is small compared to the complete surrounding of the chambers. If there are no electrons of high energy above the atmosphere, there should be little difference between the two cases. The counting rates shown in Fig. 3 are unadjusted and the fluctuations indicated are the statistical probable errors only. The absorption coefficient, μ, derived from $I = I_0 e^{-\mu h}$, is (180 g/cm²)⁻¹. However, if the Gross transformation,

$$I = I_0 \mu h \int_{\mu h}^{\infty} \frac{e^{-x} dx}{x^2},$$

is used, then an absorption coefficient of (215 g/cm²)⁻¹ gives the best fit to the data and fits only the data of the case without lead. Inasmuch as an ion chamber is a non-directional detector, we believe the Gross transformation to be more significant.

Since the distribution of burst sizes is similar to that of Bridge and Rossi and the absorption curve of Fig. 3 indicates a monotonic increase of burst rate, we believe (a) that on the plateau in the upper atmosphere, where the counting rate is constant, we were measuring a direct effect of the primaries; (b) that the absorption coefficient of this portion is that associated with a nuclear cross section of 1.0×10^{-25} cm²; and (c) that an ever diminishing portion of this primary radiation still exists at lower altitudes.[2] The departure of the burst rate from the Gross transformation at low altitudes may be due to the diminishing of the energy of these primaries in normal ionization through the atmosphere.

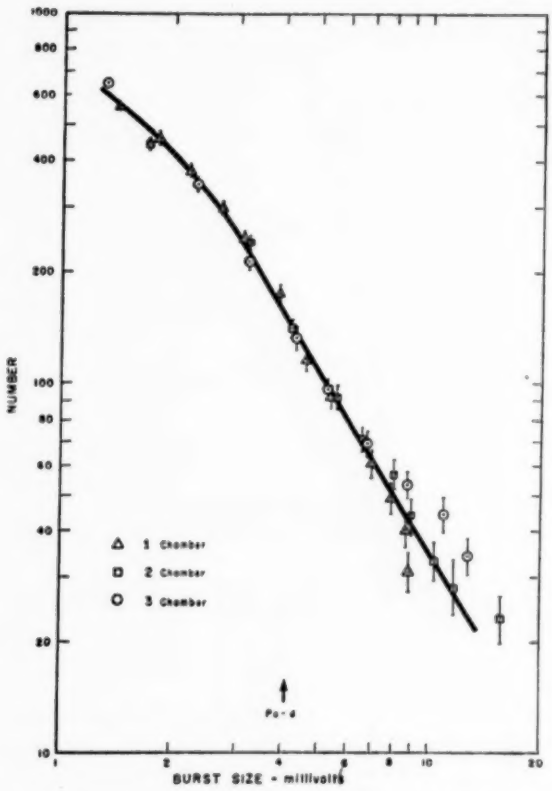

FIG. 2. Integral number—size curve of bursts recorded above 180,000-feet altitude.

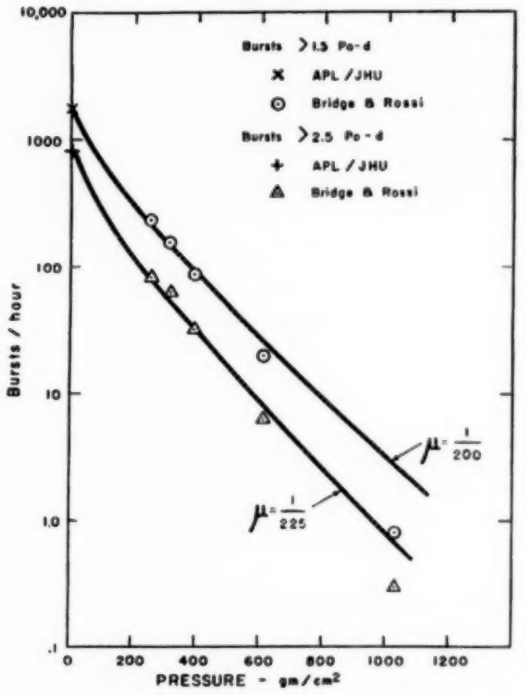

FIG. 3. Bursts/hour vs. pressure. Composite plot of V-2 data and data from reference 1 for the case without lead. The smooth curves are Gross transformations with $\mu = (200 \text{ g/cm}^2)^{-1}$ and $(225 \text{ g/cm}^2)^{-1}$, respectively.

We are grateful for the help given by Mr. Bridge and Professor Rossi and their colleagues in the preparation of this experiment.

* Supported by the Navy Bureau of Ordnance under NOrd 7386.

** Now at the Department of Terrestrial Magnetism, Carnegie Institution of Washington.

[1] H. Bridge and B. Rossi, Phys. Rev. 71, 379 (1947); H. Bridge, B. Rossi, and R. Williams 72, 257 (1947).

[2] Compare D. Broadbent and J. Janossy, Proc. Roy. Soc. A190, 497 (1947)

(n, p) and (n, α) Disintegrations of Nitrogen by Fast Neutrons

P. HUBER AND A. STEBLER
Physics Department, University of Basle, Switzerland
November 10, 1947

THE emission resonance of protons and α-particles from nitrogen has been observed several times.[1] Barschall and Battat[2] accurately determined the resonances with monochromatic neutrons of varied energy.

Our work was done with a continuous neutron spectrum by using neutrons from a *d-d* reaction with a suitable graphite moderator. The disintegrations of nitrogen were observed in an ionization chamber fitted with a linear amplifier and a "pulse spectrograph."[3] The measured energies correspond with the energy of the charged particles produced by the disintegration. The energy scale was calibrated with α-particles from uranium: $E(U^{234})=4.78$ Mev, $E(U^{238})=4.18$ Mev.[4] As the α-particles and the protons have a different saturation at high pressures in the ionization chamber, two different energy scales had to be used in the upper part of Fig. 1.

The (n, p) and (n, α) resonances in nitrogen were distinguished by recording the disintegrations at different pressures in the ionization chamber (2 and 15 kg (weight) per cm²). The results plotted in Fig. 1 show that only the (n, α) reactions can be observed if the pressure is lowered from 15 to 2 kg per cm². The (n, p) reactions vanish in the energy range considered (>1.2 Mev) as a consequence of the big wall effects for protons.

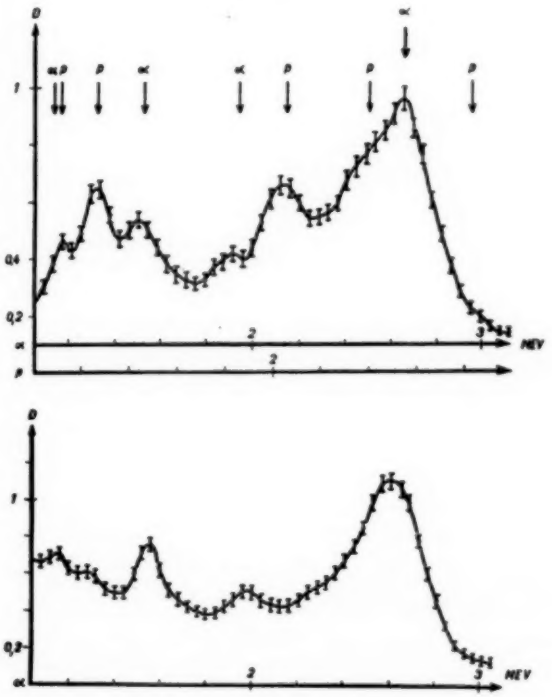

FIG. 1. Pulse distribution plotted against energy. D = relative number of pulses per energy interval. 18,000 pulses >1 Mev. Ionization chamber filled with nitrogen at a pressure of: (above) 15 kilograms (weight) per cm², energy of primary neutrons, 2.9 Mev, thickness of graphite moderator, 21 cm; (below) 2 kilograms (weight) per cm², energy of primary neutrons 2.8 Mev, thickness of graphite moderator 17 cm.

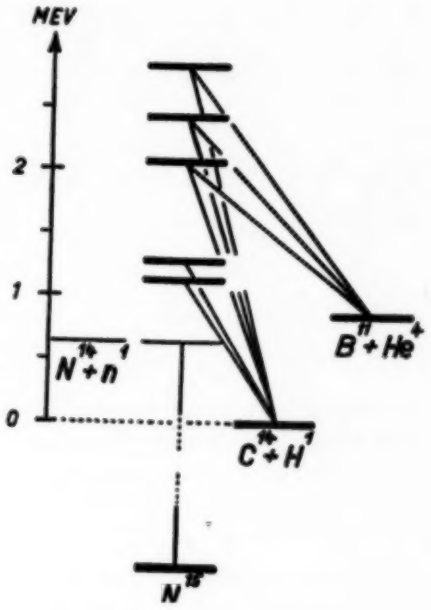

FIG. 2. Energy levels.

Three of the seven resonances are connected with (n, α) disintegrations. According to the results of Barschall and Battat, our lowest resonance corresponds to a (n, α) as well as to a (n, p) disintegration. The two (n, p) resonances of highest energy cannot be determined quite accurately as both are situated near the main (n, α) group. Yet they have been observed in all records so that their existence seems to be proved.

TABLE I. Energies in Mev.

Present measurements (n, α)	Present measurements (n, p)	Barschall and Battat* (n, α)	Barschall and Battat* (n, p)	Wilhelmy (n, α)	Zagor (n, α)	Maurer (α, n)	Hansen
1.14±0.04	1.11±0.04	1.21	1.18				
	1.27±0.03		1.33		1.33		1.31
1.54±0.04				1.42	1.64	1.40	1.75
1.97±0.06					1.94		1.94
	2.06±0.06		2.08	2.04	2.15	2.00	2.31
	2.40±0.1			2.59	2.64	2.16	2.58
	2.82±0.1				2.98	2.70	2.93
				3.21		3.25	3.18
						3.49	
						3.74	3.7
						3.86	3.82

* For the conversion of the measured neutron energies into the figures given here, we used $Q(n, p)=0.63$ Mev, $Q(n, \alpha)=-0.24$ Mev.

Table I contains the energy values of earlier papers and our new determinations. If the resonances are interpreted as energy levels of the intermediate nucleus N^{15}, it is possible to coordinate with each energy level (Fig. 2) a

(n, p) and a (n, α) disintegration insofar as the energy of the α-particles was measurable. The energy difference $E(n, p)-E(n, \alpha)$ of corresponding transitions must be equal to the difference of the Q values: $Q(n, p)-Q(n, \alpha)$ $\sim$0.9 Mev.

[1] E. Wilhelmy, Zeits. f. Physik **107**, 769 (1937); H. I. Zagor and F. A. Valente, Phys. Rev. **67**, 133 (1945). This paper contains references to previous work.
[2] H. H. Barschall and M. E. Battat, Phys. Rev. **70**, 245 (1946).
[3] D. Maeder, Helv. Phys. Acta **XX**, 139 (1947).
[4] Alder, Huber, and Metzger, Helv. Phys. Acta **XX**, 234 (1947).

On the Resolving Time and Genuine Coincidence Loss for Geiger-Mueller Counters*

C. E. MANDEVILLE AND MORRIS V. SCHERB
Bartol Research Foundation of the Franklin Institute, Swarthmore, Pennsylvania
November 6, 1947

THE coincidence method is one which has been widely used in experiments relating to nuclear disintegrations and cosmic radiation. In investigations of nuclear reactions and radioactive nuclei by coincidence techniques, the use of a very short resolving time ($\tau \leq 0.1$ microsecond) would have the obvious advantage of minimizing accidental coincidences arising from the presence of a strong background of uncorrelated phenomena. Circuit design has not been the limiting factor in achieving such short resolving times; the difficulties lie in the Geiger-Mueller counter mechanisms. A number of workers[1-4] have reported substantial losses in the counting of genuine coincidences when employing G-M counters in coincidence circuits having resolving times less than one microsecond. These losses have been attributed to fluctuating time delays (as much as one microsecond) between the initial ionizing event and the change in the potential of the counter wire of sufficient magnitude to register.

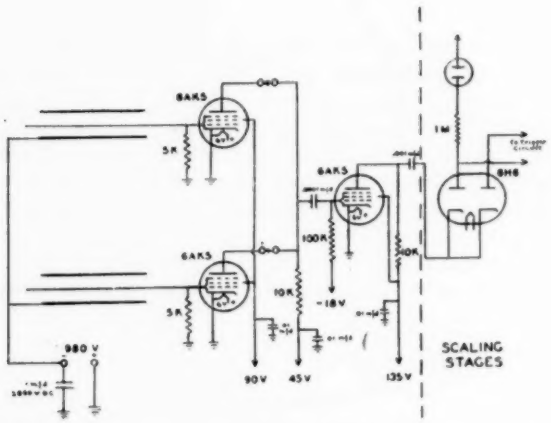

FIG. 1. Fast coincidence circuit—resolving time 0.08 microsecond.

Coincidence studies of radioactive nuclei have been in progress for some time at this laboratory and recent attempts to use resolving times under one microsecond have yielded preliminary results of a promising nature.

Thin-walled Geiger-Mueller counters were constructed to the following specifications: sensitive counting volume—5 cm in length, 1.5 cm in diameter; thickness of glass walls —0.013 cm; anode wire diameter—0.0075 cm; aquadag cathode thickness—0.0013 cm.

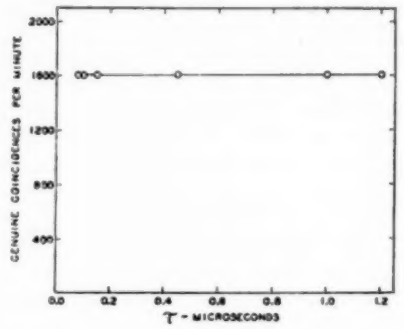

FIG. 2. Genuine coincidences as a function of the resolving time.

The counters were washed in a sulphuric acid solution and rinsed in distilled water before the cathode coating was applied. After baking in vacuum for 2 hours at 420°C to drive off occluded vapors, the anode wires were flashed and the counters filled with an argon-ether mixture to a pressure of 12 cm Hg. The operating potential for these counters was 980 volts.

For operating resistors of 1000 to 5000 ohms, the counter pulse shapes were examined on a fast sweep oscilloscope. The pulse rise time as viewed on the oscilloscope was 0.15 microsecond, the rise time of the oscilloscope amplifier. The actual rise time of the counters may be less than this amount. The pulses had a uniform amplitude of several volts.

A matched set of 2 of these Geiger-Mueller counters was operated in coincidence with the circuit shown in Fig. 1. The anode wires were connected directly to the grids of the Rossi valves as indicated. For an operating resistance of 5000 ohms, the counters delivered a negative pulse of approximately 4.5 volts to the grids of the 6AK5's. The resolving time of the circuit was varied by altering the values of the input grid resistors and the bias of the output tube. The coincidence circuit was checked for delays in one channel with respect to the other and for inter-channel coupling which might give rise to spurious coincidences.

Genuine coincidences were produced by a collimated source of hard beta-rays which were allowed to traverse both counters. As the resolving time, τ, was reduced from 1.2 microseconds to 0.08 microsecond, no loss in genuine coincidences was observed. More than 1600 genuine coincidences were recorded at each point to insure a high statistical accuracy. The genuine coincidence rate is plotted as a function of the resolving time in Fig. 2. As a check on

the results obtained, radioactive sources of Sc^{46}, Ti^{51}, and Ta^{182} were placed between the counters, and the beta-gamma coincidence rate was determined as a function of the resolving time. No losses in the genuine coincidence rate were observed down to the shortest resolving time used.

No variations in these results were observed when four pairs of counters of the type described above were tested.

The results obtained suggest that for these particular counters, the delay times are a fraction of one-tenth of a microsecond, and that long delays reported by other workers are not inherent in all Geiger-Mueller counters. It has been suggested that long time delays are due to the presence of electronegative vapors.[5,6] Rossi and Nereson[7] have reported delays of a few tenths of a microsecond in brass-walled argon-alcohol counters used in cosmic ray experiments. Counter delays of a tenth microsecond or less have also been reported.[8–10]

For argon-alcohol counters of diameter 1.2 cm, an extrapolated delay time of 0.04 microsecond has been calculated.[9] This result is in agreement with the fundamental experiments of Ramsey[11] and the recent analysis of Korff.[12]

Circuit limitations prevented the investigation of coincidence losses at resolving times less than 0.08 microsecond. A fast rise time amplifier is now in development for extending observations to 10^{-8} second, since no counter delays have as yet been detected.

Geiger-Mueller counters of this type should widen the use of the coincidence method and in particular should aid in the search for short-lived metastable states.[10,13]

Stimulating discussions with W. E. Ramsey and with Professor W. C. Elmore of Swarthmore College are gratefully acknowledged. We are indebted to Dr. Elmore for having measured the rise time and other counter pulse characteristics with his apparatus. Austin G. Nester of the Bartol Research Foundation constructed the Geiger-Mueller counters.

* Supported by the Office of Naval Research.
[1] J. V. Dunworth, Nature **144**, 152 (1939).
[2] J. Rotblat, Proc. Roy. Soc. **A177**, 260 (1941).
[3] A. Roberts, J. R. Downing, and M. Deutsch, Phys. Rev. **60**, 544 (1941).
[4] W. E. Ramsey, Phys. Rev. **58**, 476 (1940).
[5] M. E. Rose and W. E. Ramsey, Phys. Rev. **59**, 616 (1941).
[6] C. G. Montgomery and D. D. Montgomery, Rev. Sci. Inst. **18**, 411 (1947).
[7] Bruno Rossi and Norris Nereson, Phys. Rev. **62**, 417 (1942).
[8] H. K. Ticho, Rev. Sci. Inst. **18**, 271 (1947).
[9] H. den Hartog, F. A. Muller, and N. F. Verster, Physica **13**, 251 (1947).
[10] L. Madansky and M. L. Wiedenbeck, Phys. Rev. **12**, 185 (1947).
[11] W. E. Ramsey, Phys. Rev. **57**, 1022 (1940).
[12] S. A. Korff, Phys. Rev. **72**, 477 (1947).
[13] S. DeBenedetti and F. K. McGowan, Phys. Rev. **70**, 569 (1946).

On the Solutions of Radial Wave Equations

AUREL WINTNER
Department of Mathematics, Johns Hopkins University, Baltimore, Maryland
November 12, 1947

FOR a fixed value, $W=W_0$, of the eigen parameter, the separation of the spherical harmonics in a Schrödinger equation, belonging to a potential of the type $V=V(r)$, is known to reduce the three-dimensional wave equation to the ordinary differential equation[1]

$$(r^2R')'/(r^2R)+W_0-l(l+1)/r^2-V(r)=0, \qquad (1)$$

for $R=R(r)$, where $R'=dR/dr$ (and $8\pi^2\mu/h^2=1$). Let the constant W_0 be in the range of "bound electrons," so that

$$W_0\geqq 0, \quad \text{and} \quad V(r)\geqq 0 \quad \text{for} \quad 0<r<\infty, \qquad (2)$$

while the potential is a sum of the form

$$V(r)=Ar^{-a}+Br^{-b}+\cdots, \qquad (3)$$

in which $a, b, \cdots$ and $A, B, \cdots$ are positive constants.

In the case of the hydrogen atom, the sum (3) reduces to a single term, with $a=1$ and $A=Ze^2>0$. In this case, the solution of Eq. (1) leads[2] to Laguerre functions, and the preponderant factor behaves, roughly, as e^{-kr} if $r\to\infty$. The success of this substantially explicit method depends on the accidental applicability of the classical theory (Riemann-Fuchs) of "regular" singular points of linear differential equations,[3] a circumstance due to the particular choice, Ze^2/r, of $V(r)$.

Because of the same circumstance, a closer inspection of the characteristic equation and of the recursion formulae is possible. It reveals that the coefficients of the Laguerre functions[4] obey a certain law of positive regularity. It will not be necessary to give a description of this law, since it turns out to have nothing to do with the specific nature of a Coulomb force or, for that matter, with the possibility of *some* "explicit" integration of Eq. (1). In fact, it will be proved below that the situation is as follows:

If the potential *graph*, $V=V(r)$, over the half-line $0<r<\infty$ of the (r, V) plane, besides satisfying condition (2), satisfies a certain *qualitative* condition (that specified by the inequalities (12) below), then Eq. (1) possesses for $0<r<\infty$ a positive solution which not only is *a Laplace transform in the real domain*, say

$$R(r)=\int_0^\infty e^{-rq}\phi(q)dq, \quad \text{where} \quad 0\leqq q<\infty, \qquad (4)$$

but belongs to a Laplace transform of a *non-negative* density, which, in addition, is *non-increasing* when q increases. In other words, the function $\phi(q)$ occurring in Eq. (4) is subject to

$$\phi(q)\geqq 0 \quad \text{and} \quad d\phi(q)\geqq 0 \quad \text{for} \quad 0\leqq q<\infty. \qquad (5)$$

Needless to say, Eq. (4) is claimed to represent an *exact* solution of Eq. (1), rather than just an approximation, asymptotic to some solution as $r\to\infty$. If the distribution determined by $\phi(q)$ is known,[5] a positive solution of Eq. (1) follows from Eq. (4), whereupon the "other" (linearly independent) solution of Eq. (1) is supplied by the product

$$R(r)\cdot\int_r^\infty \{pR(p)\}^{-2}dp, \qquad (6)$$

in which R denotes the first solution. This can, of course, be verified by substituting the function (6) into Eq. (1) and assuming that the latter is satisfied by the first factor of the product (6).

The existence of a solution $R(r)$ of the type in question will be concluded from the following theorem:[6] Suppose that $f(x)$ is any function possessing at every positive x derivatives of arbitrarily high order, and that the latter satisfy the conditions

$$(-1)^{n+1}d^nf(x)/dx^n \geqq 0 \quad \text{for} \quad n=0, 1, 2, \cdots; \quad 0<x<\infty. \quad (7)$$

Then the differential equation,

$$y''+f(x)y=0, \quad (8)$$

has a positive solution which is representable in the form

$$y(x)=\int_0^\infty e^{-xq}d\phi(q), \quad 0<x<\infty, \quad (9)$$

where $\phi(q)$ is a certain non-decreasing function which (since only $d\phi$ occurs) can be normalized by $\phi(0)=0$.

In order to apply this general theorem to the wave equation, put

$$f(r)=W_0-l(l+1)r^{-2}-V(r) \quad (10)$$

and $y=rR$. Then an easy calculation transforms Eq. (1) into an Eq. (8), where $x=r$. Since Eq. (9) becomes identical with Eq. (4), where $R=y/r$, it follows that

$$R(r)=\left\{\int_0^\infty e^{-rq}d\phi(q)\right\}/r. \quad (11)$$

But if the identity

$$1/r=\int_0^\infty e^{-rp}dp$$

is substituted into Eq. (11), a straightforward contraction reduces Eq. (11) to Eq. (4), since $\phi(0)=0$.

What remains to be verified is that the assumptions (7) for the existence of a solution of the form (9) are satisfied in the present case. But Eq. (10) shows that the case $n=0$ of the conditions (7), where $d^0f/dx^0=f$, is contained in the assumption (2) for a bound electron, and that the other conditions (7) reduce to

$$(-1)^n d^nV(r)/dr^n \geqq 0, \quad \text{where} \quad n=1, 2, \cdots; \quad 0<r<\infty. \quad (12)$$

Clearly, the conditions (12) are satisfied by $V(r)=r^{-a}$ if $a>0$. Hence, they are satisfied by any potential of the form (3). They are also satisfied if $V(r)=e^{-r}/r^a$, since they are satisfied if $V(r)=e^{-r}$ (they are satisfied by $V(r)=V_1(r)V_2(r)$ if they are satisfied by both $V=V_1$ and $V=V_2$).

If $r=x$, Eq. (1) and Eq. (10) represent the particular case $g(x)=x^2$, $h(x)=f(x)$ of the general self-adjoint differential equation $(gz')'+hz=0$. It is not hard to verify that the above deduction can be extended to the case of the latter differential equation as soon as the conditions (7) are satisfied by both $f=-g^{-\frac{1}{2}}$ and $f=h$.

[1] E. Schrödinger, *Abhandlungen zur Wellenmechanik* (J. A. Barth, Leipzig, 1928), p. 3.
[2] E. Schrödinger (see the above), pp. 4–10 and pp. 131–134.
[3] E. G. C. Poole, *Introduction to the Theory of Linear Differential Equations* (Clarendon Press, Oxford, 1936), Chap. V.
[4] (See reference two.)
[5] A. Wintner, Am. J. Math. **69**, 88 (1947).
[6] A. Wintner (see the above), p. 91.

Stark Spectrum of H_2O*

S. GOLDEN**
Harvard University, Cambridge, Massachusetts
AND
T. WENTINK, R. HILLGER, M. W. P. STRANDBERG
Research Laboratory of Electronics, Massachusetts Institute of Technology, Cambridge, Massachusetts
November 18, 1947

THE Stark spectrum of the rotation line of H_2O[1] at 22,235.22±0.05-mc/sec. has been observed, using higher electric fields than previously reported.[2] The apparatus used is similar to types described by others,[3,4] utilizing 1.25 cm silver wave guide with a 6 kc/sec. square wave electric field oriented parallel to the electric vector of the microwave radiation. At fields of 7500 volts/cm, four of the six components predicted by theory were completely resolved.

The unperturbed line had a minimum breadth of approximately 250 kc/sec.; because of the irregularities in the perturbing electric field, the components had widths of approximately 500 kc/sec.

Figure 1 shows the experimental data and fitted curves for the Stark splitting. It appears that the unresolved $M=0, 1$ line has a "center of gravity" approximating the splitting of the $M=1$ line. This is to be expected since the latter is doubly degenerate and the former a single line; the resulting computed intensity ratio is 36/70. The relative intensities of the components qualitatively follow a

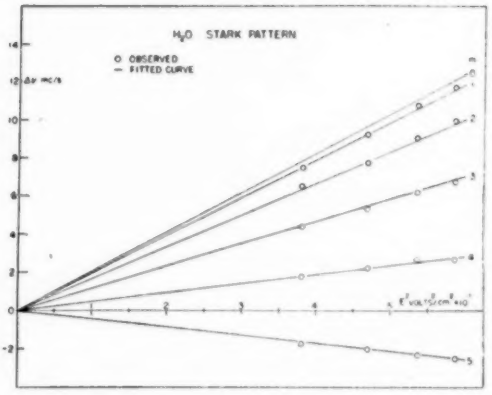

FIG. 1. H_2O Stark pattern.

theoretical (J^2-M^2) law, $(J=6)$, but this has not been substantiated by integration over the components.

The experimental data can be represented by the formula

$$\Delta\nu=(20.65-1.003M^2)E^2\times10^{-8} \text{ mc/sec.},$$

where $M=0, 1, 2, 3, 4, 5$; E=electric field strength in volts/cm. The probable error of fit is approximately 0.3 percent. This is to be compared with the theoretical formula calculated by means of conventional perturbation theory:

$$\Delta\nu=(18.42-0.9165M^2)E^2\times10^{-8} \text{ mc/sec.},$$

with the dipole moment equal to 1.84×10^{-18} esu-cm.[5]

Certain of the direction cosine matrix elements involved in the calculation were determined from the line strengths for H_2O calculated by King, Hainer, and Cross[6] while others were determined by interpolation from tables of line strengths by these same authors.[7] The term values involved in the second-order perturbation theory were taken from the assignments by Randall, Dennison, Ginsburg, and Weber[8] with the exception that the observed microwave absorption frequency was used in place of that computed from the assigned term values.

Despite favorable agreement between the experimentally and theoretically derived formulas, the existing discrepancy requires some comment. From the theoretical point of view there are three possible sources of error. Induced polarization effects due to the Stark field have been examined and for the present case may be safely neglected. There is some uncertainty in the dipole moment, particularly since the value usually obtained involves an implicit averaging over the various vibrational states of the molecule. The most serious error is probably in the use of the rigid rotor wave functions in the theoretical calculations.

Experimentally, the greatest source of error is in the determination of the field strength, since the field is not homogeneous over the cross section of the wave guide. Calculations show that corrections for fringing of the field near the side walls of the wave guide are negligible. However, the error in the measured field strength can be as much as ± 2 percent because of lack of centering of the Stark electrode and the wave shape of the applied Stark voltage.

The ratio of the constant and M-dependent coefficients in the formulas is 20.59 for the observed data and 20.10 for the theoretical formula, giving a 2.5 percent agreement. This ratio is independent of both field strength and dipole moment.

To apply the theory described to our measurements, a value for the dipole moment of 1.94 ± 0.06 Debye units would be required.

* This work has been supported in part by the Signal Corps, the Air Materiel Command, and O. N. R.

** National Research Council Predoctoral Fellow.

[1] C. H. Townes and F. R. Merritt, Phys. Rev. 70, 558 (1946) and references noted therein.

[2] D. K. Coles, Westinghouse, in private communication to Prof. E. B. Wilson, Jr., Harvard, observed the Stark displacement of this transition, without resolution, at fields considerably lower than those used here.

[3] R. H. Hughes and E. B. Wilson, Jr., Phys. Rev. 71, 562 (1947).

[4] B. P. Dailey, Phys. Rev. 72, 84 (1947).

[5] See, for example, *Tables of Electric Dipole Moments*, Tech. Report No. II, Laboratory for Insulation Research, Massachusetts Institute of Technology.

[6] G. W. King, R. M. Hainer, and P. C. Cross, Phys. Rev. 71, 433 (1947).

[7] G. W. King, R. M. Hainer, and P. C. Cross, J. Chem. Phys. 12, 210 (1944).

[8] H. M. Randall, D. M. Dennison, N. Ginsburg, and L. Weber, Phys. Rev. 52, 160 (1937).

Proceedings of the American Physical Society

Minutes of the Meeting of the Ohio Section at Oberlin on November 1, 1947

THE Ohio Section of the American Physical Society met at Oberlin on November 1, 1947. The titles of the papers presented are listed below, and are followed by such abstracts as were made available for publication. A discussion of the problem of registration of physicists was held by a Committee under the chairmanship of H. P. Knauss. The Section heard the Sigma Xi lecture of Professor J. R. Dunning of Columbia University.

LEON E. SMITH, *Secretary*

1. **A Direct Measurement of the Current-Voltage Relation in Charging and Discharging a Capacitor.** CARL E. ROWE, *Oberlin College.*
2. **Continuous Casting of Metals.** N. P. GOSS, *Cleveland, Ohio.*
3. **The Production of Axially Symmetric Magnetic Fields.** E. F. SHRADER AND R. L. GARWIN, *Case Institute of Technology.*
4. **Properties of Thin Ferromagnetic Films.** E. C. CRITTENDEN, JR., *Case Institute of Technology.*
5. **Artificial Growing of Quartz Crystal.** D. R. HALE, *Brush Development Company.*
6. **The Electro-Optic Effect in Primary Phosphate Crystals.** HANS JAFFE, *Brush Development Company.*
7. **Rectangular Analogs of Helmholz Coils.** RICHARD A. BETH AND J. S. KROHMER, *Western Reserve University.*
8. **The Design of a 30-Mev Betatron.** E. C. GREGG, JR., *Case Institute of Technology.*
9. **Study of Activation of Oxide-Coated Cathodes.** W. F. HODGE, *Nela Park Laboratories of General Electric Company.*
10. **A Method of Measuring Nuclear Magnetic Moments.** JOHN R. ZIMMERMAN AND DUDLEY WILLIAMS, *Ohio State University.*
11. **Some Advantages of English Absolute over English Gravitational Units.** CONRAD E. RONNEBERG, *Denison University.*
12. **Reflections of Radar Waves.** PAUL B. TAYLOR, *Aircraft Radio Laboratory, Wright Field.*

ABSTRACTS

Rectangular Analogs of Helmholtz Coils. J. S. KROHMER AND R. A. BETH, *Western Reserve University.*—A pair of rectangular rather than circular coils can be used to approximate a uniform magnetic field.[1,2] The rectangular coils may be preferred in order to extend the region of uniformity in a direction transverse to the field or in order to avoid the difficulties involved in making sufficiently large circular coils.

If two identical rectangular coils are connected in series and coaxially placed with corresponding sides parallel, the magnetic field H along their common axis can be expressed in a series of *even* powers of the distance w from the geometric center of the system. For given rectangle sides, $a>b$, *the spacing* D *between the planes of the coils can be chosen* $(=D_0)$ *so that the coefficient of* w^2 *vanishes*, thus giving the best field uniformity in the same sense in which the Helmholtz spacing (equal to the radius) gives the best uniformity for circular coils.

With the "best spacing," D_0 cm, between coils, the field on the axis near the center of the system of two rectangular coils is

$$H=(4ni/D_0)h_0(1-Cx^4+\cdots)\text{oersted},$$

where n is the number of turns in each coil, i is the current in abamperes, and $x=w/D_0$.

[1] F. K. Harris, Nat. Bur. Stand. J. Research 13, 391 (1934).
[2] R. H. Lyddane and A. E. Ruark, Rev. Sci. Inst. 10, 253 (1939).

A Method of Measuring Nuclear Magnetic Moments. JOHN R. ZIMMERMAN AND DUDLEY WILLIAMS, *Ohio State University.*—Three methods of observing nuclear magnetic moments have recently been reported. The work described in the present report is based on an extension and modification of one of the methods described by Roberts. The method involves a nuclear Paschen-Back effect, and magnetic resonances in solid or liquid samples are observed at

radiofrequencies. The coil containing the sample forms part of a simple LC oscillator and is located in a uniform magnetic field, the intensity of which can be varied and also subjected to a small 60-cycle modulation. When the condition for resonance $h\nu = \mu H/I$ is realized, the amplitude of oscillation shows marked changes, which can be detected by a radio receiver or by means of audio-amplifier circuits to be described. The resonance peaks are displayed on a cathode-ray oscilloscope. The interpretation of the signals observed with the audio-amplifier is somewhat simpler than that of the signals from the receiver. The sensitivity is comparable with the receiver super-regenerative-oscillator technique recommended by Roberts. Difficulties are encountered in reducing the oscillator power to a point where saturation effects are negligible. The accuracy with which magnetic moments can be determined is limited by the accuracy of magnetic field measurements. The preliminary values obtained for H^1 and F^{19} are

$$H^1 = 2.788 \pm .028 \text{ nuclear magnetons},$$
$$F^{19} = 2.625 \pm .017 \text{ nuclear magnetons}.$$

The work is being continued with slight modifications for determining magnetic moments of other nuclei.

Design of a 30-Mev Biased Betatron. E. C. GREGG, JR., *Case Institute of Technology.*—The biased betatron now under construction[1] has an equilibrium orbit radius of 17.2 cm and a peak orbital magnetic field of 6000 oersteds. The use of a complete laminated iron core, bucking coil wound about the core, and a biasing direct current[2] reduces considerably not only the physical size of the machine (for a given energy) but also the size of the capacitor bank required to tune the betatron to resonance. The driving frequency of 180 c.p.s. is obtained from a frequency tripling transformer. The outside dimensions of the betatron are 46″×28″×16″ with a total weight of 5000 pounds, while the .05 hy reactor necessary to bypass the direct current is water-oil cooled and totals 500 pounds of copper. The betatron-reactor combination requires 460 kva of power factor correction at 3250 volts and dissipates about 12 kw of power. Calculations show that the current feedback resulting from connecting the bucking coil in parallel with the main coil reduces the magnetic non-linearities of the core to about 0.1 percent at the time of electron ejection. An underground vault for housing the machine with an appropriate control room has just been completed.

[1] This work is being supported in part by a grant from the Research Corporation.
[2] W. F. Westendorp, J. App. Phys. 16, 657 (1945).

A Method of Studying the Thermionic Emission of Oxide-Coated Cathodes in Gaseous Conduction Devices. W. F. HODGE, *Lamp Development Laboratory, General Electric Company.*—The procedure for the activation of oxide-coated cathodes in tubes containing a gaseous atmosphere has been determined in the past by measurements made in vacuum and by trial and error methods in practical usage. Based on a method, described by Found, for measuring the thermionic emission of such cathodes in a gaseous atmosphere, an experimental means giving a sensitive indication of the activity of such cathodes has been developed. This consists of plotting positive ion current to a probe located in the vicinity of the cathode against cathode heating current or temperature. The result of this procedure is a determination of the point where zero field emission becomes insufficient to carry the arc current, a lower temperature for this point indicating greater activity. Measurements can be made quite rapidly, an advantage in a study of cathodes that may change their activity considerably in a short period of operation. The method is being used in the study of fluorescent lamp cathodes. It would be equally applicable to other gas-filled discharge devices, such as thyratrons.

Electro-optic Effects in Crystals of the Primary Phosphate Type. HANS JAFFE, *Brush Development Company.*—Non-centric crystals are known to have electro-optic effects analogous to the Kerr effect in liquids but differing from this effect by a linear dependence of optic retardation on applied electric fields. The linear electro-optic effect is of particular interest in that case where the applied field is parallel to the propagation of the light beam and where this is parallel to the optic axis of the crystal. This condition can be realized only in one class of uniaxial crystals of which the primary phosphates of potassium and ammonium are representative. Half-wave retardation in these crystals is obtained by 8400 and 9400 volts, respectively, for green light independent of the thickness of the crystal plate. The effect is useful for modulating a light beam with acoustic signals, for fast-working shutters, and for color switching.

Minutes of the Meeting of the New York State Section at Union College, November 8, 1947

THE Fall Meeting of the New York State Section of the American Physical Society was held at Union College, Schenectady, New York, on Saturday, November 8, 1947. An attendance of 120 members and visitors was recorded. The following programme of invited papers was presented:

Greetings. CARTER DAVIDSON, *Union College.*

Dedication of the South Physics Laboratory, Union College. SHERMAN MILLER, *American Locomotive Company.*

Ultrasonics in War and in Basic Research. H. B. HUNTINGTON, *Rensselaer Polytechnic Institute.*

Electron Accelerators. W. F. WESTENDORP, *General Electric Company.*

I. Demonstration Experiments

Model to Illustrate Action of Mass Spectrograph. F. J. NORTON, *General Electric Company.*

A Simple X-Ray Intensity Meter. A. T. GOBLE, *Union College.*

Geomagnetic Surveying with a New Electronic Magnetometer. H. R. LARSEN, *Gurley Instrument Company.*

The Question of the Existence of Single Magnetic Poles. HERTA R. LENG, *Rensselaer Polytechnic Institute.*

Chromatographic and Fluorescence Analysis for the Isolation and Purification for Spectroscopic Studies of Pigments Synthesized by Micro-organisms. M. O'L. CROWE AND A. WALKER, *Division of Laboratories and Research, New York State Department of Health.*

Mechanical Model of Chain Reaction in Nuclear Fission. LEWI TONKS, *General Electric Company.*

II.

Rocket Propulsion (Motion Pictures of V-2 Launchings). R. W. PORTER, *General Electric Company.*

On the preceding afternoon visits were made to General Electric Research Laboratory and the American Locomotive Company plant. The Union College Chapter of Sigma Xi invited the Society to an evening lecture on the Future of Nuclear Research by John R. Dunning, of Columbia University.

C. L. ANDREWS, *Secretary*